

THERMIONIC ELECTRON  
EMISSION PROPERTIES OF NITROGEN-INCORPORATED  
POLYCRYSTALLINE DIAMOND FILMS

By

William (Hank) Paxton

Dissertation

Submitted to the Faculty of the  
Graduate School of Vanderbilt University  
in partial fulfillment of the requirements

for the degree of

DOCTOR OF PHILOSOPHY

in

Electrical Engineering

May, 2013

Nashville, Tennessee

Approved:

Professor Jim L. Davidson

Professor Weng P. Kang

Professor Norman H. Tolk

Professor D. Greg Walker

Professor Mike Alles

*To my dearest wife, Megan*

*To my loving parents, Lucy and Bill Paxton*

*And*

*To my sister and her family, Crissy, Todd, and Kate*

## ACKNOWLEDGMENTS

I am very grateful for my academic advisor, Dr. Jim Davidson for giving me the opportunity to pursue this research. It would be impossible for me to summarize the vast amount of insight he has bestowed on me since I began working with him during the summer prior to my undergraduate senior year at Vanderbilt. The freedom that Dr. Davidson has awarded me has allowed me to develop into a stronger scientist with the confidence to solve any problem that may arise. In addition to Dr. Davidson, I am also highly appreciative of Dr. Weng Poo Kang for his always intuitive advice and suggestions. His inquisitive approach to the interpretation of results has helped to mold me into a vigilant researcher devoted to rigorous methodology and collecting the most accurate results possible. Moreover, I feel that the advice Dr. Kang has given me on matters outside of research will certainly become increasingly more helpful as I move forward into my professional career.

I would also like to thank Dr. Norman Tolk, Dr. Greg Walker, and Dr. Mike Alles for serving on my Ph.D. committee. Over the past several years, Dr. Tolk and I have developed a strong academic relationship that has allowed me the opportunity to branch out into other areas of science beyond those discussed in this dissertation. I have also had the pleasure of collaborating with Dr. Walker on several occasions which I feel has greatly helped to further my understanding of this research. Though I have not had many opportunities to work with Dr. Alles directly, the encounters we have had together have always proven extremely insightful.

I would also like to acknowledge my present and ex-colleagues for their valuable technical assistance. Particularly, I feel that many of the experiments performed in this research would not have been possible without the aid of Mick Howell. His ever astonishing ingenuity has aided me with the design and implementation of many of my testing apparatuses. I feel that Mick will be a highly useful resource in any endeavor that I may encounter following the successful completion of my Ph.D.

This work would not have been possible without the financial support from the TN-SCORE (Tennessee Solar Conversion and Storage using Outreach) program. This support has not only provided me with a research assistantship and research funding, but has also afforded me the opportunity to participate in community outreach programs such as Vanderbilt Student Volunteers for Science. I would further like to recognize The Graduate School at Vanderbilt whose travel grants have allowed me to present my work at conferences around the world.

Much of the credit for my success while pursuing my Ph.D. is due to my wife, Megan. Her role as a fellow Ph.D. student at Vanderbilt (Clinical Psychology) has enabled her to relate and commiserate with me during the challenges of graduate school and research. Though always supportive, she has helped to prevent me from becoming completely consumed with my research. Her love and companionship have helped to make my journey through graduate school one of the most memorable yet and I look forward to many more journeys with her.

, Lastly, I would like to thank my family who has always been both supportive and encouraging during my graduate work. I have been so blessed to have my parents, Bill and Lucy, my sister, Crissy, my brother-in-law, Todd, and my new niece, Kate, as

some of my most influential contacts. I know they are all extremely proud of me and look forward to what the next chapter of my life has in store.

## TABLE OF CONTENTS

	Page
DEDICATION _____	<i>ii</i>
ACKNOWLEDGEMENTS _____	<i>iii</i>
LIST OF TABLES _____	<i>x</i>
LIST OF FIGURES _____	<i>xi</i>
CHAPTER I. INTRODUCTION _____	1
History of thermionic emission and vacuum devices _____	1
Motivation for energy conversion research _____	3
Today’s energy climate _____	3
Current large-scale power generation methods _____	5
Current small-scale power generation methods _____	6
Renewable power generation technologies _____	7
Thermionic energy conversion _____	8
Research objectives _____	9
Organization of this dissertation _____	10
CHAPTER II. DIAMOND:GROWTH, PROPERTIES, AND CHARACTERIZATION _____	12
Diamond background _____	12
Fabrication of diamond films _____	13
Substrate selection and preparation and the nucleation process _____	14
Film deposition _____	17
Characterization of diamond films _____	20
Material properties of diamond _____	25
Doping of diamond _____	26
P-type diamond _____	27
N-type diamond _____	27

Nitrogen-incorporated diamond films _____	28
Hydrogen in diamond _____	29
Electron transport _____	29
Electron affinity _____	31
Desorption of hydrogen from diamond _____	34
Deuterium in diamond _____	38
Applications of diamond _____	39
Diamond as a solid state electronic material _____	39
Diamond in vacuum microelectronics _____	43
Use of diamond in thermionic energy converters _____	47
CHAPTER III. THERMIONIC ENERGY CONVERSION _____	50
Thermionic emission _____	50
Richardson equation derivation _____	51
Thermionic energy conversion _____	55
Thermionic energy converter design considerations _____	57
Production of thermionic energy converters _____	61
Current thermionic cathodes _____	62
Metallic cathodes _____	62
Oxide coated cathodes _____	64
Lanthanum hexaboride cathodes _____	65
Overview _____	65
CHAPTER IV. PROPOSED RESEARCH _____	66
Introduction to the proposed research _____	66
Fabrication of nitrogen-incorporated diamond thermionic cathodes _____	68
Characterization of the thermionic emission from diamond films _____	71
Investigation of hydrogen's influence on thermionic emission _____	73
Determination of the activation energy of hydrogen in diamond _____	74
Exploration of deuterium as an alternative to hydrogen _____	76
Investigation into the operation of diamond in gaseous environments _____	76
CHAPTER V. DEVICE FABRICATION AND TESTING _____	80

Deposition and characterization of diamond films _____	80
Sample preparation and deposition process _____	80
Characterization of diamond samples _____	82
Testing apparatus _____	85
Apparatus for testing in vacuum environments _____	85
Apparatus for testing in gaseous environments _____	89
Data collection and system control _____	94
Current vs. Temperature (CVT) Configuration _____	96
Isothermal (IT) Configuration _____	98
Influence of gaseous species on the thermionic emission from diamond _____	99
CHAPTER VI. THERMIONIC EMISSION CHARACTERIZATION IN VACUUM _____	101
As-grown nitrogen-incorporated films _____	101
Thermionic emission behavior of as-grown samples _____	101
Effect of hydrogen on the thermionic emission from diamond _____	105
Characterization technique _____	105
Comparison of as-grown and hydrogenated diamond samples _____	106
Analysis of hydrogen's effects on thermionic emission _____	108
Determination of the optimal hydrogenation procedure _____	111
Influence of temperature on the hydrogenation of diamond _____	111
Influence of time on the hydrogenation of diamond _____	115
Influence of microwave power on the hydrogenation of diamond _____	118
Effects of varying hydrogenation recipes _____	120
Desorption process of hydrogen in diamond _____	120
Diamond sample preparation _____	122
Isothermal emission behavior of hydrogenated diamond films _____	123
Calculation of the activation energy of hydrogen in diamond _____	125
Desorption deuterium from diamond _____	129
Isothermal emission behavior of deuterated diamond films _____	132
Summary of the desorption of deuterium from diamond _____	139
CHAPTER VII. THERMIONIC EMISSION CHARACTERIZATION IN GASEOUS ENVIRONMENTS _____	140
Molecular nitrogen _____	140

Behavior of diamond thermionic cathodes in a N <sub>2</sub> environment _____	141
Methane _____	143
Behavior of diamond thermionic cathodes in a CH <sub>4</sub> environment _____	145
Analysis of the thermionic emission behavior in CH <sub>4</sub> _____	149
Water vapor _____	153
Behavior of diamond thermionic cathodes in a H <sub>2</sub> O environment _____	154
Analysis of the thermionic emission behavior in H <sub>2</sub> O _____	157
Molecular hydrogen _____	162
Behavior of diamond thermionic cathodes in a H <sub>2</sub> environment _____	163
Analysis of the thermionic emission response to H <sub>2</sub> _____	171
Increased operating temperature in H <sub>2</sub> _____	174
Nitrous Oxide _____	175
Behavior of diamond thermionic cathodes in a N <sub>2</sub> O environment _____	176
Analysis of the thermionic emission behavior in N <sub>2</sub> O _____	180
 CHAPTER VIII. CONCLUSION AND RECOMMENDATIONS _____	 184
 Observed effects of hydrogen in diamond _____	 184
Gaseous environment effects on thermionic emission _____	185
Gases that diminish thermionic emission _____	185
Gases that enhance thermionic emission _____	186
Potential thermionic energy conversion performance _____	189
Recommendations for future work _____	192
 LIST OF PUBLICATIONS _____	 194
 REFERENCES _____	 195

## LIST OF TABLES

Table	Page
<b>Table 2.1</b> Comparison of diamond to silicon, boron nitride, and copper.....	25
<b>Table 2.2</b> Comparison of the activation energies obtain from diamond films with differing orientations using various methods. It can be see that most studies agree that the activation energy of 100 oriented diamond films is around 1.5eV .....	36
<b>Table 3.1</b> Description and definition of symbols used in Equations 3.13-15 which describe the three mechanisms of heat loss for a thermionic energy converter in operation as described by J.H Ingold.....	60
<b>Table 3.2</b> Comparison of tungsten surface contaminant on the work function.....	63
<b>Table 3.3</b> Comparison of the work function values and Richardson constant values of some commonly use thermionic cathode oxide coatings .....	64
<b>Table 6.1</b> Measurements of the bond energy from hydrogen desorption studies using various experimental approaches .....	128
<b>Table 6.2</b> Activation energies and pre-exponential factors obtained from previous deuterium desorption studies.....	136
<b>Table 7.1</b> A few possible low pressure dissociation channels resulting from the impact of an electron with a methane molecule.....	150
<b>Table 7.2</b> Qualitative description of the response of the emission current to the presence of water vapor .....	158

## LIST OF FIGURES

Figure	Page
<b>Figure 1.1</b> Graph of the world energy consumption by fuel type in terms of million tons of oil equivalence (MTOE).....	4
<b>Figure 1.2</b> Current estimates of world oil production from the year 1900 through 2100 based on a 2006 study by BP. The three peaks represent the three possible times in which the world will reach peak production. ....	5
<b>Figure 1.3</b> Flow diagram of the components of a typical coal fueled power plant beginning with the fuel handling through the energy conversion. ....	6
<b>Figure 2.1</b> Image of the diamond lattice .....	12
<b>Figure 2.2</b> SEM image of diamond crystals forming on a scratched silicon substrate .....	16
<b>Figure 2.3</b> Schematic diagram of the biased enhanced diamond growth processes during the first two hours of deposition presented by Stoner and colleagues. ....	17
<b>Figure 2.4</b> Schematic of an (a) HFCVD apparatus and (b) MPCVD apparatus .....	19
<b>Figure 2.5</b> General Raman spectra of gem quality diamond excited at wavelengths of 229.9 nm at room temperature demonstrating the first, second, and third order Raman peaks .....	21
<b>Figure 2.6</b> Typical XRD patterns for diamond samples with (a) (100) surface facets and (b) (111) surface facets .....	22
<b>Figure 2.7</b> SEM spectra of polycrystalline diamond films with (a) (111) triangular faces, (b) (100) square faces, and (c) cauliflower-like small crystalline aggregates.....	24
<b>Figure 2.8</b> Current-Voltage curves of the diamond film as grown, annealed, and hydrogenated from M.I. Landstrass and K.V. Ravi's 1989 study.....	30
<b>Figure 2.9</b> Band diagrams of a semiconductor with (a) positive electron affinity and (b) negative electron affinity. $E_g$ represents the bandgap; $\Phi$ , the work function; $E_o$ , the vacuum level; $E_f$ , the Fermi level; and $E_c$ and $E_v$ , the conduction and valence band energy levels, respectively. ....	32
<b>Figure 2.10</b> Band diagram and corresponding atomic arrangements of a clean, hydrogenated, and oxygenated diamond surface. ....	34

<b>Figure 2.11</b> a) Decrease in hydrogenation coverage as a function of anneal time for various annealing temperatures. b) First order desorption fit of the data indicating an activation energy of 21 kcal/mol .....	37
<b>Figure 2.12</b> Scanning electron micrograph of boron doped diamond resistors patterned via oxygen plasma etching on an aluminum nitride substrate .....	40
<b>Figure 2.13</b> Current-voltage characteristics of an all diamond pn diode with boron and nitrogen as the n- and p-type dopants respectively .....	41
<b>Figure 2.14</b> Fabrication of the vertical diamond field effect transistor by M.W. Geis.....	42
<b>Figure 2.15</b> Inverse capacitance squared vs. bias voltage of the diamond field effect transistor seen in Figure 2.13. The linear relationship implies the diamond-SiO <sub>2</sub> interface is extremely well behaved.....	42
<b>Figure 2.16</b> (a) Potential energy of an electron U(x) as a function of distance from the metallic cathode. Here “-eFx” is the externally applied potential, “U <sub>p</sub> ” is the total potential well depth, and “-e <sup>2</sup> /4x” is the image potential. (b) Band bending as a function of the radius of curvature of a tungsten “needle” emitter .....	44
<b>Figure 2.17</b> (a) Scanning electron micrograph of the lateral diamond microelectronic diode. The cathode and anode are both patterned out of a single uniformly deposited nanocrystalline diamond film and isolated by SiO <sub>2</sub> . (b) Current-voltage characteristics of the device in (a) which is able to achieve a “turn-on” voltage of 5V .....	45
<b>Figure 2.18</b> Left: Fabrication process for diamond pyramidal cold cathodes. Right: SEM image of fabricated emitters .....	46
<b>Figure 2.19</b> (a) Scanning electron micrograph of the diamond triode vacuum microelectronic device. The cathode here is a diamond pyramid with a tip radius of curvature on the order of 5 nm and the gate is silicon. SiO <sub>2</sub> is used to insulate the gate from the cathode. (b) Anode current-voltage behavior of the diamond triode device at different gate voltages. With the gate biased at 20V, an amplification factor of 250 was achieved .....	47
<b>Figure 2.20</b> Thermionic emission current vs. cathode temperature of a nitrogen-incorporated ultra-nanocrystalline diamond films by R. J. Nemanich.....	48
<b>Figure 3.1</b> Energy diagram of “pillbox” problem. The region from “a” to “b” represents a cavity inside a homogenous crystalline material. The entire material and the cavity are said to be at a constant uniform temperature. This diagram neglects space charge effects and assumes that the distance “x” is large enough such that image potential can also be neglected.....	53

<b>Figure 3.2</b> Potential diagram of a thermionic energy converter showing the increased potential barrier electrons must overcome in order to be emitted into the vacuum in the presence of a space charge region .....	58
<b>Figure 4.1</b> Thermionic emission results from previous work on a boron-doped polycrystalline diamond film. It can be seen by the solid line that the emission current data (points) followed closely with the Richardson equation. Thermionic emission current obtained from this sample was too low to be practical due to the high work function of 4.43 eV .....	69
<b>Figure 4.2</b> Schematic diagram of a typical thermionic testing configuration .....	72
<b>Figure 5.1</b> Scanning electron micrograph of a diamond sample grown under the previously described conditions.....	83
<b>Figure 5.2</b> Scanning electron micrograph of a sample grown uninterrupted for less time under the same conditions as the sample in Figure 5.1. Well defined smooth square faces indicative of 100 orientations can easily be discerned as well as deteriorated triangular faces suggesting crystals with 111 orientations are also present.....	84
<b>Figure 5.3</b> Raman spectroscopy indicating predominantly diamond ( $sp^3$ ) composition with minimal graphitic ( $sp^2$ ) content.....	85
<b>Figure 5.4</b> A) Diagram of the electrical feedthrough. B) Photograph of the mounted sample .....	87
<b>Figure 5.5</b> A) Top view of the vacuum chamber. Note that there is no direct line of sight between the sample being tested and either the ion gauge or the ion pump. B) Side view of chamber to demonstrate placement of the sample.....	88
<b>Figure 5.6</b> Photograph of testing apparatus .....	89
<b>Figure 5.7</b> Schematic of the testing apparatus for the incorporation of gaseous species into the vacuum gap .....	91
<b>Figure 5.8</b> Step-by-step process used to prepare the water vessel chamber used to introduce water vapor into the vacuum chamber. The first two steps were meant to remove other species that could interfere with results. The second two steps were meant to allow water vapor to freely enter the chamber.....	93
<b>Figure 5.9</b> Schematic of the testing apparatus for the incorporation of species that are in the liquid state at room temperature into the vacuum gap .....	94
<b>Figure 5.10</b> Electrical schematic of the thermionic emission testing configuration. The sample to be tested was resistively heated by a Lambda power supply ( $V_{\text{substrate heater}}$ ). The anode was biased by a separate high voltage power supply with the grounds of the two power supplies tied together.	

Electron emission current was monitored by a floating picoammeter in series with the anode power supply. ....	95
<b>Figure 5.11</b> Flow diagram depicting the Labview control loop for the current vs. temperature tests.....	97
<b>Figure 6.1</b> Thermionic emission current behavior of an as-grown diamond sample as a function of temperature .....	102
<b>Figure 6.2</b> Richardson plot of the thermionic emission data seen in Figure 6.2. It is clear that the plot is not linear contrary to what would be expected from the Richardson equation. Rather there was a distinct transition temperature in which both the work function and Richardson constant increased.....	103
<b>Figure 6.3</b> Comparison of the thermionic emission testing results from Test #1 and Test #2 of an as-grown sample before hydrogenation. Test #1 was an as-grown diamond sample and the thermionic emission current was observed to increase with temperature according to the Richardson equation until ~800°C, upon which the emission current began to decrease. Test #2 was performed on the same sample after a cool down period. No emission current above the noise level was observed up to a maximum testing temperature of 800°C. The solid line represents the fit to the Richardson equation of Test #1 data.....	107
<b>Figure 6.4</b> Comparison of the thermionic emission testing results from Test #1, Test #2, and Test #3. The electron emission current from the sample after hydrogenation was significantly higher than the previous runs. The solid line represents the fit of Test#3 to the Richardson Equation. ....	108
<b>Figure 6.5</b> Visual depiction of the as-grown diamond sample, A) compared with a hydrogenated sample, B). The as-grown sample was grown in a methane-starved hydrogen-rich environment resulting in some concentration of hydrogen on the diamond surface and in the diamond bulk. Exposure of the sample to a hydrogenation treatment increased both surface and bulk concentrations resulting in higher emission current levels but little change in work function. ....	110
<b>Figure 6.6</b> As-grown thermionic emission current vs. temperature behavior for Set A. It can be seen that the emission current behavior was similar for each sample. The discrepancies likely were a result of the polycrystalline nature of the diamond films .....	113
<b>Figure 6.7</b> Comparison of the performance of each sample before and after hydrogenation from Set A.....	114

**Figure 6.8** Maximum current densities obtained from each film as a function of temperature at which they were achieved for each hydrogenation treatment in Set A. It can be seen that the maximum emission current decreased with increasing temperature until the final temperature of 850°C .....115

**Figure 6.9** Emission current density vs. cathode temperature of samples B1, B2, and B3 hydrogenated for 1, 2, and 4 hours respectively. It can be seen that increased exposure time not only decreased the maximum emission current density values slightly but also decreased the temperature at which the samples achieve their maximum current densities.....116

**Figure 6.10** Maximum emission current density values as a function of temperature at which they were achieved for each hydrogenation treatment. It can be seen that there was a trend of decreasing thermionic emission performance as the duration of hydrogenation treatment increased .....117

**Figure 6.11** Emission current density vs. cathode temperature of samples C1, C2, and C3 hydrogenated at pressures of 550, 700, and 850 Watts, respectively. It can be seen that increased microwave power had little effect on emission current .....119

**Figure 6.12** Maximum emission current density values as a function of temperature at which they were achieved for each hydrogenation treatment. It can be seen that there microwave power had little influence on maximum emission current density values .....119

**Figure 6.13** Normalized emission current for two samples (sample A: 600°C, 650°C, 750°C; sample B: 700°C, 725°C, 775°C) at different operation temperatures. The small vertical and horizontal lines within each data point represent the error of the ammeter and the pyrometer respectively.....124

**Figure 6.14** First-order plots of emission current for temperatures between 600°C and 775°C. Two samples were measured (Sample A: 600 °C, 650 °C, 750 °C; Sample B: 700 °C, 725 °C, 775 °C).....125

**Figure 6.15** Arrhenius plot of rate constants obtained in Figure 3. The slope is equal to  $-E_A$ , found to be 1.23eV and the y-intercept is equal to  $\ln(k_o)$  found to be  $2.5 \times 10^3 \text{ s}^{-1}$  .....126

**Figure 6.16** Morse diagram representing the difference in Zero Point Energies (ZPE) between hydrogen and deuterium. As deuterium has a higher mass, it will have a lower vibration energy implying that it will have a larger activation energy than hydrogen.....131

**Figure 6.17** Normalized thermionic emission current behaviors as a function of time .....133

<b>Figure 6.18</b> First order desorption plot of the normalized isothermal thermionic emission current behaviors. The linear trend at each temperature indicates the desorption followed first order kinetic behavior.....	134
<b>Figure 6.19</b> Arrhenius plot of the desorption data. The deviation from linearity at lower temperatures incates tunneling could have played a role in the desorption mechanism.....	134
<b>Figure 6.20</b> Generic parabolic potential diagram comparing the classical to the tunneling desorption mechanism. ....	135
<b>Figure 6.21</b> Fit of the k values at each temperature accounting for tunneling.....	137
<b>Figure 6.22</b> Tunneling fit to the hydrogen desorption data from the previous section .....	138
<b>Figure 7.1</b> Isothermal thermionic emission behavior of an as-grown nitrogen-incorporated diamond cathode in a molecular nitrogen gaseous environment. It can be clearly seen that nitrogen had a negative effect on the emission performance from diamond cathodes likely due to the decreased mean-free-path of electrons traveling from the cathode to the anode .....	142
<b>Figure 7.2</b> Isothermal thermionic emission current behavior of an as-grown nitrogen-incorporated diamond cathode in the presence of methane gas. Four runs were performed and each run tested at 600°C, 625°C, 650°C, 675°C, and 700°C. Little effect can be seen in the emission current (blue points) as methane pressure (red points) increased. Plots for 675°C and 700°C were not shown as they exhibited the same behavior as the other temperatures. The anode voltage was increased from 200V used in Runs 1 and 2 to 400V in Run 3 and 600V in Run 4. Again, no effect was observed with increasing voltage .....	147
<b>Figure 7.3</b> Isothermal emission current testing of a hydrogenated diamond sample in the presence of methane gas. A small positive increase in emission current (blue points) can be seen as the methane pressure (red points) was introduced into the chamber. Plots for the 675°C and 700°C runs were not shown as the variations in emission current were too large to decipher any significant changes in emission current .....	148
<b>Figure 7.4</b> Semi-log plots of the percent of total ionization of the primary methane dissociation products as a function of pressure. Data has been digitized from a previous study by G. Drabner and colleagues.....	151
<b>Figure 7.5</b> Semi-log plots of the percent of total ionization of the secondary methane dissociation products as a function of pressure. Data has been digitized from a previous study by G. Drabner and colleagues .....	151

**Figure 7.6** Semi-log plots of the percent of total ionization of the tertiary methane dissociation products as a function of pressure. Data has been digitized from a previous study by G. Drabner and colleagues .....152

**Figure 7.7** Thermionic emission current behaviors of diamond films operating in a low pressure water vapor environment. The four testing runs shown are categorized by the temperature at which they were performed and are labeled accordingly. It can be seen that the emission current increased in the presence of water vapor at the lower temperatures but increased at higher temperatures.....157

**Figure 7.8** Isothermal emission current behavior of an as-grown diamond film with hydrogen leaked in for the temperature 600°C, 625°C, and 650°C. The blue data represents the current while the red data represents the pressure in the chamber. For all graphs, it can clearly be seen that there was an increase in emission current when the hydrogen pressure was increased in the chamber .....166

**Figure 7.9** Isothermal emission current behavior of a hydrogenated diamond film with hydrogen leaked in for the temperatures 600°C, 625°C, and 650°C. The blue data represents the current while the red data represents the pressure in the chamber. For all graphs, it can clearly be seen that there was an increase in emission current when the hydrogen pressure was increased in the chamber .....167

**Figure 7.10** Example of the residual plot performed for all data runs which allowed for direct calculation of the increase in current upon hydrogen being leaked into the chamber .....168

**Figure 7.11** Plot of the emission current increase in the influence of hydrogen gas as a function of the current before the start of the leak-in (baseline current). A clear relationship can be seen where the magnitude of increase increased with baseline current. Two possible trend lines were found to describe this relationship: linear and power.....170

**Figure 7.12** Plots of the emission current vs. temperature after the third testing runs for the as-grown (a) and hydrogenated (b) diamond sample.....171

**Figure 7.13** Emission current response of the as-grown diamond sample to the introduction of a low pressure nitrous oxide environment. Graphs a), b), and c) are the behavior for the four runs performed at 600°C, 625°C, and 650°C, respectively .....178

**Figure 7.14** Emission current behavior of a hydrogenated diamond sample in the influence of a low pressure nitrous oxide environment. Graphs a), b), and c) are the behavior for the four runs performed at 600°C, 625°C, and 650°C, respectively .....180

<b>Figure 7.15</b> a) Magnitude of the emission current decrease from baseline vacuum levels upon exposure of the cathodes to nitrous oxide. b) Percent of emission current decrease from vacuum levels .....	181
<b>Figure 8.1</b> Potential output current of an all diamond thermionic energy converter with molecular hydrogen as the interelectrode gas at a pressure of 5.5 $\mu$ Torr .....	191
<b>Figure 8.2</b> Potential output power of an all diamond thermionic energy converter with molecular hydrogen as the interelectrode gas at a pressure of 5.5 $\mu$ Torr .....	191

# CHAPTER I

## INTRODUCTION

This chapter is meant to introduce the focus of the present research. A brief history of thermionic emission is presented along with its potential applications to the field of energy conversion. Existing power generation technologies are also discussed to emphasize the motivation behind the present research. Finally, the goals and objectives of the research are discussed along with an organization of this dissertation.

### 1.1 History of thermionic emission and vacuum devices

Thermionic emission is a long understood principal that has played a crucial role in not only the history of electronic devices but also our modern understanding of physics. Though E. Becquerel is credited with first observing this phenomenon in 1853, little became of his research until Thomas Edison took interest in the subject in the late 19<sup>th</sup> century.[1, 2] While working with his famed incandescent light bulb, Edison observed that, following extended operation periods, a dark residue consistently formed on the inside surface of the glass enclosure. Upon closer examination, Edison noted that there always appeared to be a white strip in the residue in the plane of the filament.[2] In 1883, after three years of failed attempts to understand the cause of this white strip, Edison decided to position an additional electrode adjacent to the filament. To his surprise, current was observed to flow when it was biased positively with respect to the filament. This finding indicated that it was Becquerel's thermionic emission that was causing this nuisance. Edison's observation led him to file the first patent for what is now known as the "thermionic diode." [2, 3]

With Edison's findings coming nearly a decade before the discovery of the electron, the scientific community struggled to comprehend the effects he was observing. This is clear from the first paper presented on the effect by E.J. Houston (per Edison's request) at the International Electrical Exposition in Philadelphia in 1884.[4] Houston stated:

*"The question is, what is the origin of this current? How is it produced? ... we cannot conceive the current as flowing across the vacuous space...I have no theory to propound as to the origin of this phenomena."*[4]

Though Edison soon abandoned attempts to understand this anomaly, his co-worker and chief science adviser to the Edison Electric Light Co. of England, Ambrose Flemming, continued research in this topic.[2] In 1890, Flemming published the first observations of the rectifying properties of the thermionic diode in his paper titled: *On Electric Discharge between Electrodes at Different Temperatures in Air and in High Vacua*. [5] By 1904, Fleming had finally invented the vacuum tube diode as we know it, closely followed by the invention of the triode vacuum tube amplifier by Lee De Forest in 1906, thereby marking the beginning of today's electronic industry.[6] Though these vacuum devices have largely been replaced by the semiconductor, thermionic emitters are still used in many applications including florescent lighting,[7] electron microscopy,[8] CRT displays,[9] and perhaps most importantly, energy conversion, which is the focus of the present research.[10]

## 1.2 Motivation for energy conversion research

Over the past century, the world's demand for electrical energy has been rapidly increasing and is projected to continue to rise significantly in the foreseeable future. Despite this increasing demand, methods used to generate electrical power have remained relatively

unchanged. Further, the growing scarcity of fossil fuels illustrates the urgency to utilize renewable energy sources. The present research explored the use of diamond in a recently unexplored method for directly converting thermal energy into electrical energy known as thermionic energy conversion.

### 1.2.1 Today's energy climate

A major driving factor in the rapid industrialization of countries like the United States during the 20<sup>th</sup> century was the relatively cheap cost of fossil fuels. Fossil fuels were able to maintain a relatively low price point for several decades as there were very few other industrialized nations. Assessing today's energy climate becomes more difficult as developing countries such as China and India are experiencing similar rapid industrialization, thereby drastically increasing the worldwide demand for fuel. To further exacerbate the situation, the United Nations has predicted that the world's population will reach nine billion by the year 2050, with the majority of this growth occurring in developing countries.[11] This population boom, coupled with the world's increasing standard of living, paints a dire picture for the world's future energy climate.

As depicted in Figure 1.1, the 2009 World Energy Outlook Report states that a large majority of the world's power is derived from coal and oil. Both of which are considered non-renewable resources that many fear will be exhausted in the near future if current predictions hold.[12]

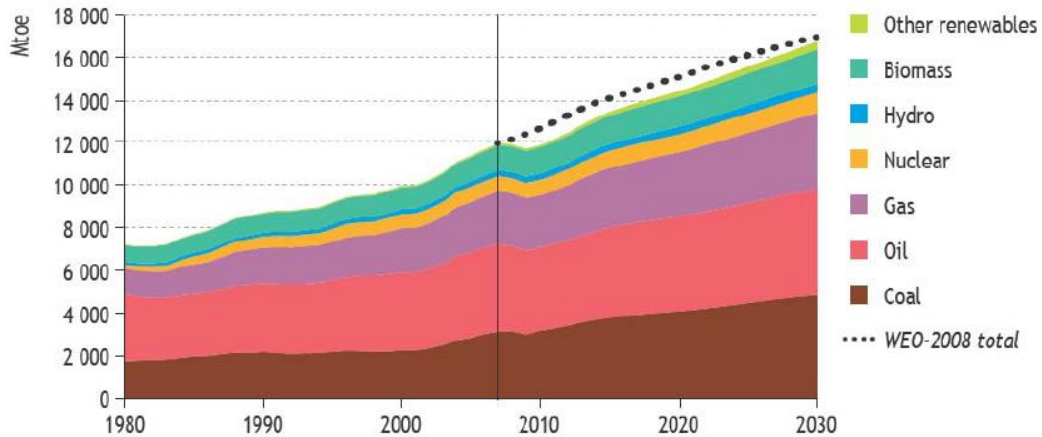


**Figure 1.1** Graph of the world energy consumption by fuel type in terms of million tons of oil equivalence (MTOE)[12]

Accordingly, in 2006, a report was released by British Petroleum (BP) stating that the total identified or proven world oil reserves was 1,200 billion barrels of oil.[12] Accounting for the current estimated undiscovered oil reserves, the world is expected to reach its peak oil production in the next few decades as seen in Figure 1.2.[11]

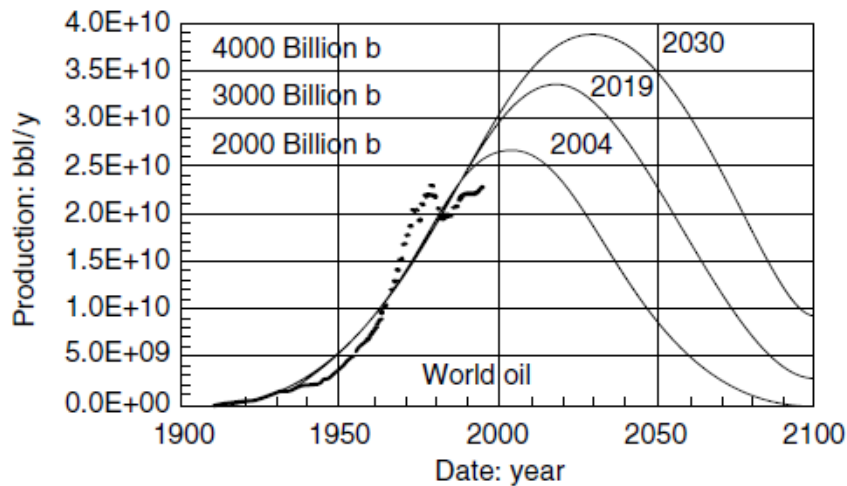


**Figure 1.2** Current estimates of world oil production from the year 1900 through 2100 based on a 2006 study by BP. The three peaks represent the three possible times in which the world will reach peak production.[11]

Though the situation is not as dire as oil, our coal resources are also dwindling. Another study by BP has estimated that the world's proven recoverable coal resources are around 909 billion tons which is expected to last for the next 164 years at 2004 consumption use.[11] Unfortunately the use of coal has increased by an average of 6% from 2002 to 2005. Thus, if this current trend continues, our coal reserves could be depleted much sooner.[11] Additionally, many associate coal-fired power plants with extreme negative environmental and health impacts leading several countries (such as the United States) to adopt policies to limit the use of coal power generation technologies.[13]

### 1.2.2 Current large-scale power generation methods

There are currently numerous methods in existence for the generation of electrical power but few are applicable to meeting the world's large-scale energy demands. The current predominate methods involve a complex multistep conversion of thermal into electrical energy which begins with acquiring a heat source. In the vast majority of plants, this thermal heat source comes from either the burning of fossil fuels or a controlled nuclear reaction. Thermal energy is then converted into mechanical energy by a multiphase working fluid. Lastly, the mechanical energy is converted into electrical energy through large turbines which are then used to drive generators. This multistep process results in high energy loss which consequently leads to relatively low operational efficiencies. These mechanical generators require high capital investments and, due to the effects of wear and corrosion, demand substantial continuing maintenance.[14, 15] A flow diagram of this process for a typical fossil fuel plant can be seen in Figure 1.3.

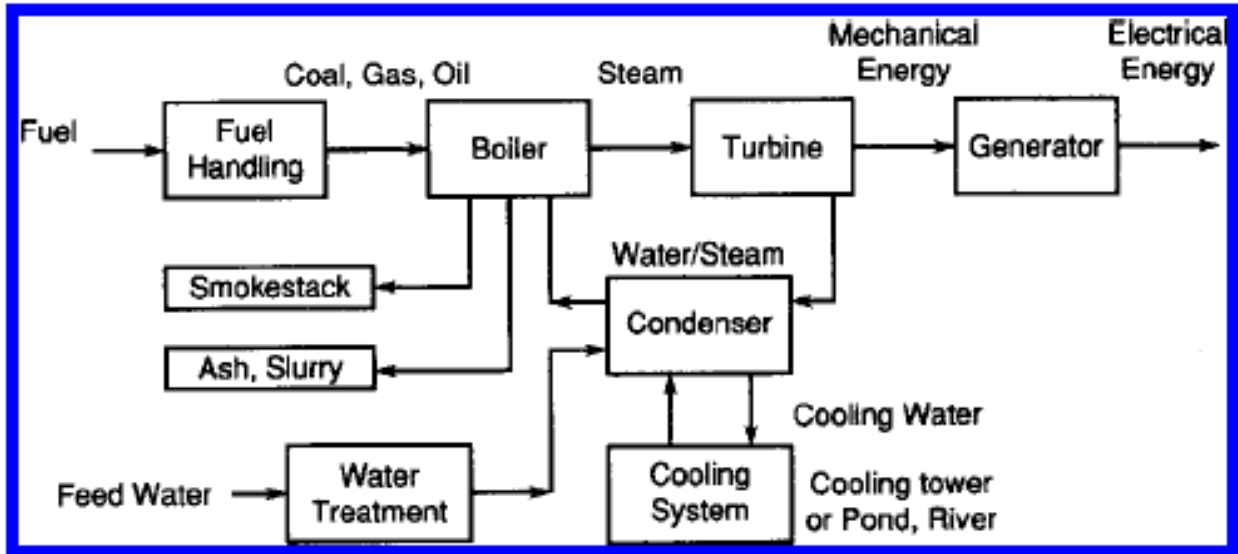


**Figure 1.3** Flow diagram of the components of a typical coal fueled power plant beginning with the fuel handling through the energy conversion.[15]

### 1.2.3 Current small-scale power generation methods

In addition to improved large-scale power generation, the need for new forms of compact and portable power generation has been driven by explosive growth in microelectronics, space exploration, and nanotechnology. Traditional energy conversion technologies lack the portability and energy density demanded by these applications. Often, electrochemical batteries do not provide sufficient power or energy storage capacity. Other power sources, such as liquid fuels and radioactive elements, possess high energy density but require a means of efficiently converting thermal power to electrical form. In all of these applications, the minimization of moving parts is essential to the deployment of a new generation of small-scale energy conversion devices.

Compact thermoelectrics can reliably directly convert thermal energy to electrical energy with no moving parts by utilizing the thermoelectric effect. However, these systems have proven impractical in most cases due to material limitations such as the inverse relationship between

Seebeck coefficient and electrical conductivity.[16] For instance, current state of the art thermoelectric power generation devices are only able to *theoretically* achieve efficiencies less than 20%.[17]

### 1.3.3 Renewable power generation technologies

There is a current “green” movement throughout the world that is meant to discourage the use of polluting fossil fuel plants in favor of cleaner, more sustainable energy conversion technologies. Although they are outside the scope of this paper, a few of the prominent alternative energy sources will be discussed in order to provide a more complete survey of current energy production methods.

Among alternative energy technologies, photovoltaics have received the most attention. A photovoltaic (solar) cell consists of a PN semiconductor junction in which photons excite electrons into the conduction band. The output voltage is determined by the difference in the Fermi energies between the n-side and the p-side and the current is proportional to the intensity of the incident light.[18] Photovoltaics suffer from poor performance as only a fraction of the solar spectrum can be converted to electricity. For example, for a photovoltaic technology that can achieve 20% efficiency, the necessary area to provide 1MW of power is roughly equal to 26,000m<sup>2</sup> or 6.4 acres.[14]

Another commonly discussed technology is wind power generation. This fairly straight forward technology harnesses the wind through large propellers which spin and drive a turbine. In the United States and several other countries, the wind resource is large enough to meet the country’s entire energy demands.[19] The widespread adoption of wind power generation is hindered due to the natural variability of wind. In some instances, the wind may reach 20 m/s

which allows for large amounts of power to be produced, while in other instances, the wind may not be blowing at all.[19] The lack of adequate large-scale energy storage methods prevents a steady amount of electricity from being distributed leading wind power to be only a supplement to other more reliable energy conversion technologies.

#### 1.4 Thermionic energy conversion

Thermionic energy conversion (TEC) is a technology that has received little attention over the past few decades for the direct conversion of thermal energy into electrical energy.[20, 21] Not only does TEC provide an efficient stand-alone method for energy conversion but could also be incorporated into existing power generation technologies to scavenge waste heat and increase their overall power output capabilities. A thermionic energy converter is based on the process known as thermionic emission. In this process, a heated material (known as the cathode) emits electrons with energy exceeding the material's work function.[22] In a typical two electrode configuration, these emitted electrons traverse a vacuum gap and are collected by an anode.

The efficiency of a thermionic energy converter greatly depends on the ability of the cathode to emit electrons. This dependence is what led many researchers to abandon TEC research during the latter part of the 20<sup>th</sup> century due to materials available at that time. Recent observations of the electronic properties of diamond, such as its superior electron emission capabilities, have revived interest in thermionic energy conversion. The present research is meant to further characterize the thermionic emission capabilities of diamond so that an efficient TEC device can be realized.

### 1.5 Research objectives

The goal of the present research is to further investigate the thermionic emission properties of diamond films for use in thermionic energy conversion. As will be discussed later in this dissertation, a practical thermionic energy converter requires a cathode capable of efficiently emitting electrons, ergo a cathode that thermionically emits a large amount of current at relatively low temperatures. In addition to studying the performance of these films, durability and longevity must also be characterized and maximized.

The objectives of this research are to:

- Fabricate diamond thermionic cathodes capable of achieving high levels of thermionic emission current at temperatures up to 1,000°C;
- Design a testing apparatus able to accurately characterize the thermionic emission current from diamond cathodes;
- Investigate potential failure mechanisms of the diamond cathodes that could limit their implementation into a practical thermionic energy converter;
- Identify factors that affect the thermionic emission properties of diamond;
- Develop new methods to increase the performance, reliability, and longevity of diamond thermionic emitters.

### 1.6 Organization of this dissertation

This dissertation consists of eight chapters organized in the following manner:

- *Chapter I* details the background of thermionic emission and vacuum tube devices. The necessity of new and more efficient energy conversion methods is discussed and a summary of a few predominant power generation technologies is provided. An overview

of thermionic energy conversion is also presented along with the goals of the present research.

- *Chapter II* is meant to provide the reader with a strong background in diamond technologies. Current fabrication techniques as well as characterization methods of diamond films are discussed in the chapter. Additionally, the electronic properties and methods of altering these properties are explained in detail.
- *Chapter III* discusses the primary motivation behind this research, thermionic energy conversion. Thermionic emission is derived in detail allowing for a better understanding of the results obtained in this research. A brief history of thermionic energy conversion is presented along with a discussion of this technology's operating principals and design considerations.
- *Chapter IV* proposes the research to be conducted. This includes a description of the testing methods, diamond samples to be fabricated, and data collection approaches.
- *Chapter V* describes the details of the experiments conducted in the present research. This includes fabrication of diamond cathodes, construction of testing apparatuses for characterizing the thermionic emission from diamond cathodes, and design of testing configurations.
- *Chapter VI* presents the results of thermionic emission experiments executed in vacuum environments. Emission performance of as-grown and hydrogenated diamond samples was compared and the desorption of hydrogen (and deuterium) from diamond was also studied.
- *Chapter VII* presents the results of the thermionic emission studies performed in a gaseous environment. Research examined molecular nitrogen ( $N_2$ ), methane ( $CH_4$ ),

molecular hydrogen ( $\text{H}_2$ ), water vapor ( $\text{H}_2\text{O}$ ), and nitrous oxide ( $\text{N}_2\text{O}$ ) in an effort to enhance the emission performance of diamond cathodes.

- *Chapter VIII* is written to summarize the conclusions made from the present research, with recommendations provided for future work that should be explored in this area of study.

## CHAPTER II

### DIAMOND: GROWTH, PROPERTIES, AND CHARACTERIZATION

#### 2.1 Diamond background

The brilliance and rarity of diamond make it one of the most valuable, and thereby most sought after naturally occurring materials. Diamond is an allotrope of carbon with each of its four unpaired valence electrons covalently bonded to its nearest neighbor to form the “Diamond-Cubic Lattice” consisting of two intersecting Face Centered Cubic lattices (Silicon also takes this lattice structure).[23] The eight atoms encompassed in each unit cell, together with the small bond length of 1.54 Å, result in the highest atomic density of any material allowing diamond to possess many exceptional material properties.

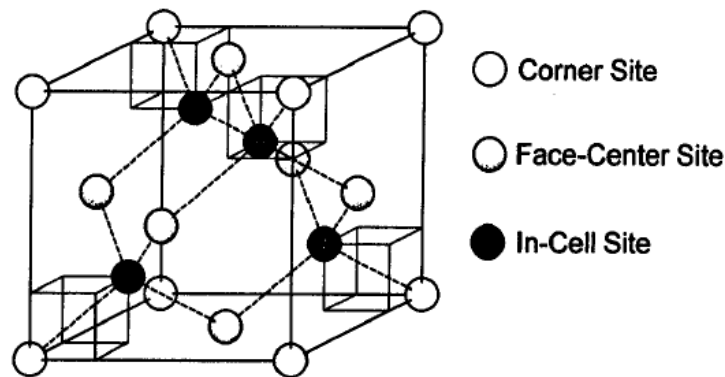


**Figure 2.1** Image of the diamond lattice.[23]

Like silicon, diamond has the ability to function as a semiconductor upon substitution of a portion of the carbon atoms with a dopant atom such as boron.[24] Recent interest in this material has been spurred by its numerous advantages over other electronic materials such as high carrier mobility, low dielectric constant, and radiation tolerance to name a few. As a wide

bandgap semiconductor, diamond has the capability to potentially function as both an effective electronic insulator and a reliable electron transport medium. The widespread adoption of this material has been hindered by the limited success in the fabrication of uniform films. The following sections will discuss the deposition processes of diamond, methods for characterizing its material properties, and also several interesting applications for which diamond is currently being utilized.

## 2.2 Fabrication of diamond films

The numerous material advantages of diamond have enticed many researchers to examine it as a potential alternative to silicon in the semiconductor industry. The major obstacle preventing the widespread use of diamond is the unconventional and often unreliable fabrication methods. Carbon is unique in that it can take on many different allotropes (i.e. graphite, carbon nanotubes, Buckminsterfullerenes, etc.) requiring precise deposition conditions in order to form diamond.[25] Further, a technique to mass produce diamond wafers, such as the Czochralski method for silicon, has not yet been developed. Current methods for the fabrication of polycrystalline diamond films consist of a 3-step process: 1) Substrate selection and surface preparation; 2) Nucleation; and 3) Film deposition. The fabrication of single-crystalline diamond films, on the other hand, is a much more complex process.

### 2.2.1 Substrate selection and preparation and the nucleation process

As with many materials, diamond can be grown as single crystalline or polycrystalline. Single crystalline films are often highly sought for electronic applications due to the long range uniformity, surface smoothness, and lack of defects. It was previously noted that the unique

lattice structure and small lattice constant provides diamond with the highest atomic density of any known material. Though this high atomic density is responsible for many of diamond's favorable material properties, it is also to blame for the current difficulties in the fabrication of single crystalline diamond. The epitaxial deposition of any single crystalline material requires a substrate with a similar lattice constant to minimize the strain arising from lattice mismatching between the two materials. Diamond substrates can be used for homoepitaxial deposition but the only substrate material with nominal success for the heteroepitaxial deposition of diamond is cubic boron nitride (c-BN).[26] The lattice structure of c-BN, zincblend, is virtually identical to the diamond lattice. In addition, the bond length between boron and nitrogen is similar to diamond allowing for a lattice mismatch between the two materials of only 1.4%.[27] Further, c-BN has a similar coefficient of thermal expansion to diamond which is necessary due to the high temperatures required for the synthesis of diamond.

The difficulties of depositing single crystalline diamond have led many researchers to explore polycrystalline diamond films, permitting a broader range of substrate materials than for single crystalline deposition. The most commonly utilized substrates for polycrystalline diamond are carbide forming materials (i.e. Si, Mo, W, etc.) which have much higher nucleation rates compared to materials which do not form carbides.[27] Nucleation has been observed to spontaneously occur at defect sites such as dislocations and slips when depositing diamond on carbide forming substrates which has lead researchers to conclude that nucleation occurs on the substrate rather than in the gas phase.[28] It has also been observed that such substrates tend to prevent the formation of graphite, which readily forms in the presence of atomic hydrogen.[28] When attempting to deposit diamond on non-diamond materials, spontaneous nucleation is often too slow for practical applications. Numerous techniques have been devised to expedite the

growth process and many of these techniques can be combined together to further improve the results. One such technique that has proven significantly important is substrate preparation.

It was previously mentioned that diamond nucleation tends to occur at defect sites. Scratching is a commonly used method to artificially introduce these defects allowing for significant growth enhancements compared to smooth surfaces (see Figure 2.2). [29, 30] Ultrasonic scratching is one established method to provide uniform substrate scratching. This process involves first suspending a hard abrasive such as diamond, silicon carbide, or boron nitride in a methanol or acetone solution. The substrate material is then placed in this slurry and vibrated ultrasonically for a period of time. The scratched substrates can either be placed directly into the deposition chamber or be subject to additional preparation techniques to further expediting the growth process.

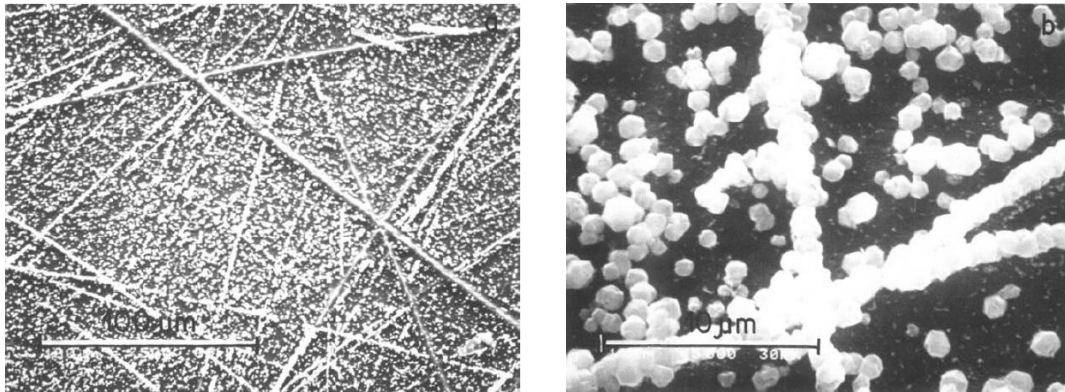


**Figure 2.2** SEM image of diamond crystals forming on a scratched silicon substrate[31]

Seeding the substrate surfaces with nanodiamond is another common method to enhance the growth rate of diamond films and often accompanies substrate scratching. Seeding can often be performed simultaneously with scratching by selecting nanodiamond as the abrasive which deposits a fraction of the nanodiamond directly into the artificially created defect sites providing

localized points for diamond nucleation. As deposition time increases, the size of these particles increases until they eventually begin to grow together, creating a uniform film. Seeding has also been shown to produce epitaxial growth of diamond films by orienting nanodiamond seeds on smooth silicon substrates.[32]

Substrate biasing is also used to accelerate the diamond growth process. Biasing can often lead to nucleation densities similar to that of scratching but on smooth unabraded surfaces, often providing improved uniformity and less contamination. A study by B.R. Stoner and colleagues compared the quality of diamond films deposited on silicon of a scratched and seeded substrate with a pristine substrate biased at 250 V.[33] Raman analysis of the two films grown under the same parameters for one hour showed that substrate biasing led to a more uniform film with higher nucleation densities and a larger number of grain boundaries.[33] B.R. Stoner proposed a five step description of the growth process with substrate bias consisting of the following process: (1) absorbed oxygen and amorphous carbon initially present on the substrate are either etched away or begin to form Si-O and Si-C, respectively with the surface; (2) oxygen is etched away and carbon “islands” form; (3) carbides reach a critical thickness preventing further growth, thus providing an excess concentration of carbon on the substrate surface permitting small clusters favorable to diamond formation; (4) continued biasing promotes etching of the surface but not of the stable diamond nuclei; and (5) this continues until there is a complete coverage of the surface with diamond nuclei.[33] This diamond growth process described by Stoner and colleagues is depicted in Figure 2.3.

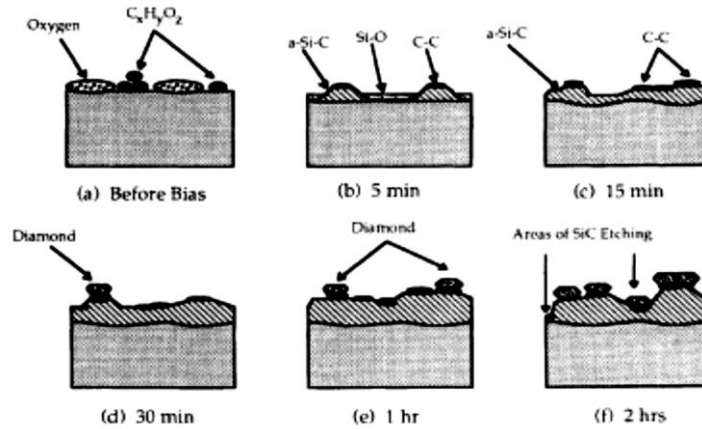


**Figure 2.3** Schematic diagram of the biased enhanced diamond growth processes during the first two hours of deposition presented by Stoner and colleagues.[33]

### 2.2.2 Film deposition

The predominant method for diamond deposition, chemical vapor deposition (CVD), uses a high energy source to break apart gas species which eventually settle on a substrate in a desired manner. The high energy required for CVD can be derived from a number of sources such as microwaves, heat, or electrons, to name a few. This section will focus on the two most commonly used methods for the deposition of diamond: Microwave Plasma-enhanced Chemical Vapor Deposition (MPCVD) and Hot Filament Chemical Vapor Deposition (HFCVD).

To date, the simplest and most reproducible method for diamond deposition is HFCVD.[27] In the HFCVD process, a filament or series of filaments is heated to extreme temperatures often in excess of 2000°C. This intense thermal energy causes gas species to ionize and dissociate when directed near the filament which eventually reform on the desired substrate. Metals with a high tolerance to hydrogen, such as tungsten, are the preferred filament materials due to their increased lifetimes. The simplicity and ability to easily scale to large area deposition has made this method attractive to many researchers.

MPCVD reactors use microwaves, in the 2.45 GHz range, to initiate a plasma which is formed by the microwave induced oscillation of electrons. These electrons collide with gas atoms and molecules to generate high ionization fractions.[34] MPCVD reactors produce a very stable and reproducible environment allowing for long deposition times of hundreds of hours. In addition, the cost of MPCVD reactors has been drastically reduced over the past 20 years due to the high availability of microwave power supplies.[27] A diagram of a MPCVD chamber can be seen in Figure 2.4 (b).

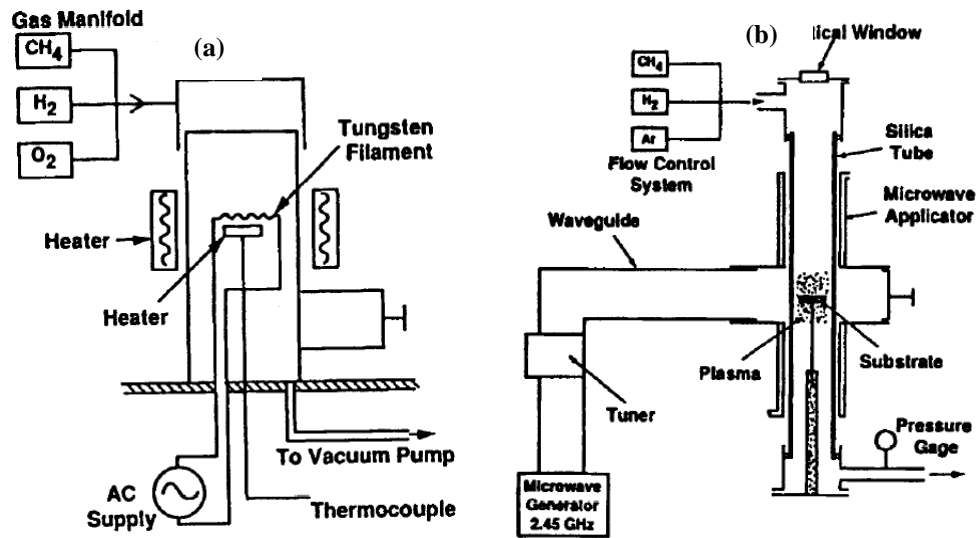


**Figure 2.4** Schematic of an (a) HFCVD apparatus and (b) MPCVD apparatus[27]

In each of these processes, deposition conditions play a crucial role in the ability to form diamond. A notable study by Hayashi and colleagues examined the dependence of substrate temperature on diamond nucleation rate.[35] In this study, diamond films were deposited via MPCVD and the substrate temperature monitored with an infrared pyrometer. An external ellipsometer was used to measure the substrate thickness while under vacuum. Hayashi and colleagues observed a sharp increase in nucleation density with increasing temperature up to a

temperature around 860°C followed by a slight decline up to the maximum tested temperature of 950°C.[35] This observation implies the existence of an optimal substrate temperature for promoting diamond nucleation.

In addition to the substrate temperature, gas pressure and composition have been observed to affect the deposition process. The gases typically involved in the CVD process are molecular hydrogen and a carbon containing gas (often methane). Semiconducting diamond requires a third gas such as boron (in the form of trimethylboron) for p-type doping or phosphorus (in the form of phosphine) for n-type doping.[36] Previous research has shown that low CH<sub>4</sub>:H<sub>2</sub> mixture ratios (0.1-0.5%) provide high quality diamond crystals with cubo-octahedral morphology but low nucleation densities.[27, 37] Alternatively, high CH<sub>4</sub>:H<sub>2</sub> mixture ratios (1.2-1.4 %) provide increased nucleation densities and film coverage, but also higher non-diamond components.[27, 37] Studies have also examined chamber pressure effects on the growth process and determined that the highest nucleation densities occur at lower pressures around 5 Torr.[27] It is difficult to present more detail on the influence of deposition conditions on diamond growth as many of the exact growth parameters for certain diamond morphologies are not available due to proprietary constraints. Accounting for all of the discussed factors involved in diamond deposition demonstrates the difficulty of utilizing it as a mass-produced electronic material.

### 2.3 Characterization of diamond films

Often the ability to characterize deposited films can be as important as growing the films. Thus far, several factors have been discussed in this dissertation that affect the growth of diamond films allowing for countless combinations of structural morphologies (grain size,

orientation, graphitic content, etc.), electrical characteristics (carrier concentration, mobility, and work function), and mechanical properties (hardness, thermal conductivity, refractive index, etc.). This wide range of variation between diamond films necessitates the ability to accurately quantify all of these properties.

Perhaps the most widely used method for examining diamond films is Raman spectroscopy given that it is non-destructive and requires little to no sample preparation.[38] Raman spectroscopy employs a monochromatic light source to examine the frequency change of the incident photons upon interaction with a sample. These photons are absorbed by the sample and reemitted at a shifted frequency providing information on the vibrational, rotational, and other low frequency transitions of the molecule.[39] Raman spectroscopy is often used for observation of sp<sup>3</sup> and sp<sup>2</sup> bonding and also for the determination of crystal size.[38, 40] Though diamond (sp<sup>3</sup>) has a relatively large Raman scattering cross section, it is still two orders of magnitude less than that of graphite (sp<sup>2</sup>), making this technique much more sensitive to sensing sp<sup>2</sup> bonding over sp<sup>3</sup> bonding. Typical Raman spectroscopy measurements only observe the first order peak at 1332 cm<sup>-1</sup>, however, the ideal diamond lattice should reveal a second order peak in the spectral range from 0 to 2690 cm<sup>-1</sup> and a third order peak has been observed at wavenumbers from 3650 to 3760 cm<sup>-1</sup>. [41] A general Raman spectrum of gem quality diamond at room temperature can be seen below in Figure 2.5.

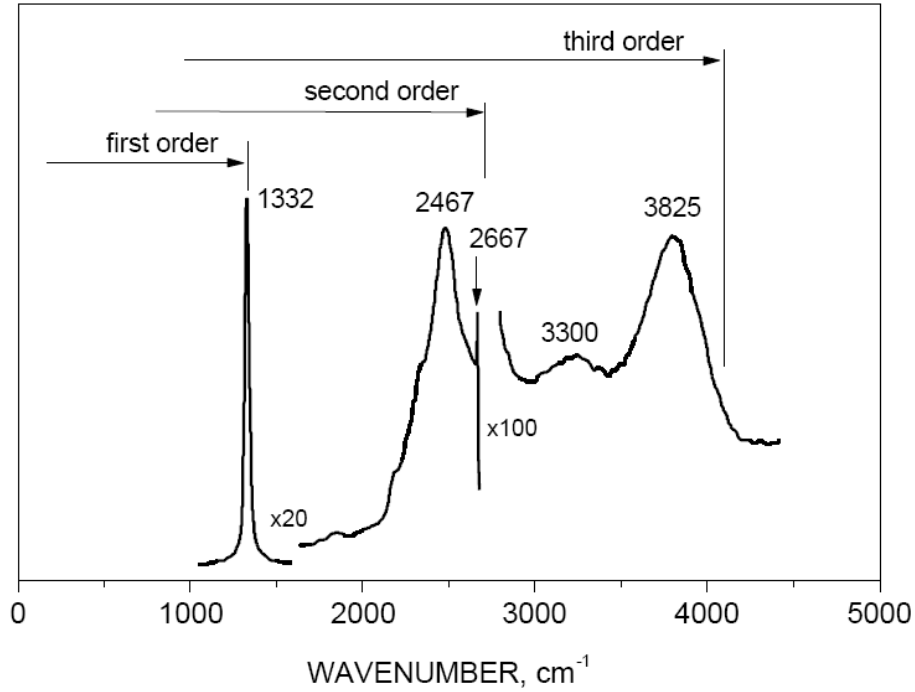


**Figure 2.5** General Raman spectra of gem quality diamond excited at wavelengths of 229.9 nm at room temperature demonstrating the first, second, and third order Raman peaks [41, 42]

X-ray Diffraction (XRD) is also frequently used to characterize the composition of films. XRD can measure the crystal structure of materials through the diffraction scattering of an incident X-ray beam. By analyzing the diffraction angles, the spacing between adjacent crystal planes can be determined and compared to values for known materials.[43] Figure 2.6 presents the typical XRD peaks for diamond films with (100) and (111) facets.

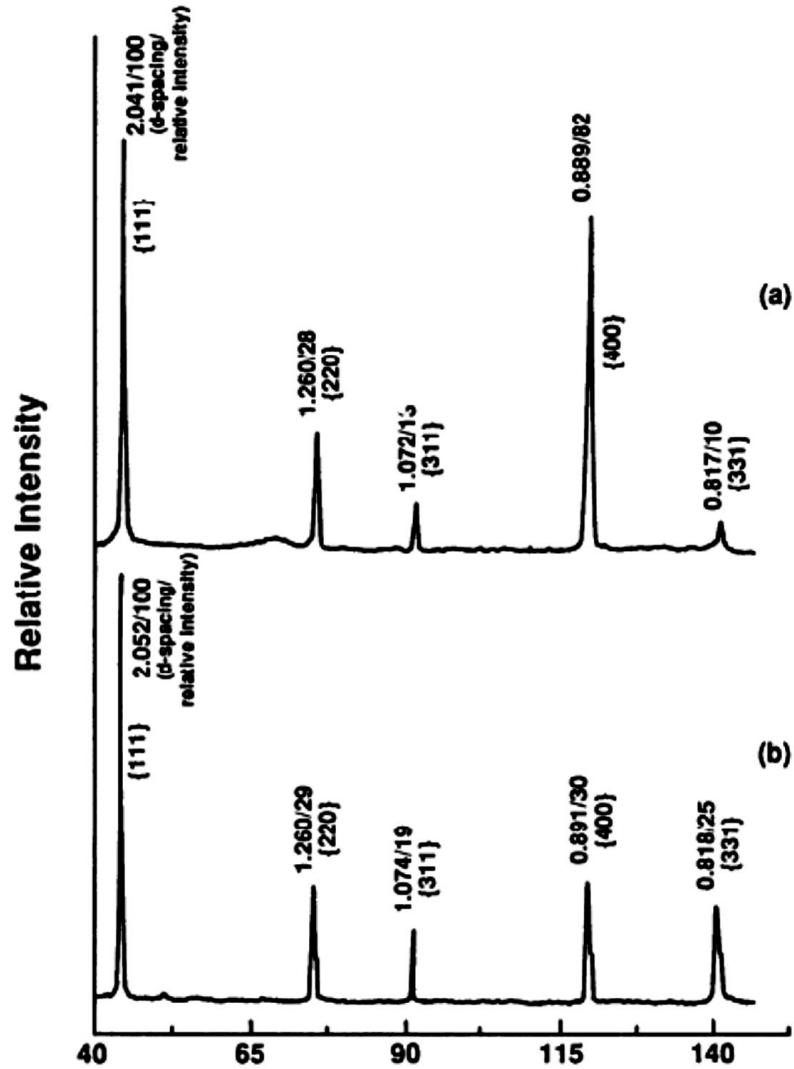


**Figure 2.6** Typical XRD patterns for diamond samples with (a) (100) surface facets and (b) (111) surface facets[34]

A detailed analysis of the chemical bonding and surface species can be obtained through X-Ray Photoelectron Spectroscopy (XPS). XPS is performed in a high vacuum environment by irradiating a sample with high energy X-rays causing electrons with sufficient energy to emit from the sample. Examining the energy distribution of these emitted electrons provides information on the energy distribution of the electronic states in the material.[44] Similar to XPS,

Ultra-violet Photoelectron Spectroscopy (UPS) irradiates a sample with ultra-violet light also causing electrons to be emitted.[45] This energy distribution obtained from UPS can be used to determine the work function of a sample.

Microscopy methods are often used to qualitatively observe the structure of diamond films. Scanning Electron Microscopy (SEM) and Atomic Force Microscopy provide basic information on the surface morphology and roughness.[23, 46] Because SEM requires a conducting film for adequate imaging, micron-sized insulating diamond is often unable to be imaged. Accordingly, Transmission Electron Microscopy (TEM) is another tool which uses high energy electrons to tunnel through a sample allowing individual atoms to be imaged providing information on crystal orientation and internal defects.[46]

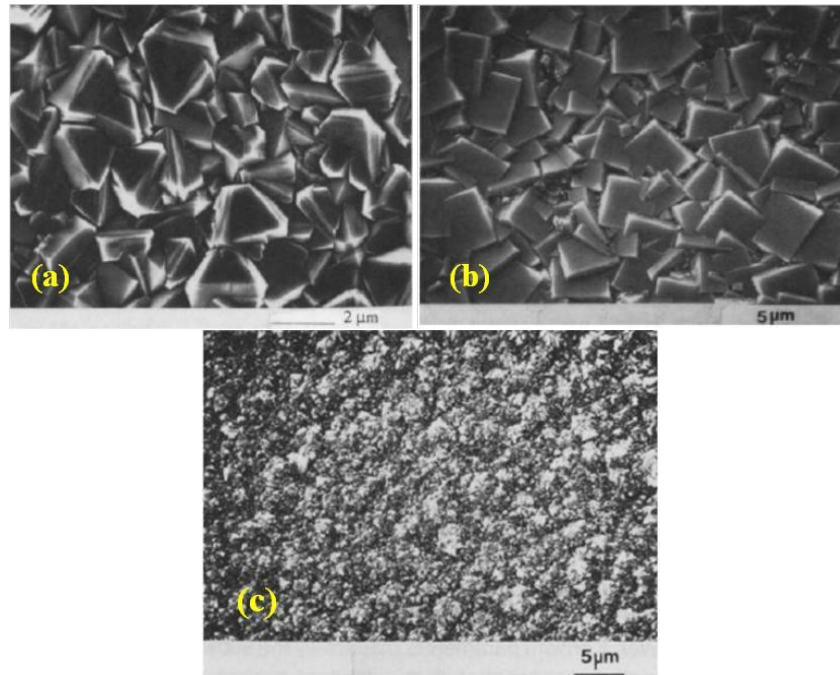


**Figure 2.7** SEM spectra of polycrystalline diamond films with (a) (111) triangular faces, (b) (100) square faces, and (c) cauliflower-like small crystalline aggregates[47]

When dealing with semiconducting diamonds, precise electronic characterization is desired. Secondary Ion Mass Spectroscopy (SIMS) can help quantify the doping concentration and species of diamond films.[48] SIMS bombards a sample with high energy ions which in turn ionizes and ejects atoms from the sample's surface. These ejected atoms are then analyzed by their mass to provide information on elemental concentrations. Simple current-voltage and capacitance-voltage analysis can provide basic information on the electronic properties and can often be used in place of SIMS when exact carrier concentration values are not required.

#### 2.4 Material properties of diamond

Recent advances in the ability to fabricate diamond films have spurred new research into the use of diamond as an electronic material. Diamond's unique combination of superior electronic and material properties could lead a promising future in the electronics industry.

As previously mentioned, diamond shares its lattice structure with silicon. This structure is known as face-centered diamond cubic. Similar to face-centered cubic lattices with 8 corner atoms and 6 face centered atoms, the diamond cubic lattice has four additional atoms forming an adjacent interpenetrating lattice that is spaced one quarter of a cube diagonal from the former.[49] The 8 atoms per unit cell encompassed in this structure, coupled with carbon's strong chemical bonding, gives diamond the highest atomic density of any material and is responsible for many of its superior properties.[50] Diamond has the highest hardness, molar density, thermal conductivity, and sound velocity as well as the lowest compressibility and bulk modulus of any other known material.[34] A few of diamond's material properties compared with other materials can be seen below in Table 2.1.

**Table 2.1** Comparison of diamond to silicon, boron nitride, and copper

Property	Units	Diamond	Silicon	Boron Nitride	Copper
Thermal Conductivity	W/cm*°C	20 [34]	1.5 [34]	13 [34]	3.8 [34]
Longitudinal Sound Velocity	m/s	18,000 [34]	7,500 [34]	7,000 [34]	4,760 [34]
Knoop Hardness	kg/mm <sup>2</sup>	5,700-10,400 [34]	940-980 [51]	4,500 [34]	40 [34]
Young's Modulus	x10 <sup>11</sup> dynes/cm <sup>2</sup>	105 [34]	11.3 [34]	900 [52]	12.8 [34]
Density	g/cm <sup>3</sup>	3.52 [34]	2.42 [34]	2.3 [53]	8.9[34]

### 2.5 Doping of diamond

Diamond differs from typical semiconductors in that it possess a large bandgap of 5.45eV compared with silicon at 1.1eV.[50] Acting as a wide bandgap semiconductor, diamond has the ability to function as both a strong electrical insulator as well as a good conductor with the incorporation of dopant atoms. However, a major limiting factor preventing the widespread adoption of diamond as an electronic material is its asymmetric doping problem. For instance, boron is easily incorporated into the diamond lattice through substitution resulting in p-type doping. In fact, naturally occurring boron doped diamond is prevalent and are colloquially referred to as “blue diamonds.” Conversely, n-type doping has proven extremely difficult.[36] The following sections seek to further elaborate on this asymmetrical doping problem.

The wide bandgap nature of diamond makes the identification of suitable dopant species a challenging task. Problems also arise after identifying such a species as the substitutional incorporation of non-carbon atoms has proven challenging. For example, diffusion is a widely used method for doping typical semiconductors but is extremely difficult in diamond due to its compact lattice allowing only the diffusion of species smaller than or comparable to carbon at reasonable temperatures.[36] Further, while ion implantation is also often used for doping other

semiconductors, it is problematic in diamond due the metastability of the  $sp^3$  bonding of the carbon in diamond with respect to the stable  $sp^2$  bonding configuration of graphite. The crystal damage associated with ion implantation often converts to graphite upon annealing.[54] As a result of these difficulties, the prevailing method for doping diamond has proven to be the incorporation of a dopant species during the growth process.

### 2.5.1 P-type diamond

It has been mentioned that p-type doping of diamond has proven easier than n-type doping. The predominate method for achieving p-type conductivity is through the addition of boron containing species into the deposition gas mixture. Success has been made using gaseous TriMethylBoron (TMB) as the boron containing species.[55] It has been widely documented that the acceptor level of substitutional boron in diamond lies at 0.37eV above the valence band allowing for thermal activation at reasonably low temperatures.[56] Hole motilities exceeding  $1000\text{cm}^2\text{V}^{-1}\text{s}^{-1}$  and resistivities less than  $10^{-2}\Omega\text{cm}$  have been reported emphasizing diamond's ability to act as a p-type semiconductor.[57]

### 2.5.2 N-type diamond

Several species have been examined as potential n-type donors in diamond including nitrogen, phosphorus, and sulfur. Currently, phosphorus stands as the best candidate with a donor level located at 0.6eV below the conduction band.[36] Though the phosphorus atom is much larger in size than carbon and has a high equilibrium formation energy, phosphorus concentrations up to  $5*10^{19}\text{cm}^{-3}$  have been achieved with electrical activity in the (111) direction.[36] Sulfur has also been shown to act as a substitutional n-type dopant with marginal

success. Regardless of the donor level being positioned favorably at only  $\sim 0.37\text{eV}$  below the conduction band, useful concentration levels (exceeding  $10^{15}\text{cm}^{-3}$ ) have yet to be achieved.[58] Interestingly, it has been documented that the incorporation of  $\text{H}_2\text{S}$  into the deposition gases not only provides n-type conductivity but also improves the quality of the diamond by reducing graphitic content.[58] Finally, nitrogen as an n-type dopant in diamond must be discussed as it is of particular interest to the present research.

### 2.5.3 Nitrogen-incorporated diamond films

To date, numerous studies have been conducted examining the role of nitrogen on the electronic properties of diamond. With a  $-3.4\text{eV}$  formation energy, nitrogen easily enters the diamond lattice as a substitutional dopant atom making nitrogen doped diamond uncomplicated to fabricate (relative to other dopant species).[59] Unfortunately, previous research has shown that substitutional nitrogen doping does not significantly influence the electronic properties of diamond due to its deep donor level at  $1.7\text{eV}$  below the conduction band.[36] However, the addition and subsequent incorporation of nitrogen during the deposition process promotes defect-induced energy bands allowing conduction band carrier “hopping”, thus aiding in electron transport through the material.[60]

In addition to altering the electrical properties of diamond, nitrogen has also been shown to affect the growth process. The presence of nitrogen in the deposition processes has been documented to increase the growth rate of diamond films, allowing for uniform film coverage to be achieved faster.[61] Previous studies have also suggested that the presence of nitrogen in the grain boundaries leads to enhanced electron transport.[62] The subsequent increase in conductivity is favorable for electron emission as it provides a higher flux of electrons traveling

normal to the diamond surface.[63] Given these benefits which nitrogen offers over other possible n-type dopants in diamond, the present research chose to utilize nitrogen-incorporated diamond films.

## 2.6 Hydrogen in diamond

The numerous effects hydrogen has on the electrical properties of current widely used semiconductors have sparked recent research into its influence on diamond. For example, hydrogen has been shown to alter the properties of silicon through the passivation of donors and acceptors as well as unwanted deep recombination centers such as transition metals.[64] However, hydrogen's influence in diamond is much less understood. This is likely due to the lack of available published research compared to other more prevalent materials such as silicon. Indeed, while interest in diamond for its electronic properties continues to increase rapidly, much debate still exists as to the roles hydrogen may play.

### 2.6.1 Electron Transport

A study published by M.I. Landstrass and K.V. Ravi in 1989 is among the first to note the influence of hydrogen on the electrical properties of diamond.[65] In their study, diamond films were grown on silicon wafers via chemical vapor deposition with methane and hydrogen as the gas species. An electrical contact to the diamond film was made from deposited chromium and gold. Contact to the silicon was made with sintered aluminum. Current-Voltage characteristics were obtained first at room temperature from these as-deposited films through the described contacts. The current-voltage data was then recollected at room temperature following a thermal anneal at 800°C for one hour in flowing nitrogen. A final current-voltage test was

performed after the sample was exposed to a hydrogen plasma at 400°C for one hour. Examination of the results found in this study (Figure 2.8) demonstrates that the resistivity greatly increased after the heat treatment, in comparison to the as-grown resistivity. Furthermore, the resistivity was observed to recover back to its initial state after the hydrogenation procedure.[65] This study was one of the first to report that hydrogen can positively enhance the electron transport through diamond films.

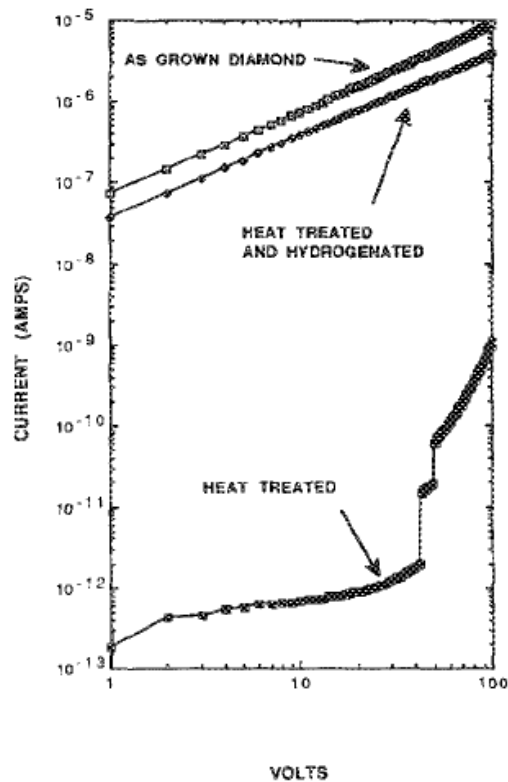


**Figure 2.8** Current-Voltage curves of the diamond film as grown, annealed, and hydrogenated from M.I. Landstrass and K.V. Ravi's 1989 study[65]

In a later follow-up study, the same authors postulated that the resistivity of the hydrogenated diamond crystals was governed by shallow acceptor levels.[66] Subsequent

annealing of the samples removed the hydrogen activating the deep donors, thus pinning the Fermi level and giving rise to the observed high resistivity. This follow-up study also observed a nonlinear behavior of the I-V curve from a MPCVD deposited film post heat treatment suggesting a continuous density of states present in the bandgap.[66] Contrary to these findings, studies on both dc plasma deposited and natural diamond appear to exhibit discrete energy levels in the bandgap.[66] To date, it remains unclear what causes these observed differences between diamond grown via opposing methods.

### 2.6.2 Electron Affinity

Hydrogen has also been shown to influence the band structure of diamond films, namely their electron affinity. Previous work by Cui and colleagues examining the effect of hydrogen on CVD diamond films and subsequent electron emission behavior, concluded that hydrogen termination decreases the effective barrier for electron emission by lowering the electron affinity.[67] Further, as previously mentioned, diamond films can demonstrate a negative electron affinity (NEA) whereby the vacuum level lies below the conduction band minimum.[68-71] A band diagram of an NEA material is illustrated in Figure 2.9.

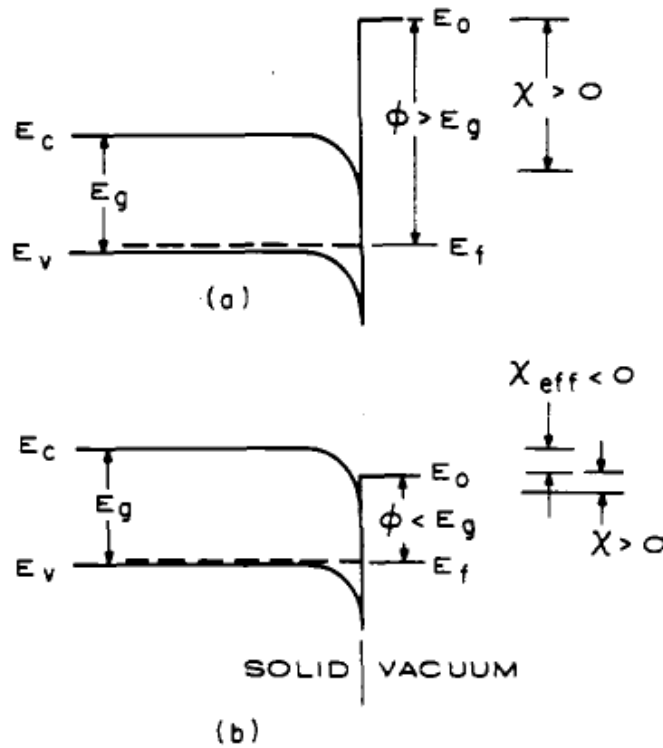


**Figure 2.9** Band diagrams of a semiconductor with (a) positive electron affinity and (b) negative electron affinity.  $E_g$  represents the bandgap;  $\Phi$ , the work function;  $E_o$ , the vacuum level;  $E_f$ , the Fermi level; and  $E_c$  and  $E_v$ , the conduction and valence band energy levels, respectively.[72]

R.U. Martinelli and D.G. Fisher provide a particularly excellent description of the electron emission from an NEA material by comparing the photoemission process for both conventional emitters and NEA emitters.[72] They first described the photoemission of a conventional emitter by a three basic processes: 1) Photons excite electrons from the valence band into the conduction band. The electrons must have energy equal to or greater than the vacuum level in order to be emitted. 2) The excited electrons migrate to the surface but lose energy through collisions which typically results in an energy loss of approximately 1eV for every 100Å traveled. The distance required to reach the surface (referred to as the escape depth)

is dependent on the excitation energy of the radiation, the absorption processes, and the energy dependence of the transport process. 3) Electrons with sufficient energy after the collision losses are emitted into the vacuum while electrons not meeting this criteria decay to the conduction band minimum.[72]

According to Martinelli and Fisher, NEA emitters function similarly to conventional emitters in that excited electrons migrate across to the emitter surface losing energy to collisions. However for an NEA emitter, the electrons without sufficient energy that decay to the bottom of the conduction are in thermal equilibrium with the lattice remaining a few kT above the conduction band minimum. These thermalized conduction band electrons can survive for relatively long periods of time allowing them to diffuse distances as far as several microns which are typically quite a few orders of magnitude longer than the escape depths. It is here that the advantages an NEA emitter has over a conventional emitter can be seen. As the thermalized electrons diffuse to the NEA surface, they are then able to emit into the vacuum as the vacuum level lies below the conduction band, thus dramatically increasing the emission efficiency.[72]

Diamond has been shown to be one the few known materials to exhibit negative electron affinity. In the first published study to suggest this, F.J. Himpsel and colleagues in 1979 examined a (111) oriented single crystal diamond sample by photoemission spectroscopy whereby emission was observed down to the conduction band minimum indicating a negative electron affinity.[68] However, it was not until later that this phenomenon was directly attributed to hydrogen.

The observed NEA of the diamond surface is believed to result from the surface dipole layer hydrogen introduces.[73] Hydrogen has a lower electronegativity than the corresponding carbon in diamond resulting in a surface C-H bond that is polarized with a positive charge,  $\delta^+$ , on

the H atom. This charge provides a potential step that pulls the vacuum level below the conduction band minimum by a distance equal to the C-H bond length. Accordingly, adsorbates with higher electronegativities (such as oxygen) will increase the electron affinity.[73] A visual depiction of this process is presented in Figure 2.10.

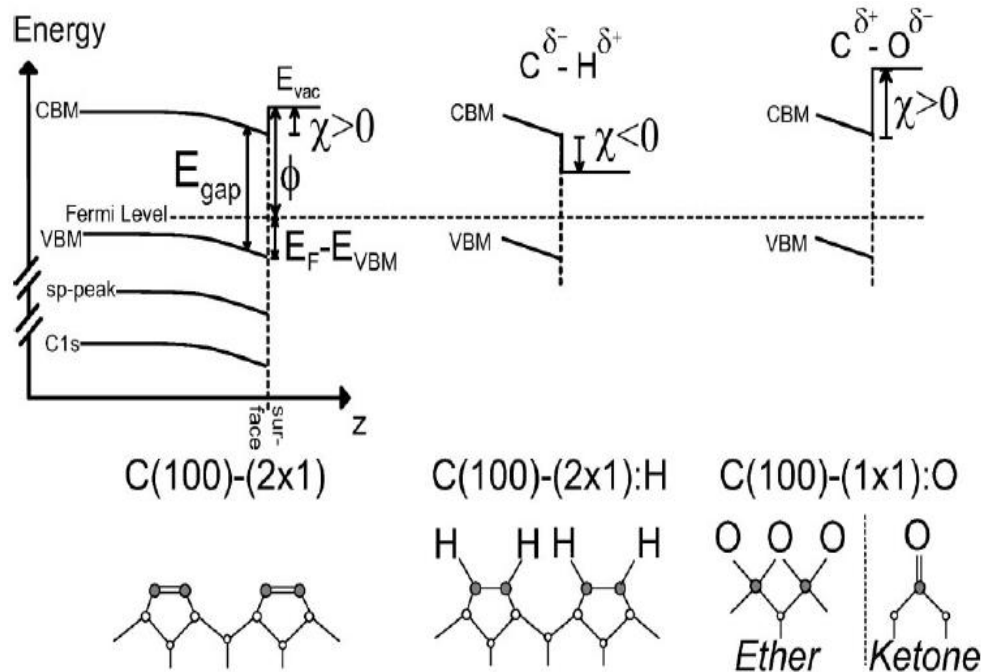


**Figure 2.10** Band diagram and corresponding atomic arrangements of a clean, hydrogenated, and oxygenated diamond surface.[73]

### 2.6.3 Desorption of hydrogen from diamond

A detailed discussion has been presented demonstrating hydrogen's ability to influence the electrical properties of diamond. Though this influence is thought crucial to diamond's superior thermionic emission abilities, it also dramatically limits the operating temperatures of such cathodes. It was previously discussed that the annealing of diamond films leads to an increased resistivity of diamond films which is observed to recover upon exposure to a hydrogen

plasma.[65] It can be deduced from this observation that annealing removes the beneficial effects of hydrogen. Similar observations have been made in experiments studying the thermionic electron emission properties of diamond films. Typical experiments characterizing the thermionic emission properties of a material consist of increasing the temperature in gradual steps while observing the emission current at each step. Such experiments performed on various diamond films have all noted a distinct decrease in this emission current beginning around 800°C with this trend continuing for the subsequent higher temperature steps.[74, 75] This observation is consistent with previous research describing the isothermal desorption behavior of hydrogen in diamond.[76] Thus, in order to improve the performance of diamond thermionic emitters, the hydrogen desorption mechanism must be fully understood.

Several previous studies have attempted to determine the activation energy of hydrogen in diamond using a wide variety of methods, including direct recoil spectroscopy (DRS), thermal desorption spectroscopy (TDS), reflection high-energy electron spectroscopy (RHEED), and electron-stimulated desorption time-of-flight spectroscopy (ESD-TOF), among others. The hydrogen desorption phenomena can be described by the Polanyi-Wigner equation seen below.

$$R_d = k_m * N^m = N^m * k_m^0 * \exp(-E_m/RT) \quad (2.1)$$

Where:  $k_m$  is the rate constant,  $m$  is the formal order;  $E_m$ , the activation energy; and  $k_m^0$ , the pre-exponential factor.[77] It is clear from Table 2.2 that a large range of hydrogen activation energies have been obtained for diamond surfaces.

**Table 2.2** Comparison of the activation energies obtain from diamond films with differing orientations using various methods. It can be see that most studies agree that the activation energy of 100 oriented diamond films is around 1.5eV

Diamond Face	Ea (eV)	Method	Reference
001	0.91	RHEED	[78]
111	1.25	Change in x	[79]
100	3.15	TDS	[80]
100	1.48	Theory	[81]
100	1.60	ESD-TOF	[82]
100	1.47	TPD	[83]
100	1.69	Ion Spectroscopy	[84]

One notable study by T. Nishimori and colleagues in 1995 measured the time evolution of the surface hydrogen coverage,  $\theta_H$ , via the electron-stimulated desorption yield of  $H^+$  ions with a time-of-flight mass spectrometer.[78] Figure 2.11a shows the time evolution curves obtained in this study of  $\theta_H$  during a thermal annealing at temperatures ranging from 1095°C to 1270°C. By assuming the hydrogen desorption is a first-order reaction, Equation 2.1 can be rewritten as Equation 2.2.

$$\theta_H = \exp(-k_{ds}t) + C_{diff}/k_{ds} \quad (2.2)$$

Where:  $k_{ds}$ : the desorption coefficient;  $t$ : time; and  $C_{diff}$ : the hydrogen segregation rate from the bulk.[78] Nishimori and colleagues then performed a least-squares fit of the data in Figure 2.11a with respect to Equation 2.2 (seen in Figure 2.11b) to obtain an activation energy,  $E_a$ , of 21 kcal/mole for the desorption of hydrogen from diamond.[78]

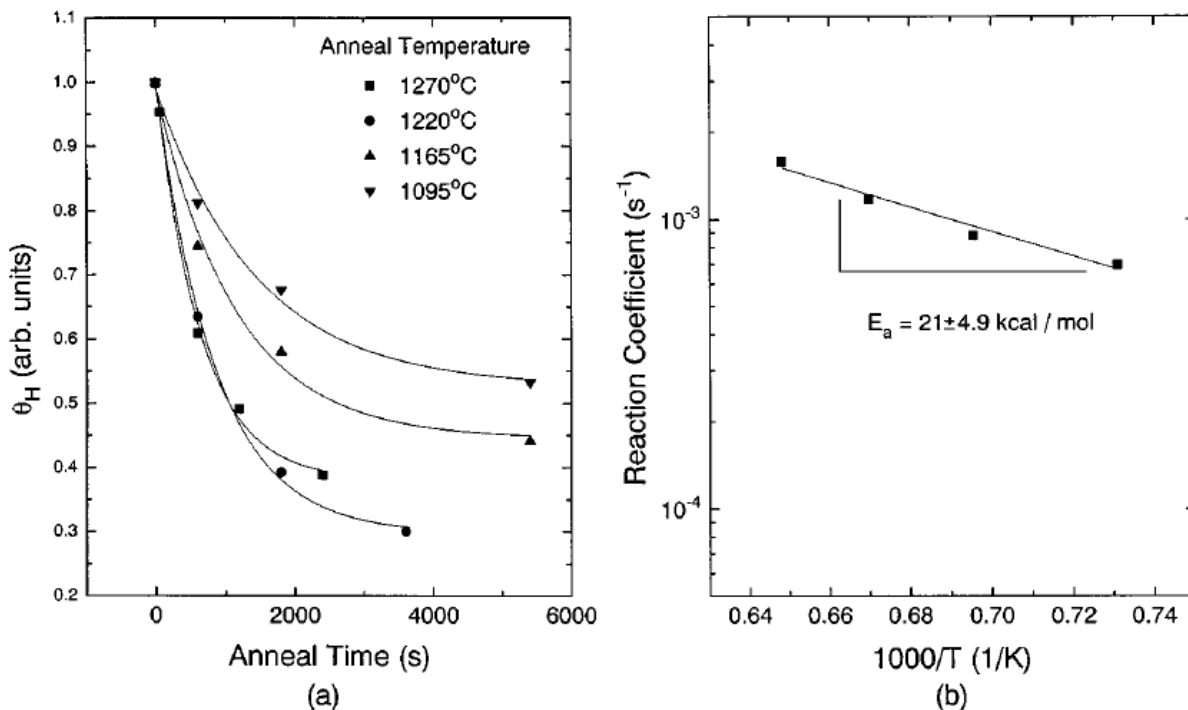


**Figure 2.11** a) Decrease in hydrogenation coverage as a function of anneal time for various annealing temperatures. b) First order desorption fit of the data indicating an activation energy of 21 kcal/mol[78]

Previous research has suggested that large measured surface hydrogen concentrations correspond to two hydrogen atoms per surface carbon atom implying a dihydride surface configuration.[85] Taking this into account, A.V. Hamza and colleagues postulated that the desorption process consists of the “unimolecular decomposition of two adjacent dihydrides to form two adjacent monhydrides”.[82] Examination of the large variation in activation energies for the desorption process of hydrogen in diamond emphasizes the need for further studies. Indeed, wide-spread utilization of diamond as an electronic material is unlikely without a better understanding of this process.

#### 2.6.4 Deuterium in diamond

Hydrogen has been shown to be responsible for many of the superior electron emission properties of diamond films. Unfortunately, the relatively low activation energy promotes rapid desorption of hydrogen at elevated temperatures leading to a temperature ceiling of around 800°C for a diamond thermionic emitter. This relatively low value (when compared to tungsten which operates in excess of 1500°C) drastically limits the applicability of these films. One method to combat this problem is through the use of deuterium rather than hydrogen. Deuterium has the same electrical properties as hydrogen but with twice the atomic mass. It can therefore be postulated, based on kinetic isotope theory, that more thermal energy will be required to dissociate the C-H bond than the C-D bond.

A study by Baumann and Nemanich in 1998 examined the surface of diamond films with photoemission spectroscopy upon exposure to both hydrogen and deuterium plasmas.[86] This study observed that the negative electron affinity attributed to hydrogen termination could be removed by annealing a sample at 1100°C. In contrast, deuterium terminated diamond still exhibited NEA after annealing to 1200°C. It was found that heating of the sample to 1250°C was required to completely remove the NEA from the surfaces.[86] These findings demonstrate that deuterium may be a viable replacement for hydrogen in diamond films. Furthermore, replacing hydrogen with deuterium could allow for operation at higher temperatures thereby increasing the overall thermionic emission current able to be extracted from a diamond cathode.

## 2.7 Applications of diamond

Diamond's unique material properties have generated interest in a wide range of applications from vacuum microelectronics to machine equipment. A selected sampling of electronic applications for diamond will now be discussed.

### 2.7.1 Diamond as a solid state electronic material

Though diamond can be found in many common items such as drill bit coatings and heat dissipaters, its future in the electronic industry seems the most promising. Diamond's relatively large bandgap of 5.45eV (compared to silicon at 1.1eV) allows it to act as an extremely effective electronic insulator with measured resistivity values exceeding  $10^{15}\Omega\text{-cm}$ . [23] This, coupled with the relatively low resistivities obtained by doping diamond, has led many researchers to examine its solid state applications. Solid state devices, such as resistors, diodes, and transistors, have already been fabricated with advances consistently being made each year.

A resistor is the simplest solid state device able to be fabricated with diamond. By modifying the dopant concentrations, a wide range of resistivities can be achieved. The Vanderbilt University Diamond Lab has fabricated boron-doped diamond resistors on insulating aluminum nitride substrates. [87] The resistors, patterned via oxygen plasma etching, can be seen below in Figure 2.12. Ohmic behavior was achieved from these resistors for low to medium current levels but at higher current levels, increased resistivity was observed due to thermal excitation from joule heating. [87] Unlike conventional resistors that would fail under such conditions, diamond's tolerance to high power allowed for continued operation. [87]

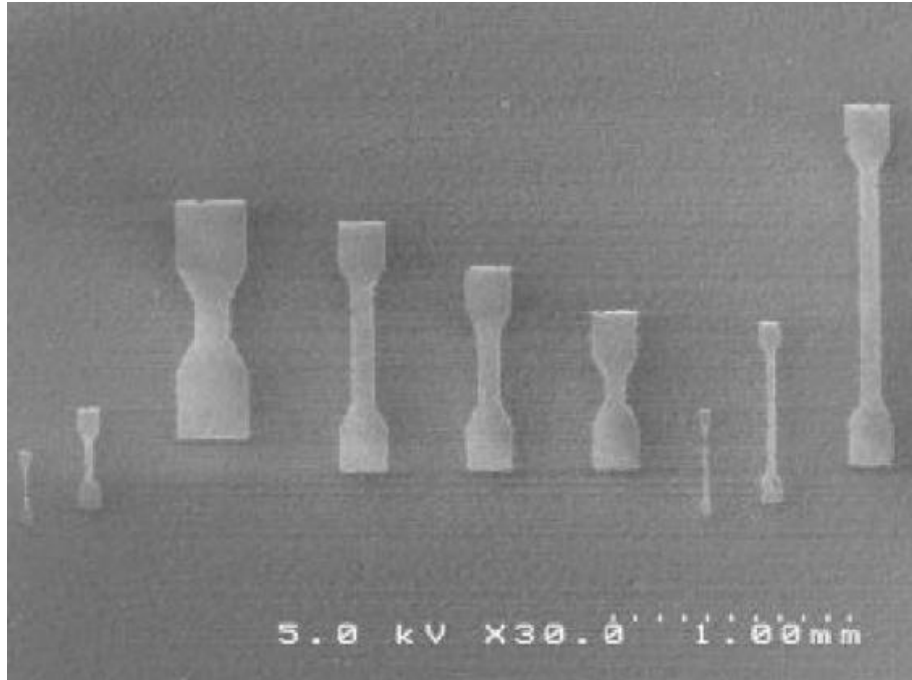


**Figure 2.12** Scanning electron micrograph of boron doped diamond resistors patterned via oxygen plasma etching on an aluminum nitride substrate[87]

The diode is yet another solid state device that has been fabricated with diamond. The large bandgap of diamond limits the intrinsic carrier concentrations to levels less than  $10^{10}\text{cm}^{-3}$  at temperature below  $1000^\circ\text{C}$  allowing for a large range of stable predictable operating temperatures.[88] This, combined with diamond's extremely high break down field of  $10^7\text{ V/cm}$ , makes it an ideal candidate for use in a diode.[89] A. Aleksov and colleagues constructed such a diode with boron and nitrogen as the p- and n-type dopants respectively in 2003. This device exhibited adequate current rectifying properties with no observable reverse bias break down over the voltages tested (Figure 2.13).[90] Thus, all diamond diodes could be utilized for future applications which require operation in harsh environments.

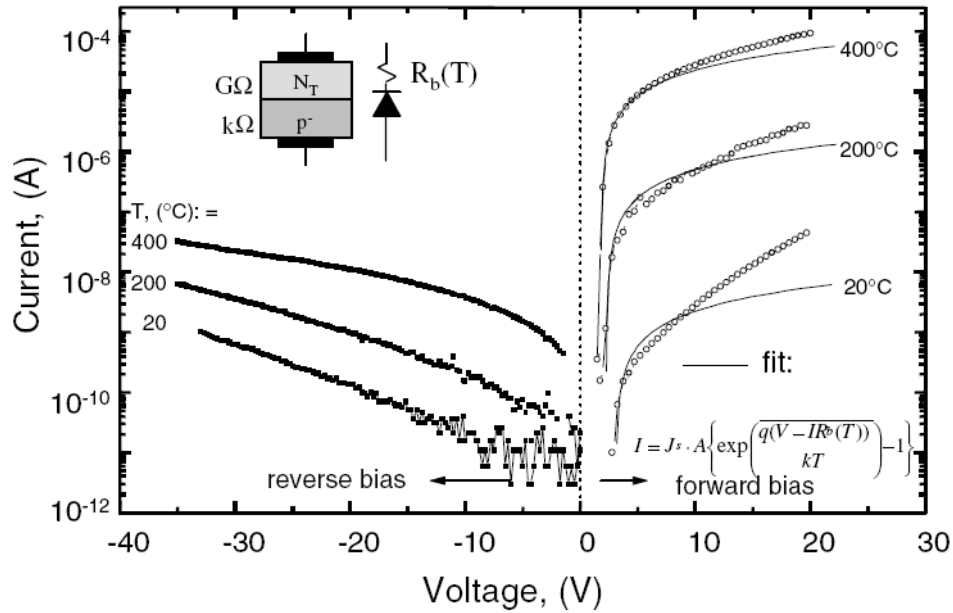


**Figure 2.13** Current-voltage characteristics of an all diamond pn diode with boron and nitrogen as the n- and p-type dopants respectively.[90]

In addition to the above devices, solid state diamond transistors have also been fabricated. One example, by M. W. Geis, was a vertical field effect transistor constructed entirely from homoepitaxial diamond layers with different boron doping concentrations similar to a MESFET (metal semiconductor field effect transistor).[91] The gate oxide layer for this device was SiO<sub>2</sub>. Figure 2.14 shows the fabrication process of Geis's device while Figure 2.15 shows the inverse capacitance squared-bias voltage relationship obtained in his study. Examination of the inverse capacitance squared vs. bias voltage plot revealed a straight line indicating that the diamond SiO<sub>2</sub> interface is extremely well behaved unlike other semiconductors such as GaAs.[91] The compatibility of diamond with SiO<sub>2</sub> could make future all-diamond integrated circuits easier to fabricate by utilizing existing oxide deposition methods.

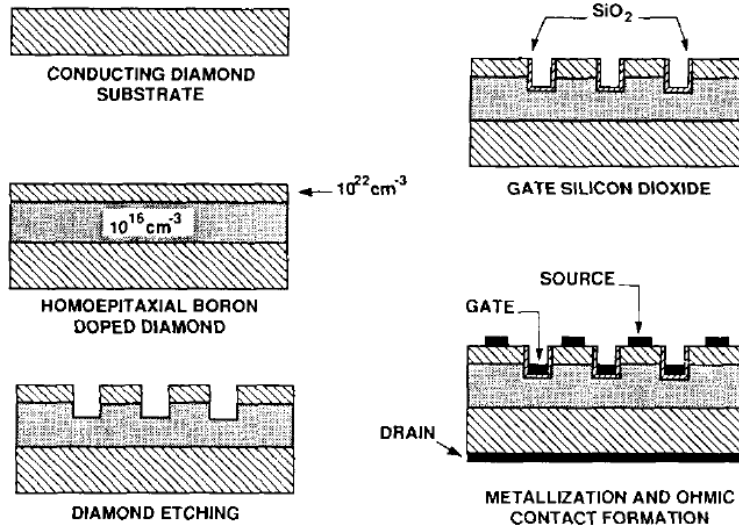


**Figure 2.14** Fabrication of the vertical diamond field effect transistor by M.W. Geis[91]

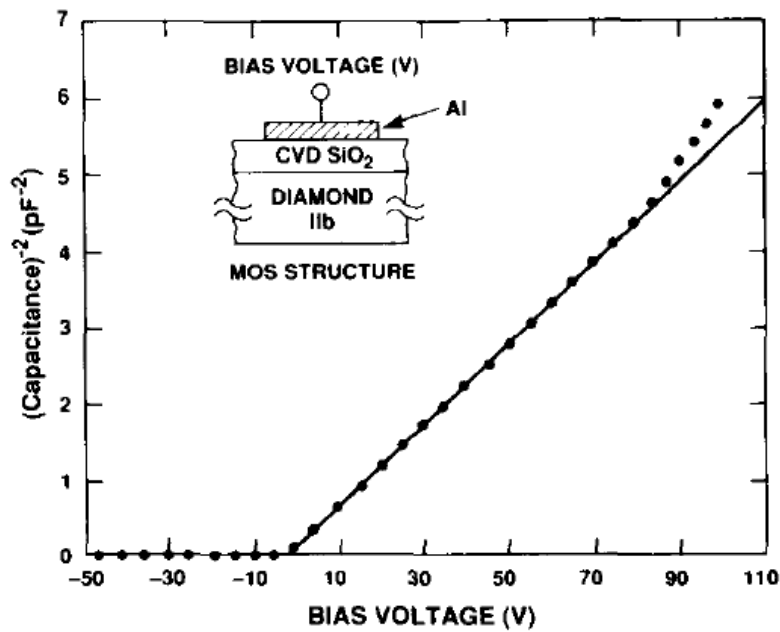


**Figure 2.15** Inverse capacitance squared vs. bias voltage of the diamond field effect transistor seen in Figure 2.13. The linear relationship implies the diamond-SiO<sub>2</sub> interface is extremely well behaved[91]

In 2009, researchers at the University of Glasgow achieved a major milestone in the advancement of diamond solid-state electronic devices. It was desired to create a transistor able to operate in the terahertz range for automotive collision detection. Given that the device would need to be able to operate in harsh environments, diamond was the ideal candidate.[92] This research led to the creation of a diamond transistor with a gate length of 50nm.[92] Perhaps in the future, when silicon transistors reach a scale at which they are physically and financially impractical to fabricate, diamond may step in to fill the void.

### 2.7.2 Diamond in vacuum microelectronics

In addition to the many solid state applications previously discussed, diamond has also become of interest in the reemerging field of vacuum microelectronics. Though vacuum devices were largely replaced by the semiconductor during the 20<sup>th</sup> century, recent advancements in fabrication technologies have led many researchers to reexamine them. Vacuum microelectronic devices, such as the diode and triode, offer many advantages over their solid-state counterparts. For example, in a solid state device, the transport of electrons is largely governed by the semiconducting material's electronic properties. However, this is not the case in vacuum devices as the electrons are transported through a vacuum in which the only limiting factor on their velocity is the speed of light; thus the problems of crystal imperfections that plague the solid-state industry are alleviated allowing for less burdensome fabrication processes. The ability to achieve high electron velocities in vacuum microelectronic devices also allows for much higher frequency switching than traditional solid-state devices.[93]

The vacuum devices of the early 20<sup>th</sup> century required large amounts of power as they utilized thermionic emission to extract electrons from the inefficient cathodes of the day.

Thermionic emission from these inefficient cathodes typically involved heating them to temperatures in excess of 1,500°C in order to achieve usable current which resulted in large amounts of wasted power. Current vacuum microelectronic devices are substantially more efficient as they employ the quantum mechanical tunneling process, known as Fowler-Nordheim emission. This emission process, often referred to as field emission, occurs at room temperature when the cathode is exposed to high voltages.[94] Field emission typically requires large electric fields on the order of 10 MV/cm in order to obtain practical current levels. This high voltage requirement can be overcome by fabricating cathodes resembling needles with very sharp radii of curvature creating high local fields at the tip. The band bending that is achieved through the fabrication of cathodes with sharp tips can be seen in the energy band diagrams in Figure 2.16.

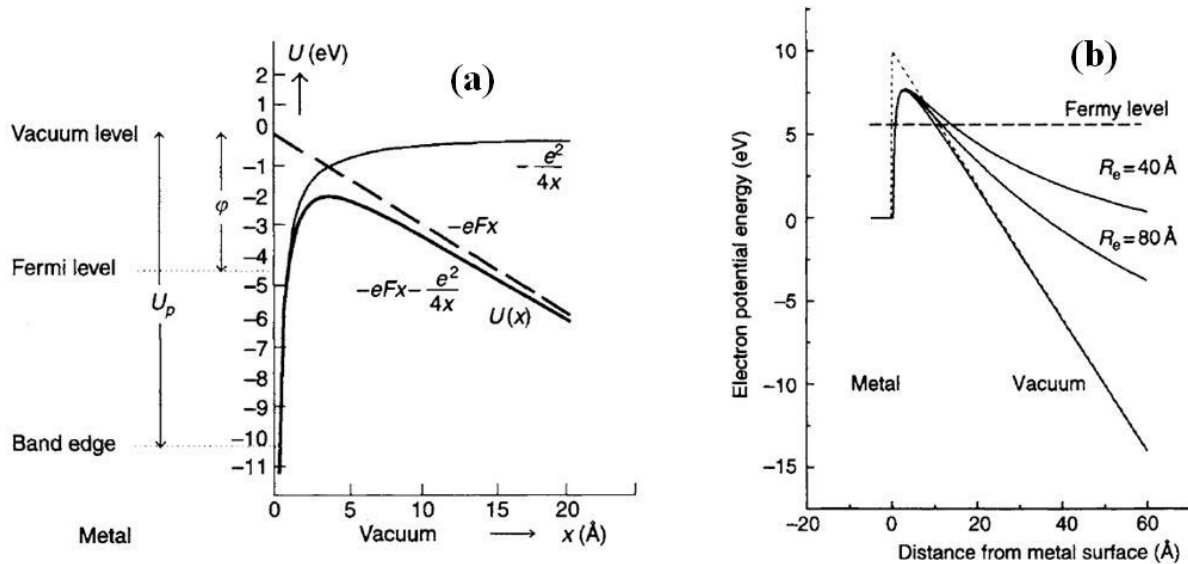


**Figure 2.16** (a) Potential energy of an electron  $U(x)$  as a function of distance from the metallic cathode. Here “ $-eFx$ ” is the externally applied potential, “ $U_p$ ” is the total potential well depth, and “ $-e^2/4x$ ” is the image potential. (b) Band bending as a function of the radius of curvature of a tungsten “needle” emitter.[93]

Current research at Vanderbilt University is examining diamond as material for vacuum microelectronic devices with both vertical and lateral configurations. The lateral configuration is similar to a two dimensional structure in which the cathode, anode, and emission current all exist in the same plane. Lateral type rectifying diodes created at Vanderbilt consist of several “finger-like” cathode emitting tips.[95-97] Both the cathode and the anode are patterned from a nanocrystalline diamond film deposited on an oxidized SOI wafer using  $\text{SiO}_2$  as the electrical insulator between the two.[95-97] This patterning can achieve extremely close cathode-anode spacings leading to “turn on” fields as low as 5V.[98] A scanning electron micrograph and current-voltage plots of these devices can be seen in Figure 2.17.

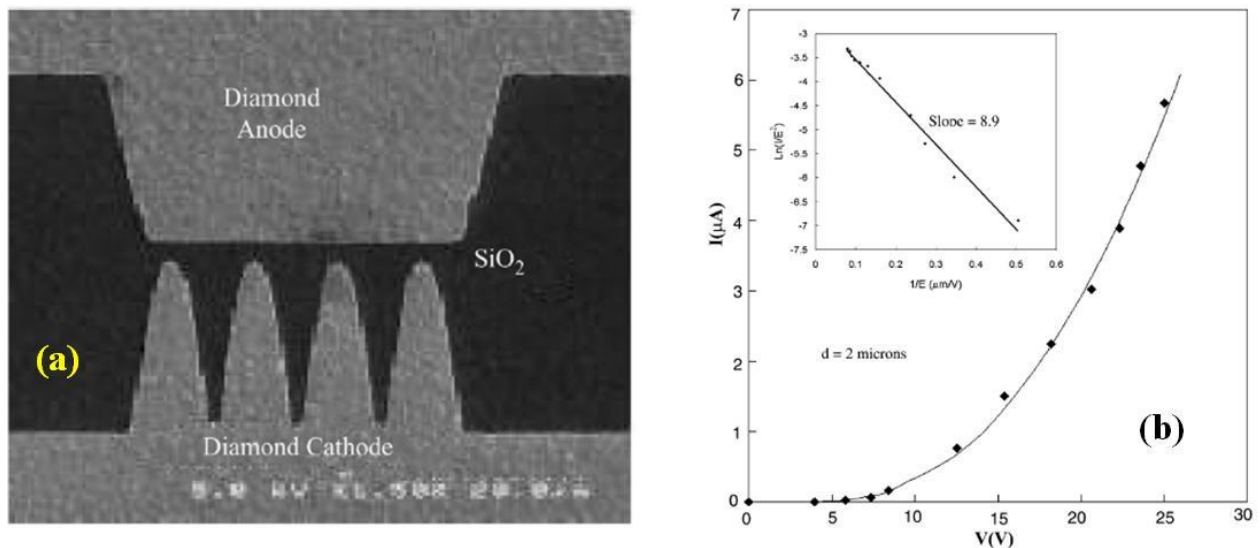


**Figure 2.17** (a) Scanning electron micrograph of the lateral diamond microelectronic diode. The cathode and anode are both patterned out of a single uniformly deposited nanocrystalline diamond film and isolated by  $\text{SiO}_2$ . (b) Current-voltage characteristics of the device in (a) which is able to achieve a “turn-on” voltage of 5V.[98]

As earlier mentioned, research at Vanderbilt is also examining diamond vacuum devices with a vertical configuration. These devices consist of three dimensional pyramid arrays with

each pyramid having an extremely sharp radius of curvature on the order of 5nm.[99] In Figure 2.18, the complex fabrication process of these pyramids for use as vacuum diodes can be seen.

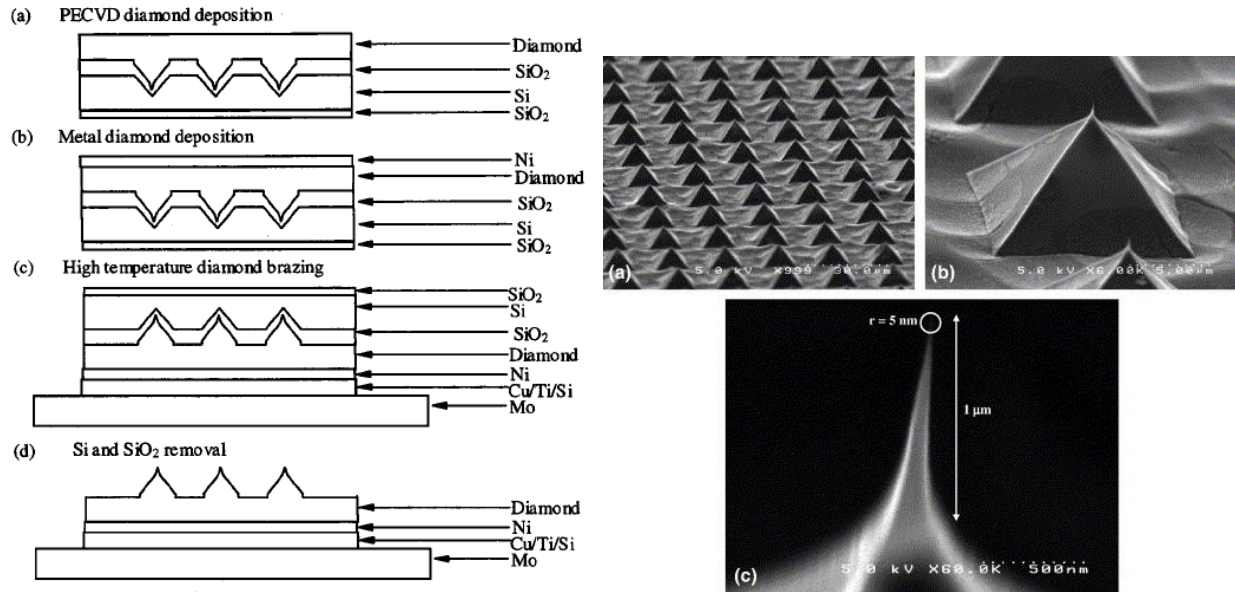


**Figure 2.18** Left: Fabrication process for diamond pyramidal cold cathodes. Right: SEM image of fabricated emitters[99-102]

Perhaps the most interesting application of these pyramidal diamond emitters is for use in vacuum triodes with transistor-like behavior consisting of three electrodes: a cathode, an anode, and a gate. The gate is biased positively and positioned close to the anode and is meant to extract electrons from the cathode tip to be collected by the anode. The incorporation of a gate allows for smaller anode voltages, creating a more practical device. The first device of this type, known as the “Spindt cathode,” was fabricated in 1968 for use in field emitter displays.[93] The diamond triodes fabricated at Vanderbilt are similar to the Spindt cathode. Diamond is the emitter in the Vanderbilt devices, while the gate is fabricated out of silicon (Figure 2.19). Such devices are able to obtain exceptionally high amplification factors (change of anode voltage over

change in gate voltage) on the order of 250 with the gate biased at only 20 V.[98] There is currently very little research outside of Vanderbilt on the topic of diamond vacuum micro/nanoelectronic devices but the several advantages this technology has over current solid state devices could result in its utilization in numerous future applications.

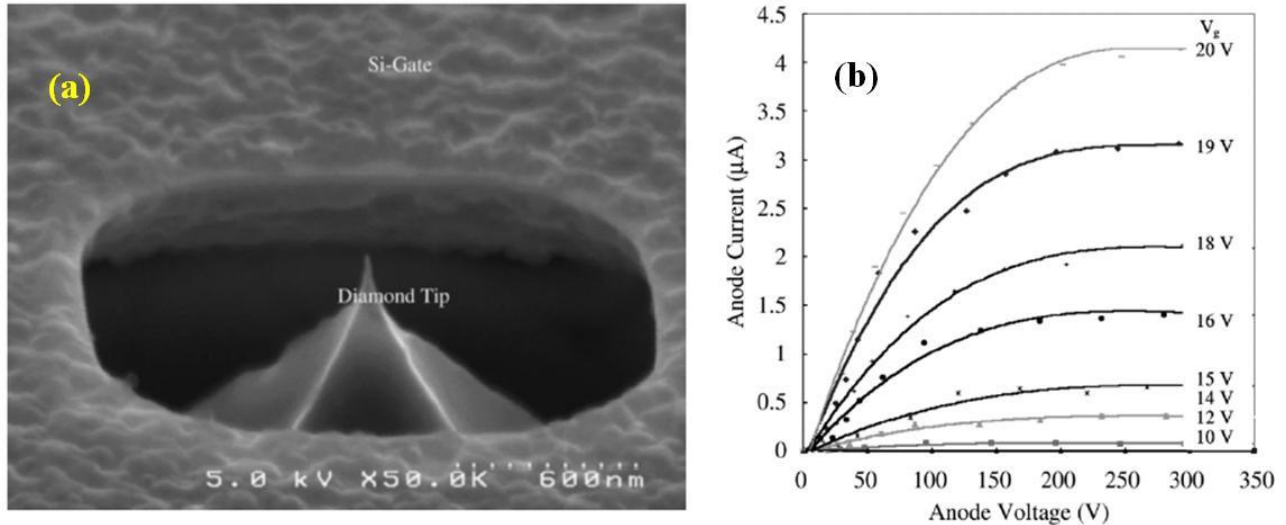


**Figure 2.19** (a) Scanning electron micrograph of the diamond triode vacuum microelectronic device. The cathode here is a diamond pyramid with a tip radius of curvature on the order of 5 nm and the gate is silicon. SiO<sub>2</sub> is used to insulate the gate from the cathode. (b) Anode current-voltage behavior of the diamond triode device at different gate voltages. With the gate biased at 20V, an amplification factor of 250 was achieved[98]

### 2.7.3 Use of diamond in thermionic energy converters

Given that the focus of this research is to examine the use of diamond as an electrode material for thermionic energy conversion, it is only fitting that previous research on this topic is discussed. The exploration of diamond as a vacuum field emitter has gone hand in hand with investigations into its thermionic emission properties. Several research groups, including the Vanderbilt Diamond Lab, have shown diamond to be an outstanding thermionic emitter.[103,

104] The wide bandgap nature of diamond requires it to be “doped” with other species to obtain its superior electronic properties. One such study, by R. J. Nemanich at Arizona State University in 2009, deposited ultra nanocrystalline diamond films on a metallic substrate via MPCVD to observe the thermionic emission current as a function of temperature.[105] Analysis of the emission current vs. temperature behavior with respect to the Richardson equation revealed nitrogen-incorporated ultra nanocrystalline diamond to have a work function of 1.29 eV and Richardson constant of  $0.84 \text{ Acm}^{-2}\text{K}^{-2}$ . [105] The thermionic emission current vs. temperature plot from this study can be seen below in Figure 2.20. These results were verified by M. Suzuki and colleagues on similar nitrogen incorporated nanocrystalline diamond films.[74]

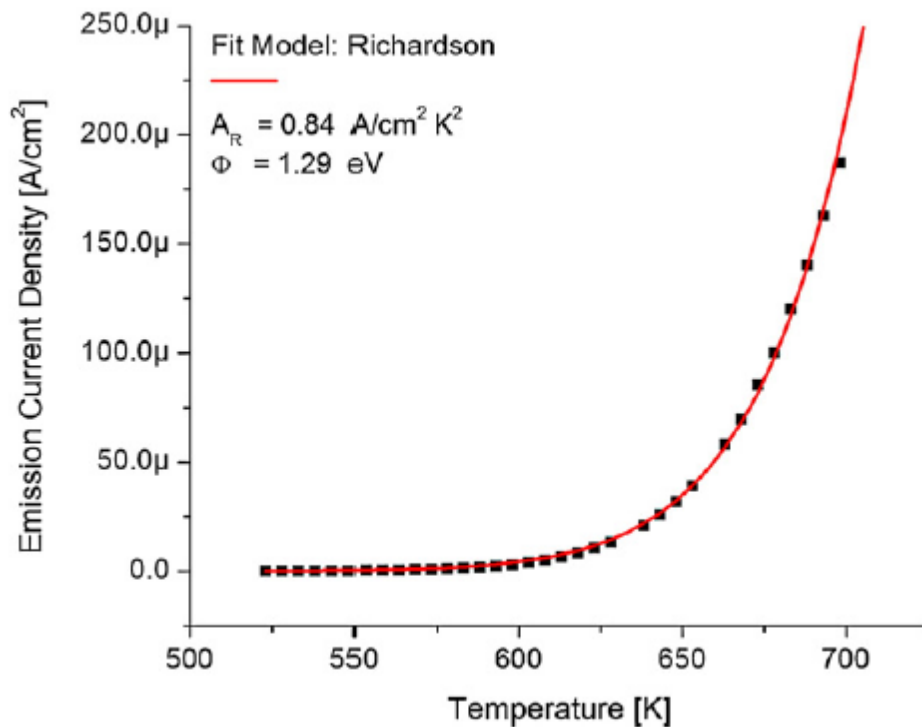


**Figure 2.20** Thermionic emission current vs. cathode temperature of a nitrogen-incorporated ultra-nanocrystalline diamond films by R. J. Nemanich[105]

A follow-up study by Nemanich studied the thermionic emission from phosphorus doped diamond films on molybdenum substrates. As Section 2.5.2 outlines, phosphorus acts as a true n-type dopant in diamond films with a relatively shallow donor level of 0.6 eV below the conduction band.[36] Thermionic emission testing, performed in the same manner as Nemanich's previously discussed experiment, established that phosphorus-doped diamond films possess a work function and Richardson constant of 1.18 eV and  $0.003 \text{ A/cm}^2\text{K}^2$ , respectively.[106] Though the phosphorus-doped diamond films had a much lower work function than the nitrogen-incorporated diamond films, the phosphorus-diamond samples were not able to achieve thermionic emission current levels as high as the nitrogen-diamond samples. This is due to the extremely low Richardson constant demonstrating that an efficient thermionic emitter must have both a low work function and a high Richardson constant.

These findings implicate diamond as an efficient electron emitter for thermionic applications such as thermionic energy conversion. Implementation of diamond into such devices has been hindered due to its relatively low temperature ceiling around  $750^\circ\text{C}$ . All known studies, including those performed at Vanderbilt, have observed that the emission current begins to deviate from the equations governing thermionic emission in that it decreases with temperature rather than continuing to increase exponentially.[74-76] This has often been attributed to hydrogen desorption which was discussed in more detail in Section 2.6.3. Little research has been performed to fully understand this mechanism so that diamond based thermionic emitters can operate at higher temperatures allowing for higher current levels to be achieved. Accordingly, a better understanding of this mechanism is one of the primary objectives of the present research.

## CHAPTER III

### THERMIONIC ENERGY CONVERSION

#### 3.1 Thermionic emission

Thermionic emission is a core component of the present research. As previously mentioned, this phenomenon occurs when thermal energy is imparted to a cathode causing the emission of electrons. The fundamental equation describing this process is known as the Richardson equation and is represented in Equation 3.1.

$$J = AT^2 e^{-\Phi/kT} \quad (3.1)$$

where J: Cathode thermionic emission current density (A/cm<sup>2</sup>); A: Cathode Richardson constant (A/cm<sup>2</sup>K<sup>2</sup>); T: Cathode temperature (K);  $\Phi$ : Cathode work function (eV); and k: the Boltzmann Constant (8.617 x 10<sup>-5</sup> eV/K).[22]

This equation is based on thermodynamic and quantum mechanical principles and is the accepted equation for electron current flow at a boundary over a certain potential barrier. For thermionic emission, this potential barrier is known as the material's work function. In addition to the work function, the Richardson constant is the other material specific parameter in Equation 3.1 which was first derived by Dushman using quantum theory for an ideal metallic emitter to be 120 A/cm<sup>2</sup>K<sup>2</sup>. [107]

A common misconception amongst researchers is that the values of "A" and " $\Phi$ " are constant for a certain material. In reality, there are numerous factors that must be taken into account which cause these values to have large variability. The following section seeks to provide a detailed understanding of this process by deriving the Richardson equation.

### 3.1.1 Richardson equation derivation

Though the Richardson equation (Eq. 3.1) appears simple and straightforward at first glance, its derivation is somewhat complex. Derivation of this fundamental equation is necessary in order to fully grasp the concepts explored in this research. The derivation presented below does not follow O.W. Richardson's original paper in which his namesake equation was originally presented as he did not initially derive a value for the Richardson constant.[22, 108] It was not until later that S. Dushman quantified this value (though he did not account for the two possible spin states of an electron thus he was off by a factor of two).[107] In order to maintain a constant use of variables, the following derivation follows a manuscript by W.B. Nottingham titled "Thermionic Emission" unless otherwise stated .[109]

To begin this derivation of the Richardson equation, three fundamental assumptions must first be made regarding electrons in a material.

1. Inter-electronic forces are neglected. This provides that electrons behave as particles with three degrees of freedom described by a six-dimensional phase space (three coordinates and three momentum components)
2. An extension in phase space of  $h^3$  is required for each quantum state
3. The Pauli Exclusion Principle must be accounted for which limits the number of electrons in a given quantum state to two (each with opposite spin)[110]

With these three assumptions in place, the derivation can begin. An expression must first be made to describe the maximum likelihood of occurrence distribution of electrons in phase space that is consistent with basic principles of thermodynamics. This equation must account for the total number of quantum states for a certain system and the two possible spin states of an electron in each quantum state described by the Pauli Exclusion Principle.[110] Additionally, as

we are dealing with electrons, a statistical equation to describe the probability distribution of electrons in the system should be included which is represented by the Fermi function.

Accounting for these parameters, a maximum likelihood function can be expressed as follows:

$$f(\varepsilon)dxdydzdp_xdp_ydp_z = 2 \frac{dxdydzdp_xdp_ydp_z}{h^3} \left[ \frac{1}{e^{\frac{\varepsilon-\mu}{kT}} + 1} \right] \quad (3.2)$$

where  $\varepsilon$ : electron energy;  $\mu$ : chemical potential;  $h$ : Plank's constant;  $k$ : Boltzmann constant;  $T$ : Temperature; and  $x, y, z, p_x, p_y, p_z$ : the spatial and momentum coordinates, respectively.

The “ $\varepsilon$ ” in Equation 3.2 represents energy and can generally be separated into two terms, kinetic and potential. The concentration of electrons is contained in the “ $\mu$ ” term, also referred to as the Fermi Level, and is a function of temperature. The coordinate and momentum grouping divided by  $h^3$  seen in the right-hand side of Equation 3.2 represents the number of quantum states in this extension and the double occupancy is accounted for in the factor of 2 in front (Assumption 3). Finally, the bracket term in the right-side of the equation (the Fermi function) is the probability distribution function of a certain quantum state at energy,  $\varepsilon$ , being occupied.

A very useful equation for electron transport calculations can be derived from Equation 3.2 known as the “Electron Flow Equation” and can be seen in Equations 3.3 and 3.4.

$$N(\varepsilon_x)d\varepsilon_x = 2 \frac{(2\pi mkT)}{h^3} \ln \left( 1 + e^{-\frac{\varepsilon_x - \mu}{kT}} \right) d\varepsilon_x \quad (3.3)$$

and 
$$\varepsilon_x = \frac{p_x^2}{2m} \quad (3.4)$$

where  $N(\varepsilon_x)$ : number of electrons at an energy  $\varepsilon_x$ ;  $m$ : electron mass; and  $h, \mu, k, T,$  and  $p_x$ : the same as defined for Equation 3.2.

The Electron Flow Equation (EFE) described in Equations 3.3-4 represents the number of electrons that cross a unit area in unit time with kinetic energy associated with the positive  $x$  direction of motion over a certain energy range. In other words, the EFE allows for the number

of electrons crossing a boundary perpendicular to the x direction to be computed. With the EFE in place, an equation of electron current can be formulated.

The derivation continues with inspection of the “Pillbox Problem”, which represents a rectangular cavity positioned inside a homogenous single crystal with every region at a constant uniform temperature. This special scenario allows for exact calculation of the random currents arising at the boundaries. For simplicity, space charge effects will be neglected but will be discussed in later sections. An energy diagram of the “Pillbox Problem” is graphically shown below in Figure 3.1.

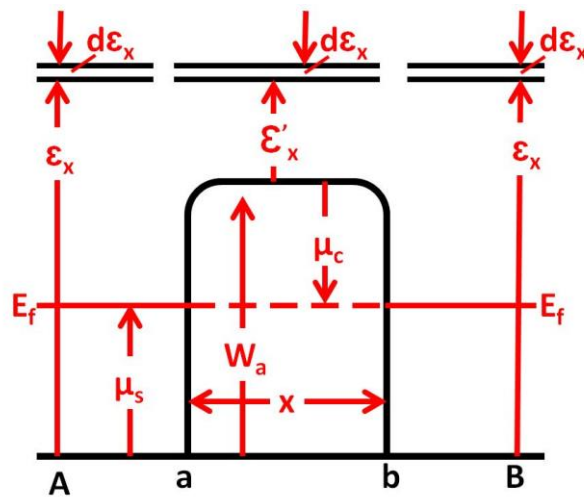


**Figure 3.1** Energy diagram of “pillbox” problem. The region from “a” to “b” represents a cavity inside a homogenous crystalline material. The entire material and the cavity are said to be at a constant uniform temperature. This diagram neglects space charge effects and assumes that the distance “x” is large enough such that image potential can also be neglected.

Figure 3.1 represents the potential energy of an electron as function of distance as it travels from “A” to “B.” The region from “A” to “a” is the potential in the homogeneous crystal and is assumed to be uniform. The region from “a” to “b” is the empty cavity region that the

electron must traverse and has a potential defined as  $W_a$ . As previously noted, space charge is neglected leaving the dominant force acting on an electron to be the image potential it leaves behind as it departs the surface. To simplify this case, calculations will be made for the distance “x” being greater than  $10^{-5}$  cm, which reduces the image potential to levels that can be neglected.

The EFE can now be used to calculate the number of electrons approaching the interface at “a” with energies between  $\varepsilon_x$  and  $\varepsilon_x + d\varepsilon_x$ . In the absence of any temperature or electric field gradients, the electron flow must exist in steady-state (thus net flow equal to 0) implying the current traveling from the left across “a” must equal the current traveling from the right across “a”. The Fermi level in the crystal “ $E_f$ ” is located at  $\mu_s$  which is referenced here as positive. The thermal equilibrium condition previously noted allows for the Fermi levels on either side of the cavity to be at the same energy thus aligned. Using the EFE, the equations for the electron currents in both directions can be written as:

$$N_{x,s}d\varepsilon_x = \frac{2(2\pi mkT)}{h^3} \ln \left( 1 + e^{-\frac{\varepsilon_x - \mu_s}{kT}} \right) d\varepsilon_x \quad (3.5)$$

$$N_{x,c}d\varepsilon_x = \frac{2(2\pi mkT)}{h^3} \ln \left( 1 + e^{-\frac{\varepsilon'_x - \mu_s}{kT}} \right) d\varepsilon_x \quad (3.6)$$

where  $N_{x,s}$ : electrons flowing from the surface across “a” and  $N_{x,c}$ : electrons flowing from the cavity across “a”.

The steady-state electron flow provides that Equations 3.5 and 3.6 must be equal allowing for Equation 3.7 to be realized.

$$\varepsilon_x - \varepsilon'_x = \mu_s - \mu_c = W_a \quad (3.7)$$

The work function seen in the Richardson equation of the crystal can then be defined upon inspection of Equation 3.7 and is represented in Equation 3.8.

$$\frac{-\mu_c}{e} = \frac{W_a - \mu_s}{e} = \Phi \quad (3.8)$$

Finally, the Richardson equation can be seen by integrating Equation 3.5 with respect to  $\epsilon_x$  using limits of integration from  $W_a$  to  $\infty$  and using the definition of work function from Equation 3.8 to arrive at the total electron current that crosses the boundary at “a” from the surface.

$$J_s = \frac{4\pi mk^2 e}{h^3} T^2 e^{-\frac{\Phi}{kT}} \quad (3.9)$$

with the Richardson constant A defined as:

$$A = \frac{4\pi mk^2 e}{h^3} = 120 \text{ A/cm}^2\text{K}^2 \quad (3.10)$$

Though, the above derivation proves fairly straight forward, it must be kept in mind that, at the time the Richardson equation was developed, the physics community was just beginning to fully understand the structure of the atom. This perhaps explains why so many years passed between the time Edison first noted his observations of the electron current arising from his light bulb filaments in the 1880’s and when it was described by Richardson and Dushman in the early 1900’s.[3, 22, 107, 108]

### 3.2 Thermionic energy conversion

With an understanding of thermionic emission in place, applications in which it can be utilized can now be discussed. This section seeks to describe in detail one such application, thermionic energy conversion. There are several possible ways to conceptualize a thermionic energy converter. One possible conceptualization was presented by R.S. Rasor describing a thermionic energy converter as a thermodynamic heat engine cycle similar to a modified Rankine cycle.[111] All heat engines require a working fluid which Rasor portrays as electrons. The function of the cathode in such a heat engine is to act as an “electron boiler” while the anode functions as the electron condenser. These two components result in an electric pressure

(i.e. voltage) difference to produce work. The difference between the heat of vaporization of the electrons from the emitter and the heat of condensation of the electrons into the collector directly equals the amount of electrical work produced per electron.[111]

In a more general description, a thermionic energy converter consists of three components: a cathode, an anode, and the necessary electrical connections between the two. In a basic thermionic converter, the cathode and anode are separated by a vacuum gap. There exist other configurations that incorporate gaseous species into this gap to improve performance and will be discussed later. As thermal energy is imparted to the cathode, electrons with sufficient energy will thermionically emit from the surface and accelerate through the vacuum gap where they collect at the anode. The electrons then drive a load as they are cycled back to the cathode through the electrical connections. Though conceptually simple, there are several factors that must be considered for an efficient device to be realized.

From the above description, a cathode must be chosen with superior thermionic emission abilities for use in a thermionic energy converter. Referencing the Richardson equation, this can be accomplished by having a low work function with a high Richardson constant. Electrons leaving the cathode must then experience an electromotive force (EMF) to be accelerated through the vacuum gap. This EMF arises from the work function difference between the cathode and anode thus requiring an anode with a lower work function than the cathode. As thermionic emission from the anode must also be accounted for, an anode must be chosen that acts as a poor thermionic emitter implying a material with a high work function and low Richardson constant be selected. It can then be seen that two conflicting requirements have been presented: it is desired to have an anode with a high work function to prevent reverse electron emission yet the anode must have a lower work function than the cathode to create an EMF to

accelerate the electrons across the vacuum gap. G. Medicus and G. Wehner were the first to note these requirements in 1951.[112] Indeed, these conflicts have proven to be a major design hurdle for the construction of an efficient thermionic energy converter.

### 3.3 Thermionic energy converter design considerations

The criteria that must be accounted for when constructing an efficient thermionic energy converter will now be further elaborated upon. As previously mentioned, a basic thermionic converter consists of a cathode and an anode separated by a vacuum gap. In the absence of an applied electric field, the only potential driving electrons through the gap is the work function difference between the cathode and the anode. As small cathode-anode separation distances are typically difficult to achieve, the resulting field is often small, permitting the creation of a space charge region immediately in front of the cathode. P.M. Marchuk first presented an alternate method of mitigating this space charge by incorporating an ionizing vapor into the vacuum gap and will be discussed in detail later.[113] The presence of this space charge region requires electrons to have higher energies than simply the work function in order to be emitted. A band diagram from a study by J. Ingold, presented in Figure 3.2, helps to clarify this.[21]

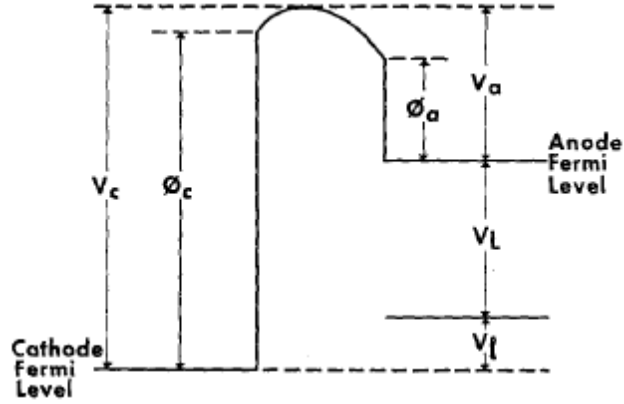


**Figure 3.2** Potential diagram of a thermionic energy converter showing the increased potential barrier electrons must overcome in order to be emitted into the vacuum in the presence of a space charge region.[21]

The band diagram of a thermionic energy converter in Figure 3.2 allows for a mathematical description of the electrical output characteristics to be presented. The new barrier,  $V_c$ , seen in Figure 3.2 resulting from the space charge requires the Richardson equation to be rewritten to incorporate  $V_c$  instead of the cathode work function,  $\Phi_c$ .

$$J_c = A_c T_c^2 \exp \left[ - \left( \frac{eV_c}{kT_c} \right) \right] \quad (3.11)$$

With:  $J_c$ : the cathode thermionic emission current;  $A_c$ : cathode Richardson constant;  $T_c$ : cathode temperature; and  $V_c$ : cathode potential barrier for electron to be emitted into the vacuum.[21]

The reverse emission from the anode must then also be accounted for as thermionic emission occurs from all materials when heated to temperatures above 0K. An equation can be derived for this anode reverse emission current similar to that shown for the cathode current in Eq. 3.11 using the Richardson equation as seen below.

$$J_a = A_a T_a^2 \exp \left[ - \left( \frac{eV_a}{kT_a} \right) \right] \quad (3.12)$$

Where  $J_a$ ,  $A_a$ ,  $T_a$ , and  $V_a$  are defined in the same manner as Equation 3.11 but with respect to the anode.[21]

To derive the theoretical efficiency and power output capabilities of a thermionic energy converter it must be assumed that the device is in steady state. That is, the heat input from the cathode equals the heat loss from the cathode. The heat loss from the cathode is dominated by three mechanisms: 1) Cooling from the electron emission:  $P_e$ ; 2) Radiated heat loss from the cathode:  $P_r$ ; and 3) Heat conducted away from the cathode through the electrical connections:  $P_l$ . Equations for these three terms (assuming the reverse emission from the anode is negligible) were derived by J. H. Ingold in 1961 and can be seen below in Equations 3.13-15 with descriptions of the variables presented in Table 3.1.[21]

$$P_e = J_c(V_c + 2\theta_c) \quad (3.13)$$

$$P_r = \epsilon\sigma\left(\frac{e}{k}\right)^4 (\theta_c^4 - \theta_a^4) \quad (3.14)$$

$$P_l = \left(\frac{k}{a_c}\right)\left(\frac{a}{l}\right)\left(\frac{e}{k}\right)(\theta_c - \theta_o) - \frac{1}{2}J_c^2 a_c \rho \left(\frac{l}{a}\right) \quad (3.15)$$

**Table 3.1** Description and definition of symbols used in Equations 3.13-15 which describe the three mechanisms of heat loss for a thermionic energy converter in operation as described by J.H Ingold[21]

Symbol	Meaning	Units
$J_c$	Cathode thermionic emission current density	A/m <sup>2</sup>
$\theta_c$	$kT_c/e$	V
$\theta_a$	$kT_a/e$	V
$\theta_o$	$kT_o/e$	V
$T_c$	Cathode temperature	K
$T_a$	Anode temperature	K
$T_o$	Ambient temperature (load temperature)	K
$\epsilon$	Effective emissivity of cathode	unitless
$\sigma$	Stephan-Boltzmann constant	W/m <sup>2</sup> *K <sup>4</sup>
$k$	Thermal conductivity of cathode lead	W/m*K
$\rho$	Electrical resistivity of cathode lead	$\Omega$ *m
$a$	Cross-sectional area of cathode lead	m <sup>2</sup>
$l$	Length of cathode lead	m
$a_c$	Cathode surface area	m <sup>2</sup>

The energy conversion efficiency,  $\eta$ , of a thermionic energy converter can then be described using Equations 3.11-15. Equation 3.16 below is one expression for  $\eta$  that was presented by J.H. Ingold in 1961 which made the assumption that the reverse thermionic emission from the anode is negligible.[21]

$$\eta = \frac{J_c V_L}{J_c(V_a + V_L + V_L) + 2J_c\theta_c + P_r + P_l} \quad (3.16)$$

A separate study by J.M. Houston in 1959 obtained a similar equation for the efficiency without neglecting the reverse emission from the anode. Houston concluded that an ideal thermionic converter could obtain efficiency values of up to 90% of the Carnot efficiency.[20] This extremely high energy conversion efficiency greatly exceeds many of the current technologies thus leading to the impetus behind this research.

### 3.4 Production thermionic energy converters

Thermionic energy conversion (TEC) is not a new concept. During the early to middle 20<sup>th</sup> century both the USA and USSR began intensive research on this technology driven by the need for compact, reliable, efficient energy conversion methods for space applications. The design configuration pursued by both countries is known as the “in-pile thermionic generator.”[111, 114] This configuration utilized the same cylindrical fuel rods used in other nuclear reactor technologies but employed the cladding around the fuel rod to act as a cathode. The anode was positioned around the cathode separated by cesium-vapor filled gap cooled by the reactor’s liquid metal coolant. Another typical variation used for space application consisted of heating the cathode by the reactor’s liquid metal coolant and using the coldness of space as a heat sink for the anode.[115]

The first practical TEC device, demonstrated by P.M. Marchuk in the USSR in 1956, incorporated a cesium vapor into the vacuum gap to mitigate space charge effects.[113, 114] Although the United States later followed, they eventually abandoned this research for space applications while the USSR continued to make advancements.[114] Between 1970 and 1984, the USSR designed and implemented two TOPAZ type in-pile reactor units to power the COSMOS satellite. The next generation generator, TOPAZ-II, was developed for future missions to Mars but was never implemented as interest in these missions faded.[115] Regardless, the Soviet TOPAZ reactors were able to achieve impressive power generation capabilities. A typical TOPAZ reactor required only around 11 kg of Uranium<sup>235</sup> and was able to output 5kW of power from the 150kW of thermal power generated from the nuclear source.[116] As of 2000, the Russian Federal space agency that emerged after the fall of the Soviet Union had resumed

research on TOPAZ type reactors for deep space mission that could deliver tens to hundreds of kilowatts for periods of up to 10 years.[116]

Radionuclide thermionic generators were another implementation of thermionic energy conversion that gained interest during the middle part of the 20<sup>th</sup> century. The isomite battery is one such example of a radionuclide thermionic generator developed by McDonnell Douglas Co. These fairly small cells, measuring up to 3 cm in height and diameter, operated at relatively low cathode temperatures leading to poor efficiencies of less than 1%. These low efficiencies combined with the relatively low output power (1-20mW) led to the eventual abandonment of this technology.[115]

### 3.5 Current thermionic cathodes

As seen from the Richardson equation, virtually any material can theoretically function as a thermionic cathode but certain materials exhibit much higher thermionic emission performance than others. It has been previously stated that materials with low work functions and high Richardson constants are the most desired for thermionic applications. The remaining part of this chapter is devoted to discussing a few of the current technologies in use today.

#### 3.5.1 Metallic cathodes

Typical metallic thermionic emitters utilize metals such as tungsten, tantalum, and rhenium. The high work function of these materials often requires high operating temperatures in order to achieve the desired current levels. High temperatures can be advantageous in certain circumstances as they allow for electronegative contaminating gases to rapidly evaporate allowing such cathodes to operate in relatively poor vacuum conditions. This property explains

why metallic materials are often chosen for use in ionization gauges for pressure measurement.[117]

Early thermionic applications often utilized bare tungsten emitters; however, the high temperatures required for such cathodes to achieve practical current densities often resulted in immense power requirements and created several engineering challenges. Given these reasons, the use of bare tungsten cathodes was abandoned for use in the vast majority of thermionic applications in favor of other, better performing materials. Surprisingly, it was later found that by contaminating a tungsten cathode with electropositive elements such as thorium and cesium, the work function could be lowered, allowing for increased thermionic emission currents at lower temperatures than with pure tungsten.[118, 119] Table 3.2, reproduced from a review paper by R. O. Jenkins, compares the various tungsten contaminants with respect to the work function.

**Table 3.2** Comparison of tungsten surface contaminant on the work function[119]

Surface Contaminant	Work Function (eV)
Clean	4.54
Ce	2.7
Th	2.7
Ba	1.6
Cs	1.5

As can be seen in Table 3.2, extremely low work functions can be achieved by contaminating a tungsten emitter. However, the surface contaminant usually evaporates when the cathode is heated to operating temperatures, thus requiring the contaminant to be constantly replenished.[119] This constraint limits the applicability of this type of cathode with a few exceptions. For example, several practical implementations of thermionic energy converters

utilize cesium coated tungsten cathodes in which the problem of contaminant evaporation is solved by the incorporation of cesium vapor into the vacuum gap. This not only provides a means to replenish the evaporated cesium but also mitigates the space charge problem previously discussed.[114]

### 3.5.2 Oxide coated cathodes

In 1904, A. Wehnelt made the discovery that the introduction of an oxide layer on a metallic emitter could greatly enhance the thermionic emission current. In his experiment, Wehnelt coated platinum cathodes with various oxides. He found that oxide coatings composed of rare-earth metals such as barium, strontium, and calcium allowed for large increases in thermionic emission current at comparatively low temperatures.[120] It is now known that these observations were due to the extremely low work functions of the oxide cathodes. Table 3.3 shows the work function and Richardson constant of a few commonly used oxides.

**Table 3.3** Comparison of the work function values and Richardson constant values of some commonly use thermionic cathode oxide coatings[120]

Oxide Composition	$\Phi$ (eV)	A (Amps/cm <sup>2</sup> K <sup>2</sup> )
CaO	1.77	129 - 249
SrO	1.27	4.07 - 258
BaO	0.99	2.88 - 272
CaO + SrO + BaO	1.24	0.0083

Though oxide coated cathodes exhibit the desired low work functions and high Richardson constants, attempts to extract more than  $\sim 1$  A/cm<sup>2</sup> dc current can cause rapid degradation of the oxide coating. Due to this, oxide coated cathodes are most commonly used in low power dc or short pulse high power devices.[119]

### 3.5.3 Lanthanum Hexaboride cathodes

Lanthanum hexaboride (LaB6) has become a widely used cathode for precision and state-of-the-art applications. LaB6 cathodes have the advantage of long operating lifetime, low work function, and chemical stability at high operating temperatures over other cathodes.[121] Despite these advantages, the high cost (arising from complex fabrication processes) has limited the use of LaB6 to high-end applications such as electron microscopy.[122]

### 3.6 Overview

The topics discussed in the chapter are meant to provide the reader with at least a basic knowledge of thermionic emission and its application in energy conversion so that the research presented in the following sections can be better understood. The vast potential of thermionic energy conversion technology has been outlined such that the motivation of this research can be appreciated. Though diamond was not examined explicitly in this chapter, the discussions presented in *Chapter II* should allow the conclusion to be reached that diamond is perhaps the most promising material for the creation of a practical thermionic energy converter. The research presented in the following chapters seeks to further the understanding of diamond for this purpose.

## CHAPTER IV

### PROPOSED RESEARCH AND APPROACH

The purpose of this research is to study diamond cathodes for use in thermionic emission applications by exploring various methods to increase the emission current output, stability, and operational lifetime. This has been achieved by directing research into two main areas. The first area investigates methods to modify the diamond cathodes to achieve higher emission current levels at lower temperatures than typical as-grown diamond cathodes. This part of the research deals with the study, development, and characterization of various hydrogen (and deuterium) plasma exposures to diamond samples which is thought to beneficially enhance their thermionic emission properties but has never been quantitatively examined in detail. The second part of the research investigates operational environment as a means to increase the performance of diamond cathodes. This is accomplished by observing the response of thermionic emission current to the introduction of various low pressure gaseous species. The following section summarizes the significance of this research and presents the approach used to achieve these goals.

#### 4.1 Introduction to the proposed research

Thermionic energy conversion (TEC) drew a great of deal attention during the mid-20<sup>th</sup> century as an efficient means of directly converting thermal energy into electrical energy.[20, 21, 111, 114, 123] However, due to material limitations of the day, the vast potential of this technology was never reached. TEC is based on the widely understood physical principal of thermionic emission which describes the thermal emission of electrons from a heated cathode.

As a cathode is heated above zero Kelvin, it can be predicted, based on Fermi-Dirac statistics, that some of the cathode's electrons will have energies equal to or greater than the cathode's work function. The work function is the energy required for an electron to be emitted into the vacuum. This process can be described by the Richardson equation (Equation 4.1).[22, 109]

$$J = AT^2 e^{-\Phi/kT} \quad (4.1)$$

Where: J: Current Density ( $A/cm^2$ ); A: Richardson Constant ( $A/cm^2K^2$ ); T: Temperature (K);  $\Phi$ : work function (eV); and k: Boltzmann constant ( $8.617 \times 10^{-5}$  eV/K). It follows from the Richardson equation that high thermionic emission current densities can be achieved from a material with a high Richardson constant and a low work function.

As mentioned earlier, the idea of utilizing this phenomenon for energy conversion is not new. During the mid-20<sup>th</sup> century, a great deal of research went into thermionic energy converters in an attempt to achieve an efficient means of converting thermal energy into electricity with limited success. Some approaches did achieve useful output currents of  $\sim 20 A/cm^2$  at an output voltage of between 0.5V to 1.5V and operated continuously for 5 or more years.[111, 114] Unfortunately these devices were handicapped by low operational efficiencies ( $\sim 20\%$ ) due to material limitations leading many researchers to de-emphasize thermionic converters in favor of other conversion techniques. At the time of this technology's peak interests, the best available materials had work functions between 4 - 5 eV which corresponds to useable current densities only at temperatures exceeding 2000 °C. Although effective work functions could be lowered (e.g. by modifying the surface with cesium) these adsorbate techniques typically do not hold up to high fields or long operation times. Also, the thermal sources required for the very high operation temperatures of past TEC devices (e.g., nuclear

pile), limited this technology to unmanned space operations due to safety considerations.[111, 114]

The preceding sections have presented a detailed background for the proposed research that will now be discussed. The objective of this research is to explore means to increase the thermionic emission performance of diamond cathodes for use in thermionic applications. The primary motivation for this research lies in TEC which has the capability to revolutionize today's energy climate by providing one of the most efficient methods of converting thermal energy directly into electrical energy.[20, 21] Studies have shown that this technology can approach total energy conversion efficiencies of 90% of the Carnot limit, which is a vast improvement over current technologies.[20, 21] Impacts of this research could potentially stem beyond TEC into other applications that utilize thermionic emission including fluorescent lighting, electron microscopy, and cathode ray tube (CRT) displays, among others. The following sections outline the tasks performed to accomplish the goals of this research.

#### 4.2 Fabrication of nitrogen-incorporated diamond thermionic cathodes

The proposed research seeks to utilize diamond as the cathode material in a thermionic energy converter. Intrinsic single crystalline diamond is an extremely poor electrical conductor with a large bandgap of 5.5eV making it an unsuitable candidate for electronic applications such as thermionic emission.[50] The electronic properties of diamond can be improved through the incorporation of certain impurities into the diamond lattice.[36, 56, 58] Further, the use of polycrystalline diamond has been shown to have enhanced electron transport over single crystalline diamond.[124] Previous work examining polycrystalline, p-type, boron-doped, diamond films revealed this type of diamond to be a reliable thermionic electron emitter that

closely followed the Richardson equation. However, the emission current at temperatures up to and exceeding 1,100°C was too low to prove useful in most thermionic applications.[125] In order to extract more current at lower operating temperatures, this research employs diamonds with n-type semiconducting behavior.

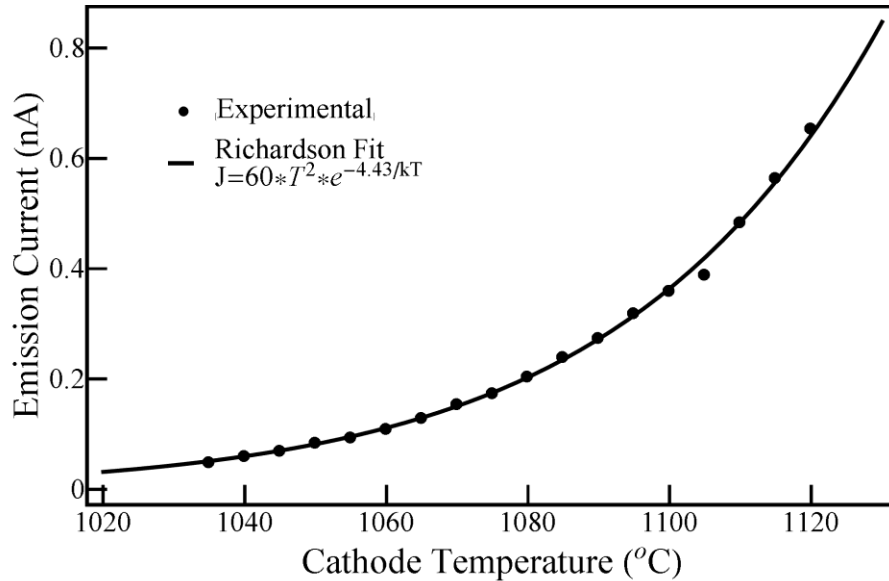


**Figure 4.1** Thermionic emission results from previous work on a boron-doped polycrystalline diamond film. It can be seen by the solid line that the emission current data (points) followed closely with the Richardson equation. Thermionic emission current obtained from this sample was too low to be practical due to the high work function of 4.43 eV.[125]

As discussed in Section 2.5, diamond suffers from an asymmetrical doping complex in that n-type behavior is much more difficult to achieve than p-type behavior.[36] Among the possible n-type dopants, sulfur, phosphorus, and nitrogen have garnered the most attention. Successful incorporation of sulfur and phosphorus into the diamond lattice has been achieved allowing diamond to behave as a traditional n-type semiconductor while attempts to use nitrogen have proven more complex.[36, 58] Though nitrogen readily incorporates into the diamond

lattice during fabrication, its deep donor level positioned 1.7eV below the conduction band would typically imply that impractically high temperatures would be required to activate the nitrogen dopants to achieve n-type behavior.[59, 60] Still, studies have demonstrated that nitrogen-incorporated diamond can indeed act as a typical semiconductor. It is believed that the incorporation of nitrogen promotes defect induced energy bands within the bandgap allowing for conduction band carrier “hopping” which increases electron transport with n-type behavior.[60]

The present research will use nitrogen as the incorporated species in the diamond thermionic cathodes for several reasons with the primary reason being deposition concerns. It was mentioned in Section 2.6 that many widely used techniques to dope typical semiconductors are not favorable with diamond. The most successful and widely used method for doping diamond is through the incorporation of dopant gases into the chamber during deposition. The gas species often used for n-type doping, phosphorus and sulfur (in the form of phosphine and hydrogen sulfide respectively), are both extremely toxic gasses. Conversely, the incorporation of nitrogen requires only the use of N<sub>2</sub> gas which is nontoxic at the amounts used during chemical vapor deposition. Further, a substantially larger portion of previously reported work has examined nitrogen as it is the primary defect found in naturally occurring diamond.[126, 127]

A suitable method has been identified for the fabrication of nitrogen-incorporated diamond samples using Microwave Plasma-enhance Chemical Vapor Deposition (MPCVD). In this method, the plasma is maintained with hydrogen while methane is fed in as the carbon source. Dry nitrogen gas is also fed into the chamber in order to make the films nitrogen-incorporated. As previous studies have demonstrated that graphite has a relatively high work function, it is desired to deposit samples with minimal graphitic content.[128] This can be accomplished by depositing the films in a “methane starved” environment which has been shown

to drastically reduce carbonaceous content other than diamond.[27, 37]The quality of the films can then be assessed by means of Raman spectroscopy and scanning electron microscopy.

#### 4.3 Characterization of the thermionic emission from diamond films

Multiple methods have been used in the past to characterize a material's thermionic emission properties. A common method is through the use of an electron energy analyzer which provides a spectrum of electrons emitted from the sample.[129] Electron emission can be stimulated by either thermal energy causing thermionic emission or electromagnetic energy causing photo emission. By analyzing the spectrum of the emitted electrons, a detailed analysis of the range of emitted electron energies can be made allowing for highly accurate work function values to be calculated from the tested sample.[129] Unfortunately, these described methods using electron energy analyzers have several disadvantages. They are not able to determine the sample's total output current as a function of temperature which prevents calculation of the sample's Richardson constant. Additionally, electron energy analyzers, for thermionic emission tests, only allow for measurements to be taken at a single temperature at a time.

Other more practical methods use simpler setups consisting of a heated cathode and positively biased anode separated by some known distance in a vacuum. Infrared radiation is often used in such testing apparatuses as it is a non-contact method and can achieve relatively high temperatures.[74, 105] Being a non-contact method is advantageous as it does not introduce another circuit into the testing configuration allowing for typical low-side current monitoring and simple temperature measurements using a thermocouple. This type of testing configuration is graphically depicted in Figure 4.2.

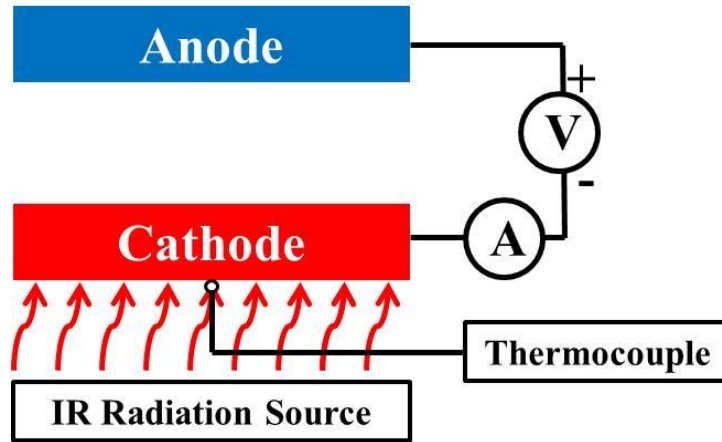


**Figure 4.2** Schematic diagram of a typical thermionic testing configuration

Difficulty arises when attempting to control the temperature of IR radiation sources as it is slow, making it problematic to obtain exact temperatures. Further, this slow temperature response makes the implementation of a PID (Proportional, Integral, and Derivative) control loop challenging, thus preventing the isothermal emission current testing. IR radiation sources are also expensive and require large amounts of power to achieve the temperatures necessary for thermionic experiments. This research uses a modified version of Figure 4.2 where instead of using an infrared heat source, the samples are resistively heated with DC power, allowing for precise, almost instantaneous temperature control. Though this method solves the problems of temperature control when using an IR radiation source, the ability to measure the sample's temperature becomes more difficult as it introduces an additional circuit into the apparatus. A thermocouple cannot be applied because it is a contact method. Contacting a thermocouple to the heating circuit will output erroneous temperatures because it will draw current. It may be possible to avoid this problem by coating the thermocouple with an electrically insulating material that has a high thermal conductivity such as boron nitride. Rather than attempt this and risk inaccurate temperature measurements, it has been concluded that a non-contact temperature

monitoring method such as a pyrometer should be used. The exact testing apparatus will be discussed in detail in the following chapter.

#### 4.4 Investigation of hydrogen's influence on thermionic emission

As discussed in detail *Chapter II*, hydrogen is responsible for many of the enhanced electronic properties of diamond. It has been widely documented that hydrogenated diamond films exhibit extremely low to negative electron affinities.[67, 68, 73] Additionally, hydrogen drastically increases the electron transport in the bulk of the diamond leading to low resistivities.[65] Both of these effects have the potential to enhance the thermionic emission capabilities of diamond films. Though many studies have seen hydrogen enhance the thermionic emission from diamond films, no detailed studies have been made linking the two. This research examines the hydrogenation process of diamond films in an effort to provide a better understanding of the mechanism and its effects. This research performs the most detailed study to date on the topic of hydrogen's influence on the thermionic emission from diamond films.

Diamond films were deposited via MPCVD in a hydrogen-rich environment as mentioned above. The as-grown diamond samples were then tested to observe their thermionic emission properties. The samples were subsequently taken to temperatures exceeding 800°C in to remove all beneficial effects of the hydrogen from the deposition process. The samples were then be retested to study their de-hydrogenated thermionic performance. Following the second test, the samples were placed back into the MPCVD chamber and exposed to various hydrogen plasma treatments and tested a third time to assess how the exposure affects the emission properties.

The present research also examines the influence of hydrogenation treatment variables such as plasma power, sample temperature, chamber pressure, and treatment time. For each variable, 3-4 different hydrogenation treatments were performed, each with a new sample.

#### 4.5 Determination of the activation energy of hydrogen in diamond

Desorption of hydrogen from diamond films has hindered attempts to utilize diamond thermionic emitters as all beneficial effects appear to completely diminish when the samples are heated to temperatures exceeding  $\sim 700^{\circ}\text{C}$ . In order to address this occurrence, a better understanding of the desorption process is in order. Numerous studies have attempted to determine the activation energy of the hydrogen desorption process from diamond with varying success. All methods currently considered require complex and expensive equipment that typically only allow for one or two measurements to be made.[78-84] The present research seeks to further advance understanding beyond previous research by examining the isothermal emission current behavior of diamond films.

As mentioned earlier, the superior electron emission properties of diamond have been attributed to the surface hydrogen induced negative electron affinity. It has been proposed that the negative electron affinity results from a surface dipole layer formed by carbon-hydrogen bonds which creates a potential drop at the surface.[67, 68, 73] Assuming this is true, the desorption of a hydrogen atom from a surface site would result in a vacancy with a higher electron affinity (and also a higher work function) at that site implying a direct correlation between surface hydrogen concentration and electron emission current.

The assumption that the amount of thermionic emission current is directly proportional to the amount of hydrogen in the samples is the basis of the next experiment. Diamond films were

synthesized via MPCVD and first tested both to characterize their as-grown thermionic emission properties and also to remove hydrogen present from the deposition processes. The samples were then re-hydrogenated and placed back into the thermionic testing chamber. The emission current of the samples was then characterized isothermally. A PID control was constructed and implemented into the testing apparatus allowing the sample to be heated to and maintain a desired temperature over an extended period of time. It was initially believed that the emission current from the samples would decrease over an extended period of time as hydrogen desorption occurs. This current was then be analyzed with respect to the integrated rate equations to determine the activation energy of hydrogen in diamond. This experiment was executed for multiple samples at several different temperatures performing a detailed study of the hydrogen activation energy in diamond beyond what is presently known.

#### 4.6 Exploration of deuterium as an alternative to hydrogen

The primary objective of this effort is to enhance the performance of diamond cathodes for use in a thermionic energy converter. As has been shown, the beneficial effects of hydrogen begin to diminish at temperatures exceeding 700°C. Therefore, alternate species should be examined that could result in more emission at higher temperatures. Deuterium is one possible approach as it has similar properties to hydrogen but with twice the mass. This higher mass leads to the carbon-deuterium bond having a lower vibrational frequency than the carbon-hydrogen bond, thus requiring more energy to break the carbon-deuterium bond and, in turn, a higher activation energy. It then follows that a diamond cathode exposed to a deuterium plasma treatment (deuterated) might be able to emit at higher temperatures than a similar hydrogenated sample. Due to the high cost of deuterium compared to hydrogen, it would be impractical to

substitute deuterium for hydrogen during the deposition process. Rather, gas supplies were conserved by only performing deuterium treatment on samples grown in the standard hydrogen-rich, methane-starved environment that had been de-hydrogenated.

#### 4.7 Investigation into the operation of diamond in gaseous environments

Past implementations of thermionic energy converters utilized tungsten cathodes with cesium gas fed into the cathode-anode gap.[114, 123, 130-133] The cesium served two purposes. Tungsten has a relatively high work function requiring high temperatures (in excess of 2000°C) in order to achieve practical thermionic current densities. The work function can be lowered by “cesiating” the tungsten surface.[114, 123, 130] The effects of the cesium rapidly diminish during operation as the tungsten outgases when heated to operating temperatures. By incorporating cesium gas into the interelectrode gap, the cesium in the tungsten could be constantly replenished allowing for stable operation.[123] In addition to enhancing the surface chemistry, operation of tungsten cathodes in a cesium vapor environment (rather than a vacuum) has been shown to favorably affect the electron transport from the cathode to the anode.

The high emission currents required to produce necessary output power levels for TEC applications often results in space charge effects. Space charge effects are due to the negatively charged electrons traversing the cathode-anode gap which cancel out a portion of the electric field between the cathode and anode. More electrons present in the gap equate to more canceling of the electric field, further suppressing the emission current. This performance limiting effect can be mitigated (or even eliminated) through the presence of positive cesium ions in the cathode-anode gap. One method to introduce these ions is through surface ionization. When a tungsten cathode is heated to temperatures in excess of 1200 °C, I. Langmuir and K.H. Kingdon

showed that all cesium atoms that strike it are ionized resulting in positively charged cesium ions.[123, 134] These positive charges present adjacent to the emitter surface will cancel out the negative charges of the electrons, reducing the space charge effect. Cesium ions can also be produced by collision of cesium atoms with the thermionically emitted electrons from the cathode.[133] In order for ionization to occur, electron temperatures greater than 2500°C are required.[135] As this study seeks to improve the low temperature (<1000°C) thermionic emission performance of diamond films, gaseous species must be examined that produce positive ion products without the excessive heat requirements of cesium.

Hydrogen interaction with the diamond surface has been shown to be somewhat analogous to the interaction of cesium with tungsten. The exposure of diamond films to hydrogen plasma treatments creates polarized C-H surface bonds which lower diamond's electron affinity to negative levels directly correlating to a lower work function.[73] Thus, hydrogen containing gaseous species appear to be the most suitable candidates to enhance the thermionic emission performance of diamond. The next part of this research characterizes five different gaseous species, three of which are hydrogen containing. It is desired to identify a gaseous species which could interact similar to cesium which both replenishes the hydrogen desorbed from the diamond during operation and also mitigates the space charge effects arising between the cathode and the anode.

Ideally, both the current vs. temperature and isothermal emission current operation of diamond films in a vacuum environment with the operation in each gaseous species would be compared. However, this would prove extremely difficult as testing alone is predicted to alter the emission current due to hydrogen desorption (i.e. testing requires the films to be heated). Further, the polycrystalline nature of the deposited diamond leads to slight variations between samples

implying that each will emit differently making comparisons between samples unsuitable. These problems were solved by examining the thermionic emission from diamond films in both a vacuum environment and a gaseous environment in one test. The samples were first isothermally heated to a desired temperature. The emission current of the sample operating in vacuum was then taken. After some period of time, a gaseous species was introduced into the chamber and the change in emission current observed. This testing method allowed for the influence of each gas on the thermionic emission to be assessed while also eliminating error that could arise from the other methods previously mentioned.

## CHAPTER V

### DEVICE FABRICATION AND TESTING APPARATUS

This chapter focuses on the two most crucial parts of this research: the deposition of diamond films as thermionic cathodes and the construction of testing apparatuses capable of characterizing the thermionic emission properties of such cathodes. The deposition process used to deposit diamond films for this research is discussed as well as characterization techniques employed to assess the quality of the films. This chapter also describes in detail the two testing apparatuses designed for this research. The information within this chapter is essential to fully comprehending the validity of the studies presented in the subsequent chapters and will be frequently referenced.

#### 5.1 Deposition and characterization of diamond films

A deposition method was identified for the growth of nitrogen-incorporated polycrystalline diamond films for use in thermionic emission applications. The method described below allowed for diamond films with large grain sizes on the order of micrometers with minimal non-diamond carbonaceous content to be fabricated.

##### 5.1.2 Sample preparation and deposition process

Diamond samples were deposited on molybdenum 125 $\mu\text{m}$  molybdenum strips. The geometry of these substrates (30 mm length x 2 mm width x 125  $\mu\text{m}$  thick) was chosen such that they could easily be heated to temperatures approaching 1000 $^{\circ}\text{C}$  without excessive power requirements, yet sturdy enough that the fabricated samples could be easily handled.

Molybdenum was the substrate material of choice for several reasons. First, it is a material that readily forms a stable carbide which has been documented to be favorable for diamond growth and adherence.[27] Second, studies have reported that the molybdenum-diamond interface is extremely well behaved with ohmic behavior.[105] Finally, molybdenum is more resistant to hydrogen embrittlement than other materials such as tungsten which allows for straightforward handling of the sample post-deposition.[28, 136]

The preparation of the molybdenum substrate for deposition began with a mild abrasion of the substrate's surface. This step removes surface contaminants allowing for a cleaner surface. Additionally, this step promotes surface defects sites which have been shown to promote diamond nucleation during the beginning of the deposition process.[28, 31] Following the abrasion, the substrates were mechanically nucleated using a nanodiamond paste/methanol mixture. The nanodiamond particles present in the mixture become embedded in the defects introduced by the abrasion and act as seeds, thereby expediting the growth process. Excess nanodiamond paste was wiped off and the samples were then placed in the MPCVD chamber for deposition. Deposition was performed on four samples concurrently to provide a set by which the emission current could be compared directly.

The MPCVD chamber was first pumped down to its ultimate pressure of around 2 mTorr. To ensure all residual air particles were removed, hydrogen was flowed through the chamber for several minutes. The hydrogen was then turned off and the substrate stage heated to 750°C. The deposition process then began with the following parameters: 20 Torr chamber pressure, 400 SCCM (standard cubic centimeters) H<sub>2</sub>, 5 SCCM CH<sub>4</sub>, and 550 W microwave power. After the plasma was initiated and observed to be stable, the substrate stage temperature set point was then changed to 900°C. While the temperature was heating to the new set point, the pressure and

microwave power were simultaneously slowly increased to 50 Torr and 1500 W, respectively. The increasing of the pressure and microwave power took several minutes in order to maintain the integrity of the plasma. Finally, the H<sub>2</sub>, CH<sub>4</sub>, and N<sub>2</sub> flow rates were set to 450, 3.5, and 15 SCCM, respectively. This process was carried out for roughly 30 hours for each set of samples or until the diamond films achieved complete substrate coverage. Safety protocol prevented the MPCVD chamber from operating unattended overnight requiring the deposition process to cease during the evening and resume the following morning. Before restarting the processes each morning, the chamber was vented and the samples rotated in order for the diamond growth to achieve uniform film coverage. The process was deemed complete only after all of the molybdenum substrate was no longer visible.

### 5.1.3 Characterization of diamond samples

The films were first inspected via scanning electron microscopy. From the scanning electron micrograph of a film deposited under the previously discussed conditions (Figure 5.1), it can be seen that the samples exhibited a grain size on the order of several micrometers. Determination of the crystal orientation from the image was difficult due disintegration crystals arising from the repeated interruption of the deposition process for inspection of the samples.[137] Several smooth square faces which appear to be tilted with respect to the substrate can be discerned in Figure 5.1 typical of polycrystalline diamond samples incorporated with nitrogen.[61] To further investigate the crystallographic orientation of the samples, a separate sample grown uninterrupted under the same conditions for less time was imaged. Though uniform coverage was not obtained, the scanning electron micrograph of this sample in Figure 5.2 reveals both well-defined, smooth, 100 faces along with deteriorated 111 faces.

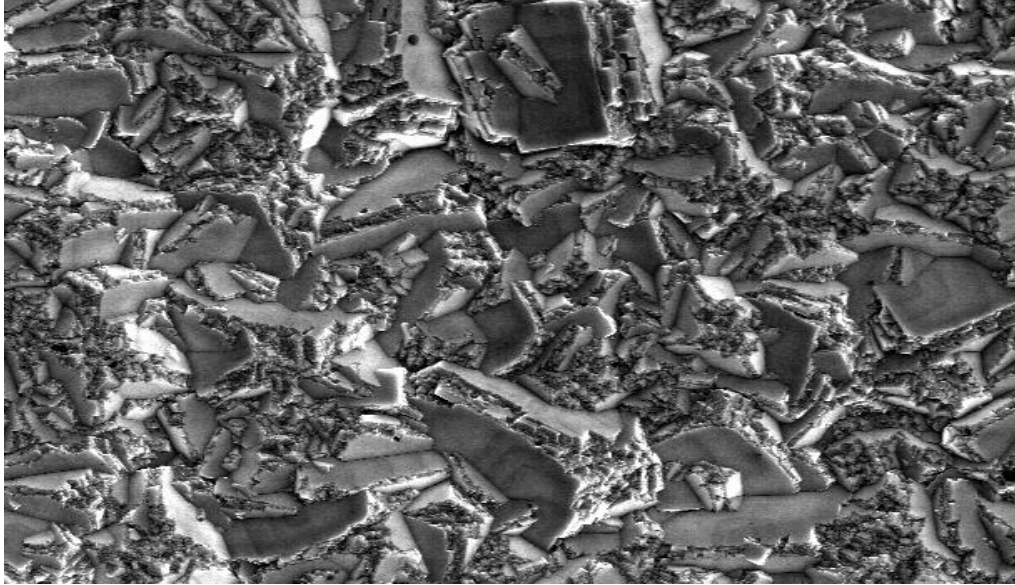


**Figure 5.1** Scanning electron micrograph of a diamond sample grown under the previously described conditions

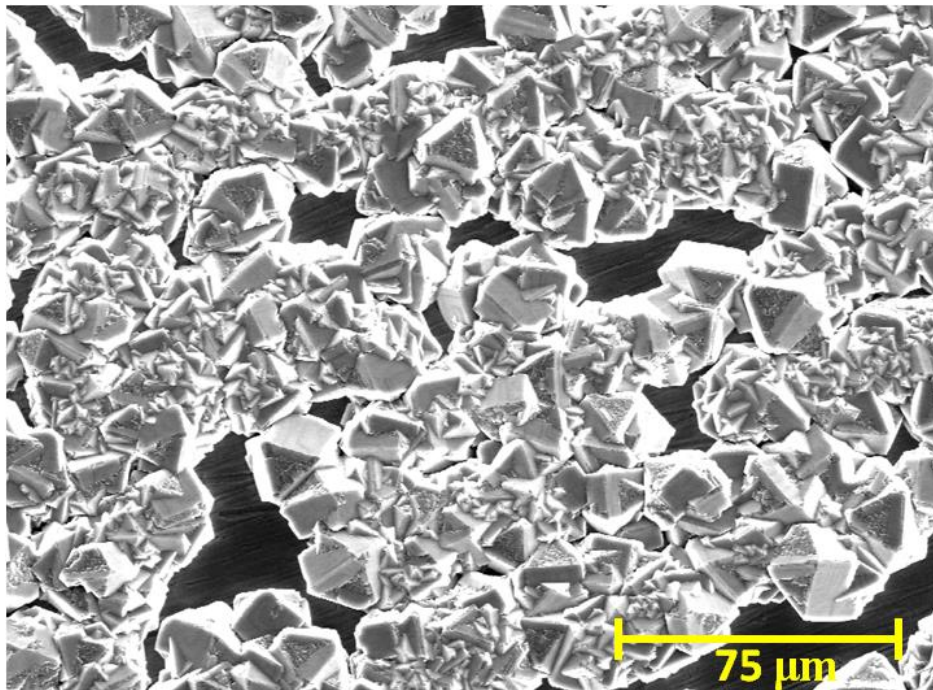


**Figure 5.2** Scanning electron micrograph of a sample grown uninterrupted for less time under the same conditions as the sample in Figure 5.1. Well defined smooth square faces indicative of 100 orientations can easily be discerned as well as deteriorated triangular faces suggesting crystals with 111 orientations are also present.

Raman Spectroscopy measurements were also performed on a diamond sample post deposition by Dr. Arnold Burger at Fisk University. As mentioned in Section 2.3, Raman spectroscopy is a non-destructive characterization technique that provides information on the vibrational, rotational, and other low frequency transitions of the molecule.[39] Analysis of these results (Figure 5.3) demonstrated a strong diamond ( $sp^3$ ) response at  $1334\text{ cm}^{-1}$  and with a small graphite ( $sp^2$ ) response around  $1580\text{ cm}^{-1}$ . Because this technique has been shown to be much more sensitive to graphite over diamond,[40] it can be concluded that these nitrogen-incorporated diamond samples are predominately diamond with little graphitic content.

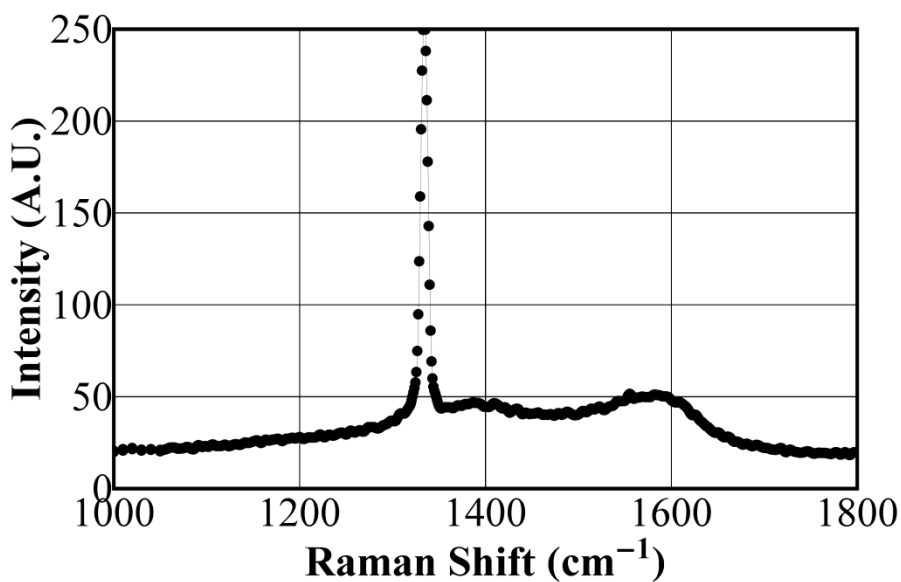


**Figure 5.3** Raman spectroscopy indicating predominantly diamond ( $sp^3$ ) composition with minimal graphitic ( $sp^2$ ) content

## 5.2 Testing apparatus

A reliable, efficient, and inexpensive method for characterizing the thermionic emission properties from the above diamond films was designed. Two testing chambers were constructed employing this method, each chamber for different types of experiments.

### 5.2.1 Apparatus for testing in vacuum environments

The thermionic emission behavior of nitrogen-incorporated diamond films was examined in both vacuum and gaseous environments. Vacuum environment testing, required for all hydrogenation and desorption studies (presented in *Chapter VI*), was performed in a custom built vacuum chamber capable of evacuating to pressures on the order of  $1 \times 10^{-8}$  Torr. The body of this testing apparatus consisted of a six-way cross with flange sizes of 6 inches to which the sample holder, viewport, turbo molecular pump, ion gauge, and ion pump all attached.

A sample holder was constructed out of a three pronged copper high power feed-through. Two of these prongs were meant to physically hold the sample while the third (which is electrically isolated from the other two) functioned as the anode. Brass wire connectors were fitted over both of the holder prongs to provide a means to secure the diamond samples which are grown on thin strips of molybdenum as described in Section 5.1. The method used for heating these samples consisted of applying DC power which created heating gradients throughout the sample with the hottest part being the middle. A glass aperture was employed to prevent emission current from sites other than those of interest and also to allow for accurate determination of the emission area so that emission current densities could be calculated. The below figure is a photograph of a mounted sample in this configuration.

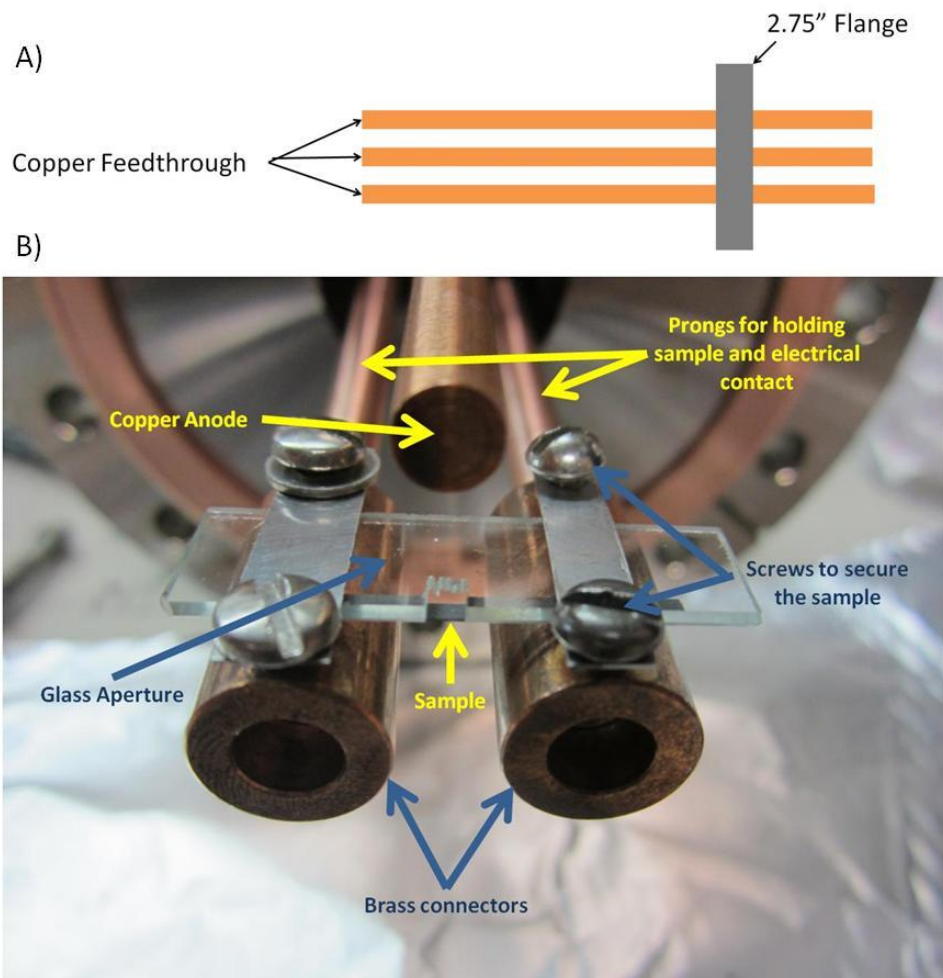


**Figure 5.4** A) Diagram of the electrical feedthrough. B) Photograph of the mounted sample

The temperature of the sample was monitored with an Omega non-contact dual color pyrometer positioned externally from the chamber. The pyrometer was able to observe the sample through a six inch viewport positioned normal to the sample. As this temperature measurement method requires detailed knowledge of the sample's emissivity, the pyrometer measured the back side of the sample, which was simply the molybdenum substrate, rather than the front diamond side. (Molybdenum has a well-documented emissivity which allowed for the pyrometer to be easily calibrated)

The primary pumping mechanism for this chamber was a Duniway ion pump that was activated after the chamber had been pumped down to a pressure of around  $1 \times 10^{-6}$  Torr by means of a turbo molecular pump stand. The pressure was measured with a Bayard Alpert style ion gauge tube. As both the ion pump and ion gauge operate on the principal of electron emission, both are prone to emitting stray electrons. To avoid these stray electrons from interfering with device testing, both were positioned without a direct line of sight to the sample (see Figs. 5.5-5.6).

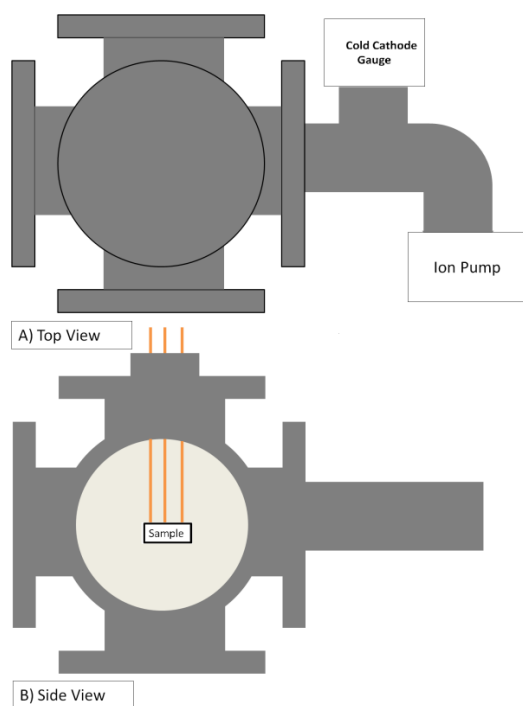


**Figure 5.5** A) Top view of the vacuum chamber. Note that there is no direct line of sight between the sample being tested and either the ion gauge or the ion pump. B) Side view of chamber to demonstrate placement of the sample

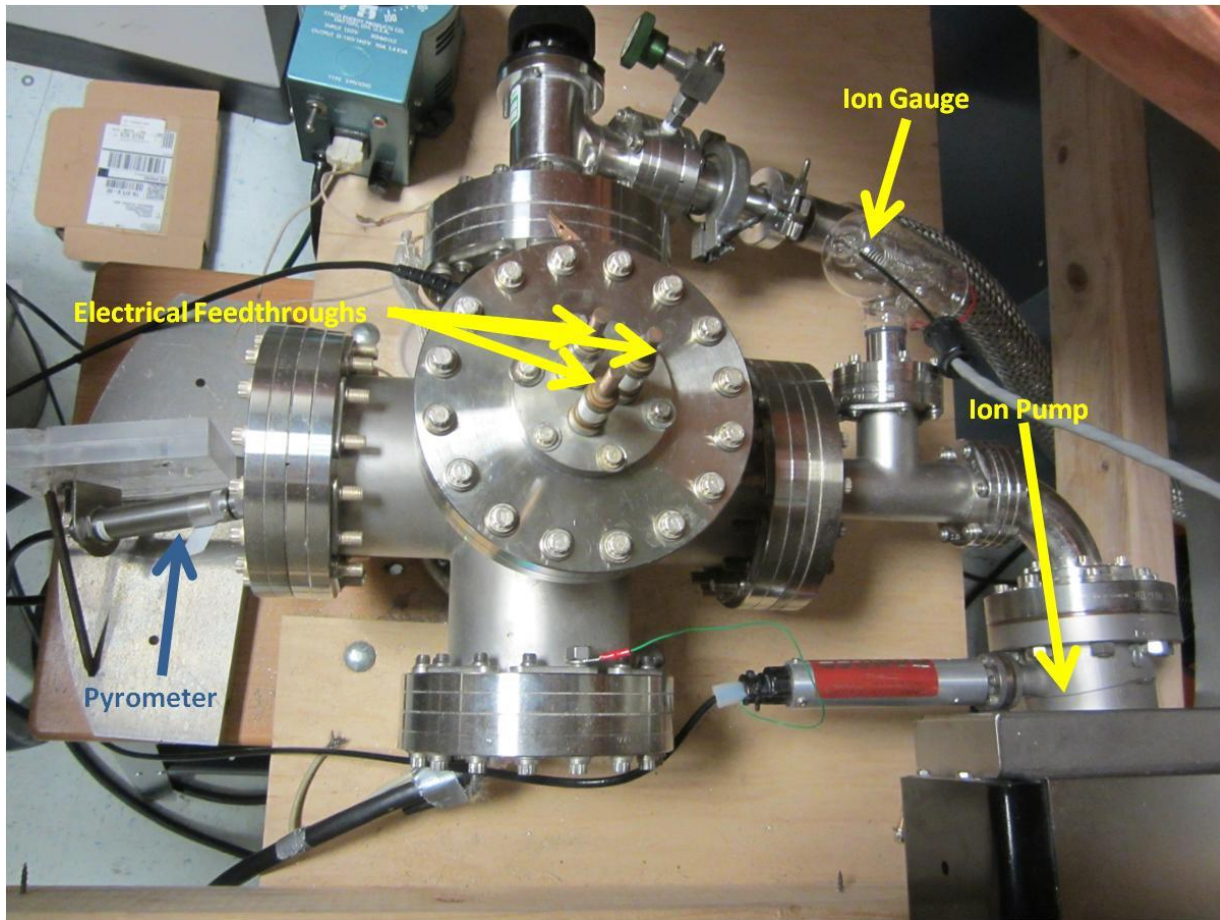


**Figure 5.6** Photograph of testing apparatus

### 5.2.2 Apparatus for testing in various gaseous environments

It was discussed in previous sections that recent studies have observed an increase in thermionic emission current from nitrogen-incorporated diamond films by incorporating methane into the gap between the cathode and the anode.[106] The present research further explored this concept by studying the influence of multiple gaseous species on the thermionic emission current. This required the construction of a second testing chamber that solely utilized a turbo molecular pump rather than the ion pump discussed above. This was because ion pumps are

extremely slow compared to turbo molecular pumps and can only operate effectively at low pressures ( $<10^{-6}$  Torr) and it was desired to fill the chamber with higher gas pressures.

The second testing apparatus functioned much the same as the one discussed in Section 5.2.1, but was also equipped with a Residual Gas Analyzer to measure the chemical makeup of the gaseous species present in the chamber. Substances that exist in the gas phase as well as those which exist in the liquid phase at room temperature were tested in this research.

Methane, molecular nitrogen, molecular hydrogen, and nitrous oxide were the four substances examined which exist in the gas phase at room temperature. Each of these species was contained in a tank of compressed gas equipped with a regulator to control the pressure to the chamber. The tanks were attached to the chamber by means of a high vacuum variable leak valve. Connections from the tank to the leak valve were made with copper piping that was first evacuated to remove all water vapor and other contaminants that could be present. Upon pressuring the copper piping with the desired gas, the testing apparatus was ready for testing. Gaseous species were able to be incorporated into the chamber to a desired pressure by simply opening the leak valve. The testing method used to characterize these gaseous species' influence on the thermionic emission from diamond is discussed later.

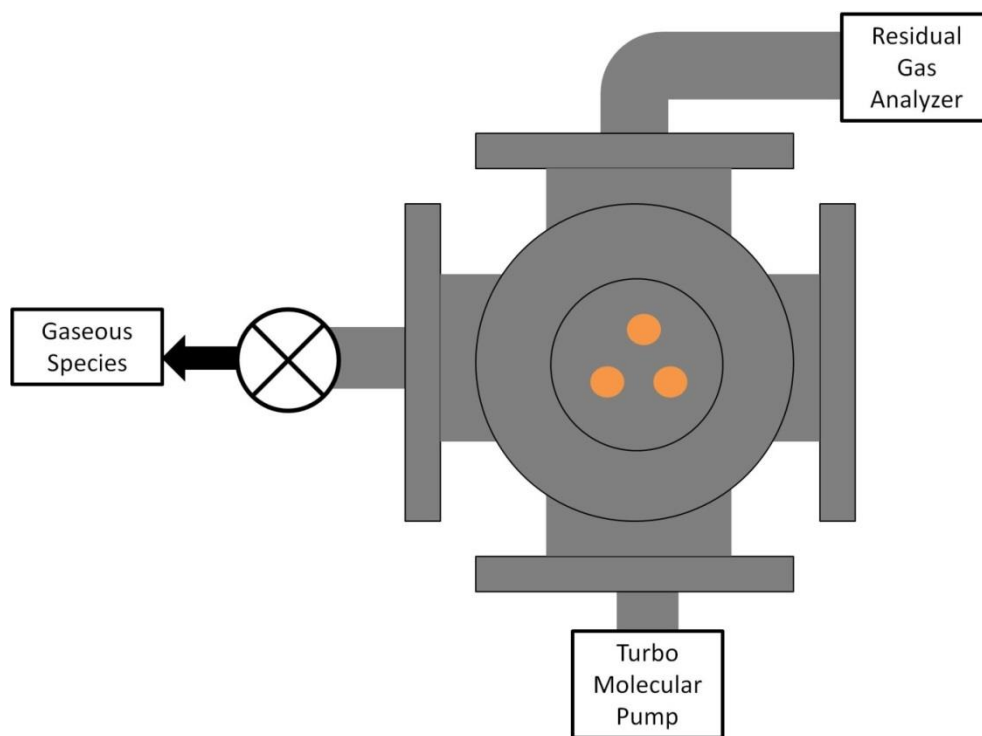


**Figure 5.7** Schematic of the testing apparatus for the incorporation of gaseous species into the vacuum gap

Testing with H<sub>2</sub>O proved more difficult than the above gaseous substances as it exists in the liquid phase at room temperature. Water vapor was fed into the vacuum chamber from a custom-designed water vessel chamber. The water vessel chamber, constructed with stainless steel to prevent corrosion/rust accumulation, was equipped with three valves and a viewport. The preparation of this vessel consisted of a four step process which was shown to prevent the inclusion of any other gaseous species during experimentation. This processes consisted of first pumping down the clean, empty water vessel with a turbo-molecular pump to pressures on the order of  $5 \times 10^{-7}$  Torr to remove the atmospheric gasses present in the vessel. After a period of several hours, the turbo-molecular pump was valved off and deionized water was sucked into the chamber through a leak valve. The line that fed the deionized water to the leak valve had all air

removed. Water was continually fed into the vessel until a desired level was achieved which was gauged through the viewport. At this point, the leak-valve to the water line was closed and the vessel was attached to the gaseous environment testing chamber through a second leak valve (the same leak valve used in the gaseous species experiments). The whole vessel was then heated to temperatures on the order of 75°C by means of heating wraps. The heating was meant to both increase the vapor pressure of the water to provide enough vapor for experimentation and also to prevent freezing of the water upon entering the testing apparatus. A step-by-step visual description of this process can be seen below in Figure 5.8. Construction of this configuration allowed testing to be performed in the same manner as the other tests on gaseous species permitting direct comparison of all results.

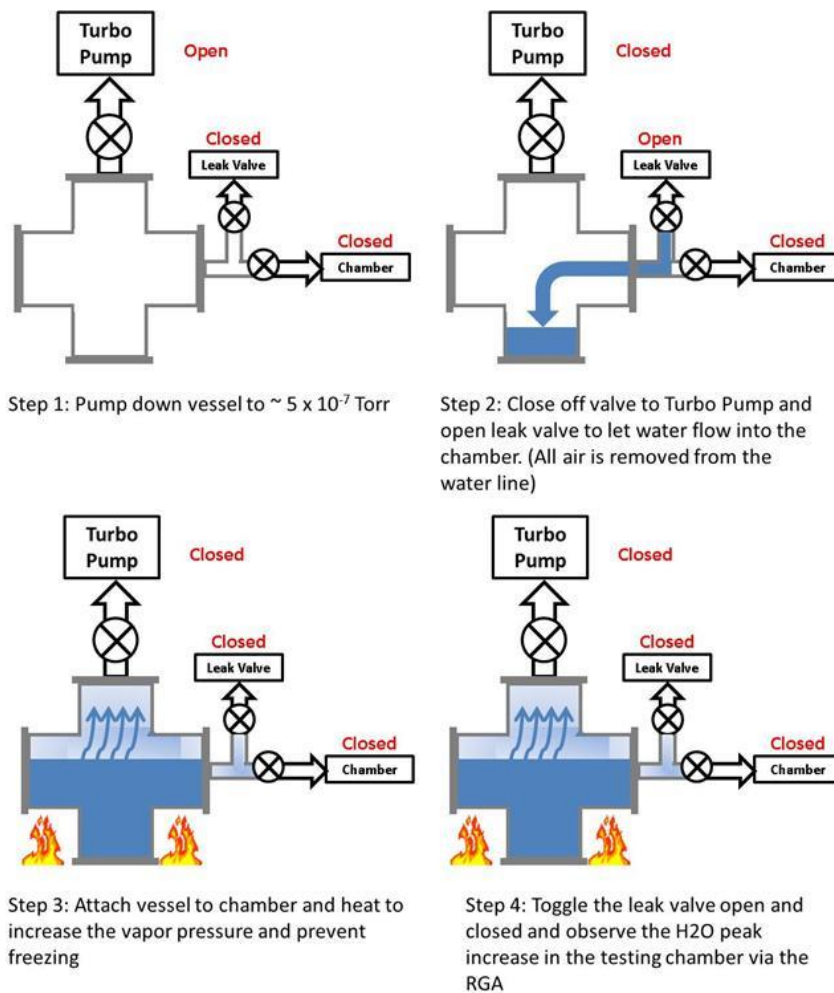


**Figure 5.8** Step-by-step process used to prepare the water vessel chamber used to introduce water vapor into the vacuum chamber. The first two steps were meant to remove other species that could interfere with results. The second two steps were meant to allow water vapor to freely enter the chamber.

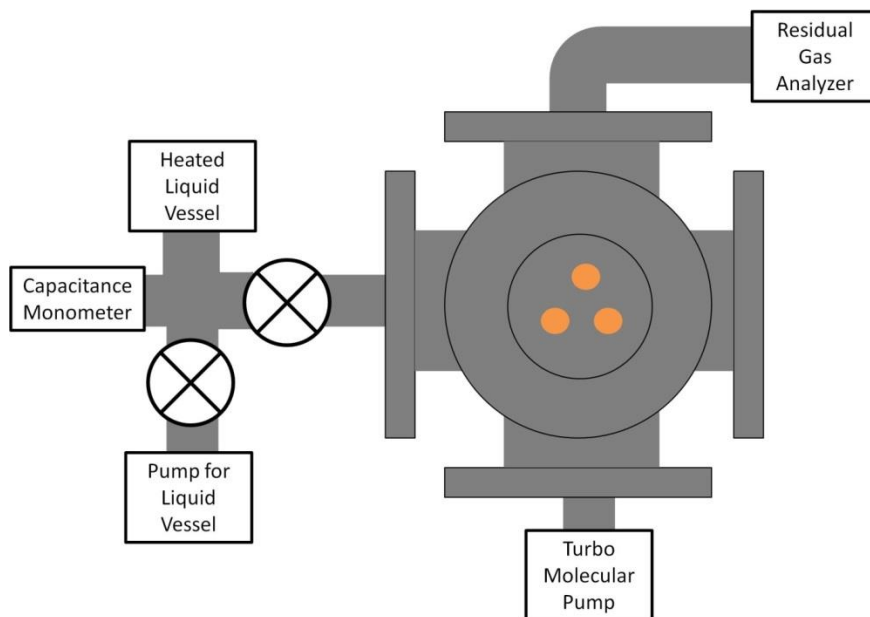


**Figure 5.9** Schematic of the testing apparatus for the incorporation of species that are in the liquid state at room temperature into the vacuum gap.

### 5.3 Data collection and system control

As previously mentioned, the sample holder was equipped with an electrically isolated prong that acted as the collector anode. Low fields ( $<1 \text{ V}/\mu\text{m}$ ) were applied to the sample as it was desired to measure only thermionic emission current. High fields could lead to tunneling thus promoting erroneous results. This anode voltage,  $V_{\text{anode}}$ , was held at a fixed voltage for all tests performed in this research. The emission current was required to be measured in series between the anode and the power supply as the high currents required to heat the sample made the expected low emission current values (pA) hard to decipher. The ammeter chosen for this purpose was a USB powered RBD Instruments 9103 floating picoammeter capable of floating at voltages up to 1000V.

The temperature was controlled by adjusting the current through the sample. The power supply used for this was a Lambda GENH20-38 capable of outputting up to 38 A. (this power

supply will be referred to as  $V_{\text{substrate heater}}$  henceforth.) Both the Lambda power supply and the Omega pyrometer are equipped with Ethernet interfaces which allowed both to be controlled by an external computer.

In addition to the two testing chambers, two testing configurations were also designed for this research. Both testing configurations were connected to the testing apparatus following the schematic diagram in Figure 5.10. One of the testing configurations was designed to observe the thermionic emission current behavior as a function of temperature; while the other was designed to monitor the isothermal emission current behavior as a function of time. Both of these testing configurations were controlled by Labview System Design Software, a commonly used research software that allows for the simultaneous control of several components all communicating with different protocols.

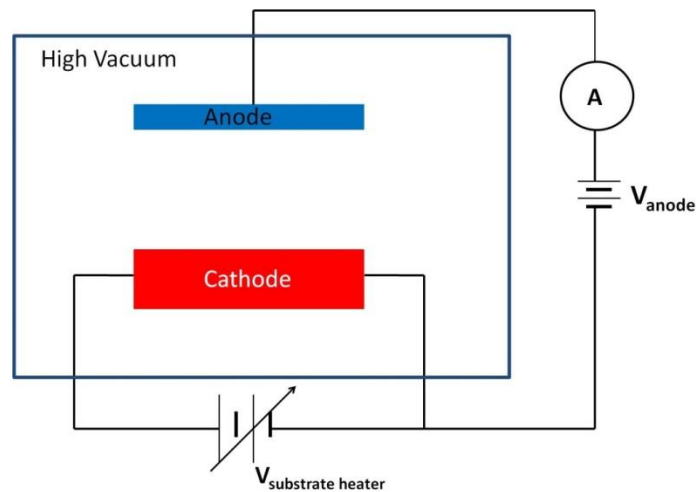


**Figure 5.10** Electrical schematic of the thermionic emission testing configuration. The sample to be tested was resistively heated by a Lambda power supply ( $V_{\text{substrate heater}}$ ). The anode was biased by a separate high voltage power supply with the grounds of the two power supplies tied together. Electron emission current was monitored by a floating picoammeter in series with the anode power supply.

### 5.3.1 Current vs. Temperature (CVT) Configuration

The first testing configuration, the CVT Configuration, was designed for experiments where it was of interest to study the thermionic emission current behavior of diamond films at several temperatures. Data collected in this method was meant to be analyzed with respect to the Richardson equation (previously described) to determine the thermionic emission parameters such as the sample's work function and Richardson constant. Testing with the CVT Configuration consisted of first heating the sample to a desired starting temperature by slowly increasing the power through the sample with the  $V_{\text{substrate heater}}$  power supply. Once the desired starting temperature was achieved, the CVT Configuration control loop was initiated. This control loop entailed first increasing the current through the sample by 0.05A which corresponded to a roughly 3-5°C temperature increase. The control loop would then pause for 25 seconds to let the temperature stabilize. Finally, five emission current data points and 5 temperature data points were collected simultaneously and averaged to give one emission current/temperature data point. This process was then repeated until the desired temperature was reached. A flow diagram depicting the process can be seen below in Figure 5.11.

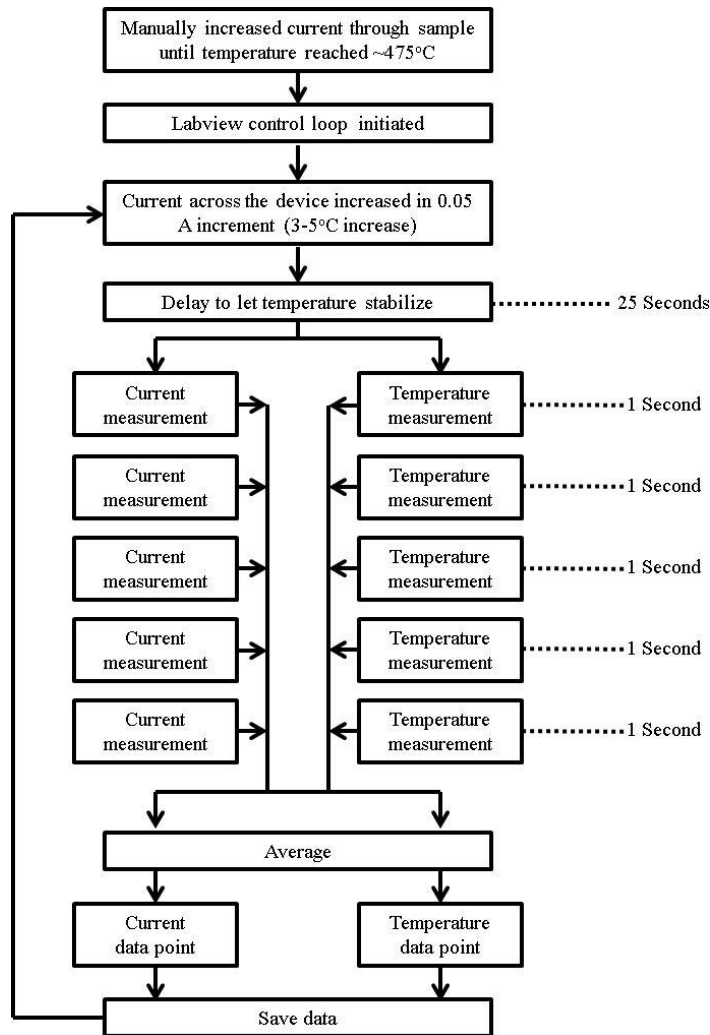


**Figure 5.11** Flow diagram depicting the Labview control loop for the current vs. temperature tests.

When the desired maximum testing temperature was achieved, the control loop was stopped, the data saved, and the temperature of the sample manually lowered by decreasing the power of  $V_{\text{substrate heater}}$  until no power was flowing through the heating circuit.

### 5.3.2 Isothermal (IT) Configuration

Experiments such as those meant to determine the activation energy of hydrogen in the diamond films required a more advanced control configuration. These experiments were performed isothermally over long periods of time whereby the emission current was constantly monitored. This was accomplished by incorporating a commonly used temperature control method known as a PID control loop. The “P” element stands for “proportional” and accounts for the current error at time  $t$  or the present error. The “I” element accounts for the past error integrated up to time  $t$ . The last element, the “D” element, accounts for the derivative at the instant of time  $t$  which predicts the future error.[138] After calibrating the P, I, and D constants, this control loop was able to precisely control the temperature of the sample with a standard deviation typically less than  $1^{\circ}\text{C}$ .

The IT Configuration began with inputting the desired cathode temperature into the Labview control program. As the pyrometer is unable to read temperature values less than  $\sim 475^{\circ}\text{C}$ , the PID portion of the control loop was not able to be initiated with the sample at room temperature. This problem was solved by starting the PID control loop after the Labview control system had slowly heated the sample to  $500^{\circ}\text{C}$  by increasing the current through the heating circuit current in small 0.05 A steps. The PID loop was then able to heat the sample from the  $500^{\circ}\text{C}$  starting temperature to the desired temperature, which typically took a few minutes. Collection of the thermionic emission current data was not begun until after it was observed that the temperature had reached the desired set point. After the amount of collected data was deemed sufficient for each particular experiment, the set point temperature was then able to be changed for further testing. The above process was repeated until testing had been performed at all

desired temperatures after which, the data saved, control loop stopped, and the temperature manually decreased until no power was traveling through the heating circuit.

#### 5.4 Influence of gaseous species on the thermionic emission from diamond

In addition to vacuum testing, the thermionic emission performance of nitrogen-incorporated diamond cathodes in various gaseous environments was also performed. These experiments were all performed using the testing apparatus earlier described in Section 5.2.2 utilizing the PID control loop in the isothermal configuration (Section 5.3.2). As mentioned, the chamber was equipped with a residual gas analyzer (RGA) to allow for direct verification of the composition of the gasses fed into the chamber. Operation of the RGA consisted of three steps: First, the chamber was pumped down for a period of ~24 hours. Second, the RGA was initialized with the leak valve closed to establish a baseline of all species present in the chamber. Finally, the desired species were leaked into the chamber. The configuration was deemed ready for testing when only the documented spectrum of the desired species was seen in the chamber. During testing, the RGA was shut off to prevent the collection of stray electrons by the anode

Each testing run characterized the isothermal emission current response to the introduction of various low pressure gaseous environments at five temperatures: 600°C, 625°C, 650°C, 675°C, and 700°C (in increasing order). At each testing temperature, the isothermal emission current was first monitored in a vacuum environment on the order of  $1 \times 10^{-7}$  Torr for a period of time to establish a baseline emission current trend. A gaseous species was then fed into the chamber to a pressure of ~5.5  $\mu$ Torr ( $N_2$  equivalent) measured at the pump for a period of ~60 seconds after which, the leak valve was closed and the chamber evacuated back down to  $1 \times 10^{-7}$  Torr levels. It was required to measure the pressure at the pump as all available pressure

measurement techniques operate on the principal of electron emission. Attaching such a gauge directly to the chamber could lead to unreliable results if stray electrons are collected by the anode. The gaseous species were fed into the chamber twice at each testing temperature. Upon completion of testing, the data was analyzed to determine the emission current response to the introduction of each gaseous species. The results from these experiments are presented in *Chapter VII*.

## CHAPTER VI

### THERMIONIC EMISSION CHARACTERIZATION IN VACUUM

This chapter presents the results of the thermionic emission experiments performed in a vacuum environment. Thermionic emission characterizations of both as-grown and hydrogenated diamond films are presented and compared. The isothermal emission current of diamond films exposed to various plasma conditions was also explored to better understand the hydrogen desorption process from diamond.

#### 6.1 As-grown nitrogen-incorporated diamond films

This portion of the research began by examining the thermionic emission current of nitrogen-incorporated diamond films immediately after deposition before exposure to any hydrogenation treatments. The Richardson constant and work function of samples in this “as-grown” state were calculated by observing the emission current vs. temperature trend of the samples.

##### 6.1.1 Thermionic emission behavior of as-grown samples

A nitrogen-incorporated diamond sample was first prepared according to the method described in Section 5.1. Thermionic emission testing for this experiment was performed in vacuum testing apparatus (Section 5.2.1) using the Current vs. Temperature (CVT) testing configuration.

Observation of the electron emission current above background began at 485°C and increased with temperature up to a maximum testing temperature of 640°C. A plot of the emission current vs. temperature can be seen below in Figure 6.1.

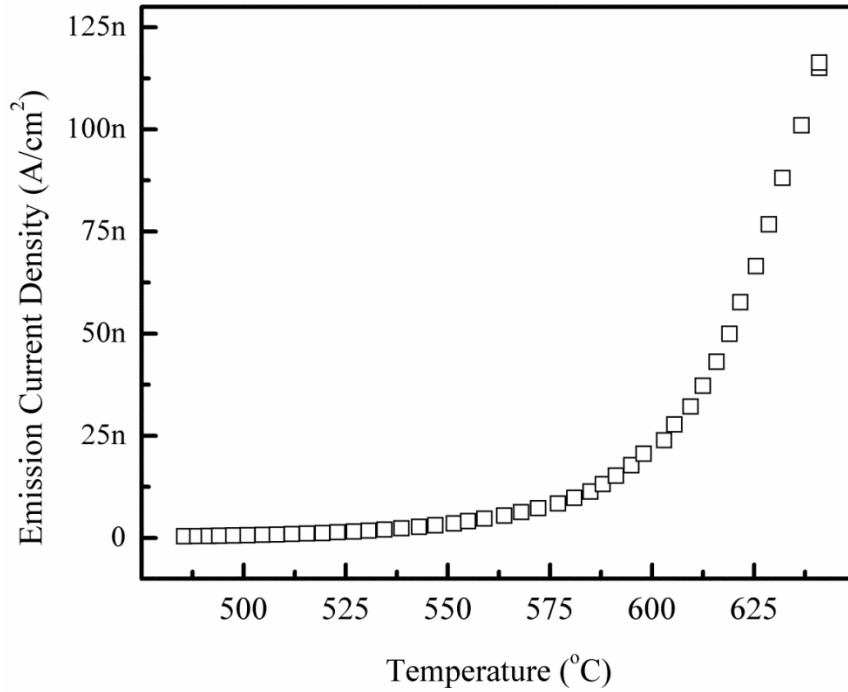


**Figure 6.1** Thermionic emission current behavior of an as-grown diamond sample as a function of temperature

As previously mentioned, the thermionic emission current arising from a heated cathode is described by the Richardson equation (Equation 6.1). [22, 109]

$$J = AT^2 e^{-\Phi/k_b T} \quad (6.1)$$

Where: J=Current Density (A/cm<sup>2</sup>); A=Richardson Constant (A/K<sup>2</sup>cm<sup>2</sup>); T=Temperature (K); Φ=work function (eV); and k=Boltzmann constant (8.617 x 10<sup>-5</sup> eV/K). The emission parameters “A” and “Φ” were determined by rearranging Eq. 6.1, taking the natural logarithm of

both sides of the equation (Eq. 6.2), and plotting  $\ln(J/T^2)$  against  $-1/kT$ . In the resulting “Richardson plot,” the slope and y-intercept correspond to the work function and natural log of the Richardson constant respectively.

$$\ln\left(\frac{J}{T^2}\right) = -\frac{\Phi}{k_b T} + \ln(A) \quad (6.2)$$

Analysis of the thermionic emission current data from the as-grown diamond sample with respect to Eq. 6.2 did not exhibit the expected linear relationship across the entire temperature range. Rather, the work function and Richardson constant varied with temperature. From Figure 6.2, it can be seen that there was a distinct transition region in which the work function and Richardson constant both increased.

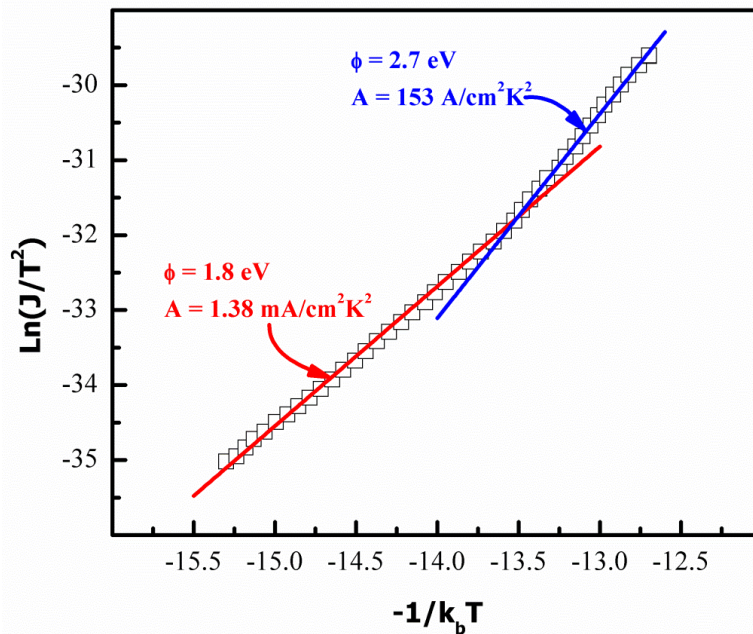


**Figure 6.2** Richardson plot of the thermionic emission data seen in Figure 6.2. It is clear that the plot is not linear contrary to what would be expected from the Richardson equation. Rather there was a distinct transition temperature in which both the work function and Richardson constant increased.

It should be noted that the Richardson constant value in the high temperature regime of  $153\text{A}/\text{cm}^2\text{K}^2$  is larger than the theoretical value of  $120\text{A}/\text{cm}^2\text{K}^2$ . Past research on this topic has indicated that the calculation of this constant requires several factors to be taken into account beyond Richardson's initial model.[139] These factors lead to large variations in this value for different materials and values much larger than  $120\text{A}/\text{cm}^2\text{K}^2$  have been well documented.[105]

The results shown in Fig. 6.2 not only exhibit a strong temperature dependence on diamond's work function but also its Richardson constant, which are consistent with previous thermionic emission studies on other wide bandgap materials. Examining the emission properties of emissive oxides, M. Myojo derived several equations describing the change in both work function and Richardson constant as linear relations to the natural logarithm of the ratio of the conduction band concentration to the donor level concentration.[140] It has been noted in previous sections that the donor level of nitrogen in diamond is  $1.7\text{eV}$  below the conduction band.[141] At the temperatures tested in this study, it can be assumed that a negligible amount of donors were ionized. Conversely, the conduction band concentration has a strong dependence on temperature resulting from the defect-induced energy bands that nitrogen presents in diamond.[60] According to M. Myojo, this increase in conduction band carrier concentration accounts for the observed increase in work function as well as Richardson constant with increasing temperature.

Thermionic emission testing results from as-grown nitrogen-incorporated diamond demonstrated that much higher emission current density values can be achieved compared to those seen from boron-doped diamond films.[142] Unfortunately, these current levels are lower than viable application levels, prompting further investigations.

## 6.2 Effect of hydrogen on the thermionic emission from diamond

Previous sections of this dissertation have provided substantial documentation on the beneficial effects that hydrogen has on the electronic properties of diamond films. For instance, it is believed that hydrogen interaction at the diamond surface is responsible for its observed negative electron affinity.[67] Hydrogen has also been shown to affect the solid state electronic properties of diamond through the passivation of grain boundaries in polycrystalline films in addition to deep traps found in single crystalline films.[65, 143] The present study sought to further the understanding of the influence of hydrogen in diamond by examining its effects on thermionic emission.

### 6.2.1 Characterization technique

A diamond sample was deposited according to the process described in Section 5.1. This “as-grown” diamond sample was first tested (Test #1) to observe its thermionic emission properties using the vacuum testing chamber in the same manner as described in Section 6.1.1. Rather than ceasing testing below 700°C (as was done in Section 6.1), testing continued up to a maximum temperature of ~900°C. It was observed that the emission current began to exhibit a strong deviation from the Richardson equation in that it transitioned into a decreasing trend with increasing temperature. Testing was halted at 900°C as the emission current had decreased to levels below measurement capability (10pA). The sample was then retested (Test #2) in the same manner and no measureable emission current was observed up to a maximum testing temperature of 800°C. After a cooling period, the sample was removed from the testing apparatus and placed back in the MPCVD chamber to be “hydrogenated.” This process consisted of exposing the sample to a low energy hydrogen plasma at the following parameters: temperature = 850°C,

hydrogen flow rate = 200 sccm, pressure = 20 Torr, and microwave power = 550 W. The duration of this process was one hour. Following hydrogenation, the sample was placed back in into the vacuum testing chamber to examine the effects the hydrogen plasma had on the thermionic emission (Test # 3).

### 6.2.2 Comparison of as-grown and hydrogenated diamond samples

Examining the data from the first two tests (Figure 6.3), it can be seen that the emission current began to decrease with increasing temperature when the sample was heated to temperatures exceeding  $\sim 800^{\circ}\text{C}$ . Though never specifically addressed, this effect has frequently been seen by other researchers and is believed to be caused by the desorption of hydrogen from the diamond cathode.[74, 75] The present study went beyond those previous observations by continuing to test up to  $900^{\circ}\text{C}$  whereby all beneficial effects of hydrogen appeared to be removed. This was verified by the lack of recovery of any measureable emission current as seen in Test # 2.

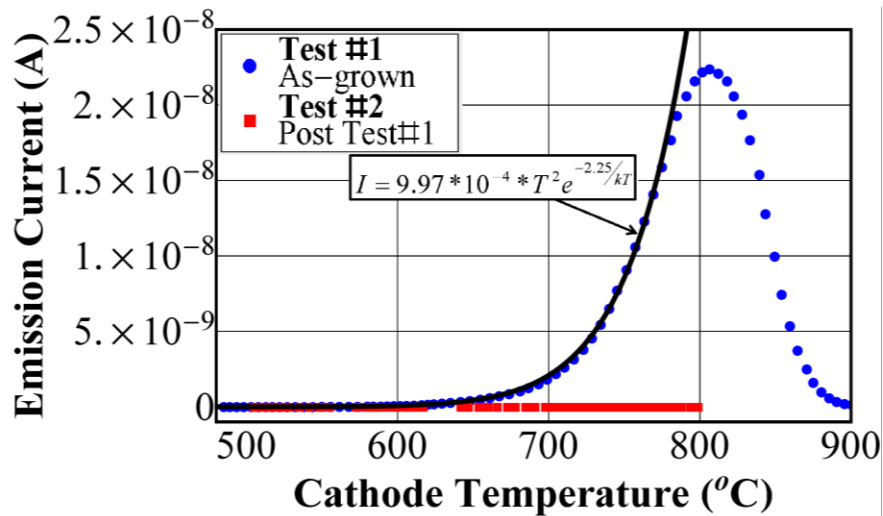


**Figure 6.3** Comparison of the thermionic emission testing results from Test #1 and Test #2 of an as-grown sample before hydrogenation. Test #1 was an as-grown diamond sample and the thermionic emission current was observed to increase with temperature according to the Richardson equation until  $\sim 800^{\circ}\text{C}$ , upon which the emission current began to decrease. Test #2 was performed on the same sample after a cool down period. No emission current above the noise level was observed up to a maximum testing temperature of  $800^{\circ}\text{C}$ . The solid line represents the fit to the Richardson equation of Test #1 data.

Upon hydrogenation of the sample, the emission current not only recovered but exceeded the emission current observed in Test #1 by four orders of magnitude, as seen in Figure 6.4. This indicates that hydrogen indeed beneficially affects the thermionic emission from diamond. Though the hydrogenated sample achieved much higher emission current levels than the as-grown sample, the emission current vs. temperature trend for Test #3 again followed the same “roll over” trend seen for Test #1 in that the emission current began to decrease with increasing temperature. Additionally, comparison of Figures 6.3 and 6.4 revealed that Test #3 began to decrease at roughly  $100^{\circ}\text{C}$  lower temperature than Test #1.

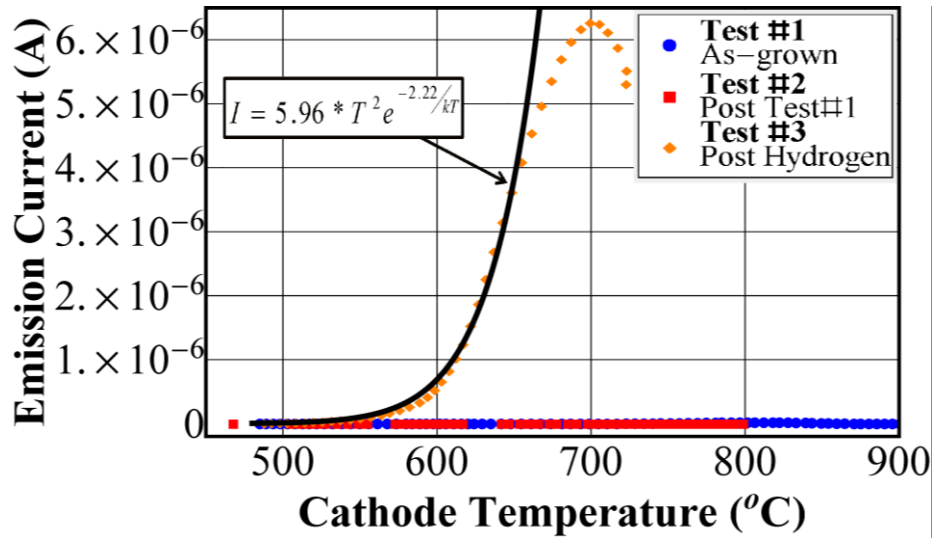


**Figure 6.4** Comparison of the thermionic emission testing results from Test #1, Test #2, and Test #3. The electron emission current from the sample after hydrogenation was significantly higher than the previous runs. The solid line represents the fit of Test#3 to the Richardson Equation.

### 6.2.3 Analysis of hydrogen's effects on thermionic emission

Comparison of the Richardson equation fits for Test #1 and Test #3 yield some interesting results. First, there was little change in the work function between the two runs. Second, the Richardson constant for Test #3 was four orders of magnitude larger than for Test #1. As the work function is simply the barrier that electrons must overcome to be emitted into the vacuum, these results indicate that exposure to a hydrogen plasma does not alter the barrier, but rather influences the emission current by means of the Richardson constant. The remainder of this section presents two possible explanations to describe these results.

The first explanation deals with a previously discussed study by Cui and colleagues.[67] Their work found that hydrogen termination on the diamond surface reduces the barrier which electrons must overcome in order to be emitted by decreasing the electron affinity.[67] As there was little change in work function from Test #1 to Test #3, it can be assumed that electron

emission primarily arose from surface sites with surface hydrogen bonds. Though Test #1 was performed with an as-grown sample that had not been exposed to the hydrogenation treatment, it was grown in a methane starved hydrogen-rich environment unavoidably resulting in some amount of hydrogen present in bulk and on the surface of the diamond films. The large increase in emission current seen in Test #3 was likely due to the hydrogenation treatment increasing the diamond's hydrogen surface concentration, thus providing more sites from which electrons can be emitted. A visual depiction of this scenario can be seen below in Figure 6.5. This increase in the amount of emission sites could explain the large increase in current seen after the hydrogenation treatment with little change in the work function. This postulated trend of increasing hydrogen concentration with hydrogen plasma exposure is consistent with previously reported studies.[144]

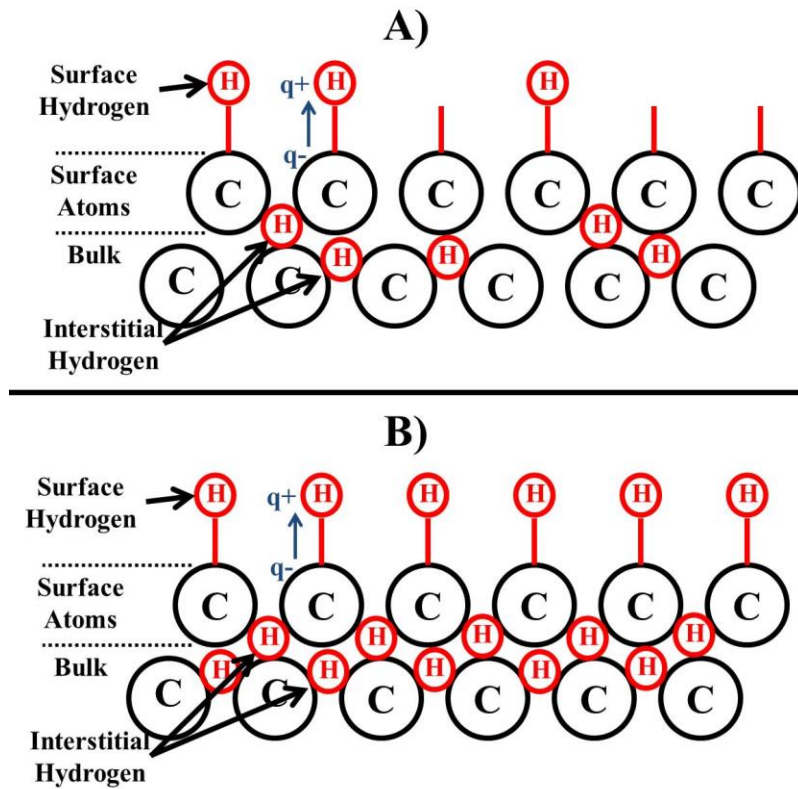


**Figure 6.5** Visual depiction of the as-grown diamond sample, A) compared with a hydrogenated sample, B). The as-grown sample was grown in a methane-starved hydrogen-rich environment resulting in some concentration of hydrogen on the diamond surface and in the diamond bulk. Exposure of the sample to a hydrogenation treatment increased both surface and bulk concentrations resulting in higher emission current levels but little change in work function.

A second possible explanation for the results obtained in the present study deals with bulk rather than surface hydrogen effects. It has been previously mentioned that hydrogen affects the electrical resistivity polycrystalline diamond films. Previous studies have observed a decrease in the resistivity of diamond films upon exposure to a hydrogen plasma which is thought to be the result of the passivation of both grain boundaries as well as deep traps present in the bulk.[143] The subsequent decrease in resistivity equates to enhanced electron transport to the diamond cathode's surface whereby a greater amount of electrons are available for emission. As

this effect deals solely with the bulk, it can be assumed that the surface chemistry is unchanged therefore the work function does not change. This explanation then accounts for the large increase observed in the Richardson constant from Test #1 to Test #3 and also the small change in work function.

Two possible mechanisms have been discussed to explain the observations made in the present study. However, it remains unclear which mechanism is more accurate or if the observations are a result of a combination of the two.

### 6.3 Determination of the optimal hydrogenation procedure

It has been shown that hydrogen is crucial to increasing the thermionic emission performance of the nitrogen-incorporated diamond films used in this research. Therefore, it was desired to determine the optimal hydrogenation procedure which would result in the best emission characteristics. Multiple sets of diamond films were synthesized consisting of three to four films per set. Each set was used to examine the influence of one distinct parameter during the hydrogenation processes such as stage temperature, pressure, and microwave power. Within each set, all but one parameter was held constant. Further, each set was grown simultaneously to minimize inconsistencies between samples.

#### 6.3.1 Influence of temperature on the hydrogenation of diamond

The influence of temperature on the hydrogenation of diamond consisted of first preparing four samples (A1, A2, A3, A4) grown in the same manner as described in Section 5.1. Each of these four samples was tested consecutively and the emission current recorded. The emission area was determined by using a caliper to measure both the aperture size and sample

width allowing the emission current density to be calculated. Using emission current densities allowed for direct comparison of each sample's thermionic emission properties. After the as-grown emission current data was taken, each sample was exposed to a hydrogen plasma treatment with pressure, microwave power, time, and hydrogen flow rate held constant at 20 Torr, 550 Watts, one hour, and 200 SCCM, respectively. The stage temperature during the hydrogenation treatment was modified for each sample ranging from 400°C to 850°C.

The thermionic emission current behavior of the initial as-grown runs for Set A can be seen in Figure 6.6. Each sample achieved similar emission current densities and reached the maximum emission current levels around 775°C. The discrepancies between films were likely due to the polycrystalline nature of the diamond films resulting in non-uniformity from sample to sample. To reduce the influence of these discrepancies on testing, it is helpful to base conclusions on the differences each sample experienced before and after hydrogenation.

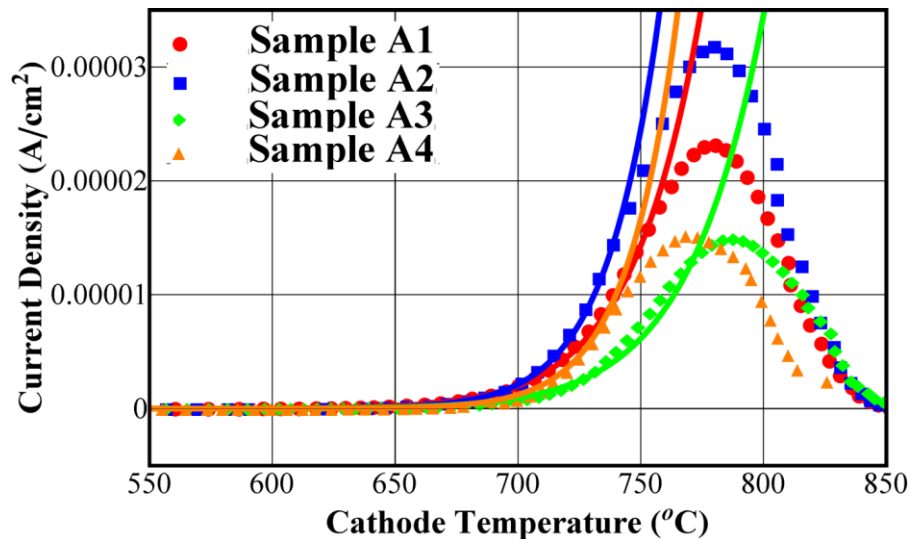


**Figure 6.6** As-grown thermionic emission current vs. temperature behavior for Set A. It can be seen that the emission current behavior was similar for each sample. The discrepancies likely were a result of the polycrystalline nature of the diamond films.

Comparison of the emission current before and after hydrogenation for each sample can be seen in Figure 6.7, while a plot of the maximum current achieved from each sample as a function of hydrogenation temperature can be seen in Figure 6.8. It was observed that the maximum emission current density decreased as the temperature at which they were hydrogenated increased with the exception of the final hydrogenation temperature of 850°C. Though a precise explanation of this trend cannot be made at this time, it was hypothesized to be a result of the two competing processes: adsorption and desorption. In the adsorption process, molecular hydrogen is fed into the MPCVD chamber and dissociates into atomic hydrogen by the microwave power. These hydrogen atoms then incorporate into the diamond films by either diffusing through the bulk or accumulating on the surface, bonding with the surface carbon atoms. Desorption results from the thermal dissociation of surface C-H bonds that has been shown to occur from diamond samples at elevated temperatures.[78, 80, 82, 84, 145-147] At low hydrogenation temperatures, adsorption was the dominant process as the temperatures to which the films are exposed are not sufficient to promote rapid desorption. As the temperature increased, the rate of the hydrogen desorption also increased resulting in a net lower concentration of hydrogen. Finally, at even higher temperatures, hydrogen can more easily diffuse through the diamond lattice thereby allowing adsorption to once again become the dominant process.

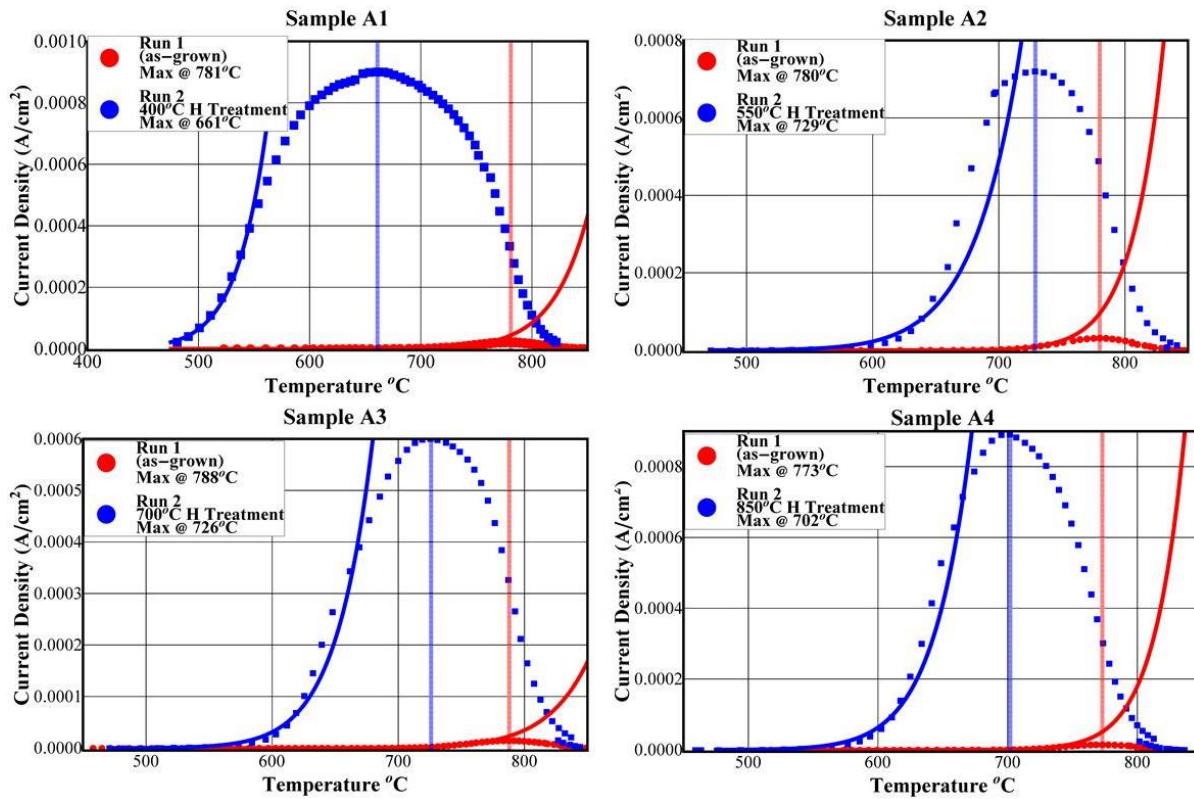


**Figure 6.7** Comparison of the performance of each sample before and after hydrogenation from Set A

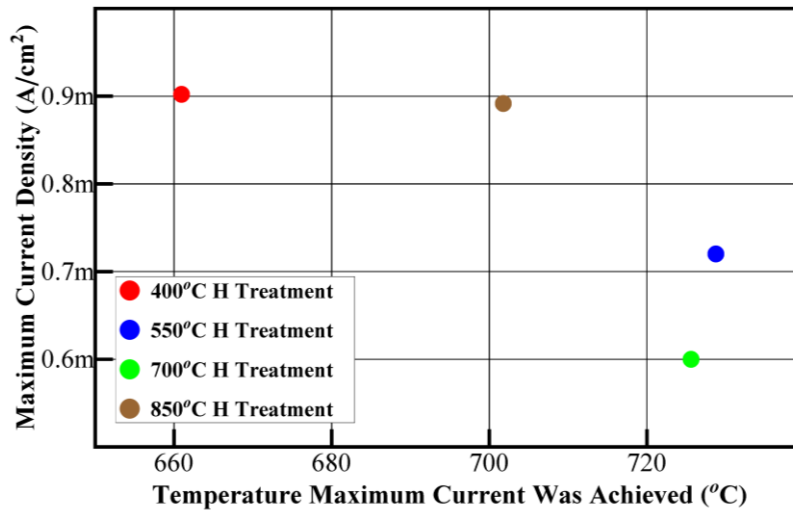


**Figure 6.8** Maximum current densities obtained from each film as a function of temperature at which they were achieved for each hydrogenation treatment in Set A. It can be seen that the maximum emission current decreased with increasing temperature until the final temperature of 850°C.

### 6.3.2 Influence of time on the hydrogenation of diamond

The effect of hydrogenation time on the emission performance was studied using Set B consisting of three samples (B1, B2, B3) grown as described in Section 5.1. Each sample was tested according to the same protocol discussed for Set A. For this set, hydrogenation time was the variable with pressure, microwave power, temperature, and flow rate held constant at 20 Torr, 550 Watts, 850°C, and 200 SCCM, respectively. The hydrogenation time was modified for each sample ranging from 1 hour to 4 hours.

Analysis of the data from Set B can be seen in Figure 6.10. Little change was observed indicating the amount of time (exceeding 1 hour) has little effect on overall performance from these devices.

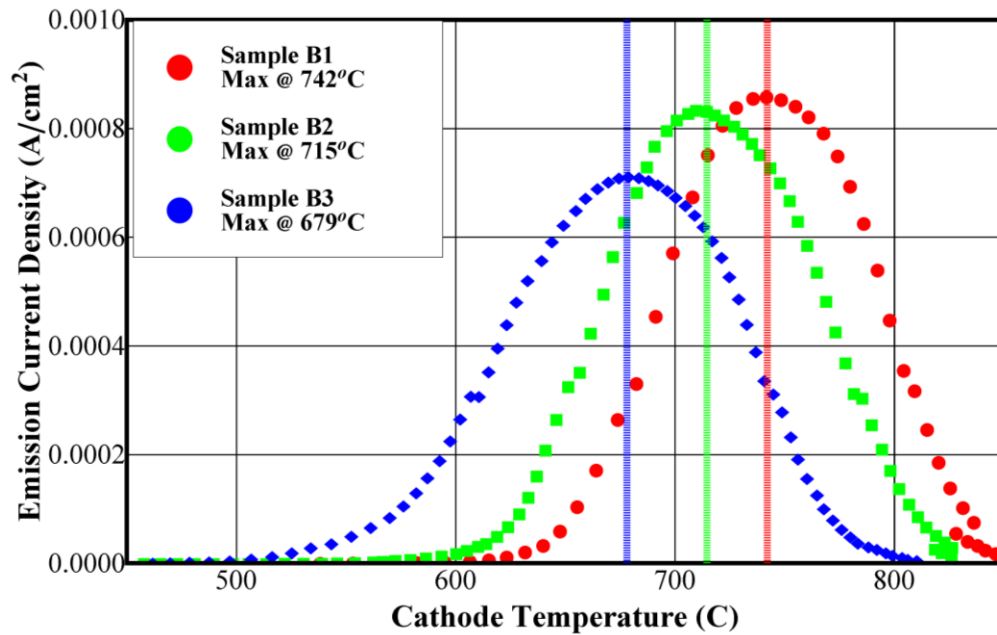


**Figure 6.9** Emission current density vs. cathode temperature of samples B1, B2, and B3 hydrogenated for 1, 2, and 4 hours respectively. It can be seen that increased exposure time not only decreased the maximum emission current density values slightly but also decreased the temperature at which the samples achieve their maximum current densities.

The influence of hydrogenation time on maximum emission current density and temperature at which these values were achieved is further illustrated in Figure 6.10. Although the effect was small, it can be seen that prolonged exposure periods to the hydrogenation treatment led to not only a decrease in maximum emission current but also a lower temperature ceiling.

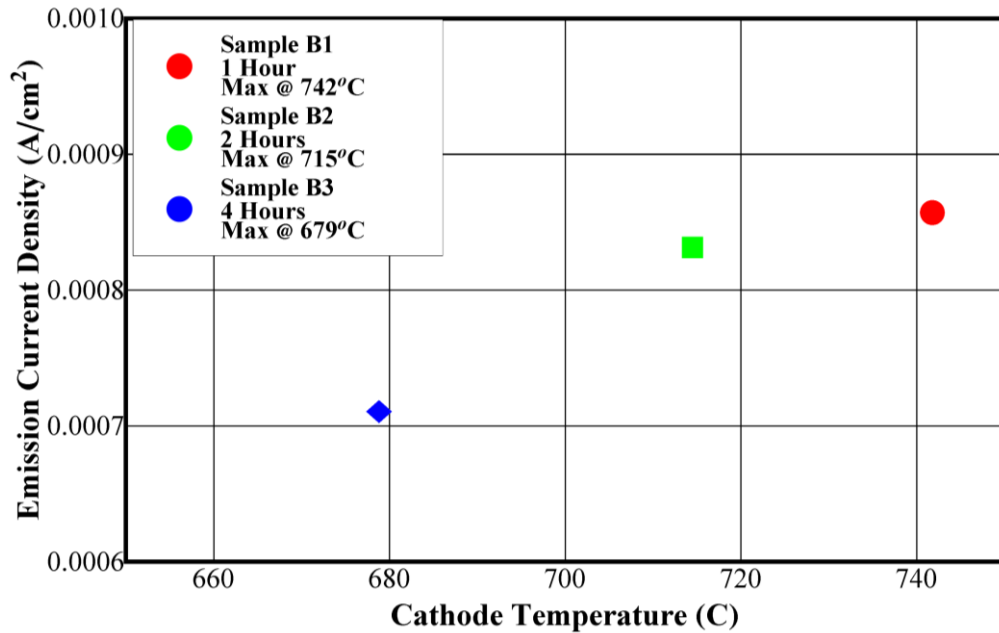


**Figure 6.10** Maximum emission current density values as a function of temperature at which they were achieved for each hydrogenation treatment. It can be seen that there was a trend of decreasing thermionic emission performance as the duration of hydrogenation treatment increased.

The emission current performance of diamond films upon exposure to a hydrogen plasma treatment of diamond films at 850°C, 20 Torr, 200 sccm H<sub>2</sub>, and 550 watts appeared to decrease as a function of hydrogenation time. Not only did the maximum emission current density each sample achieved decrease with increasing hydrogenation time, but also the temperature at which

they began the “roll over” trend, both of which are unfavorable. These effects can likely be attributed to the competing absorption/desorption mechanisms discussed for Set A. At the temperatures of 850°C performed in each hydrogenation treatment in Set B, there is likely a large amount of desorption occurring. Further, the temperature of the sample could likely be increasing during the hydrogenation treatment. The MPCVD chamber contains an inductively heated stage that the samples sit on during deposition and hydrogenation. The 850°C temperature measured during the treatment was the temperature of the stage, not the sample. Over extended periods of times, it is highly possible that the plasma imparts thermal energy on to the sample causing it to heat past the 850°C stage temperature. Thus these higher temperatures will cause the hydrogen to desorb faster. If the desorption rate is higher than the hydrogen adsorption rate caused by the plasma, then the sample will experience a net decrease in hydrogen surface concentration. This appears to be the most probable explanation for the results seen from Set B in the absence of a direct measurement of the sample temperature.

### 6.3.3 Influence of microwave power on the hydrogenation of diamond

Hydrogenating diamond films with varying microwave powers was studied with Set C consisting of three samples (C1, C2, C3), which again were grown according to the method described in Section 5.1. Microwave power was the variable in this set with temperature, pressure, flow rate, and time held constant at 850°C, 20 Torr, 200 SCCM, and one hour respectively. The power for each sample varied from 550 Watts to 850 Watts.

The effect of hydrogenation power on the electron emission of the diamond films from Set C was observed to have little effect. The plot of the emission current density vs. temperature for samples exposed to 550, 700, and 850 Watts were extremely similar with the discrepancies

being within a reasonable margin of error (Figure 6.11). This indicated that microwave power has little effect on overall emission current.

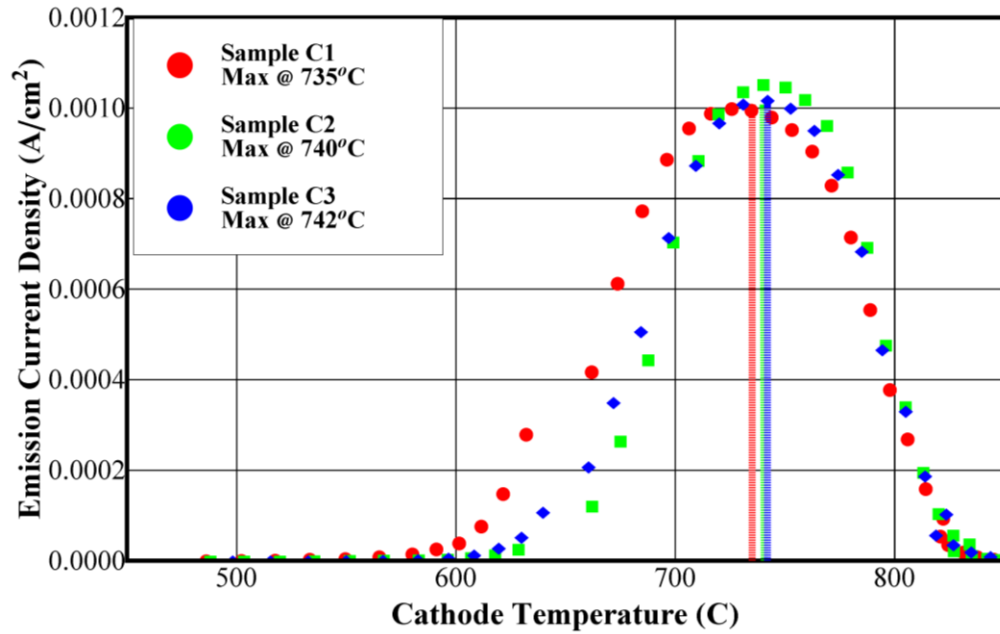


**Figure 6.11** Emission current density vs. cathode temperature of samples C1, C2, and C3 hydrogenated at pressures of 550, 700, and 850 Watts, respectively. It can be seen that increased microwave power had little effect on emission current.

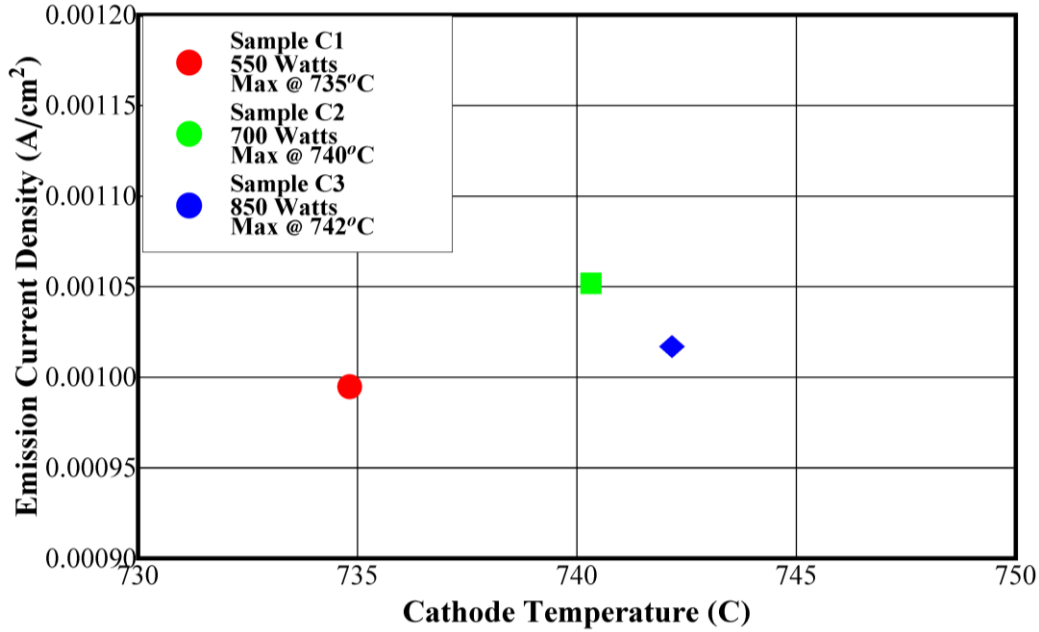


**Figure 6.12** Maximum emission current density values as a function of temperature at which they were achieved for each hydrogenation treatment. It can be seen that there microwave power had little influence on maximum emission current density values.

### 6.3.4 Effects of varying hydrogenation recipes

It has been shown in this study that hydrogenation conditions can impact emission current performance from nitrogen-incorporated diamond films. Among the parameters examined, hydrogenation temperature appeared to have the greatest effect. The sample hydrogenated at 400°C achieved the highest emission of the four temperatures tested followed closely by the 850°C treatment. Increasing hydrogenation time was shown to result in reduced emission current while hydrogenation power was determined to have a negligible effect. Based on these results, the following experiments utilized the 850°C hydrogenation treatment described in Section 6.3.1. Though the 850°C treatment achieved slightly less emission current than the 400°C treatment, it was able to achieve this current at a higher temperature and one of the goals

of the present research was to increase the temperature ceiling at which diamond films can operate.

#### 6.4 Desorption process of hydrogen in diamond

Accounts of previous works have been discussed which illustrate that hydrogen has beneficial effects on the electronic properties of diamond films. Further, the work in this dissertation has been the first to not only specifically prove that hydrogen enhances the thermionic emission of diamond films but to examine its effects quantitatively. The following study sought to further this understanding by calculating the activation energy of the hydrogen desorption process from diamond films.

Examination of the Richardson equation (Eq. 6.1) indicates that if a cathode is held at a constant temperature over a period of time, the thermionic emission current should also be constant. In other words, the Richardson equation contains no explicit time dependence. Though hydrogen desorption has been mentioned in previous thermionic emission studies involving diamond, no known studies have examined the isothermal thermionic emission current of diamond films which this study seeks to accomplish.

With any desorption reaction, hydrogen desorption can be described by the Polanyi-Wigner equation seen below.

$$R_d = \frac{d[H]}{dt} = k_m * [H]^m = [H]^m * k_m^o * \exp(-E_m/RT) \quad (6.3)$$

Where  $k_m$ : the rate constant;  $[H]$ : the hydrogen concentration;  $M$ : the formal order;  $E_m$ : the activation energy; and  $k_m^o$ : the pre-exponential factor.[77] As this study examined the isothermal desorption of hydrogen from diamond surfaces, it was useful to integrate Equation 6.3 with

respect to time to obtain equations that describe the desorption as a function of time. The integrated rate equations for zeroth, 1/2, first, and second order reactions can be seen below.

$$kt = [H_o] - [H], \text{ zeroth} \quad (6.4)$$

$$kt = 2 \left( \sqrt{[H_o]} - \sqrt{[H]} \right), \text{ } 1/2 \text{ order} \quad (6.5)$$

$$kt = -\ln \left( \frac{[H_o]}{[H]} \right), \text{ first order} \quad (6.6)$$

$$kt = \frac{1}{[H]} - \frac{1}{[H_o]}, \text{ second order} \quad (6.7)$$

Where k: the rate constant,  $[H_o]$ : the initial surface hydrogen concentration, and  $[H]$  the surface hydrogen concentration at time t.[84] The integrated rate equations seen above in Equations 6.4-6.7 provide a mathematical relationship between the initial hydrogen concentration and the concentration at time t in terms of a rate constant k. Determination of the reaction order is typically done by observing the decrease (or increase) of the concentration of a certain species as a function of time and comparing the data to Equations 6.4-6.7 to determine which has the best fit. The present study utilized a novel method to determine the desorption kinetics of hydrogen in diamond by analyzing the isothermal thermionic emission current behavior instead of directly observing the desorbed species.

#### 6.4.1 Diamond sample preparation

For this study, two diamond films (A and B) were synthesized according to Section 5.1. Both films were initially heated at 900°C in vacuum to fully desorb all hydrogen present from the deposition process. The samples were then exposed to identical hydrogenation treatments in the MPCVD chamber for one hour under the following conditions: temperature = 850°C, H<sub>2</sub> flow rate = 200 SCCM, microwave power = 550 Watts, and chamber pressure = 20 Torr. The sample

heater was then turned off and the samples were let cool in the hydrogen plasma until the temperature reached 500°C (which took ~ 5 minutes) after which, the microwave power was shut off and the chamber evacuated so the remaining sample cooling took place in a vacuum environment. It is necessary to cool the samples in the hydrogen plasma to prevent any desorption of the hydrogen while cooling. The samples were then tested separately in the vacuum testing chamber described in Section 5.2.1. The isothermal emission current was studied using the isothermal (IT) testing configuration described in Section 5.3.2.

#### 6.4.2 Isothermal emission behavior of hydrogenated diamond films

The two samples prepared for this study were tested a total of three times at three different temperatures. The first sample (A) was tested at 600°C, 650°C, and 750°C, while the second sample (B) was tested at 700°C, 725°C, and 775°C. The isothermal emission current behavior of the two samples can be seen below in Figure 6.13. The data was normalized such that  $J_0 = J(t=0) = 1$  for direct comparison. The vertical and horizontal error bars seen for each data point in Figure 6.13 represent the accuracy of the ammeter and pyrometer, respectively, according to their manufacturers' specifications. When these diamond emitters were held at a constant temperature, it was clear that the emission current decreased with time which is inconsistent with the Richardson equation as previously discussed. Additionally, it can be seen that the rate of emission current decrease became larger with increasing temperature.

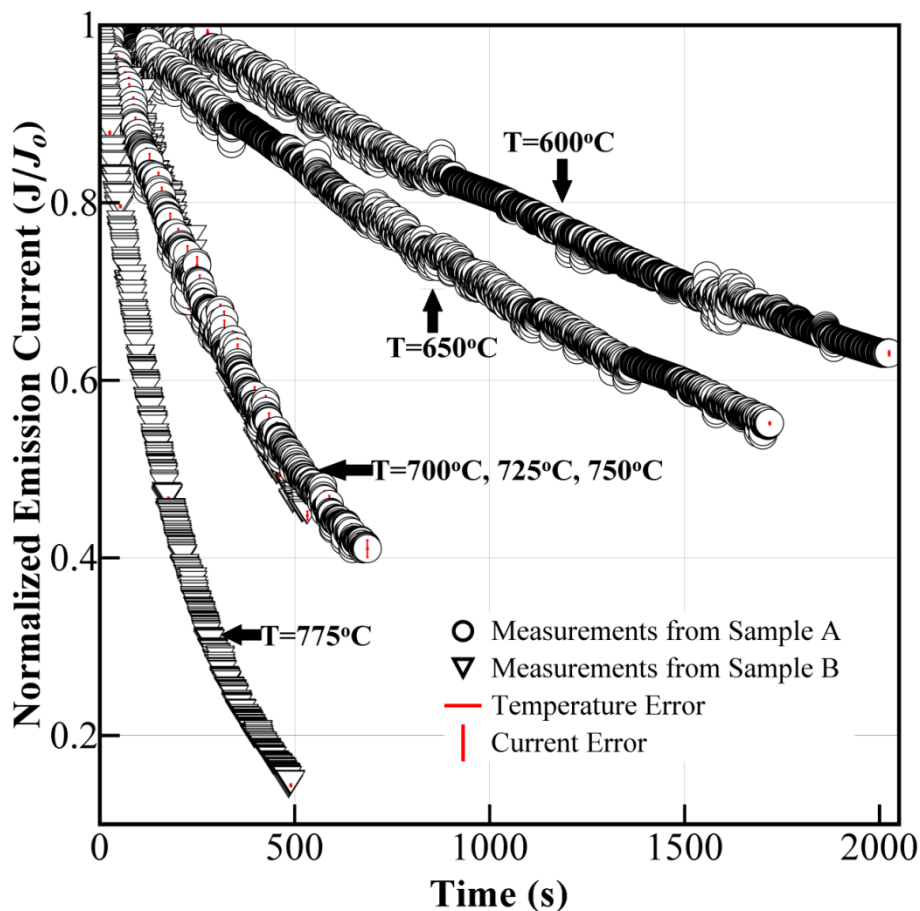


**Figure 6.13** Normalized emission current for two samples (sample A: 600°C, 650°C, 750°C; sample B: 700°C, 725°C, 775°C) at different operation temperatures. The small vertical and horizontal lines within each data point represent the error of the ammeter and the pyrometer respectively.

Previous experiments, using various other techniques, have observed that the desorption of hydrogen from CVD diamond surfaces follows the first order reaction rate.[78, 80, 82, 84, 145-147] Examination of Equation 6.6 indicates that if a reaction is first order, a plot of  $-\ln[H]/[H]_0$  versus time should yield a straight line with a slope equal to the rate  $k$ . Such a plot can be seen in Figure 6.14 with the y-axis equal to  $-\ln[J]/[J]_0$ , where  $[J]$  and  $[J]_0$  are the emission current and initial emission current respectively, and were substituted for the reactant

concentrations in Equation 6.6. In Figure 6.14, it is clear that each temperature test yielded a first order curve that was linear, indicating that a first order reaction was indeed observed.

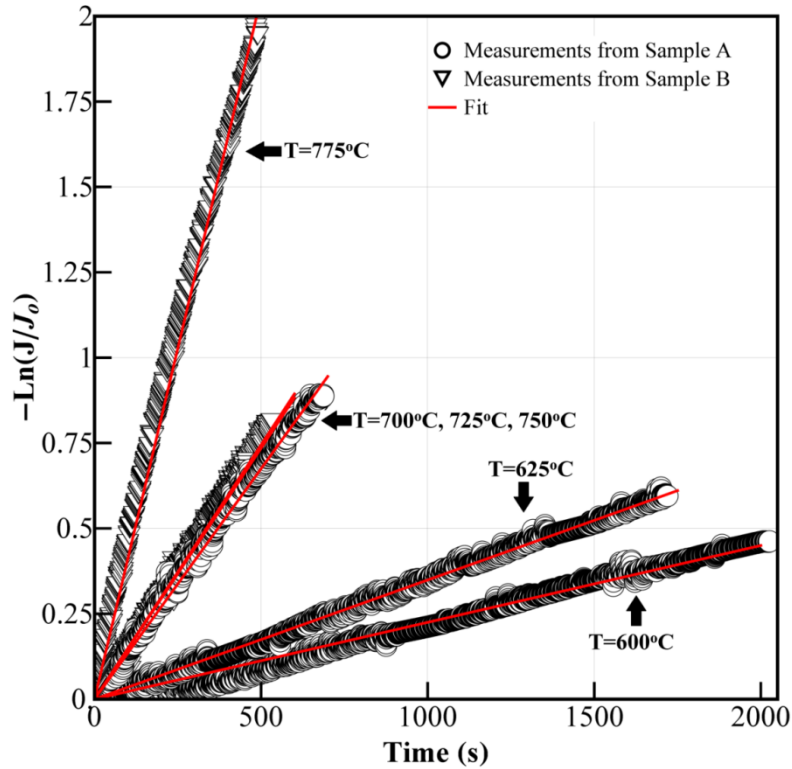


**Figure 6.14** First-order plots of emission current for temperatures between 600°C and 775°C. Two samples were measured (Sample A: 600 °C, 650 °C, 750 °C; Sample B: 700 °C, 725 °C, 775 °C).

### 6.4.3 Calculation of the activation energy of hydrogen in diamond

A thermally driven classical reaction process where a reaction energy barrier must be overcome can be described by the Arrhenius equation as:

$$k = A_H e^{-E_A/k_B T} \quad (6.8)$$

where  $T$  is temperature (K),  $A_H$  is a pre-exponential factor,  $E_A$  is an activation energy (eV), and  $k$  is the Boltzmann constant ( $8.617 \times 10^{-5}$  eV/K).[77] Upon rearrangement of the Arrhenius equation, activation energy and pre-exponential factor can be determined using the  $k$  values determined for each temperature from Figure 6.14 by plotting  $\ln(k)$  against  $1/k_b T$ . This plot can be seen below in Figure 6.15 for which an activation energy and pre-exponential constant were found to be 1.23 eV and  $2.5 \times 10^3$  s<sup>-1</sup>, respectively.

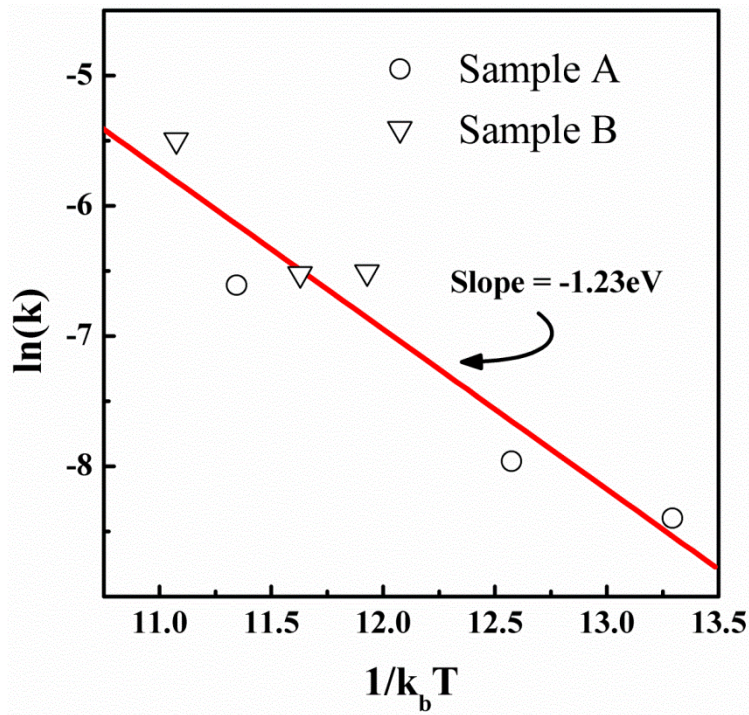


**Figure 6.15** Arrhenius plot of rate constants obtained in Figure 3. The slope is equal to  $-E_A$ , found to be 1.23eV and the y-intercept is equal to  $\ln(k_0)$  found to be  $2.5 \times 10^3$  s<sup>-1</sup>.

It has so far been assumed that the desorption of hydrogen is primarily responsible for the observed isothermal degradation of emission current and the results obtained in this study appear to add validity to this assumption.[68, 148, 149] Previous theoretical and experimental work has

demonstrated that diamond(100):H or diamond(111):H surfaces exhibit negative electron affinity. This property arises from the surface dipole moment the hydrogen-terminated surface bonds invoke. In a semiconductor, the work function can be described as the energy difference between the Fermi level and the conduction band plus the energy difference from the conduction band to the vacuum level (electron affinity). Thus a negative electron affinity equates to a lower function which, from the Richardson equation, leads to increased thermionic emission. A switch from negative to positive electron affinity has also been observed in parallel with a phase transition of the diamond surface from H-terminated (1 x 1) to hydrogen free reconstructed (2 x 1) upon thermal annealing.[150, 151] Also, post-testing exposure of degraded emission diamond films to low intensity hydrogen plasmas resulted in significantly enhanced recovery of thermionic emission capability.[76] It then follows that the desorption of a hydrogen atom from a surface site would result in a vacancy with a higher electron affinity (and also a higher work function) at that site implying a direct correlation between surface hydrogen concentration and electron emission current.

Previous studies have suggested that high surface hydrogen concentrations correspond to two hydrogen atoms per surface carbon atom suggesting a dihydride surface configuration.[85] Taking this into account, A.V. Hamza and colleagues provides suitable explanation of the first order hydrogen desorption mechanism observed in the present study. Hamza postulates that the desorption process consists of the “unimolecular decomposition of two adjacent dihydrides to form two adjacent monohydrides.”[82] Observations from the present work, that the emission current declined according to a first-order rate equation, are therefore consistent with the presence and desorption of hydrogen at its surface determining emission energetics.

Various methods have been used in previous studies attempting to determine the activation energy of the hydrogen desorption from diamond. These methods include direct recoil spectroscopy (DRS), thermal desorption spectroscopy (TDS), and reflection high-energy electron spectroscopy (RHEED), among others. A rather large range of activation energy values have been reported and can be seen below in Table 6.1. The value of 1.23eV determined from the Arrhenius behavior plotted in Figure 6.15 agrees with the median reported values around 1.25eV for (111) and 1.5-1.7eV for (100) surfaces.

**Table 6.1** Measurements of the bond energy from hydrogen desorption studies using various experimental approaches.

Diamond Face	Ea (eV)	Method	Reference
001	0.91	RHEED	[78]
111	1.25	Change in x	[79]
100	3.15	TDS	[80]
100	1.48	Theory	[81]
100	1.60	ESD-TOF	[82]
100	1.47	TPD	[83]
100	1.69	Ion Spectroscopy	[84]

In summary, this study measured the isothermal, time-dependent thermionic emission from polycrystalline diamond films at temperatures ranging from 600-800°C. The emission current was observed to degrade over time following the first-order reaction trend also observed by other previous studies using different methods. The activation energy of 1.23 eV found in this study is also in agreement with previously reported hydrogen-diamond desorption reactions on the 100 and 111 surfaces. The results obtained in the present study not only provide evidence that hydrogen has beneficial effects on the thermionic emission from diamond cathodes, but also

indicated that the magnitude of thermionic emission is directly proportional to the amount of hydrogen present in the sample.

### 6.5 Desorption of deuterium in diamond

The studies presented so far have demonstrated the beneficial effect hydrogen has on the thermionic emission from diamond films. Though the emission current has been seen to increase by several orders of magnitude upon exposure to a hydrogenation treatment compared to as-grown, it has been found that the thermionic emission performance decreased logarithmically (following a first-order trend) when heated to operating temperatures exceeding 600°C.[76, 152] This lack of stable operating performance drastically limits the applicability of hydrogenated diamond cathodes and must be addressed.

The interest in deuterium lies in the kinetic isotope effects that occur when a carbon-hydrogen (C-H) bond is substituted with a carbon-deuterium (C-D) bond. Kinetic isotope effects describe how the reaction rates of chemically identical molecules can vary simply by replacing one element of the molecule with its isotope.[153, 154] The vibrational frequency,  $\nu$ , of both the surface C-H bond and the surface C-D bond can be described as a simple harmonic oscillator (Equation 6.9).[153]

$$\nu = \frac{1}{2\pi} \sqrt{\frac{f}{\mu}} \quad (6.9)$$

$$\mu = \frac{m_C m_H}{m_C + m_H} \quad \text{or} \quad \mu = \frac{m_C m_D}{m_C + m_D} \quad (6.10)$$

Where  $f$  is the spring constant of either the C-H or C-D bond,  $\mu$  is the reduce mass,  $m_C$ ,  $m_H$ , and  $m_D$  are the masses of a carbon, hydrogen, and deuterium atom respectively.[155] Given that deuterium and hydrogen exhibit nearly identical ionization energies,[156] the spring constant,  $f$ , in Equations 6.9 can be approximated to be equal for the C-H and C-D bonds. Further, as

deuterium has twice the atomic mass as hydrogen,[157] the relatively large mass of carbon (compared to hydrogen and deuterium) allows for the effective mass,  $\mu$ , of deuterium to be simplified as being twice that of hydrogen. These assumptions allow for a simple linear relationship for the vibrational frequency of the C-H bond in terms of the C-D bond to be expressed as:

$$v_H = \sqrt{2}v_D \quad (6.11)$$

As the present study was interested in the activation energy of the deuterium bond, it was desired to express the vibrational frequency of a bond in terms of energy. The vibrational energy of a diatomic molecule is provided in Equation 6.12.

$$E_n = \left(n + \frac{1}{2}\right) h\nu \quad (6.12)$$

Where  $n$ : the vibrational quantum number,  $h$ : Plank's constant ( $4.135 \times 10^{-15}$  eV\*s), and  $\nu$ : the vibrational frequency of the bond found in Equation 2 ( $s^{-1}$ ).[153] When characterizing kinetic isotope effects, it is often useful to express the vibrational energy in terms of zero point energy (ZPE). At room temperature, virtually all molecules with a certain vibrational frequency can be approximated to be at the lowest vibrational energy level ( $n=0$ ) which is referenced as the ZPE. [154] Using the relation found in Equation 6.11, an expression can be made relating the zero point energies of the hydrogen and deuterium carbon bonds (Equation 6.13) which indicates that the C-D bond will lie energetically below the C-H bond at the same temperature.

$$ZPE_H = \sqrt{2}ZPE_D \quad (6.13)$$

In a classical reaction, the dissociation of the C-D or C-H bond can only occur when the energy of the molecule is sufficient to overcome an energy barrier known as the dissociation energy,  $D_e$ . [154] The Morse diagram presented in Figure 6.16 demonstrates that the ZPE difference between hydrogen and deuterium requires more energy be imparted to the C-D bond to overcome the dissociation energy than the C-H bond. Thus, assuming kinetic isotope effects are the only factor influencing the reaction, the desorption of deuterium from diamond should have a higher activation energy than the desorption of hydrogen.

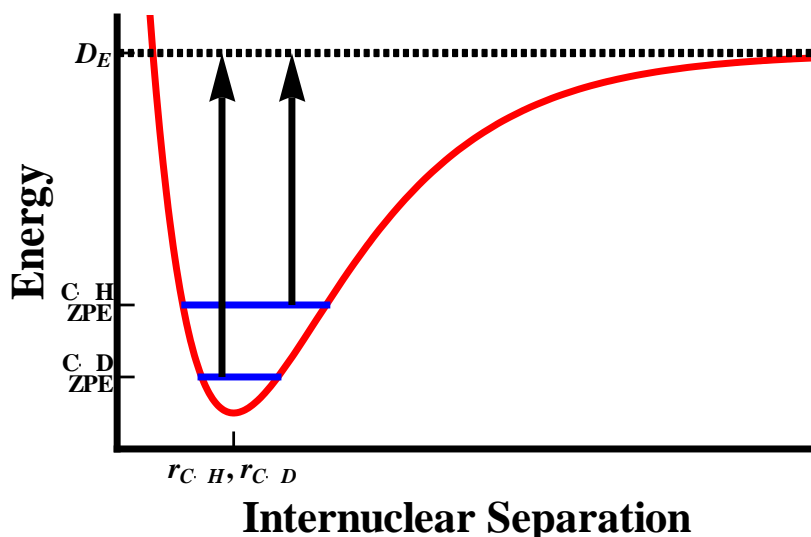


**Figure 6.16** Morse diagram representing the difference in Zero Point Energies (ZPE) between hydrogen and deuterium. As deuterium has a higher mass, it will have a lower vibration energy implying that it will have a larger activation energy than hydrogen.

In the present study, the isothermal thermionic emission current arising from a deuterated diamond sample was examined to characterize the deuterium desorption kinetics. The desorption behavior was compared to the previously reported hydrogen desorption behavior in an effort to better understand the kinetic isotope effects arising from the surface C-D bonds compared to

surface C-H bonds. The information obtained in this study was meant to provide a greater understanding of the thermionic emission phenomena from diamond and is information relevant to the future implementation of such cathodes for use in thermionic applications.

#### 6.4.1 Isothermal emission behavior of deuterated diamond films

The desorption of deuterium from diamond was studied in the same manner as the previous hydrogen desorption experiment. Two samples were prepared for this experiment (A and B) according to the method described in Section 6.4.1, but with using a deuterium plasma instead of a hydrogen plasma. The isothermal emission current behavior from each sample was examined using the IT configuration for time periods ranging from 500 to 2500 seconds at three separate temperatures providing six total points for which the desorption parameters could be calculated. Both samples were tested in order of increasing temperature with Sample A tested at 650°C, 700°C, and 750°C and Sample B tested at 675°C, 725°C, and 750°C. Isothermal emission testing at each temperature is shown in Figure 6.17. The emission current data was normalized such that  $J_0=J(t=0)=1$  to assist in the following calculation of the deuterium desorption parameters. It can be clearly seen in Figure 6.17 that the emission current followed a decreasing trend with respect to time as to be predicted from previous work.[152] The normalized emission current data was then analyzed according to the first-order reaction equation (Equation 6.14) by plotting the natural logarithm of the emission current against time (Figure 6.18).

$$-\ln \frac{[A]}{[A]_0} = kt \quad (6.14)$$

Where  $k$  is the desorption rate ( $s^{-1}$ ),  $t$  is time (s), and  $[A]/[A]_0$  is the normalized emission current.[84] The resulting linear trends indicated that the decay in emission current followed first-order reaction behavior with the slope at each temperature corresponding to the reaction

rate. A first order desorption trend was also observed for the previously discussed study on hydrogen as well as several other previous studies by other researchers, further verifying that the deuterium desorption rate was indeed being directly observed.[152, 158-160]

The rate of a classical thermally driven reaction in which a barrier must be overcome can be expressed as a function of temperature by means of the Arrhenius equation (Equation 6.15).

$$k = A_D e^{-E_{aD}/k_b T} \quad (6.15)$$

Where  $k$ : the reaction rate ( $s^{-1}$ );  $A_D$ : the Arrhenius pre-exponential constant ( $s^{-1}$ );  $E_{aD}$ : the activation energy of deuterium;  $k_b$ : the Boltzmann constant ( $8.617 \times 10^{-5} \text{ eV} \cdot \text{Kelvin}^{-1}$ ); and  $T$ : the temperature of the sample (Kelvin).[77] The desorption rate at each temperature calculated from Equation 6.14 was analyzed according to the Arrhenius equation (Figure 6.19). A linear fit of the resulting Arrhenius plot indicated an activation energy and pre-exponential constant of 1.95 eV and  $8.6 \times 10^6 \text{ s}^{-1}$ , respectively.

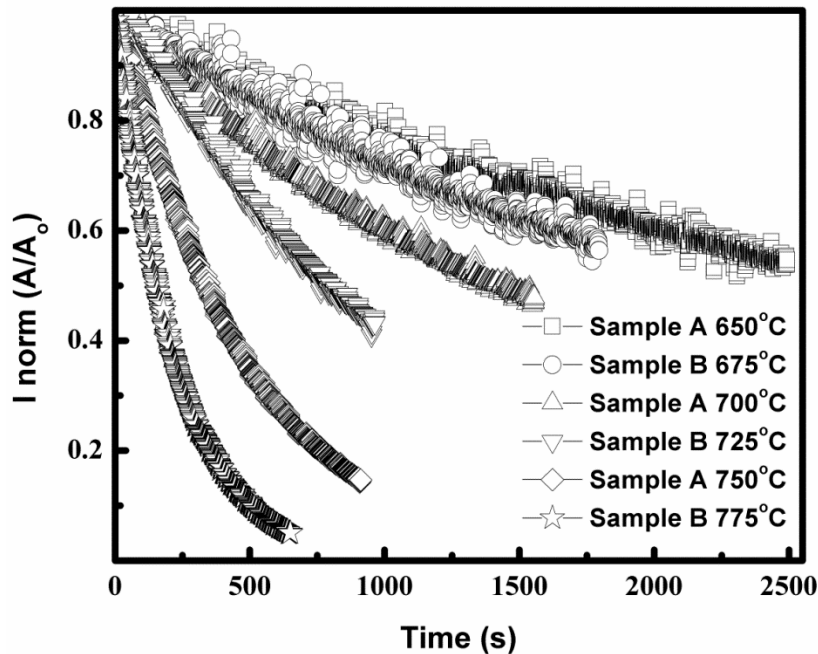


**Figure 6.17** Normalized thermionic emission current behaviors as a function of time.

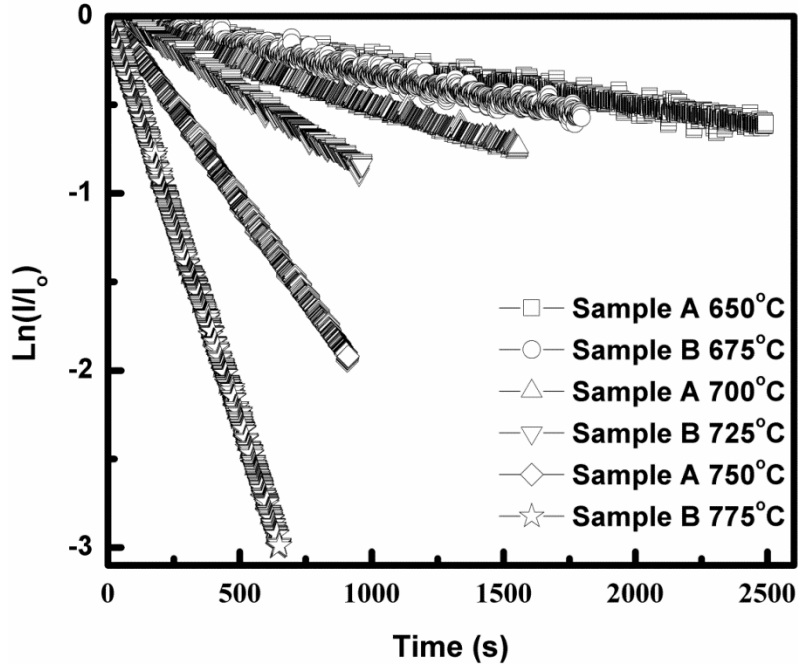


**Figure 6.18** First order desorption plot of the normalized isothermal thermionic emission current behaviors. The linear trend at each temperature indicates the desorption followed first order kinetic behavior.

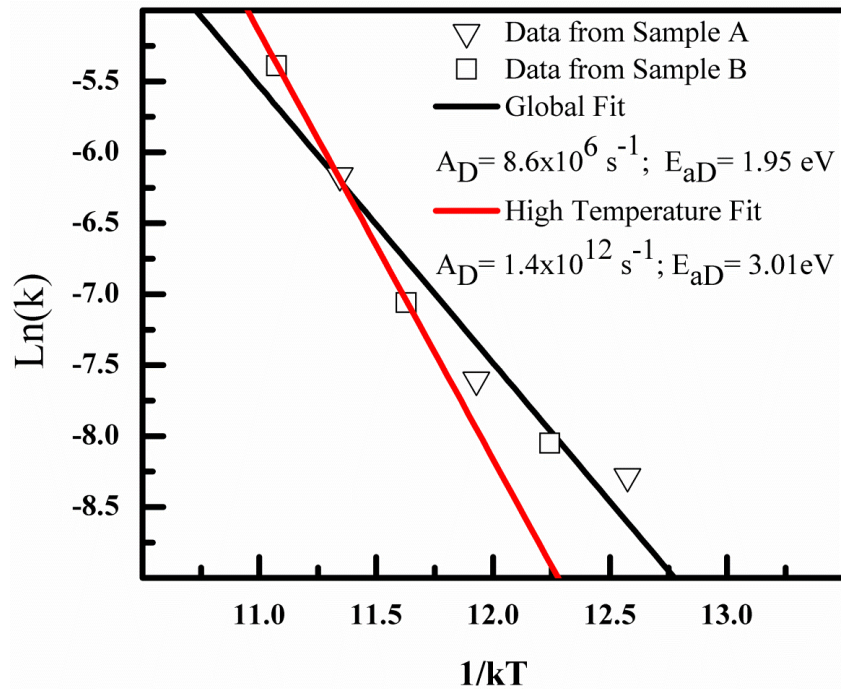


**Figure 6.19** Arrhenius plot of the desorption data. The deviation from linearity at lower temperatures incates tunneling could have played a role in the desorption mechanism.

Examination of the Arrhenius plot in Figure 6.19 yielded some unexpected results. There appeared to be a deviation from linearity at lower temperatures. According to E.V. Anslyn and D.A. Dougherty, this deviation, where the slope becomes less negative at lower temperatures, is often an indication of tunneling.[154] Rather than the classical case whereby an energy barrier must be overcome in order for a reaction to take place, tunneling allows a reaction to occur at lower energies due to the molecule's wave function passing through the barrier. This scenario is graphically depicted in Figure 6.20. As tunneling should become less significant at higher temperatures, a second fit was performed using only the higher temperatures giving an activation energy and pre-exponential factor of 3.01 eV and  $1.4 \times 10^{10} \text{ s}^{-1}$ , respectively. These values are consistent with other reported values in seen in Table 6.2.

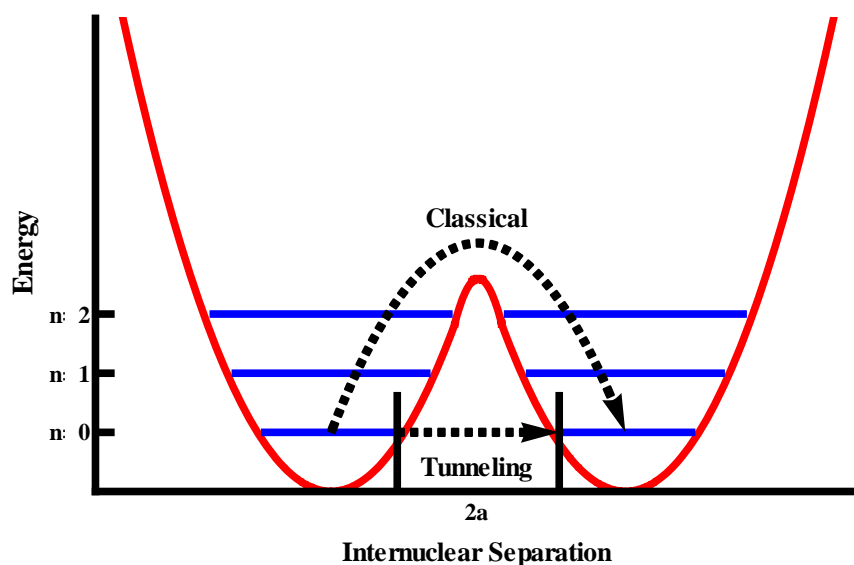


**Figure 6.20** Generic parabolic potential diagram comparing the classical to the tunneling desorption mechanism.

**Table 6.2** Activation energies and pre-exponential factors obtained from previous deuterium desorption studies

Ea (eV)	A	Source
3.82	$1.0 \times 10^{13}$	[158]
3.47	$5.0 \times 10^{12}$	[159] (Plane)
2.91	$5.0 \times 10^{12}$	[159] (Edge)
3.08	$1.0 \times 10^{13}$	[161]
3.7	$9.5 \times 10^{13}$	[160]

It is possible to account for tunneling by incorporating a pre-exponential correction factor,  $Q$ , into the Arrhenius equation above. This factor, first mathematically derived by Bell, accounts for the mass of the desorbing species ( $m$ ), the width of the barrier ( $2a$ ), the temperature ( $T$ ), and the activation energy ( $E_a$ ). The tunneling correction for the Arrhenius equation can be seen below in Equations 6.16-19.[162] It should be noted that this tunneling correction assumes parabolic potential wells as depicted in Figure 6.20.

$$k = Q A e^{-E_a/RT} \quad (6.16)$$

$$Q = \frac{\pi\alpha/\beta}{\sin(\pi\alpha/\beta)} - \alpha e^\alpha \left( \frac{e^{-\beta}}{\beta-\alpha} - \frac{e^{-2\beta}}{2\beta-\alpha} + \frac{e^{-3\beta}}{3\beta-\alpha} - \dots \right) \quad (6.17)$$

$$\alpha = E/k_b T \quad (6.18)$$

$$\beta = \frac{2a\pi^2(2mE_a)^{1/2}}{h} \quad (6.19)$$

Where  $2a$  is the width of the tunneling barrier (meters),  $m$  is the mass of the tunneling particle ( $\text{eV}\cdot\text{c}^{-2}$ ), and  $h$  is Plank's constant ( $4.135 \times 10^{-15} \text{ eV}\cdot\text{s}$ ).

A fit of the  $k$  values for each temperature was performed with respect to the tunneling equation described in Equations 6.16-19 using a Levenberg-Marquardt algorithm. The starting parameters for the fit algorithm were chosen to be the  $E_{aD}$  and  $A_D$  values obtained from the high

temperature fit in Figure 6.19. From Figure 6.21, it can be seen that a fit with a coefficient of determination ( $R^2$ ) value greater than 0.99 was found and the tunneling barrier width,  $2a$ , adjusted pre-exponential factor,  $A_D$ , and adjusted activation energy,  $E_{aD}$ , determined to be 25.3 pm,  $2.3 \times 10^{12} \text{ s}^{-1}$ , and 3.19 eV, respectively. It must be noted that though tunneling is likely the cause of the deviation from linearity in Figure 6.19 and the above best-fit parameters describe the experimental data with a strong goodness of fit, testing at several more temperatures than the six performed in this study will be required for a more accurate analysis. Regardless, the agreement of the data with Bell's tunneling equation provides strong evidence that deuterium does not desorb from diamond in a classical manner.

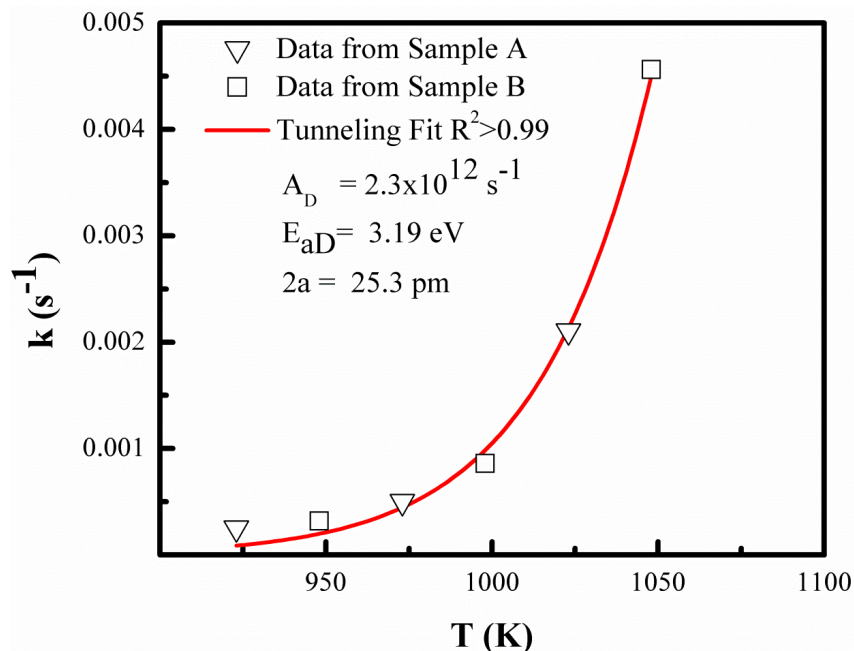


**Figure 6.21** Fit of the  $k$  values at each temperature accounting for tunneling.

The results obtained in this study indicated that tunneling plays a role in the desorption of deuterium from diamond. Assuming this is true, it can be inferred that tunneling must also influence the desorption of hydrogen from diamond. This was addressed by reexamining the hydrogen desorption data from the previous study with respect to Equations 6.16-19.[152] Though the previous hydrogen desorption data exhibited a higher variation than the deuterium desorption data in the present study, a fairly strong fit was made ( $R^2=0.84$ ) with the desorption parameters values for the tunneling barrier width, pre-exponential constant, and activation energy values equal to 78.5 pm,  $9.83 \times 10^5 \text{ s}^{-1}$ , and 1.76 eV, respectively (Figure 6.23).

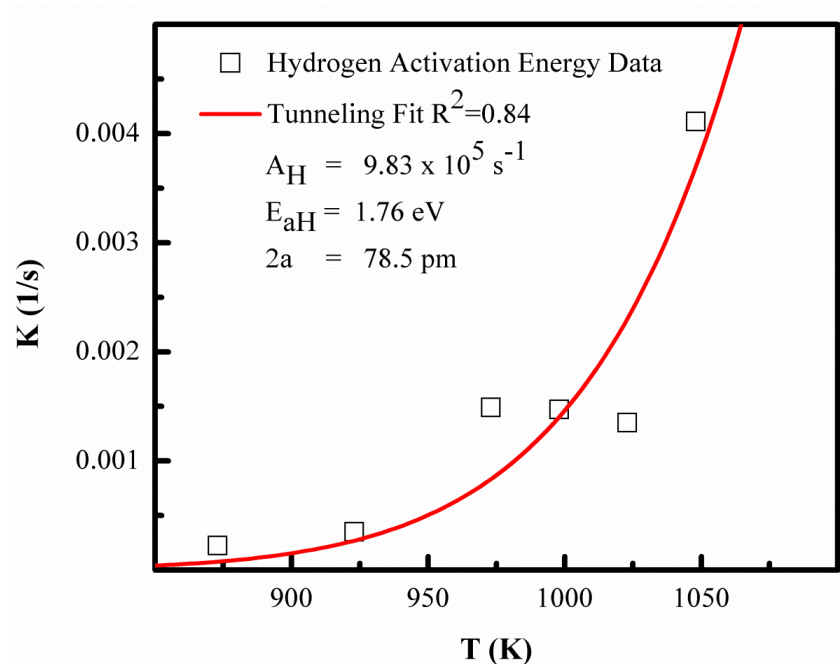


**Figure 6.22** Tunneling fit to the hydrogen desorption data from the previous section.

### 6.4.3 Summary of the desorption of deuterium from diamond

The results presented in the previous two desorption studies provide useful insight into hydrogen's role in the thermionic emission process from diamond films. The observed first order decay in emission current for both hydrogenated and deuterated diamond samples is evidence that emission current is directly proportional to the hydrogen (deuterium) concentration. Further, the present study is the first known to suggest that the desorption reaction is non-classical with contributions from tunneling. Lastly, the desorption of the C-D bond appeared to have a much higher activation energy ( $>1\text{eV}$ ) than the C-H bond. Though it is difficult to quantify, this higher activation energy should allow a deuterated diamond sample to have a much higher temperature ceiling than a corresponding hydrogenated sample resulting in improved thermionic performance. In conclusion, the research presented thus far has performed the most detailed study to date on hydrogen's role in the thermionic emission behavior of diamond films. The following chapter sought to further this research by exposing diamond films to various low pressure gaseous environments in an effort to further increase the emission performance beyond hydrogenation.

## CHAPTER VII

### THERMIONIC EMISSION CHARACTERIZATION OF GASEOUS ENVIRONMENTS

The work discussed in the previous chapter characterized the thermionic emission properties of diamond films operating in a vacuum environment. It was shown that exposure to hydrogen plasma significantly enhanced the thermionic emission performance but hydrogen's beneficial effects began to diminish when the diamond cathodes were either heated to high temperatures or operated for extended periods of time. The work presented in this chapter sought to explore a new approach, beyond hydrogenation, to increase both the thermionic emission performance and the long term emission stability of diamond films. This approach consisted of operating diamond thermionic cathodes in low pressure gaseous environments. Multiple gaseous species were studied and detailed analyses of the results are presented in this chapter.

#### 7.1 Molecular Nitrogen

The first gaseous species examined to determine its influence on the thermionic emission performance of nitrogen-incorporated diamond cathodes was molecular nitrogen ( $N_2$ ). Testing with  $N_2$  was chosen primarily to act as a control due to the easily predictable influence it should have on the thermionic emission current. Molecular nitrogen possesses a relatively high magnitude negative electron affinity of -1.8 eV.[163] The electron affinity is the energy difference between the ground state of molecule and its negatively charged anion. The electron affinity value for nitrogen indicates that the ground state of the  $N_2$  molecule lies 1.8 eV below the anion  $N_2^-$  thus  $N_2^-$  is unstable. Further, molecular nitrogen has an extremely high dissociation energy of 9.8 eV and a large (relative to the diamond lattice spacing) atomic cross section of  $\sim 10^{-16}$

$17 \text{ cm}^2$  suggesting that no reaction, bonding, or incorporation will occur when the molecular nitrogen is in contact with the diamond sample.[163, 164] Given these reasons, it can be reasonably inferred that the thermionic emission performance of diamond cathodes in a nitrogen environment would not be positively influenced, due to the reduction in electron mean-free-path. Furthermore, R.J. Nemanich and colleagues have previously operated nitrogen-incorporated diamond cathodes in a molecular nitrogen environment at pressure ranging from 10 mTorr to 1 Torr.[106] This study reported that no identifiable thermionic emission current enhancement was observed.[106] Hence the present study aimed to demonstrate the experimental technique's ability to accurately characterize the thermionic emission performance of diamond films upon exposure to low pressure gaseous environments.

#### 7.1.2 Behavior of diamond thermionic cathodes in a $\text{N}_2$ environment

Nitrogen-incorporated polycrystalline diamond cathodes were deposited according to the method described in Section 5.1 and tested in the manner described in Section 5.4. The results from one of the testing runs on an as-grown diamond sample can be seen below in Figure 7.1. While more data was collected and verified on multiple separate samples, only one complete testing run is shown as the other results exhibited the same trend. Examination of the results confirmed the hypothesis that the thermionic emission performance of diamond cathodes in the presence of nitrogen gas would not be positively affected. The emission current clearly decreased from the baseline level established in high vacuum when the nitrogen was introduced into the chamber to a pressure of  $\sim 5.5 \mu\text{Torr}$  ( $\text{N}_2$  equivalent) measured at the pump. As nitrogen is not believed to interact favorably with the emitted electrons nor affect the diamond sample itself, it was hypothesized here that this decrease in emission current was due to the mean-free-path

reduction of the electrons traversing the cathode-anode gap. A smaller mean-free-path greatly increases the scattering probability of electrons thus causing the electrons to lose kinetic energy thereby reducing the total current collected at the anode.

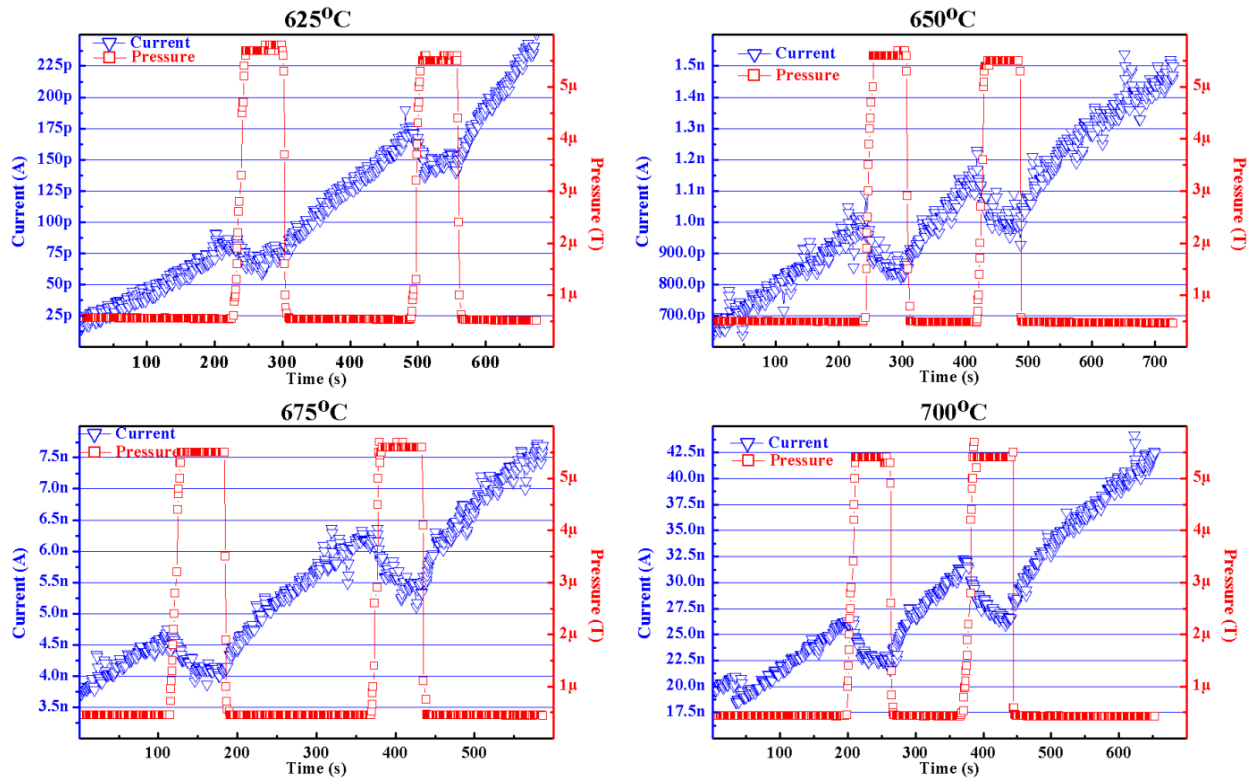


**Figure 7.1** Isothermal thermionic emission behavior of an as-grown nitrogen-incorporated diamond cathode in a molecular nitrogen gaseous environment. It can be clearly seen that nitrogen had a negative effect on the emission performance from diamond cathodes likely due to the decreased mean-free-path of electrons traveling from the cathode to the anode.

The results collected in this study indicated that molecular nitrogen gas was not a suitable candidate to improve the performance of diamond thermionic emitters. This was attributed to molecular nitrogen's relatively high magnitude negative electron affinity of -1.8 eV, high dissociation energy, and large cross-section. The results were consistent with the predicted effect  $N_2$  should have on the thermionic emission from diamond films demonstrating this testing

method's ability to assess the emission performance of diamond films upon exposure to other gaseous environments. The following sections sought to examine multiple other gaseous species that may beneficially enhance the thermionic emission of nitrogen-incorporated diamond cathodes.

## 7.2 Methane

It has long been known that transient negative ions (TNI) can result from the collision of electrons with certain molecules in the gas phase. The formation of a TNI often results in two possible outcomes.[165] One scenario, known as autodetachment, occurs when the TNI emits an extra electron.[166] If autodetachment leaves the neutral molecule in the ground state, such that the energy of the detached electron is equal to the incident electron, the process is known as elastic resonant scattering.[165, 167] Conversely, inelastic resonant scattering occurs when the neutral molecule is left in an excited state with the energy of the detached electron different than that of the incident electron.[165, 167] The other possible scenario for a TNI is through decomposition into stable negatively charged and neutral fragments known as dissociative electron attachment.[165-167] Assuming the correct gaseous vapor is chosen, it was hypothesized that dissociative electron attachment could be used to enhance the thermionic emission properties of diamond. One possible situation could be the dissociation of a hydrogen containing molecule that could allow for the in situ rehydrogenation of a diamond cathode allowing for increased operational temperature, longer stability, and higher emission current.

The ability of a molecule to form a TNI is determined by its electron affinity which is defined as the energy difference between ground states of the neutral molecule (M) and the negatively charged molecule (M<sup>-</sup>). The electron affinity is conventionally referenced as positive

if the ground state of  $M^-$  is energetically lower than that of  $M$ . [165, 166] The definition provides that, for a molecule with a positive electron affinity,  $M^-$  is stable when the attached electron exists in a bound state. [165] Thus the formation of a TNI upon impact with an incident electron typically can only occur for neutral molecules with positive electron affinities. The sign of the electron affinity is rooted in the Pauli exclusion principle which states that no two electrons in an atom/molecule can have the same atomic numbers. [110] When an electron approaches an atom/molecule, a dipole (or any higher multipole) moment is induced creating a binding potential for the electron in the atom/molecule. Some substances such as noble gases have completely occupied outer shells requiring the extra electrons to exist in shells with higher principal quantum numbers. In such cases, the binding potential is not sufficient to bind the electron thereby making the atom/molecule unstable resulting in a negative electron affinity. [168] Conversely, atoms with only a single electron missing from their outer shell allow the approaching electron to easily fill this vacancy. The binding energy in these types of atoms is sufficient to retain the electron allowing for the existence of a stable negative ion and, therefore, a positive electron affinity. [168]

One such molecule of interest with respect to thermionic applications is methane ( $CH_4$ ). Methane has a slightly positive electron affinity of 0.083 eV allowing it to easily form a TNI upon electron impacts. [166] Further, extensive studies of methane have demonstrated that its TNI state decays following dissociative electron attachment forming a mixture of negatively and positively charged products. [169-173] Previous work has also demonstrated the operation of diamond thermionic cathodes in a high pressure (up to 700 mTorr) methane environment greatly increased the emission performance compared to operation in a vacuum environment. [106] The

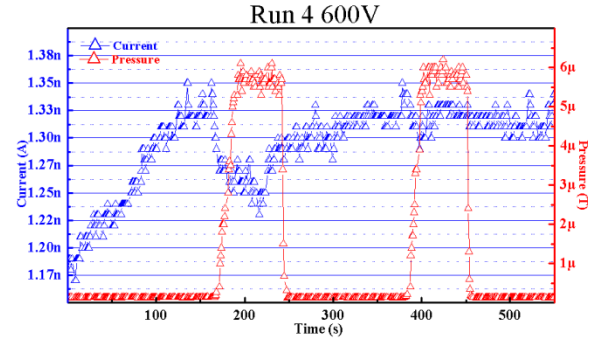
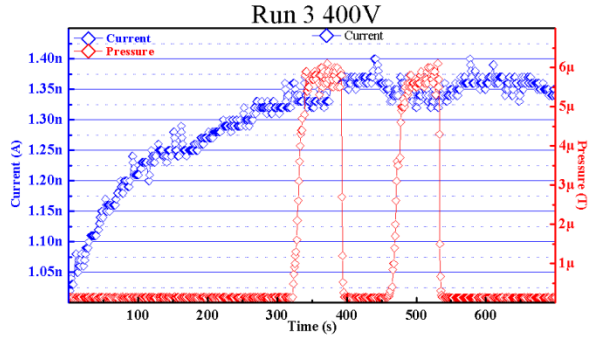
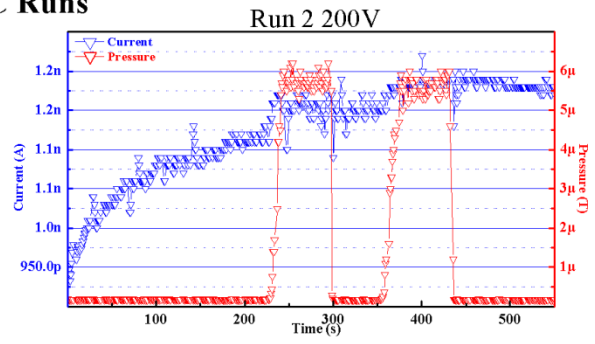
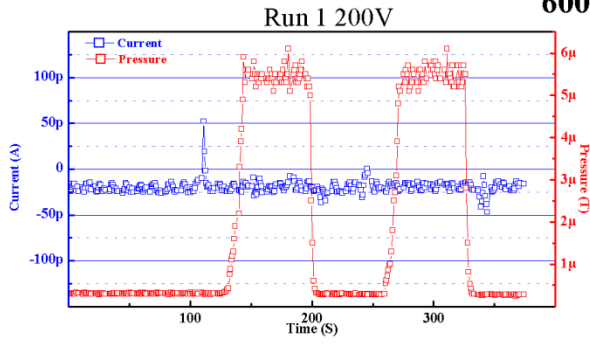
present study sought to further past research by examining the influence of low pressure methane exposure on the thermionic operation of nitrogen-incorporated diamond cathodes.

### 7.2.1 Behavior of diamond thermionic cathodes in a CH<sub>4</sub> environment

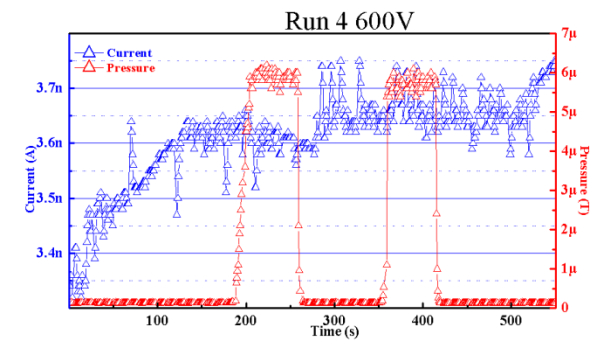
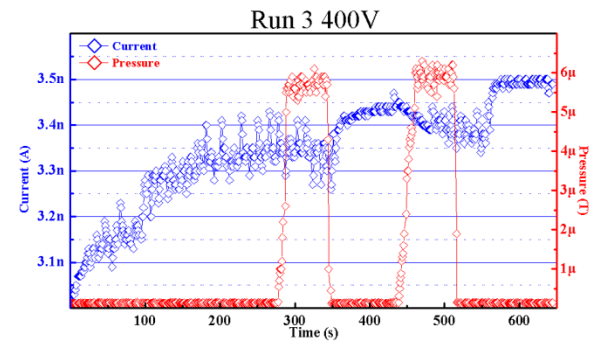
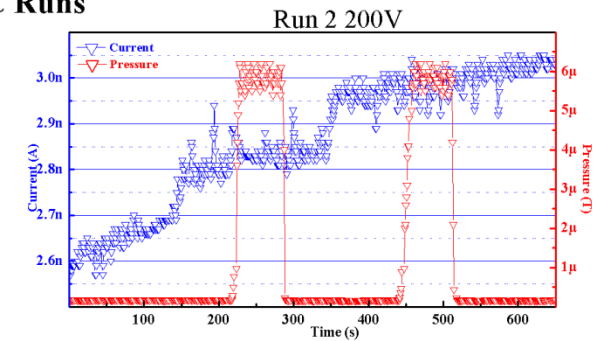
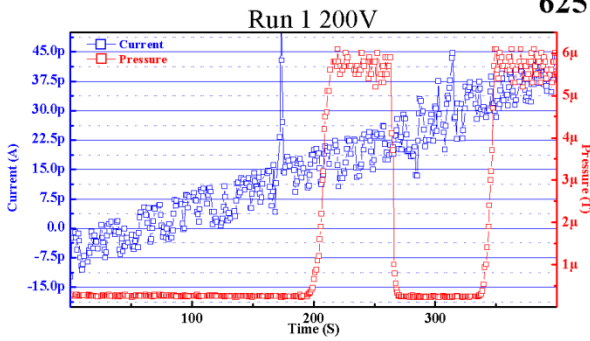
Nitrogen-incorporated polycrystalline diamond cathodes were deposited according to the method described in Section 5.1 and tested in the manner described in Section 5.4. Several tests were performed on samples in both the as-grown state and after exposure to a hydrogenation treatment. The as-grown isothermal emission current results for each test can be seen below in Figure 7.2. The results from the 675°C and 700°C yielded the same behavior as those presented below for 600°C through 650°C and are therefore not shown. Run 1 and Run 2 below were performed with the typical 200 Volt anode bias used in all other previous experiments.

Examination of the as-grown diamond tests showed that no significant effect was observed upon the introduction of methane gas into the testing apparatus. In an effort to further understand this lack of effect, Runs 3 and 4 were performed with higher anode voltages, Run 3 at 400 V and Run 4 at 600 V. Similarly, it can be seen that no observable effect could be discerned upon the introduction of methane gas.

### 600°C Runs



### 625°C Runs



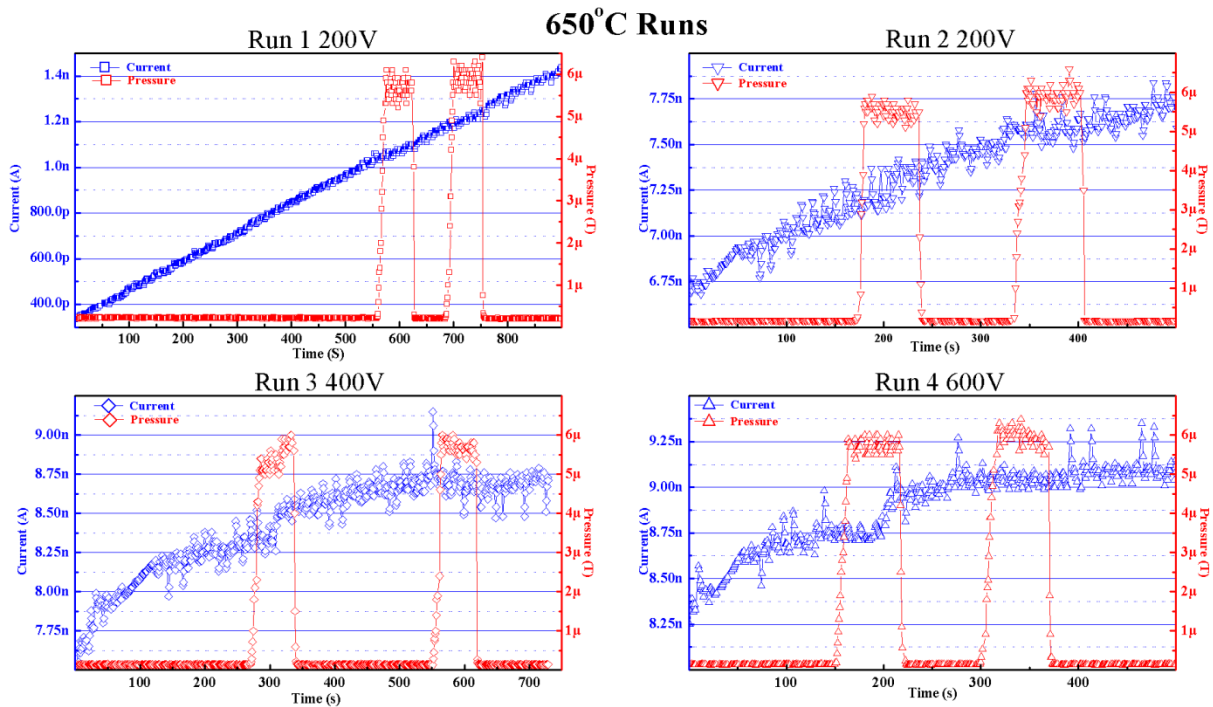


**Figure 7.2** Isothermal thermionic emission current behavior of an as-grown nitrogen-incorporated diamond cathode in the presence of methane gas. Four runs were performed and each run tested at 600°C, 625°C, 650°C, 675°C, and 700°C. Little effect can be seen in the emission current (blue points) as methane pressure (red points) increased. Plots for 675°C and 700°C were not shown as they exhibited the same behavior as the other temperatures. The anode voltage was increased from 200V used in Runs 1 and 2 to 400V in Run 3 and 600V in Run 4. Again, no effect was observed with increasing voltage.

The thermionic emission behavior of a sample after the hydrogenation treatment (which was performed after the as-grown runs) can be seen below in Figure 7.3. Unlike the as-grown sample, the emission current of the hydrogenated sample did exhibit some response to the introduction of methane into the chamber. The fact that this response appeared to be positive (emission current increased in the presence of a low pressure gaseous environment compared to a vacuum environment) agrees with previously reported work, however, the magnitude of this positive response was much smaller than that seen from the same previously reported work.[106]

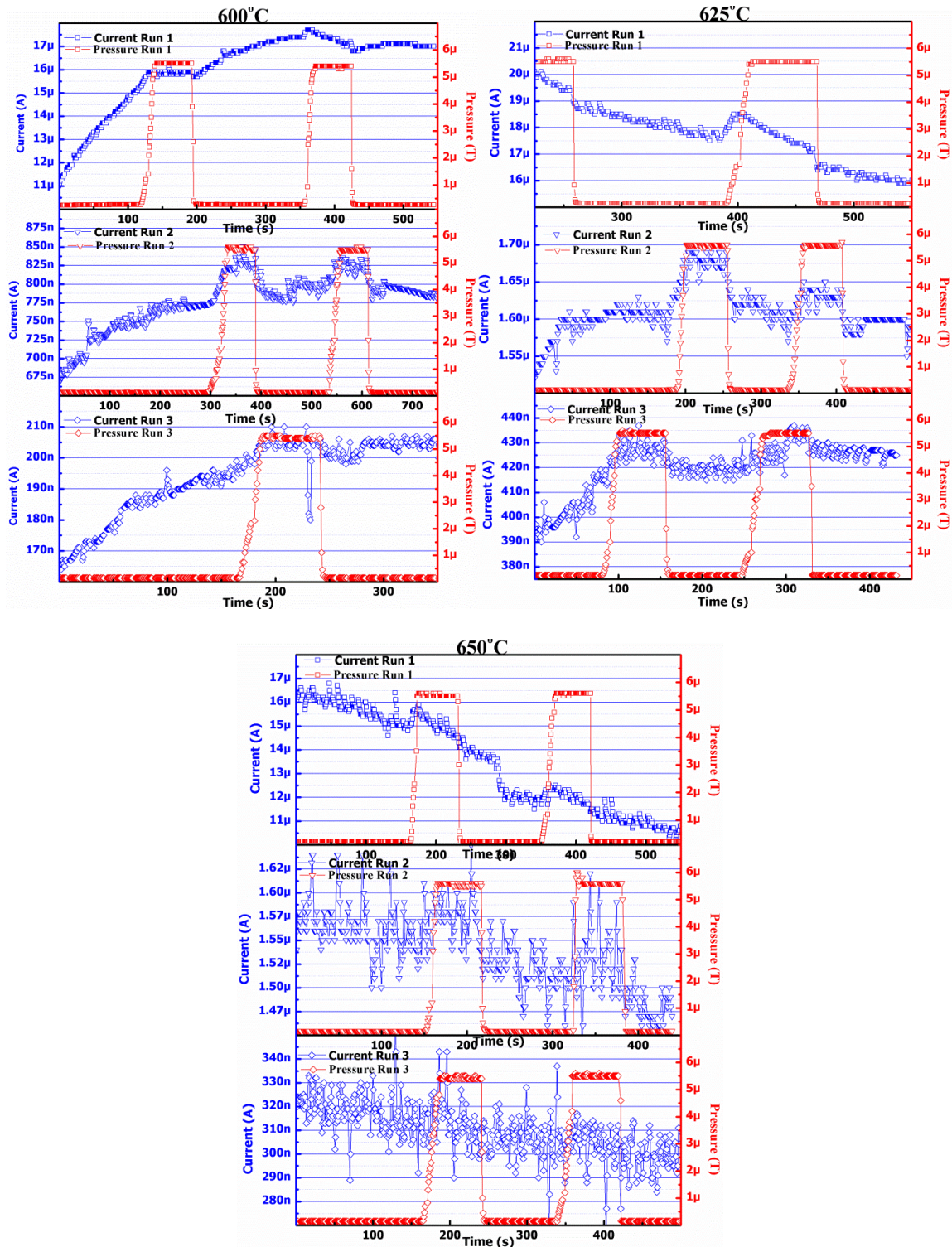


**Figure 7.3** Isothermal emission current testing of a hydrogenated diamond sample in the presence of methane gas. A small positive increase in emission current (blue points) can be seen as the methane pressure (red points) was introduced into the chamber. Plots for the 675°C and 700°C runs were not shown as the variations in emission current were too large to decipher any significant changes in emission current.

Though testing for only one sample in both the as-grown and hydrogenated state is shown, the results were verified on multiple other samples. The influence of methane on the thermionic emission properties of each film demonstrated the same behavior.

### 7.2.2 Analysis of the thermionic emission behavior in CH<sub>4</sub>

The results found in this study appear to contradict previously reported studies which examined the operation of diamond thermionic cathodes in a methane environment. While exposing diamond samples to methane environments at pressure up to 700mTorr, Nemanich and colleagues observed performance enhancement when compared to vacuum operation.[106] The discrepancies between that work and the study presented herein most likely occurred because of the different methane pressures used in each study.

Extensive work has been performed studying the electron impact effects of methane. The vast majority of these studies have focused solely on low-pressure (low mTorr to  $\mu$ Torr range) methane impact studies.[166, 171, 172] In low pressures, the primary dissociation products of the methane TNI are smaller molecules such as CH<sub>3</sub> and H ions.[174] The table below shows several of the products formed in the low pressure dissociation of the Methane TNI from the reaction:  $e^- + CH_4 \rightarrow$  Dissociation Channel. Due to the vast amount of possible charge states of the resulting molecules, the table only displays a few of the possible dissociation channels

**Table 7.1** A few possible low pressure dissociation channels resulting from the impact of an electron with a methane molecule.[171, 174]

Dissociation Channel			
CH <sub>3</sub> + H <sup>-</sup>	CH <sub>3</sub> <sup>*</sup> + H <sup>-</sup>	CH <sub>3</sub> <sup>-</sup> + H	CH <sub>3</sub> + H <sup>(+)</sup> + e <sup>-</sup> (2e <sup>-</sup> )
CH <sub>2</sub> + H + H <sup>-</sup>	CH <sub>2</sub> <sup>-</sup> + H <sub>2</sub>	CH <sub>2</sub> <sup>-</sup> + 2H	CH <sub>2</sub> <sup>+</sup> + 2H + 2e <sup>-</sup>
CH + H <sub>2</sub> + H <sup>-</sup>	CH + H + H + H <sup>-</sup>	CH <sup>+</sup> + 3H + 2e <sup>-</sup>	

At higher pressures, such as those studied by R.J. Nemanich and colleagues, the products of the methane TNI dissociation haven been shown to be much more complex than those in Table 7.1.[106] G. Drabner and colleagues performed an extensive study to examine the products of the dissociation of methane as a function of pressure.[171] Their study found that three different types of products can be formed by increasing the pressure which can be classified into primary, secondary and tertiary products. The primary products have  $m/z$  values equal to 12, 13, 14, 15, and 16 corresponding to C, CH, CH<sub>2</sub>, CH<sub>3</sub>, and CH<sub>4</sub> respectively.[171] The secondary products consist of products with  $m/z$  values of 17, 26, 27, 28, and 29 while the tertiary products consist of  $m/z$  values equal to 39, 41, and 43. The percent of ionization of these species as a function of pressure digitized from Drabner and colleagues' study is presented below in Figures 7.4-6.[171]

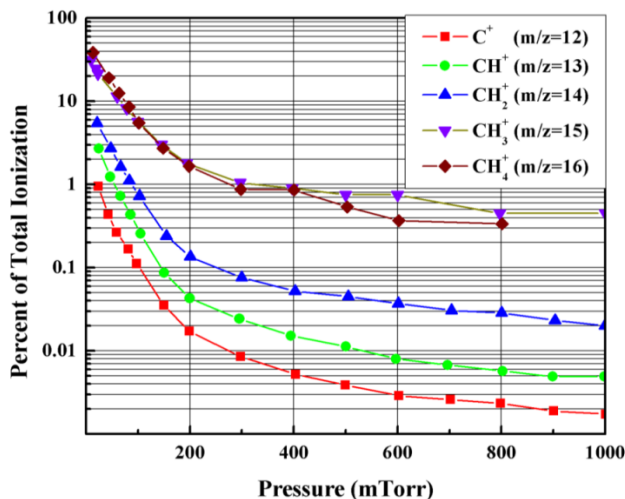


**Figure 7.4** Semi-log plots of the percent of total ionization of the primary methane dissociation products as a function of pressure. Data has been digitized from a previous study by G. Drabner and colleagues.[171]

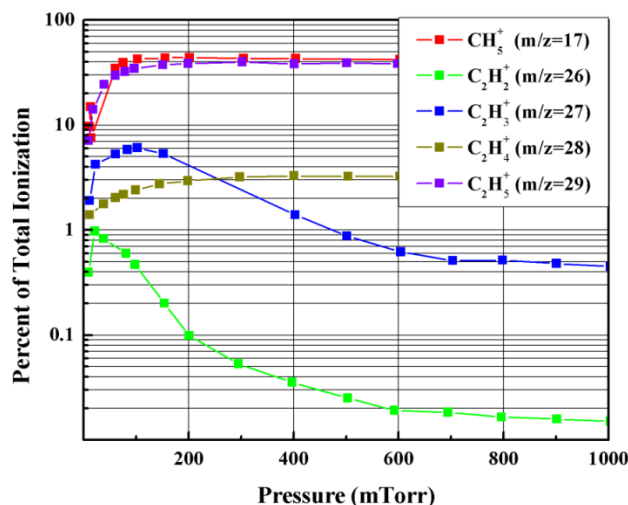


**Figure 7.5** Semi-log plots of the percent of total ionization of the secondary methane dissociation products as a function of pressure. Data has been digitized from a previous study by G. Drabner and colleagues.[171]

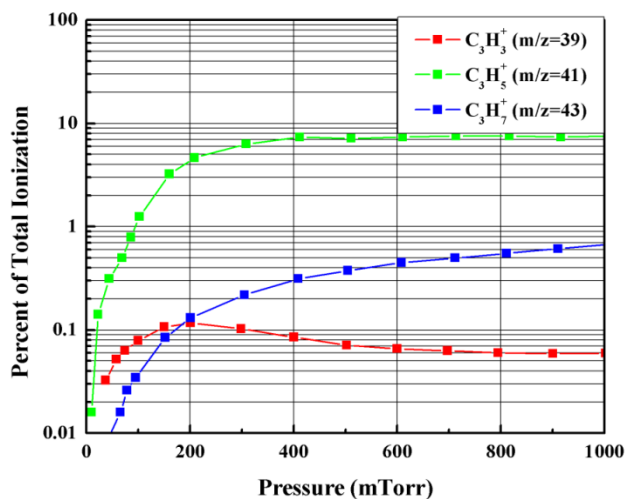


**Figure 7.6** Semi-log plots of the percent of total ionization of the tertiary methane dissociation products as a function of pressure. Data has been digitized from a previous study by G. Drabner and colleagues.[171]

Figures 7.4-6 obtained from Drabner and colleague's study indicate that the formation of primary products all greatly increase at lower pressures while the secondary and tertiary products tend to increase at higher pressures.[171] It then follows that the discrepancies between the results presented in Figures 7.2 and 7.3 and the study by Nemanich can likely be attributed to

the largely differential dissociation products of methane upon electron impact arising from the vastly different pressures used in each study. It is yet to be determined why the formation of more complex carbon chains such as the secondary and tertiary products would be more beneficial to the thermionic emission current from diamond cathodes than the simple carbon compounds found in the primary products. In summary, this study showed methane to have some enhancing effects on the thermionic emission performance of diamond cathodes. However, this enhancement is greatly dependent on pressure.

### 7.3 Water vapor

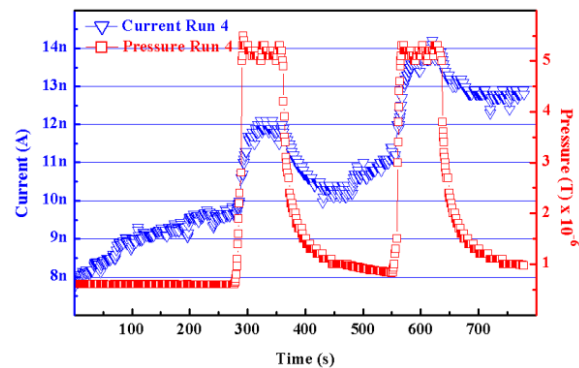
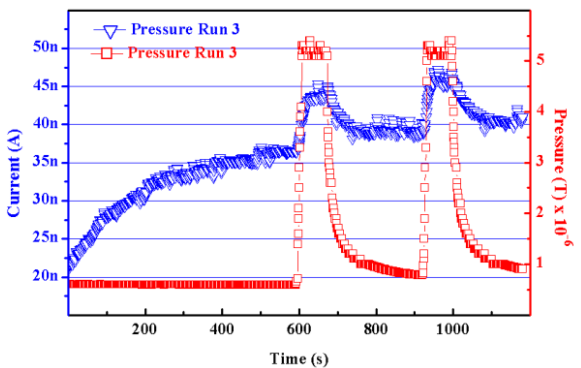
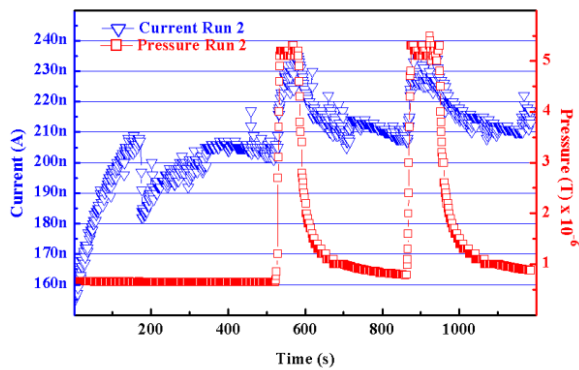
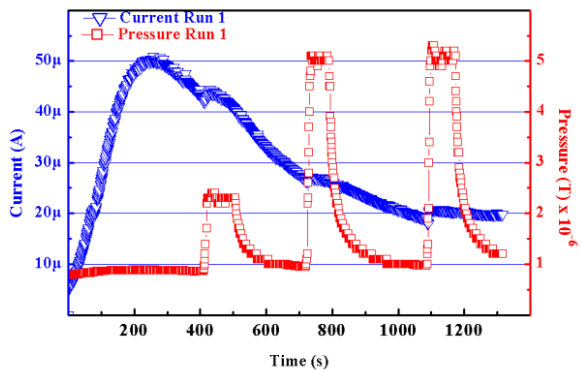
The next study to be discussed examined the operation of thermionic devices in a low pressure water vapor environment. With a relatively high electron affinity of 1.8 eV (compared to other species), water vapor was not expected to have an enhancing effect on the thermionic emission from diamond based on the previously discuss theory dealing with transient negative ions. However, there are several other reasons to study water vapor. First, there is some debate amongst previously reported work as to how water affects the electron emission from diamond. Several studies have reported that interaction of water vapor with the diamond surface lowers the electron affinity. Water vapor disassociates upon interaction with diamond into H and OH, both of which bond with the diamond surface creating a dipole that promotes negative electron affinity.[175, 176] Other studies contradict these results such as one by G. Piantanida *et al.* While observing the influence of moderate (200-300°C) heat treatments on the photoemission from diamond cathodes, G. Piantanida *et al* concluded that water vapor increased the electron affinity. Using information obtained from XPS and UPS data of their diamond films, G. Piantanida *et al* developed a surface dipole model and calculated this increase to be 0.8 eV

compared to a hydrogenated surface.[177] With these two contradicting theories, it was clear that there is much that can be learned by studying the thermionic emission from diamond in a low pressure water vapor environment. Further, should there be an enhancing effect, water vapor would be a more attractive candidate than other gaseous species as it is abundant, readily available, non-toxic, and inflammable.

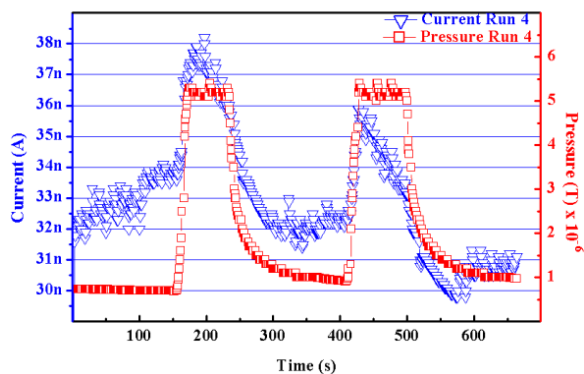
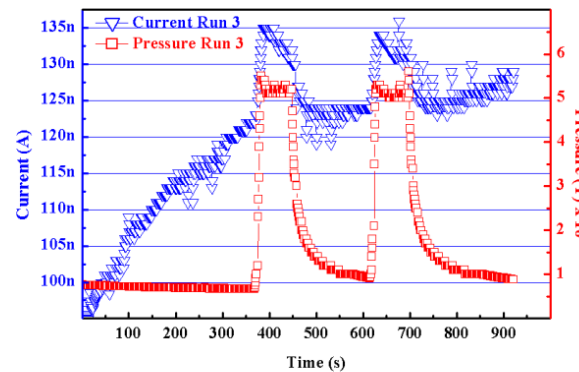
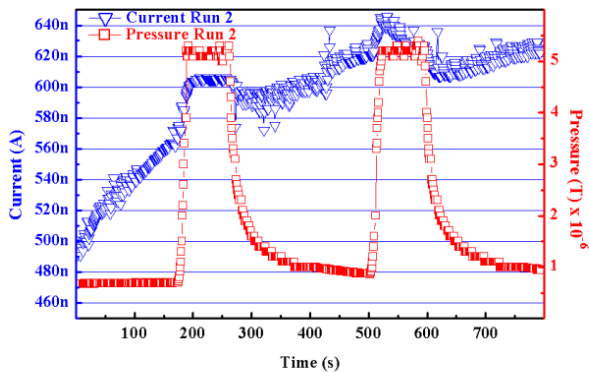
### 7.3.1 Behavior of diamond thermionic cathodes in a H<sub>2</sub>O environment

Nitrogen-incorporated polycrystalline diamond cathodes were deposited according to the method described in Section 5.1 and tested in the manner described in Section 5.4. The delivery method of water vapor in to the vacuum chamber was discussed in Section 5.2.2. Experimental difficulties restricted testing to only a hydrogenated diamond sample. The data obtained for all testing runs (Figure 7.7) indicated that water vapor has a definite effect on the thermionic emission behavior from hydrogenated diamond films. This effect appeared to be different at lower temperatures than at higher temperatures. It can be seen in that, at lower temperatures (600°C and 625°C), the thermionic emission current increased in the presence of water. Conversely, at higher temperatures (675°C and 700°C), the thermionic emission decreased when water vapor was added to the system. Testing at 650°C appeared to be a transition temperature given that during the first two testing runs, the emission current decreased but during the second two testing runs, the emission current first increased when water vapor was added then began to decrease such that there was a resulting net negative effect.

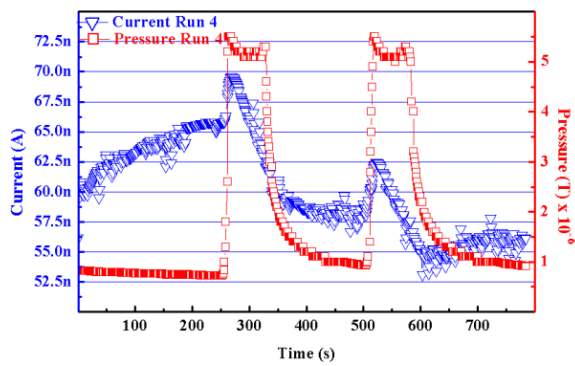
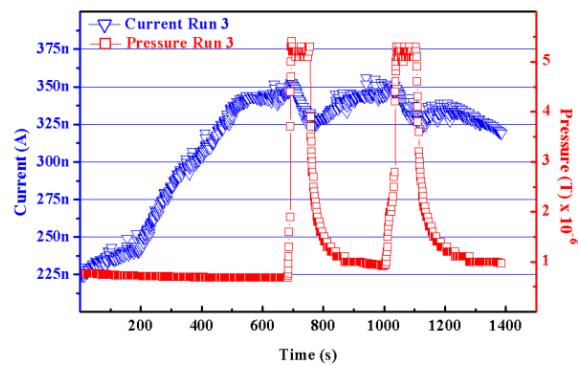
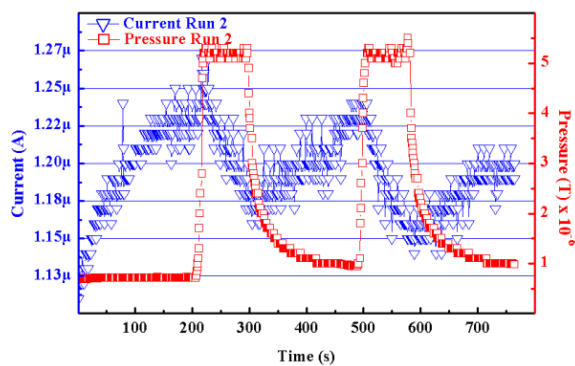
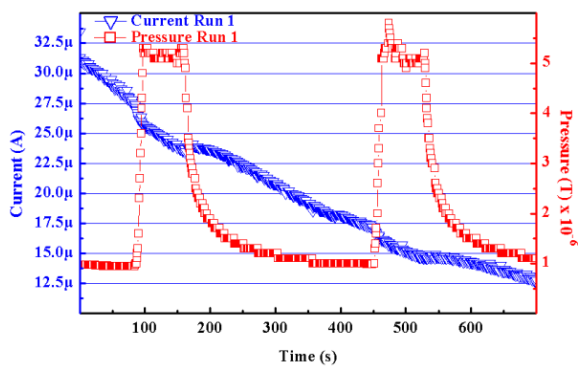
## 600°C Runs



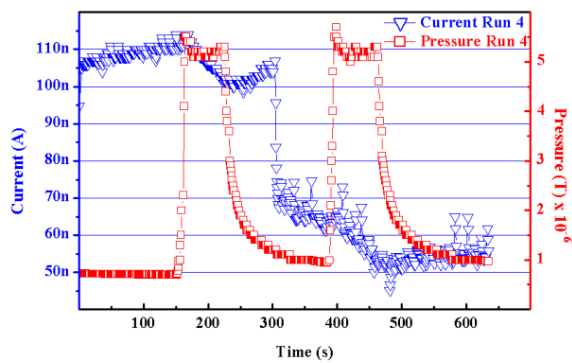
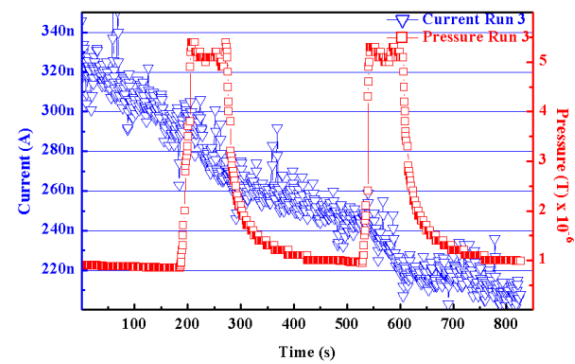
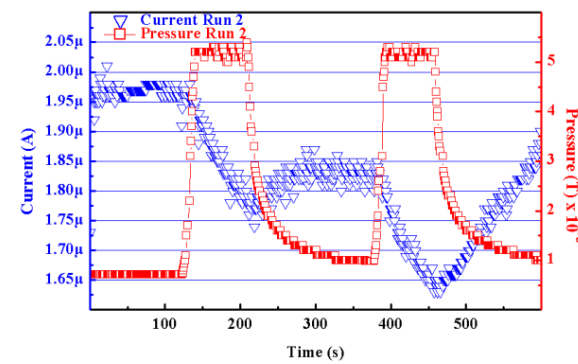
## 625°C Runs



## 650°C Runs



## 675°C Runs



## 700°C Runs

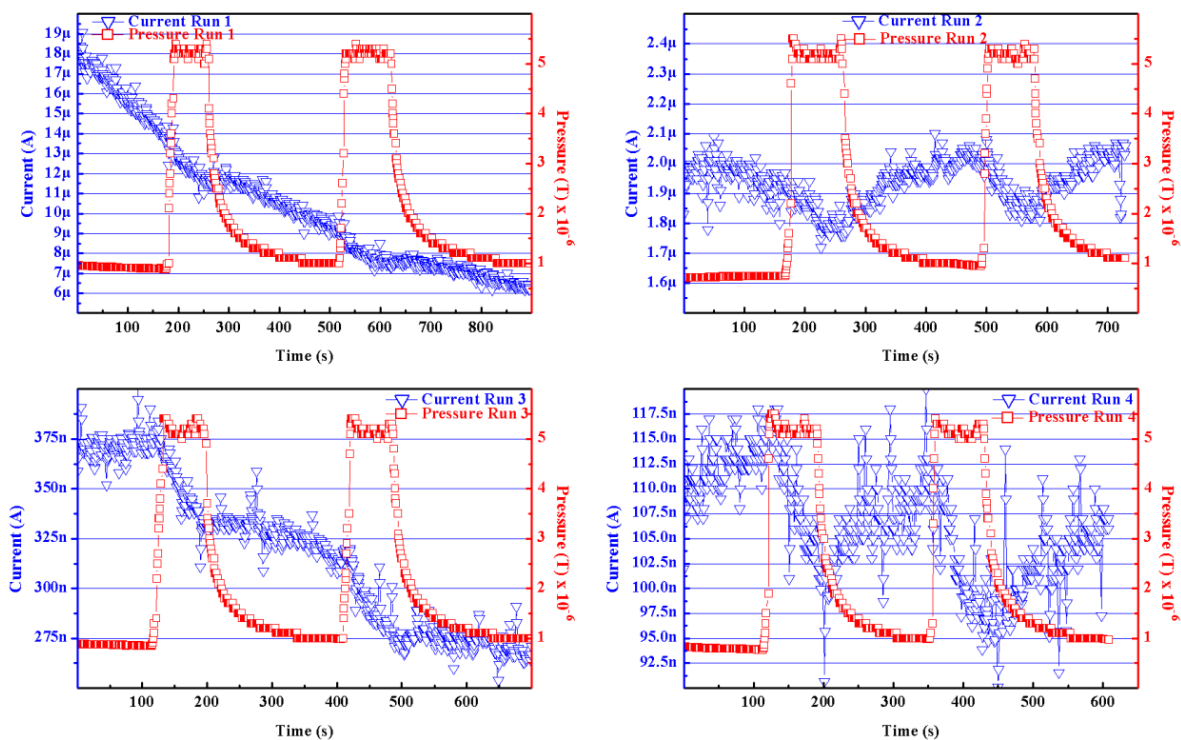


**Figure 7.7** Thermionic emission current behaviors of diamond films operating in a low pressure water vapor environment. The four testing runs shown are categorized by the temperature at which they were performed and are labeled accordingly. It can be seen that the emission current increased in the presence of water vapor at the lower temperatures but increased at higher temperatures.

### 7.3.2 Analysis of the thermionic emission behavior in H<sub>2</sub>O

The results obtained in this study indicate that water vapor has a varying effect on the thermionic emission from diamond cathodes based on temperature. It has been previously shown by A. Laikhtman *et al* that water vapor interacts differently with a hydrogenated diamond surface than with a bare hydrogen surface.[178] They observed that the exposure of a bare diamond surface to water vapor resulted in a large amount of it dissociating forming of C=O, C-O-H, and C-H chemisorbed surface structures that were mostly stable until annealing at 300°C for two hours.[178] Conversely, it was determined that the exposure of water vapor to a hydrogenated

diamond surface did not disassociate to form chemisorbed surface structures, rather it physisorbed into and on the diamond.[178] Though physisorbed water on the diamond surface has been shown to increase the surface conductivity, it is believed to readily desorb at temperatures as low as 90°C.[178, 179] In order to better analyze the varying effect water vapor has on the thermionic emission behavior from diamond films, Table 7.2 below has been prepared describing the emission current response right as the leak valve was opened (Beginning), the trend during the ~60 seconds it was open (During), the response as the leak valve was closed (End), and the resulting net change in current (Result) for each testing run.

**Table 7.2** Qualitative description of the response of the emission current to the presence of water vapor

Temperature (°C)	Run	Current Range (A)	Current Response to Leak			
			Beginning	During	End	Result
600	1	10u-50u	Increase	Increasing	Decrease	Increase
600	2	150n-240n	Increase	Stable	Decrease	Increase
600	3	20n-50n	Increase	Stable	Decrease	Increase
600	4	8n-14n	Increase	Stable	Decrease	Increase
625	2	500n-640n	Increase	Decreasing	Decrease	None
625	3	100n-135n	Increase	Decreasing	Decrease	None
625	4	30n-38n	Increase	Decreasing	Decrease	Decrease
650	1	12.5u-32u	Decrease	Stable	Increase	None
650	2	1.1u-1.3u	Decrease	Decreasing	Increase	Decrease
650	3	225n-350n	Increase	Decreasing	Increase	Decrease
650	4	50n-70n	Increase	Decreasing	None	Decrease
675	2	1.6u-2u	Decrease	Decreasing	Increase	Decrease
675	3	200n-340n	Decrease	Decreasing	None	Decrease
675	4	50n-110n	Decrease	Decreasing	Increase	Decrease
700	1	5u-20u	Decrease	Stable	Increase	Increase
700	2	1.7u-2.1u	Decrease	Decreasing	Increase	None
700	3	250n-400n	Decrease	Decreasing	None	Decrease
700	4	90n-120n	Decrease	Decreasing	Increase	Decrease

Table 7.2 indicates that at the lowest tested temperatures (600°C and 625°C), water vapor had a positive effect on the thermionic emission current. It has been previously discussed that water vapor is thought to physisorb into a hydrogenated diamond sample which increases the surface conductivity of diamond.[178] As this experiment dealt with a polycrystalline diamond sample, water vapor likely absorbed into the grain boundaries of the diamond increasing the overall conductivity of the film. A likely explanation for the results found in the low temperature tests may then be as follows: (1) Water vapor is fed into the chamber and is physisorbed into the diamond grain boundaries. (2) The physisorbed water vapor increases the conductance throughout the diamond film which in turn causes an augmented flux of electrons traveling normal to the diamond surface.[175] This larger amount of electrons available for emission increases the emission current from the sample which was reflected in the data. (3) The water vapor readily desorbs at these temperatures but is constantly replenished as long as water vapor is continually fed into the chamber. (4) When the water vapor is shut off, the majority of this water vapor desorbs causing the emission current to decrease back towards pre-water vapor levels. (5) For the 600°C tests, the emission current did not fully decrease down to the pre-water vapor because the temperature was not high enough to fully desorb all water vapor absorbed into the sample. The result was a net positive increase in emission current. Conversely, at 625°C it was observed that the emission current fully decreased down to pre-water vapor levels. This is likely due to the slightly higher testing temperature which caused more of the water vapor to be desorbed from the diamond terminating all its emission current enhancing effects. The observed low temperature response of the emission current to the presence of water vapor could also be explained by the dissociation of the water molecules.

The heating of the diamond samples for testing will inevitably result in hydrogen desorption from the diamond surface based on the previous desorption experiments. This is clearly evident when observing the sharp decreasing current trend in 600°C Run 1 test which was the first test performed after hydrogenation. The desorption of hydrogen results in a vacancy with a higher electron affinity (thus lower emission current) at that site unless it gets filled by a hydrogen atom diffusing from the bulk. When water vapor is fed into the chamber, it has been shown to disassociate and chemisorb onto bare unhydrogenated surfaces forming C-H and C-OH bonds, both of which invoke a negative electron affinity which promotes electron emission.[175, 176] This process could possibly be happening, filling the poorly emitting surface carbon vacancies allowing for the observed increased emission. Studies have indicated that the C-OH bond is not stable upon annealing for extended periods at temperatures of 500°C.[175, 180] Accordingly, the C-OH bonds are then desorbing at a much faster rate than the C-H bonds but are being constantly replenished as long as water vapor is being fed into the chamber. When the water vapor is shut off, the hydroxyl molecules rapidly desorb causing the emission to quickly decrease. Per the Arrhenius equation discussed in the previous chapter, the hydroxyl groups will desorb slower at 600°C than at 625°C accounting for the observation that water vapor resulted in a net increase in emission current at 600°C but net zero change at 625°C. Both of the proposed processes explain the observed low temperature effects and are supported by literature. It is yet to be determined which process is more accurate due to the lack of previously reported work on this topic.

At higher temperatures, 675°C and 700°C, the findings indicated that water vapor negatively affected the electron emission current. When the water vapor was first introduced into the vacuum chamber, emission current was observed to decrease followed by a decreasing trend

during the period the valve was open. Upon closure of the valve, a majority of the tests demonstrated an increasing trend but the current never reached levels up to the pre-leak trend resulting in a net negative effect. Though no previously reported research has observed an effect such as this, it is possible to make a hypothesis. The proposed process is as follows: (1) Water vapor is leaked into the chamber and dissociates form C-H and C-OH bonds.[175, 176] This dissociation occurs because several of the surface C-H bonds have been broken due to the desorption that occurs during testing. (2) According to L.M Struck and M.P. D'Everlyn, many of the C-OH bonds will further decompose into a mixture of C-O-C, C-H, and C=O bonds when heated to temperatures on the order of 1000°C.[181] Studies have indicated that the C-OH bond (unlike the C-H bond) is not stable upon annealing to temperatures of 500°C for several hours.[175, 180] Further, the stability of the water induced surface groups follows the order of  $\text{OH} > \text{C-O-C} > \text{C=O}$ . Therefore, it can be inferred that the oxide containing groups other than C-OH are also unstable upon annealing to temperatures of 500°C.[175, 180] The oxide containing species will constantly desorb from the surface and be replenished while the leak valve is open. (3) The resulting activated oxygen resulting from the desorption of the oxide containing molecules has been reported to cause the abstraction of chemisorbed hydrogen (C-H bonds).[182] Based on results from previously conducted experiments, the removal of this hydrogen will lead to decreased emission current. (4) When the leak valve is closed and water vapor is no longer fed into the chamber, the oxide containing species will be removed. (5) The observed increase in emission current toward pre-water vapor levels could be explained by the “percolation” of hydrogen diffusing from inside the bulk of the diamond to fill some of the newly vacant surface sites. It is expected that a large amount of the hydrogen contained in and on the diamond will be removed due to water vapor providing a smaller number of hydrogen atoms

available for diffusion to the surface. This may explain the small increase in emission current and the net negative emission current compared to pre-water vapor levels.

In summary, water vapor was observed to affect the thermionic emission from diamond films both positively and negatively depending on temperature. Multiple explanations have been proposed based on previously reported work which attempt to describe the observed effects. This experiment indicated that water vapor could potentially enhance the thermionic emission of diamond under certain conditions but more research will be required to determine these conditions.

#### 7.4 Molecular hydrogen

The previous vacuum thermionic emission studies discussed in *Chapter VI* demonstrated hydrogen to have a definite beneficial effect on the thermionic emission properties of diamond films. The present study sought to examine the operation of diamond thermionic cathodes in a low pressure hydrogen environment. It was believed that this could both potentially allow for better thermionic emission performance and provide a better understanding of how hydrogen affects the electronic properties of diamond. Though the molecular hydrogen anion is the simplest of all molecular anions, it has proven to be one of the more widely debated topics in molecular physics over the past 50 years. Interestingly, it was not until recently that the existence of the molecular hydrogen anion had even been verified.[183, 184]

The earliest calculations regarding the molecular hydrogen anion were performed by H. Eyring and colleagues who mathematically demonstrated that the energy required to dissociate  $H_2^-$  into H and  $H^-$  was positive. This positive energy requirement to dissociate means that energy must be added to the system in order for the reaction to occur, thus implying  $H_2^-$  to be

stable.[168, 185] The stability of the molecular hydrogen anion would appear to indicate  $H_2^-$  to have a positive electron affinity. However, all previous attempts to calculate the electron affinity of molecular hydrogen have been in disagreement with each other and a large range of electron affinity values reported, both negative and positive.[168, 186-188] Experimental observation of  $H_2^-$  has been reported several times beginning with V.I. Khvostenko and V.M. Dukel'skii in 1957.[189, 190] However, results have been met with skepticism due the experimental difficulty of deciphering  $H_2^-$  from the stable atomic deuterium anion.[189] It has not been until recently (in the last decade) that the existence and behavior of  $H_2^-$  been experimentally observed with enough confidence to be accepted by the scientific community.[184, 189, 191] It is clear that many challenges still exist to understand molecular hydrogen making it difficult to predict its influence on the thermionic emission from diamond films.

#### 7.4.1 Behavior of diamond thermionic cathodes in a $H_2$ environment

Nitrogen-incorporated polycrystalline diamond cathodes were deposited according to the method described in Section 5.1 and tested in the manner described in Section 5.4. The delivery method of molecular hydrogen in to the vacuum chamber was discussed in Section 5.2.2. The present study examined diamond films in both the as-grown and hydrogenated state. Though the results from only one sample are presented below, the data was verified by testing multiple other samples.

Emission current and pressure plotted against time for the sample in the as-grown state can be seen below in Figure 7.8. Upon inspection, it was immediately identified that leaking in hydrogen had a positive effect on the emission current at every temperature for each of the three runs on the as-grown sample at temperatures of 600°C, 625°C, and 650°C. The emission current

increased from the baseline trend when hydrogen was introduced into the chamber and decreased back toward the baseline trend when the hydrogen was shut off. Further inspection of the plots in Figure 7.8 indicated an increasing baseline trend for each run with increasing time. This trend is somewhat counter intuitive to the results previously found in the hydrogen activation energy experiment in which it was seen that the emission current decreased (rather than increased) with increasing time. Though no known reported work has observed this increasing trend, speculation can be made as to its cause.

The previous hydrogen activation energy experiment was performed using a hydrogenated sample whereas the data collected for Figure 7.8 was performed with an as-grown sample. It is believed that a hydrogenated sample has virtually all dangling surface bonds occupied by a hydrogen atom. As the sample is heated, the hydrogen atoms desorb from the surface into the vacuum resulting in decreased emission. In short, a fully hydrogenated diamond sample cannot emit any better. The reason for the poor emission from an as-grown sample, compared to a hydrogenated sample, may be because a large number of the surface carbon atoms are not bonded with a hydrogen atom. They are likely either dangling or bonded to a non-emission enhancing species such as the hydroxyl ion that easily desorbs when heated. The explanation for the increasing current trend with time seen below is thought to lie in the deposition process. As the samples were grown in a hydrogen-rich, methane-starved environment, a substantial amount of hydrogen was likely deposited within the bulk of the diamond films. When the diamond films were heated during testing, these hydrogen atoms diffused throughout the diamond and to the surface, bonding with some of the surface carbon atoms. When these bonds were made, emission current was enhanced. Though it is not believed that the emission current would ever increase to the levels seen in fully hydrogenated samples, a

small increase occurred (similar to a conditioning process) as observed in the results seen in Figure 7.8. Emission current variations in the 675°C and 700°C tests made the response of emission current to the introduction of molecular hydrogen difficult to decipher, and are therefore not shown.

Isothermal testing of the sample post hydrogenation treatment demonstrated a similar response to the as-grown sample, but with much higher emission current values (Figure 7.9). The first runs all exhibited a decreasing current trend that was expected given the previous hydrogen desorption experiments. Again, the data from the higher temperatures was not shown as the background current variations were too large to accurately quantify the current response to hydrogen.

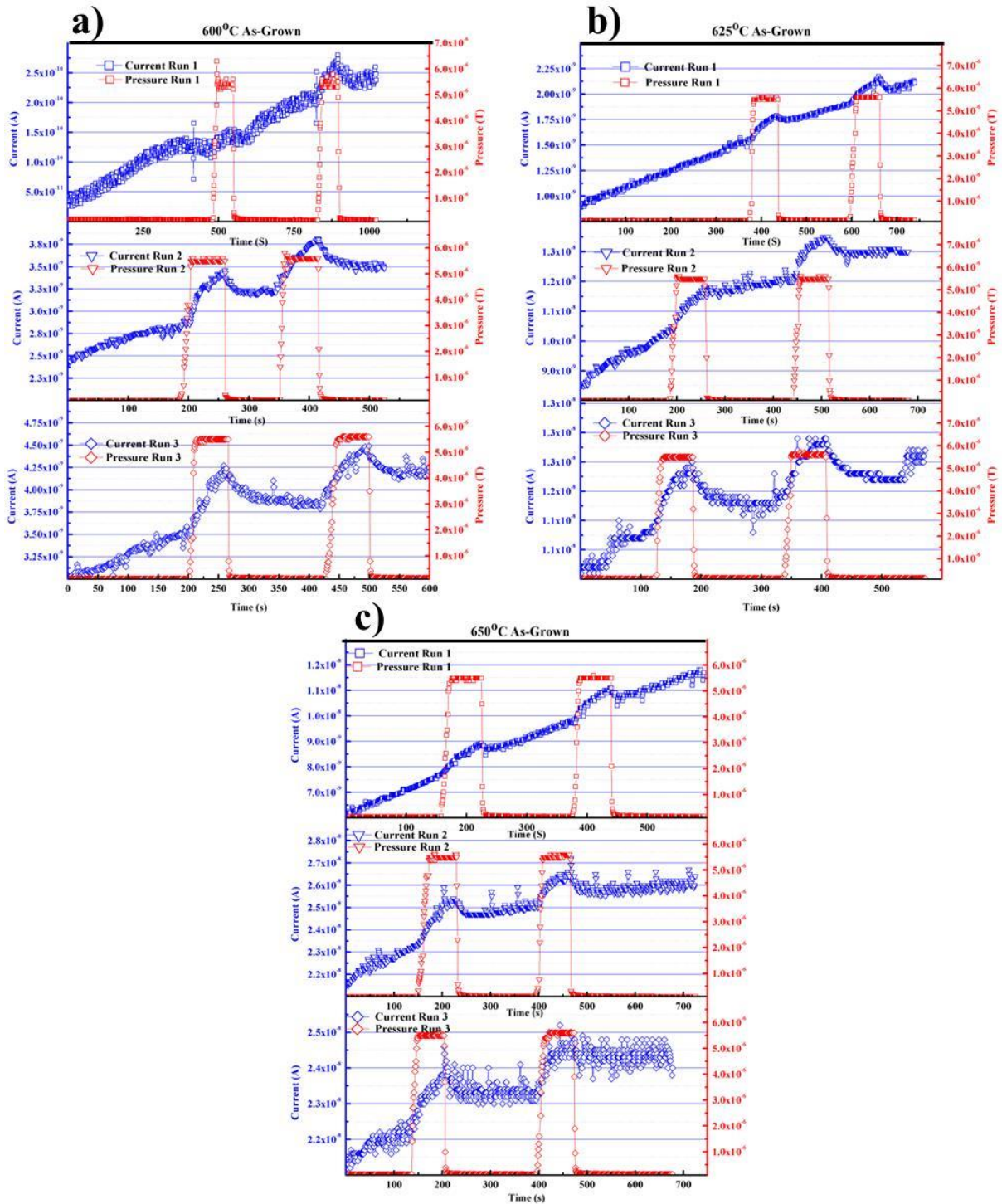


**Figure 7.8** Isothermal emission current behavior of an as-grown diamond film with hydrogen leaked in for the temperature 600°C, 625°C, and 650°C. The blue data represents the current while the red data represents the pressure in the chamber. For all graphs, it can clearly be seen that there was an increase in emission current when the hydrogen pressure was increased in the chamber.

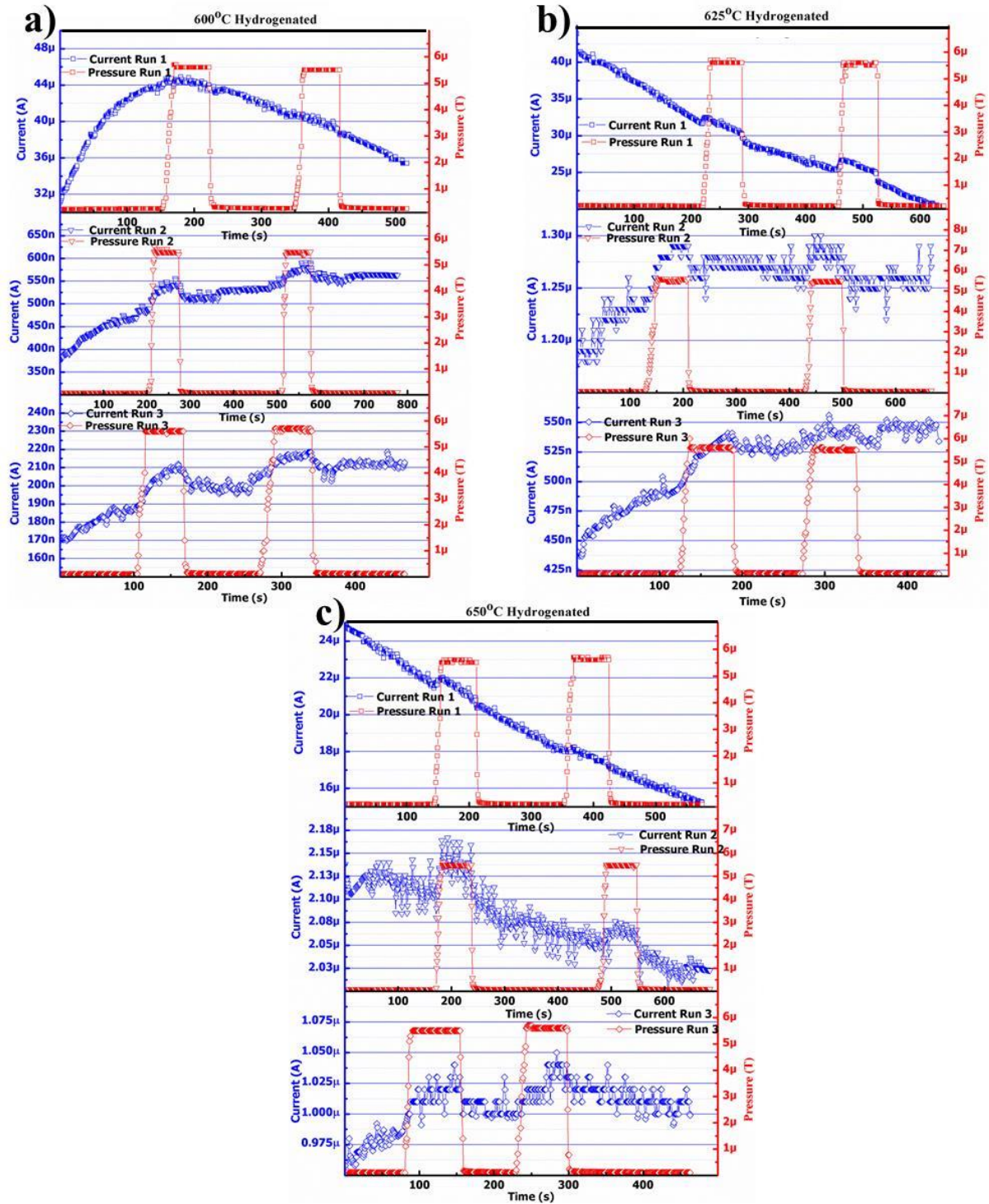


**Figure 7.9** Isothermal emission current behavior of a hydrogenated diamond film with hydrogen leaked in for the temperatures 600°C, 625°C, and 650°C. The blue data represents the current while the red data represents the pressure in the chamber. For all graphs, it can clearly be seen that there was an increase in emission current when the hydrogen pressure was increased in the chamber.

Analysis of the response to hydrogen for both the as-grown and hydrogenated testing runs was difficult due to the transient nature of the background. To allow for more accurate quantification of the current increase, a residual plot was taken of the data. A residual plot consists of determining the trend of the background and subtracting each data point from the trend line similar to a linear transformation. An example of this transformation can be seen below in Figure 7.10 for the 650°C Run 1 data.

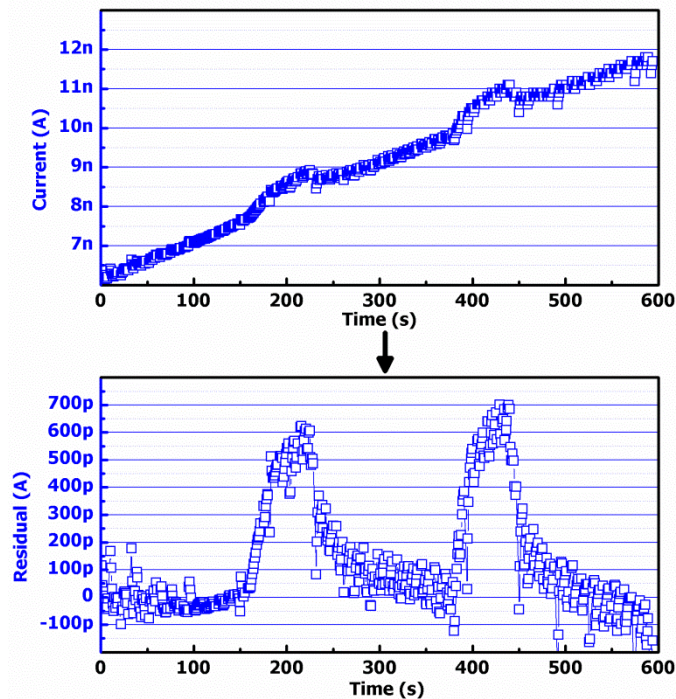


**Figure 7.10** Example of the residual plot performed for all data runs which allowed for direct calculation of the increase in current upon hydrogen being leaked into the chamber.

A plot of the current increase vs. baseline current (current before leak-in) was then performed. Figure 7.11 demonstrates a positive relationship between baseline current and the current increase in that higher baseline current equated to a higher increase in current in the

presence of hydrogen. Two possible trend lines were found that describe the observed data, one linear, the other a power function.

Though the power trend line has a higher coefficient of determination ( $R^2$ ), it is unlikely that a physical model can be derived with which it is consistent. This is due to both the dependent and independent variables being in units of Amperes. Examination of the equation for the power trend lines implies that there is some constant (units unknown) that is multiplied by amperes to the 0.8754 power. As the result of this product must be in Amperes, the constant must have units of amperes raised to the 0.1246 power which is highly improbable. Thus, a more likely description is the linear trend line.

The linear fit to the data seen in Figure 7.11 implies the baseline current can be related to the current increase by means of a simple unit-less constant. Further, the calculated linear trend line has a y-intercept of 0. This follows intuition given that when there is no baseline current (which happens at 0K as described by the Richardson equation), there can be no increase in emission current.

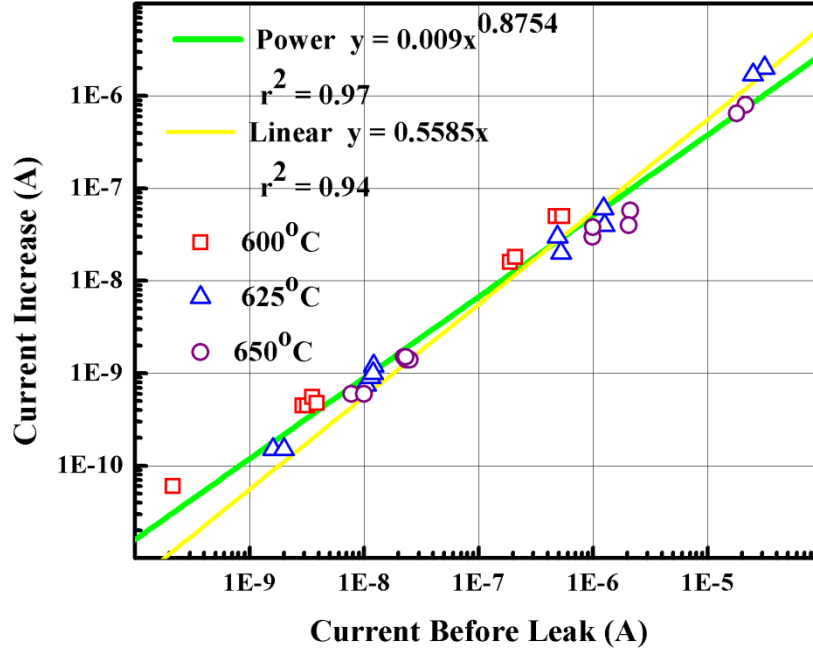


**Figure 7.11** Plot of the emission current increase in the influence of hydrogen gas as a function of the current before the start of the leak-in (baseline current). A clear relationship can be seen where the magnitude of increase increased with baseline current. Two possible trend lines were found to describe this relationship: linear and power.

Two emission current versus temperature tests were performed one after the third as-grown run and also after the third hydrogenated run, both beginning at 700°C and continuing up to 900°C. The hydrogen pressure in the chamber was constantly maintained at ~5.5 μTorr (N<sub>2</sub> equivalent) throughout both tests. From Figure 7.12a it can be seen that the as-grown sample reached its maximum emission current levels at a temperature around 815°C which is approximately 50°C higher than the value seen for the previously described as-grown emission tests. Figure 7.12b indicates that the maximum emission current was achieved at ~780°C. This is significantly above the ~700°C value found in the previous hydrogenated tests.

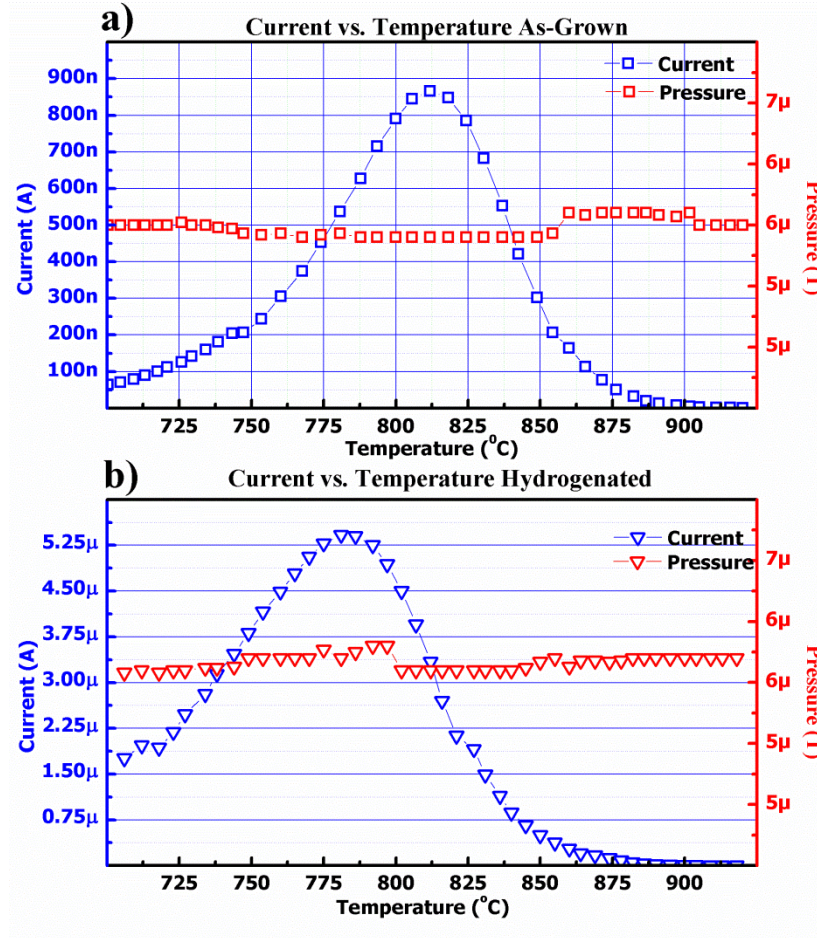


**Figure 7.12** Plots of the emission current vs. temperature after the third testing runs for the as-grown (a) and hydrogenated (b) diamond sample.

#### 7.4.2 Analysis of the thermionic emission response to H<sub>2</sub>

The above results indicate that the incorporation of hydrogen gas into the cathode-anode gap did indeed have an enhancing effect. The positive correlation between baseline current and emission current increase seen in Figure 7.11 is evidence that the reaction was a result of the electrons traversing the vacuum gap rather than direct interaction between the heated cathode and the molecular hydrogen. Attempts to hydrogenate diamond with molecular hydrogen have only proven successful at temperatures in excess of 400°C.[192, 193] The lack of temperature dependence on the emission current increase seen in the overlap of data points at different

temperatures in Figure 7.11 implies that a similar effect must have occurred at all three tested temperatures. Assuming this to be true, two possible explanations are proposed to describe the observed behavior which are consistent with previously reported work.

The first possible explanation deals with the in-situ rehydrogenation of the diamond films. As noted in previous sections, the beneficial effects hydrogen has on the thermionic emission from diamond films are due to atomic hydrogen bonding with the surface carbon atoms reducing the electron affinity. In the typical hydrogenation treatment, the atomic hydrogen results from the dissociation of molecular hydrogen into atomic hydrogen due to electron collisions. The electrons are stimulated by the microwaves in the MPCVD chamber such that they oscillate with high enough energy that when they collide with molecular hydrogen, they ionize and split into two hydrogen atoms. The atomic hydrogen then bonds with the diamond surface forming C-H bonds which are favorable for thermionic emission. This same effect may be happening when the diamond thermionic cathodes are in operation in a molecular hydrogen environment. As electrons are emitted from the diamond and accelerated towards the anode, they likely collide with the hydrogen present in the interelectrode gap. These electrons will have a large range of energies as described by Fermi-Dirac statistics with some high enough to cause the molecular hydrogen to ionize and dissociate. Some of this atomic hydrogen will migrate to the diamond cathode filling the dangling surface bonds thus increasing the emission current. When the hydrogen is shut off and evacuated from the chamber, these new emission sites desorb per Arrhenius rate kinetics causing the emission current to decrease back down toward the baseline levels. If this is the case, then this effect should increase when more electrons are traversing the vacuum gap (higher emission current) which was observed in Figure 7.11.

A second explanation deals with the mitigation of space-charge effects. During testing, the cathode and anode were biased at a fixed potential difference of 200V. Space charge effects arise when electrons begin traversing the gap between the cathode and anode. Each electron has a negative charge that cancels out some portion of the 200V potential difference; so higher emission current levels result in a larger portion of the potential being canceled. The lower the potential the cathode sees, the lower the EMF to accelerate electrons to the anode and thus a lower emission current. The operation of the diamond thermionic emission devices in a hydrogen atmosphere could possibly cancel out some of this effect through the ionization of the molecular hydrogen. The ionization of molecular hydrogen results in two products: electrons with a negative charge, and ionized hydrogen with a positive charge. The negatively charged electrons will be attracted to the anode while the positively charged ions will proceed to the cathode. From the cathodes perspective, this accumulation of positive ions at the cathode surface will resemble the positive bias originally applied, canceling out some of the space-charge effects and increasing the emission current. As more emission current would result in the creation of more positive ions, it is to be expected that a higher increase in emission current upon exposure to hydrogen gas would be seen which also agrees with the results obtained in Figure 7.11.

Both these postulated mechanisms are consistent with the observed increase in emission current upon exposure of diamond films to a low pressure hydrogen environment. It is not clear which explanation is satisfactory or rather, if the observations in this study can be better explained by a combination of the two. In any case, it was determined that the emission current increases by roughly 50% which is extremely favorable for thermionic emission applications.

### 7.4.3 Increased operating temperature in H<sub>2</sub>

In addition to the increase in isothermal emission current, the introduction of hydrogen into the interelectrode cathode-anode gap appeared to increase the temperature at which the emission current began the “roll over” behavior thus allowing for increased operating temperatures. The plots in Figure 7.12 indicate that operation in a 5.5  $\mu$ Torr (N<sub>2</sub> equivalent) hydrogen environment increased the emission temperature “ceiling” of diamond films. The insufficient information available on the interaction of molecular hydrogen with diamond at the elevated temperatures tested in the present study makes it difficult to provide a suitable explanation for the observed behavior. Additionally, the reaction between molecular hydrogen and incident electrons is still a hotly debated topic. Ample evidence has been offered to justify that hydrogen desorption is the cause of the emission current roll over seen in the vacuum experiments presented in *Chapter VI*. Hence, the faster the hydrogen desorbs, the lower the temperature will be at which the current begins to decrease. Thus it was posited that the increased temperature ceiling seen in Figure 7.12 was likely due to some amount of in situ rehydrogenation of the diamond surface. As the hydrogen desorbed from the surface, the molecular hydrogen provided additional hydrogen atoms to fill the newly formed vacancies which allowed the thermionic emission process to continue.

Both the as-grown and hydrogenated samples began the typical “roll over” behavior at much higher temperatures compared to vacuum operation which is desirable for thermionic energy conversion applications. Before the “roll over”, diamond electron emission followed the Richardson equation, whereby emission current increased exponentially with increasing temperature. It was then concluded that the operation of diamond thermionic cathodes in a low

pressure hydrogen environment allowed for higher emission current levels to be achieved which would directly equate to a better performing thermionic energy conversion device.

### 7.5 Nitrous Oxide

The final gaseous species studied in the present research was nitrous oxide (N<sub>2</sub>O). Nitrous oxide is one of the most studied species that undergoes dissociative electron attachment. Though the electron affinity N<sub>2</sub>O is widely accepted to be slightly positive at 0.2 eV,[194, 195] other experimental and theoretical calculations have reported different values.[196-198] Regardless of the reported electron affinity discrepancies, the dissociative electron attachment of N<sub>2</sub>O (Equation 7.1) has been extremely useful in mass spectrometry applications concerning the O<sup>-</sup> radical anion.[199]



It has been previously discussed that past thermionic energy converters utilized tungsten cathodes with cesium vapor fed into the cathode-anode gap. Among other reasons, this cesium was meant to mitigate space charge. In such a scenario, electrons emitted from the cathode collide with the vapor causing the cesium to ionize. The positively charged molecules then migrate to the cathode while the negatively charged ions travel to the anode resulting in decreased space charge effects.[114] Observation of the dissociative electron attachment reaction nitrous oxide undergoes (Eq. 7.1) indicates that no positively charged ions will be formed. Thus, the space charge effects which limit the performance of a thermionic emission device will be further magnified by the addition of another negatively charged species present in the cathode-anode gap. Previous studies examining the reactivity of nitrous oxide with diamond have not observed any adsorbed states of N<sub>2</sub>O on a clean C(100) surface by either EELS (high-resolution

electron energy loss spectroscopy) or TDS (thermal desorption spectroscopy) techniques.[200] These properties indicate that nitrous oxide should only have a strong negative effect on the thermionic emission performance of diamond cathodes. The present study was meant to examine this hypothesis in an effort to add further validity to both the experimental technique used in all of the gaseous studies and also to the analyses presented for results obtained from the above studies.

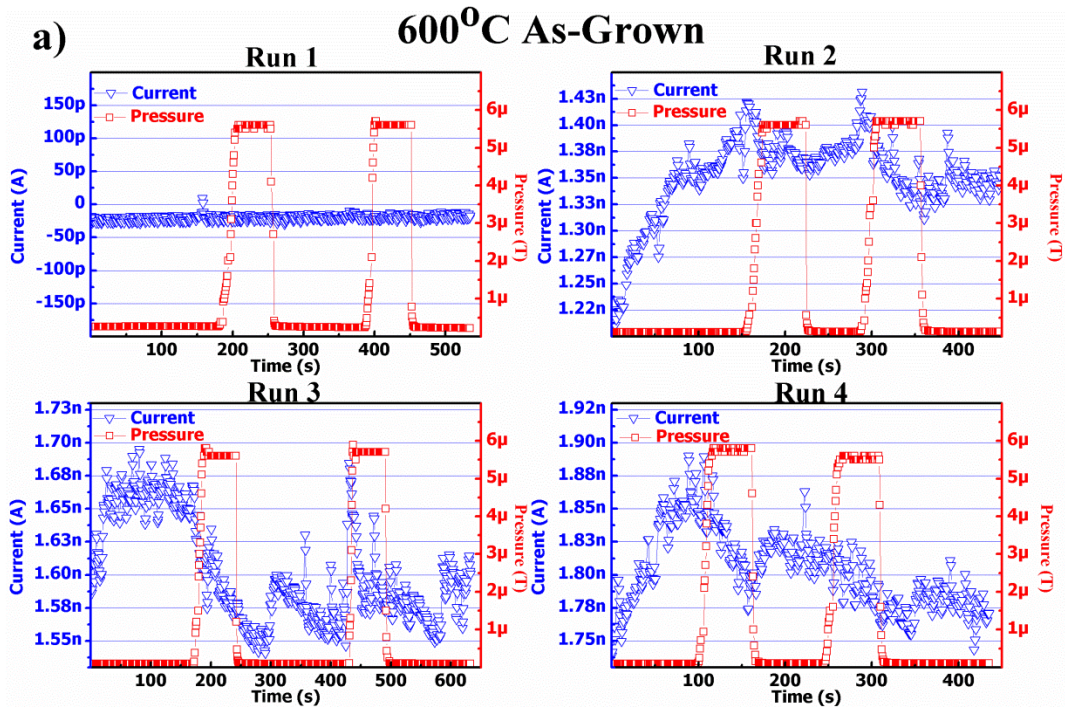
#### 7.5.1 Behavior of diamond thermionic cathodes in a N<sub>2</sub>O environment

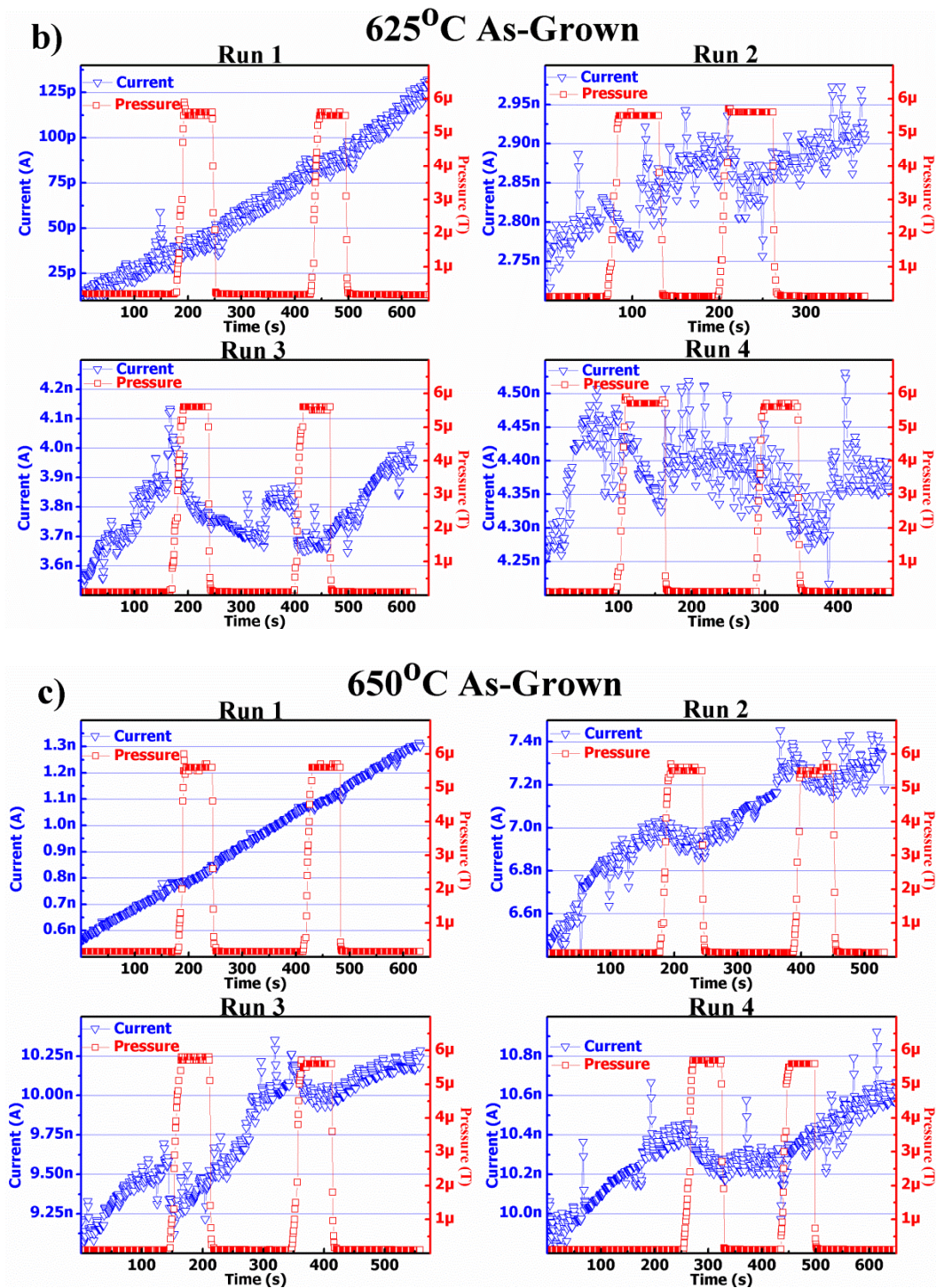
Nitrogen-incorporated polycrystalline diamond cathodes were deposited according to the method described in Section 5.1 and tested in the manner described in Section 5.4. The delivery method of nitrous oxide in to the vacuum chamber was discussed in Section 5.2.2. The present study examined diamond films in both the as-grown and hydrogenated state.

The thermionic emission current response of an as-grown nitrogen-incorporated polycrystalline diamond sample to the introduction of nitrous oxide is shown below in Figure 7.13. The graphs from 650°C and 700°C are not shown as the response was difficult to decipher do to large variations in the emission current. At all temperatures, a small change in emission current was observed for each testing run. It appeared that nitrous oxide had a negative effect such that the emission current decreased with respect to vacuum levels when the gas was introduced into the chamber.

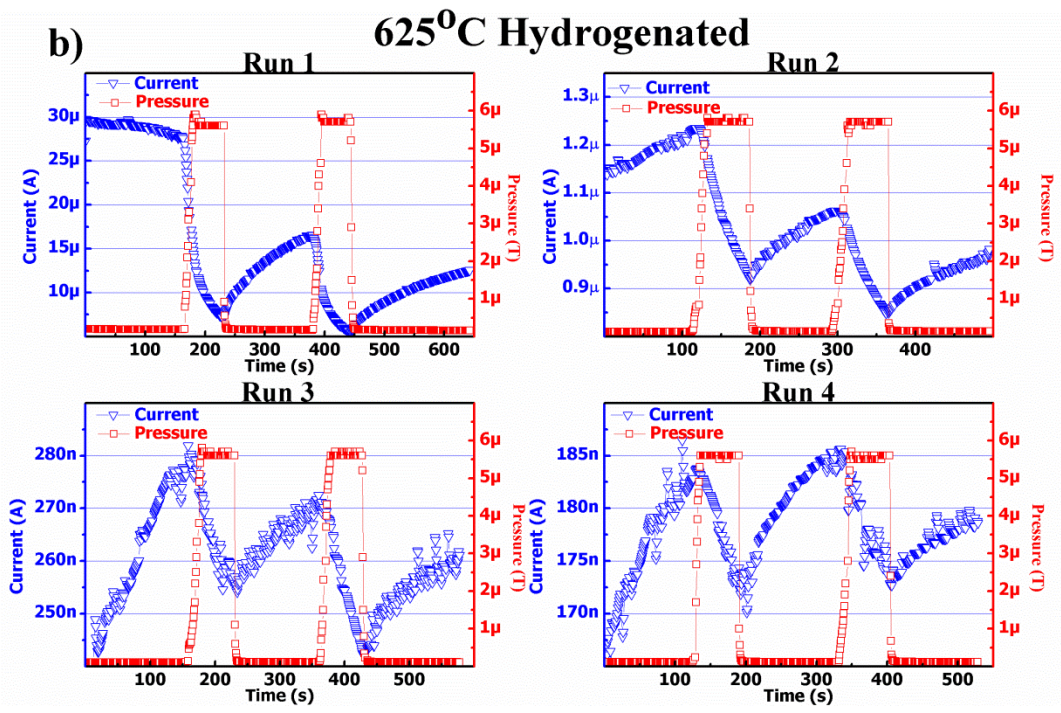
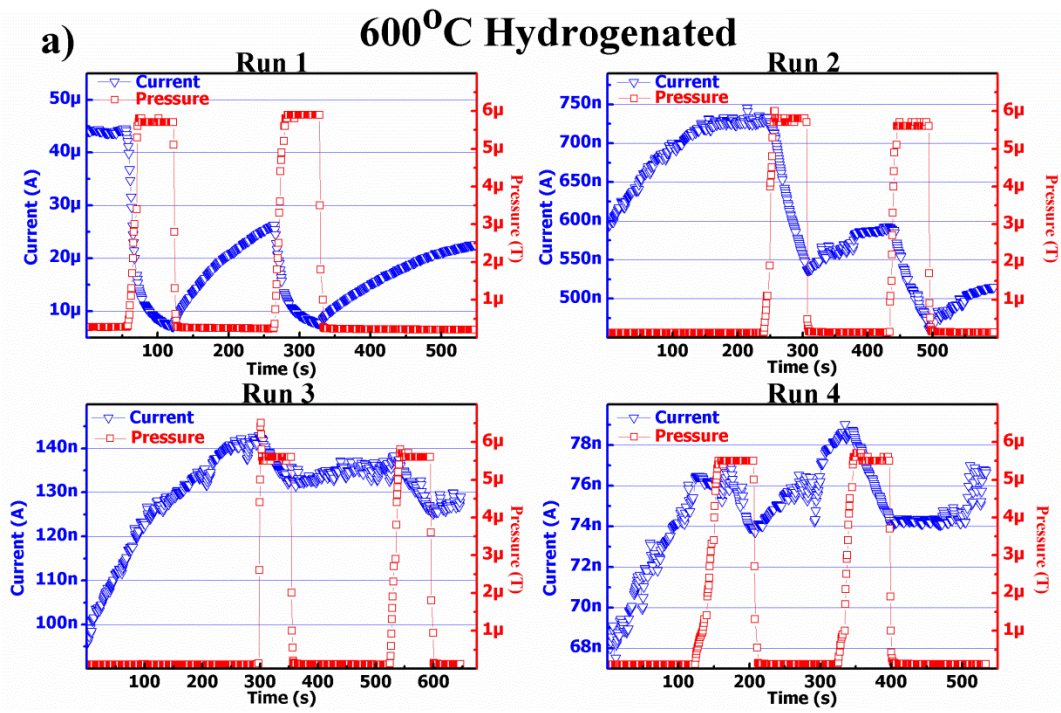
Testing after exposing the sample to a hydrogenation treatment demonstrated a more dramatic effect compared to the as-grown sample. From Figure 7.14, it can be seen that a decrease in emission current resulted from the introduction of nitrous oxide. As the leak valve was opened and N<sub>2</sub>O fed into the chamber, a sharp decline in emission current was observed.

The decline continued for the entire duration the leak valve was open. Upon closing the valve and the chamber re-evacuating to  $1 \times 10^{-7}$  Torr levels, the emission current exhibited some recovery. However, this recover did not reach pre-leak in levels.





**Figure 7.13** Emission current response of the as-grown diamond sample to the introduction of a low pressure nitrous oxide environment. Graphs a), b), and c) are the behavior for the four runs performed at 600<sup>o</sup>C, 625<sup>o</sup>C, and 650<sup>o</sup>C, respectively.



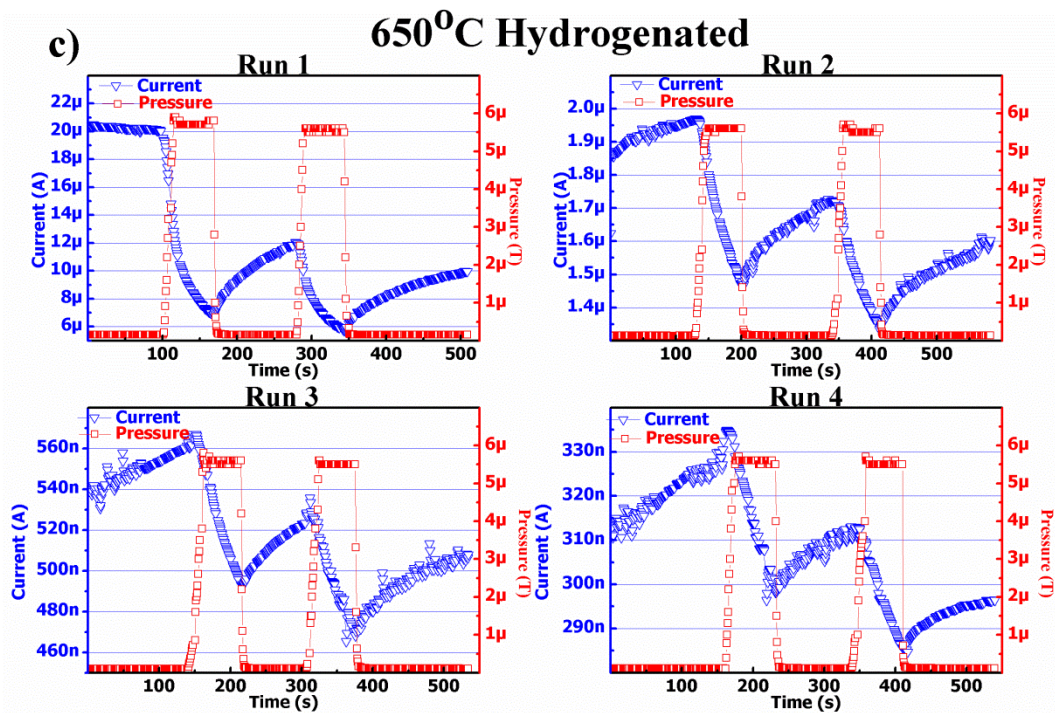


**Figure 7.14** Emission current behavior of a hydrogenated diamond sample in the influence of a low pressure nitrous oxide environment. Graphs a), b), and c) are the behavior for the four runs performed at 600°C, 625°C, and 650°C, respectively.

### 7.5.2 Analysis of the thermionic emission behavior in $N_2O$

The results presented in the previous section suggest that nitrous oxide had a negative effect on the thermionic emission from diamond films. When comparing the magnitude of decrease amongst all testing runs (as-grown and hydrogenated) it is clear that the magnitude of this decrease was larger when the baseline emission current (current before leak-in) was higher. To better understand the results in Figures 7.13 and 7.14, the magnitude of this decrease was calculated for each run in which it was easily decipherable. For runs that exhibited an increasing or decreasing baseline trend, a residual plot to accurately calculate the amount the emission current decreased was performed (this was the same method described in the previous section for the hydrogen data).

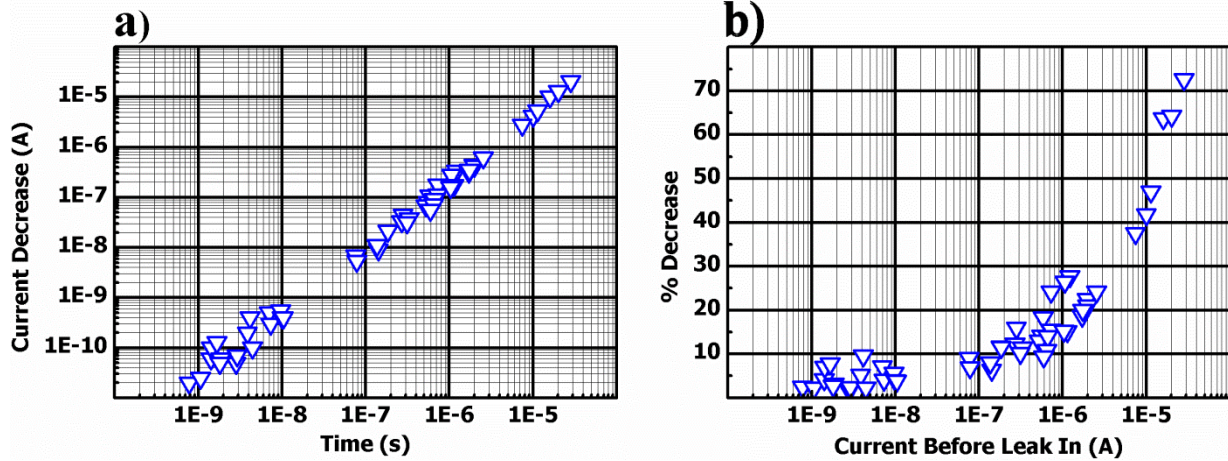


**Figure 7.15** a) Magnitude of the emission current decrease from baseline vacuum levels upon exposure of the cathodes to nitrous oxide. b) Percent of emission current decrease from vacuum levels.

The plot in Figure 7.15a indicates that there was a direct positive correlation between emission current decrease and the baseline emission current levels. Further, the percent of emission current decrease appears to also increase linearly as a function of increasing baseline current per the exponential trend on the semi-log plot seen in Figure 7.15b. The observed impact nitrous oxide had on the thermionic emission from diamond films strongly agrees with the previous predictions.

Nitrous oxide has been shown to have no observable interaction with diamond films suggesting that any effects observed in the present study should be the result of electron impact reactions with the  $N_2O$  molecules.[200] Additionally, nitrous oxide predictably dissociates into a neutral nitrogen molecule and an atomic oxygen anion (Equation 7.1) which should greatly inhibit the electron emission from all types of thermionic cathodes. As no positive ions were produced, the space charge effects between the cathode and anode were not suppressed (as would be the case with a molecule that dissociates into a positive ion). Thus, the nitrous oxide

molecules and the corresponding dissociation products likely only decreased the mean free path of electrons causing various scattering processes which inevitably led to a decrease in emission current. This is also believed to be the case in the nitrogen experiment discussed in Section 7.1. Both of these predictions were verified by the strong positive correlation of the emission current decrease with baseline emission current.

It can also be predicted that a portion of the oxygen radicals produced in the chamber likely bonded with the emission-enhancing hydrogen atoms on the diamond surface also causing further decreased emission.[182] This prediction was also confirmed upon examination of Figures 7.13 and 7.14. Should nitrous oxide present in the cathode-anode gap act as only a means to suppress emission current, the sample would have immediately resumed normal operation upon the removal of all N<sub>2</sub>O present in chamber when the leak valve was closed. The present experiment observed the emission current to show some signs of recovery though never back to the same level that would be predicted by the baseline current trend. Thus, as molecular nitrogen nor nitrous oxide effect the diamond surface,[200] it is likely that the oxygen radicals are removing some of the surface hydrogen atoms, preventing the sample from achieving full operational performance.

The present study demonstrated that the operation of diamond cathodes in a low pressure nitrous oxide environment dramatically decreased their thermionic emission performance. However, this study added further validity to this testing method. This testing apparatus/configuration has proven capable of producing results in strong agreement with well-established theory. Although other experiments in this research examined gaseous species with much less predictable behavior on the thermionic emission from diamond, the results from this nitrous oxide study increased the confidence in all results obtained with this testing method.

In summary of this chapter, several gaseous species were examined to assess their impact on the thermionic emission from diamond. The testing method used for all gaseous studies was shown to provide reliable results such that future work can continue this research. Though a detailed analysis of the results has been presented based on available research, more work is needed for the implementation of a reliable, highly performing, diamond cathode for thermionic applications. The next chapter elaborates on suggestions for furthering this research.

## CHAPTER VIII

### CONCLUSIONS AND RECOMMENDATIONS

Several experiments have been presented in this research examining the thermionic emission properties of polycrystalline nitrogen-incorporated diamond cathodes. This final chapter is meant to outline the implications of the present research. Though it is clear that this research has resulted in a better understanding of thermionic emission from diamond, much more work is required for diamond cathodes to be fully utilized for thermionic applications. Accordingly, this chapter also presents recommendations for future research.

#### 8.1 Observed effects of hydrogen in diamond

Perhaps the most useful information obtained in the present research is that hydrogen is responsible for significant enhancement of diamond's thermionic emission properties. It has been shown that exposure of diamond cathodes to a hydrogen plasma treatment greatly increases the emission current compared to an as-grown sample by as much as four orders of magnitude. Further, current vs. temperature plots of hydrogenated samples revealed that the emission current begins to decline at temperatures below 700°C limiting the capability of such cathodes. That is, isothermal emission current testing of hydrogenated diamond samples exhibited a decreasing trend with time for temperatures ranging from 600°C to 800°C. It was shown that this decreasing trend followed a first-order reaction equation with an activation energy of ~1.25 eV. These results are the first known to indicate a direct correlation between emission current and surface hydrogen concentration.

In addition to hydrogen, the desorption of deuterium from diamond was also studied. The isothermal emission current decrease of a deuterated sample followed a first-order reaction rate equation. An Arrhenius plot of the data did not exhibit a linear trend as would be expected from a classical desorption reaction. It was determined that this lack of linearity indicates that deuterium likely desorbs from diamond through quantum mechanical tunneling. The data was analyzed according to Bell's tunneling equation instead of the classical Arrhenius equation from which an activation energy of 3.19 eV was calculated with a coefficient of determination ( $R^2$ ) extremely close to 1. Assuming tunneling is indeed responsible for the desorption of deuterium from diamond, the data obtained from the hydrogen desorption experiment was reanalyzed according to Bell's tunneling equation which provided an activation energy of 1.76 eV. Though more data is required to increase the confidence of the activation energy calculations, these findings suggest deuterium requires more energy to desorb than hydrogen. The results obtained from both the deuterium and hydrogen activation energy studies indicate that a deuterated diamond sample could likely operate at higher temperatures before experiencing the effects of desorption than a hydrogenated sample.

## 8.2 Gaseous environment effects on thermionic emission

### 8.2.1 Gases that diminish thermionic emission

Diamond cathodes were exposed to five different gases to examine their effect on thermionic emission. Two gases were observed to have *negative* effects on diamond's thermionic emission properties:  $N_2$  and  $N_2O$ . Both molecular nitrogen and nitrous oxide were not predicted to favorably affect thermionic emission. Specifically, nitrous oxide was predicted to have a strong negative effect due to its well documented dissociation products upon electron interaction.

The testing method confirmed this hypothesis verifying its capability to accurately characterize each gas's influence on the thermionic emission from diamond.

### 8.2.2 Gases that enhance thermionic emission

CH<sub>4</sub>: Operation of diamond films in a methane environment was predicted to have an enhancing effect on the thermionic emission performance based on a previous study by Nemanich.[106] Though, testing of an as-grown diamond sample exhibited very little response to the introduction of CH<sub>4</sub>, testing with a hydrogenated sample appeared to have a small positive response. This positive response is in agreement with Nemanich but the magnitude of response does not reflect his findings that methane appreciably enhanced the thermionic emission of nitrogen-incorporated diamond films. It was hypothesized that this discrepancy is due to the pressures used in each study. At the high pressures Nemanich examined (up to 700mTorr), previous electron impact studies suggest that methane will decompose and reform into many different hydrocarbon molecules consisting of several carbon and hydrogen atoms.[171, 174] These same electron impact studies also imply that the low pressures used in the present research (5.5 μTorr) result in the dissociation of CH<sub>4</sub> into smaller, simpler radicals such as CH<sub>3</sub><sup>+(-)</sup> and H<sup>(+)</sup>. [171, 174] Thus, pressure likely dictates how methane will influence the thermionic emission from diamond films.

Based on the results obtained in the present research, methane was deemed an unsuitable gaseous species for increasing the thermionic emission performance of diamond. Though previous studies have shown methane to have a positive effect on the operation of diamond thermionic cathodes, previous electron impact studies suggest that this effect cannot be sustained. The complex carbon contained molecules formed during Nemanich's study will likely

coalesce on the surface of the diamond electrode. At the elevated temperatures required for thermionic energy conversion, it is probable that these carbon molecules will result in the formation of graphite or other non-diamond carbonaceous content which is not favorable for electron emission due to its high work function of  $\sim 4.5\text{eV}$ . [128, 201]

$\text{H}_2\text{O}$ : Water vapor was also examined and shown to have varying effects on the thermionic emission from diamond. Testing of a hydrogenated sample revealed that a roughly 60 second exposure to  $\text{H}_2\text{O}$  had a net positive effect at lower temperatures while at higher temperatures, it was seen to have a net negative effect. This was determined to be caused by the varying reaction water vapor has with the diamond surface at different temperatures. At lower temperatures, water is thought to interact with the diamond surface by forming C-H and C-OH bonds, both of which have been reported to invoke a negative electron affinity. [175, 176] But at higher temperatures, studies have shown that water vapor can decompose upon interaction with the diamond surface to form a mixture of C-H, C-O-C, and C=O bonds, with the latter two being unfavorable for electron emission. [181] The results in this study suggest water vapor is likely not an ideal candidate to increase the thermionic emission performance of diamond.

$\text{H}_2$ : Molecular hydrogen was the third gas shown to enhance the emission performance of diamond films and appears to be the most promising candidate for use in a diamond thermionic energy converter. For both as-grown and hydrogenated diamond samples, the emission current was observed to increase over vacuum levels. When plotting the emission current increase against baseline emission current, a distinct trend was observed such that the magnitude of this positive effect increased linearly as a function of baseline current levels. A linear regression of this data allowed an expression to be quantified with an  $R^2$  of 0.94 (Equation 8.1).

$$I_{increase} = 0.56 * I_{baseline} \quad (8.1)$$

Where  $I_{increase}$ : the thermionic emission current increase upon exposure to molecular hydrogen and  $I_{baseline}$ : emission current prior to the introduction of hydrogen. Thus, there is a roughly 50% increase in emission current when operating in a 5.5  $\mu$ Torr  $H_2$  environment.

Operation in molecular hydrogen was also observed to increase the temperature ceiling at which diamond films can operate. Recall that though hydrogenated diamond cathodes were able to achieve much higher emission current than as-grown films, they began to exhibit the “roll off” behavior (where the emission current ceases to increase exponentially with temperature and begins to decrease) at lower temperatures, limiting their performance capability. When examining the current versus temperature behavior of diamond cathodes in a constant 5.5 $\mu$ Torr  $H_2$  environment, this roll off was observed to occur at  $\sim 100^\circ\text{C}$  higher temperatures for hydrogenated films. The ability to operate at higher temperatures will allow for more emission current to be extracted from diamond thermionic emitters.

Summarizing: Out of the five gaseous species studied in this research, it is clear that molecular hydrogen is most favorable for use in diamond thermionic energy converters. Not only does exposure to a low pressure hydrogen environment result in a roughly 50% increase in emission current but also allows diamond cathodes to operate at higher temperatures permitting even more current to be extracted. It thus appears unlikely that any future thermionic energy converter implementations utilizing diamond will not take advantage of molecular hydrogen’s beneficial effects.

### 8.3 Potential thermionic energy conversion performance

As a goal of the present research was to examine diamond films for use in TEC, an analysis of the potential performance characteristics was executed. This research demonstrated that exposure of diamond samples to a hydrogen plasma significantly enhanced thermionic emission current levels at low temperatures ( $<1000^{\circ}\text{C}$ ). Unfortunately, the emission current was observed to degrade at temperatures below  $700^{\circ}\text{C}$  when operating in a vacuum environment. This research further established that exposure of diamond samples to low pressure molecular hydrogen results in increased thermionic emission current (compared to operation in vacuum) and also allows for operation at higher temperatures.

The performance of a thermionic energy converter with a nitrogen-incorporated cathode and anode was calculated based on the equations presented in *Chapter III* including all the beneficial effects identified in this work. For the cathode, this analysis used the thermionic emission parameters (Richardson constant and work function) derived for a hydrogenated diamond sample calculated from the data points prior to the “roll off” trend. The anode was modeled from the thermionic emission parameters for the low temperature operation of an as-grown diamond sample discussed in Section 7.1. The performance was extrapolated by applying the enhancing effects observed from operation in the  $5.5\ \mu\text{Torr}$  hydrogen environment. Thus, Equation 8.1 was employed to predict the increased thermionic emission current and the energy conversion performance was calculated up to temperatures just exceeding  $800^{\circ}\text{C}$ . To simplify the calculations, the TEC performance was based on a device with ideal electrical contacts and a load resistance that perfectly matched the power output.

The potential output current and power of this all diamond thermionic energy converter just described was calculated as a function of cathode temperature for an anode held constant at a

nominal temperature of 400°C (Figs. 8.1 and 8.2). Assuming the effects of both the hydrogen plasma treatment and the low pressure hydrogen environment are retained, this configuration could achieve emission current densities of 1 A/cm<sup>2</sup> with an overall output power greater than 100 mW/cm<sup>2</sup> at a cathode operational temperature of 800°C. This equates to the production of over 1 kW per square meter of electrical power from this diamond TEC configuration.

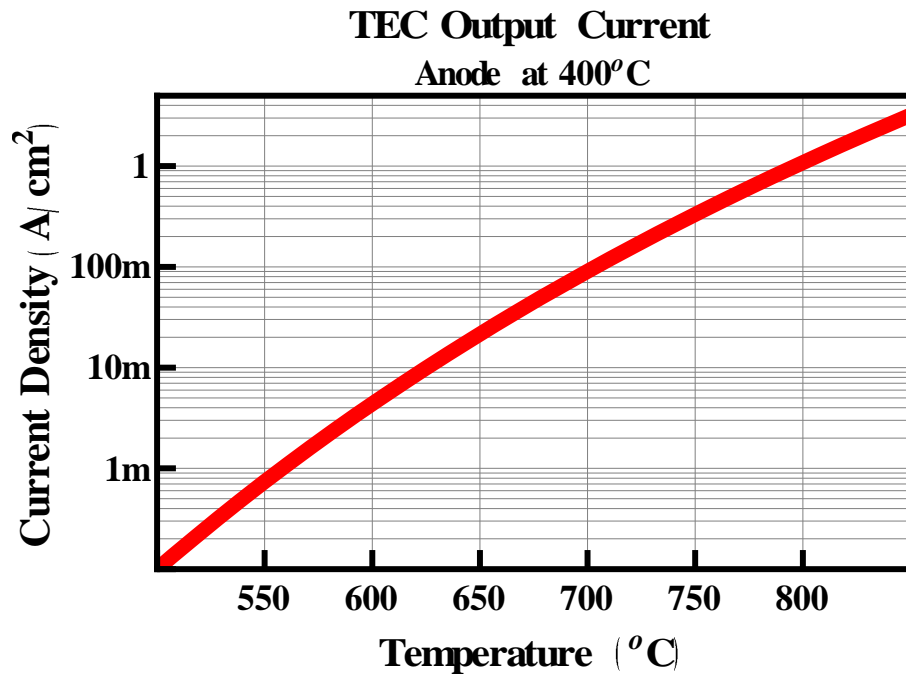


**Figure 8.1** Potential output current of an all diamond thermionic energy converter with molecular hydrogen as the interelectrode gas at a pressure of 5.5μTorr.

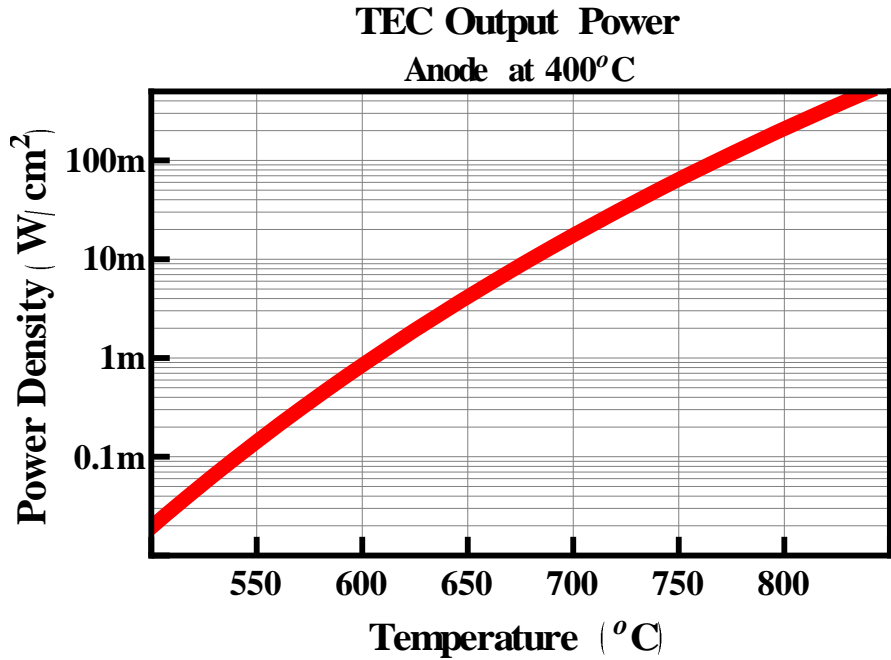


**Figure 8.2** Potential output power of an all diamond thermionic energy converter with molecular hydrogen as the interelectrode gas at a pressure of 5.5 $\mu$ Torr.

#### 8.4 Recommendations for future work

The numerous findings presented in this dissertation should encourage future research of diamond cathodes for thermionic energy conversion. It has been shown that exposure of diamond films to a hydrogenation treatment significantly enhances their thermionic emission performance. The thermal desorption of hydrogen is the primary failure mechanism of diamond emitters preventing exceptionally high emission current from being achieved. This research has shown that the desorption of hydrogen, and its isotope deuterium, is a more complex process than previously thought. The observed non-classical tunneling behavior of the desorption process should be further examined by other research using different methods.

The thermionic emission studies performed in gaseous environments presented in *Chapter VII* indicate that future implementation of a diamond thermionic energy converter may

utilize a gaseous species in order to achieve the useful power output performance described in the previous section. This is rational as all previous TEC implementations took advantage of similar effects, thus many of the engineering challenges have been addressed. Results presented in the present research pertaining to methane differed somewhat from previous work.[106] This dissertation has presented evidence suggesting the previous research utilizing high pressure methane environments would not be feasible for long term operation, follow-up studies could further clarify this matter. Such work would involve testing diamond thermionic emitters in methane environments at varying pressures.

Perhaps the most promising results obtained in this research involve exposing diamond cathodes to low pressure molecular hydrogen environments. While examining operation in pressures of  $5.5\mu\text{Torr}$ , a marked improvement in thermionic emission current was observed. Future studies should examine this effect more broadly in an effort to further characterize the performance of diamond thermionic emitters. This effort should consist of examining emission operation in different molecular hydrogen environment pressures to determine the maximum beneficial effect. This future research would lead to a better understanding of the mechanisms whereby hydrogen has emission current enhancing effects.

In conclusion, this research has provided a sound framework on which future work with diamond thermionic energy converters can be built. It is hoped that the results presented in this dissertation will reinvigorate interest in thermionic energy conversion which is a technology that could revolutionize the field of power generation.

## LIST OF PUBLICATIONS

- [1] W. F. Paxton, J. L. Davidson, W. P. Kang, and M. Howell, "Enhanced thermionic energy converter," USA, Provisional Patent, 2013.
- [2] T. D. Musho, W. F. Paxton, J. L. Davidson, and D. G. Walker, "Quantum simulation of thermionic emission from diamond films," *Journal of Vacuum Science & Technology B: Microelectronics and Nanometer Structures*, vol. 31, p. 021401, 2013.
- [3] W. F. Paxton, A. Steigerwald, M. Howell, N. Tolk, W. P. Kang, and J. L. Davidson, "The effect of hydrogen desorption kinetics on thermionic emission from polycrystalline chemical vapor deposited diamond," *Applied Physics Letters*, vol. 101, p. 243509, 2012.
- [4] W. F. Paxton, M. Howell, W. P. Kang, and J. L. Davidson, "Influence of hydrogen on the thermionic electron emission from nitrogen-incorporated polycrystalline diamond films," *Journal of Vacuum Science & Technology B: Microelectronics and Nanometer Structures*, vol. 30, p. 021202, 2012.
- [5] W. F. Paxton, T. Wade, M. Howell, N. Tolk, W. P. Kang, and J. L. Davidson, "Thermionic emission characterization of boron-doped microcrystalline diamond films at elevated temperatures," *physica status solidi (a)*, 2012.
- [6] W.F. Paxton, M. Howell, N. Tolk, W.P. Kang, and J.L. Davidson, "Nonclassical Desorption Kinetics of Deuterium from Diamond Studied by Thermionic Emission," (In serious preparation)

## REFERENCES

- [1] E. Becquerel, "Rescherches Sur La Transmission De L'Electricite Au Travers Des Gaz A Des Temperatures Elevees," *Annales de Chimie et de Physique*, vol. 39, p. 48, 1853.
- [2] P. A. Redhead, "The birth of electronics: Thermionic emission and vacuum," 1998, pp. 1394-1401.
- [3] T. A. Edison, "Method and apparatus for scanning and object and correcting image data using concurrently generated illumination data," United States Patent 307031, 1884, 1884.
- [4] E. J. Houston, "Notes on Phenomena in Incandescent Lamps," *American Institute of Electrical Engineers, Transactions of the*, vol. I, pp. 11-18, 1884.
- [5] J. A. Fleming, "On Electric Discharge between Electrodes at Different Temperatures in Air and in High Vacua," *Proceedings of the Royal Society of London*, vol. 47, pp. 118-126, January 1, 1889 1889.
- [6] "Power Vacuum Tube Applications," in *Power Vacuum Tubes Handbook, Third Edition*, ed: CRC Press, 2012, pp. 1-18.
- [7] M. Henikenius. *Fluorescent Lamp*. Available: <http://www.ustr.net/electronics/fluorescent.shtml#Overview>
- [8] V. r. Andr<sup>v</sup>o's and P. Michael, "The Scanning Electron Microscope," in *Handbook of Charged Particle Optics, Second Edition*, ed: CRC Press, 2008, pp. 437-496.
- [9] H. Mimura, "The Status of Field Emission Displays," in *Vacuum Electronics Conference, 2007. IVEC '07. IEEE International*, 2007, pp. 1-4.
- [10] G. N. Hatsopoulos and E. P. Gyftopoulos, *Thermionic energy conversion. Volume II. Theory, technology, and application*, 1979.
- [11] D. Y. Goswami and K. Frank, "Global Energy System," in *Handbook of Energy Efficiency and Renewable Energy*, ed: CRC Press, 2007, pp. 1-1-1-24.
- [12] "World Energy Outlook," International Energy Agency 2009.
- [13] J. O'Toole. (2012, Coal company announces layoffs in response to Obama win. *CNN Money*.
- [14] R. Roberts, "Energy Sources and Conversion Techniques: What is our capability of meeting the energy needs of the future within the limitations of known energy resources and energy conversion technology," *American Scientist*, vol. 61, pp. 66-75, 1973.

- [15] K. George, "Conventional Power Generation," in *Systems, Controls, Embedded Systems, Energy, and Machines*, ed: CRC Press, 2006, pp. 1-1-1-20.
- [16] L. E. Bell, "Cooling, Heating, Generating Power, and Recovering Waste Heat with Thermoelectric Systems," *Science*, vol. 321, pp. 1457-1461, September 12, 2008 2008.
- [17] K. Biswas, J. He, I. D. Blum, C.-I. Wu, T. P. Hogan, D. N. Seidman, V. P. Dravid, and M. G. Kanatzidis, "High-perfance bulk thermoelectrics with all-scale hierachical architectures," *Nature*, vol. 489, p. 5, 2012.
- [18] S. M. Sze, *Physics of Semiconductor Devices*, 2nd ed. New York, NY: John Wiley & Sons, Inc., 1981.
- [19] B. Dale, "Wind Energy Conversion," in *Handbook of Energy Efficiency and Renewable Energy*, ed: CRC Press, 2007, pp. 22-1-22-30.
- [20] J. M. Houston, *Theoretical Efficiency of the Thermionic Energy Converter* vol. 30: AIP, 1959.
- [21] J. H. Ingold, "Calculation of the Maximum Efficiency of the Thermionic Converter," *Journal of Applied Physics*, vol. 32, pp. 769-772, 1961.
- [22] O. W. Richardson, "The Electrical Conductivity Imparted to a Vacuum by Hot Conductors," *Philosophical Transactions of the Royal Society of London. Series A, Containing Papers of a Mathematical or Physical Character*, vol. 201, pp. 497-549, 1903.
- [23] S. J. Pearton, "Wide Bandgap Semiconductors - Growth, Processing and Applications," ed: William Andrew Publishing/Noyes, 2000.
- [24] R. J. Zhang, S. T. Lee, and Y. W. Lam, "Characterization of heavily boron-doped diamond films," *Diamond and Related Materials*, vol. 5, pp. 1288-1294, 1996.
- [25] R. B. Kusner, P. M. Lahti, and C. P. Lillya, "New surface allotropes of carbon," *Chemical Physics Letters*, vol. 241, pp. 522-527, 1995.
- [26] S. Koizumi, T. Murakami, T. Inuzuka, and K. Suzuki, "Epitaxial growth of diamond thin films on cubic boron nitride {111} surfaces by dc plasma chemical vapor deposition," *Applied Physics Letters*, vol. 57, pp. 563-565, 1990.
- [27] H. Liu and D. S. Dandy, "Diamond Chemical Vapor Deposition," ed: William Andrew Publishing/Noyes, 1995.
- [28] B. V. Spitsyn, L. L. Bouilov, and B. V. Derjaguin, "Vapor growth of diamond on diamond and other surfaces," *Journal of Crystal Growth*, vol. 52, pp. 219-226, 1981.
- [29] H. Maeda, S. Masuda, K. Kusakabe, and S. Morooka, "Nucleation and growth of diamond in a microwave plasma on substrate pretreated with non-oxide ceramic particles," *Journal of Crystal Growth*, vol. 121, pp. 507-515, 1992.

- [30] K. F. Turner, B. R. Stoner, L. Bergman, J. T. Glass, and R. J. Nemanich, "Observation of surface modification and nucleation during deposition of diamond on silicon by scanning tunneling microscopy," *Journal of Applied Physics*, vol. 69, pp. 6400-6405, 1991.
- [31] G. Popovici and M. A. Prelas, "Nucleation and Selective Deposition of Diamond Thin Films," *physica status solidi (a)*, vol. 132, pp. 233-252, 1992.
- [32] M. W. Geis, "Growth of textured diamond films on foreign substrates from attached seed crystals," *Applied Physics Letters*, vol. 55, pp. 550-552, 1989.
- [33] B. R. Stoner, G. H. M. Ma, S. D. Wolter, and J. T. Glass, "Characterization of bias-enhanced nucleation of diamond on silicon by invacuo surface analysis and transmission electron microscopy," *Physical Review B*, vol. 45, p. 11067, 1992.
- [34] R. F. Davis, "Diamond Films and Coatings," ed: William Andrew Publishing/Noyes, 1993.
- [35] W. D. Yasuaki Hayashi, and Russel Messier, "Temperature Dependence of Nucleation Density of Chemical Vapor Deposition Diamond," *Jpn. J. Appl. Phys.*, vol. 31, 1992.
- [36] M. A. Pinault, J. Barjon, T. Kociniewski, F. Jomard, and J. Chevallier, "The n-type doping of diamond: Present status and pending questions," *Physica B: Condensed Matter*, vol. 401-402, pp. 51-56, 2007.
- [37] R. C. Hyer, M. Green, K. K. Mishra, and S. C. Sharma, "Nucleation and growth of diamond in hot filament assisted chemical vapour deposition," *Journal of Materials Science Letters*, vol. 10, pp. 515-518, 1991.
- [38] S. Praver and R. J. Nemanich, "Raman spectroscopy of diamond and doped diamond," *Philosophical Transactions of the Royal Society of London. Series A: Mathematical, Physical and Engineering Sciences*, vol. 362, pp. 2537-2565, November 15, 2004 2004.
- [39] P. Instruments, "Raman Spectroscopy Basics," ed.
- [40] N. Wada and S. A. Solin, "Raman efficiency measurements of graphite," *Physica B+C*, vol. 105, pp. 353-356, 1981.
- [41] A. M. Zaitsev, *Optical Properties of Diamond*: Springer, 2001.
- [42] R. W. Bormett, S. A. Asher, R. E. Witowski, W. D. Partlow, R. Lizewski, and F. Pettit, "Ultraviolet Raman spectroscopy characterizes chemical vapor deposition diamond film growth and oxidation," *Journal of Applied Physics*, vol. 77, pp. 5916-5923, 1995.
- [43] J. F. Shackelford, *Materials Science for Engineers*. Upper Saddle River, New Jersey: Pearson Prentice Hall, 2005.

- [44] J. M. Hollander and W. L. Jolly, "X-ray photoelectron spectroscopy," *Accounts of Chemical Research*, vol. 3, pp. 193-200, 1970/06/01 1970.
- [45] P. van der Heide, *X-Ray Photoelectron Spectroscopy : An Introduction to Principles and Practices*. Hoboken, NJ, USA: Wiley, 2011.
- [46] P. J. Goodhew, F. J. Humphreys, and R. Beanland, *Electron Microscopy and Analysis*. London, GBR: Taylor & Francis, 2000.
- [47] W. Zhu, B. R. Stoner, B. E. Williams, and J. T. Glass, "Growth and characterization of diamond films on nondiamond substrates for electronic applications," *Proceedings of the IEEE*, vol. 79, pp. 621-646, 1991.
- [48] D. G. Brandon and W. D. Kaplan, *Microstructural Characterization of Materials: J*. Wiley, 1999.
- [49] M. N. Yoder, "Diamond Properties and Applications," in *Diamond Films and Coatings-Development, Properties, and Applications*, R. F. Davis, Ed., ed. Park Ridge: Noyes Publications, 1993, pp. 1-30.
- [50] D. R. S. Gilbert, Rajiv K., "Diamond Deposition and Characterization," in *Wide Bandgap Semiconductors - Growth, Processing and Applications*, S. J. Pearton, Ed., ed. Norwich: William Andrew Publishing/Noyes, 2000, p. 507.
- [51] A. A. Giardini, "A Study of the Directional Hardness in Silicon," *The American Mineralogist*, vol. 43, p. 13, 1958.
- [52] V. L. Solozhenko, S. N. Dub, and N. V. Novikov, "Mechanical properties of cubic BC<sub>2</sub>N, a new superhard phase," *Diamond and Related Materials*, vol. 10, pp. 2228-2231, 2001.
- [53] C. Research. Boron Nitride (BN) - Properties and Information on Boron Nitride [Online]. Available: <http://www.azom.com/article.aspx?ArticleID=78>
- [54] R. Kalish, "Doping of diamond," *Carbon*, vol. 37, pp. 781-785, 1999.
- [55] A. Wisitsora-at, W. P. Kang, J. L. Davidson, Y. Gurbuz, and D. V. Kerns, "Field emission enhancement of diamond tips utilizing boron doping and surface treatment," *Diamond and Related Materials*, vol. 8, pp. 1220-1224, 1999.
- [56] R. F. Mamin and T. Inushima, "Conductivity in boron-doped diamond," *Physical Review B*, vol. 63, p. 033201, 2001.
- [57] J. Barjon, N. Habka, C. Mer, F. Jomard, J. Chevallier, and P. Bergonzo, "Resistivity of boron doped diamond," *physica status solidi (RRL) – Rapid Research Letters*, vol. 3, pp. 202-204, 2009.

- [58] M. Nishitani-Gamo, E. Yasu, C. Xiao, Y. Kikuchi, K. Ushizawa, I. Sakaguchi, T. Suzuki, and T. Ando, "Sulfur-doped homoepitaxial (001) diamond with n-type semiconductive properties," *Diamond and Related Materials*, vol. 9, pp. 941-947, 2000.
- [59] S. A. Kajihara, A. Antonelli, J. Bernholc, and R. Car, "Nitrogen and potential n-type dopants in diamond," *Physical Review Letters*, vol. 66, pp. 2010-2013, 1991.
- [60] Y. Show, T. Matsukawa, M. Iwase, and T. Izumi, "Effects of defects introduced by nitrogen doping on electron emission from diamond films," *Materials Chemistry and Physics*, vol. 72, pp. 201-203, 2001.
- [61] G. Z. Cao, J. J. Schermer, W. J. P. v. Enckevort, W. A. L. M. Elst, and L. J. Giling, "Growth of {100} textured diamond films by the addition of nitrogen," *Journal of Applied Physics*, vol. 79, pp. 1357-1364, 1996.
- [62] S. Bhattacharyya, O. Auciello, J. Birrell, J. A. Carlisle, L. A. Curtiss, A. N. Goyette, D. M. Gruen, A. R. Krauss, J. Schlueter, A. Sumant, and P. Zapol, "Synthesis and characterization of highly-conducting nitrogen-doped ultrananocrystalline diamond films," *Applied Physics Letters*, vol. 79, pp. 1441-1443, 2001.
- [63] F. A. M. Koeck, R. J. Nemanich, A. Lazea, and K. Haenen, "Thermionic electron emission from low work-function phosphorus doped diamond films," *Diamond and Related Materials*, vol. 18, pp. 789-791, 2009.
- [64] J. P. Goss, "Theory of hydrogen in diamond," *Journal of Physics: Condensed Matter*, vol. 15, p. R551, 2003.
- [65] M. I. Landstrass and K. V. Ravi, "Resistivity of chemical vapor deposited diamond films," *Applied Physics Letters*, vol. 55, pp. 975-977, 1989.
- [66] M. I. Landstrass and K. V. Ravi, "Hydrogen passivation of electrically active defects in diamond," *Applied Physics Letters*, vol. 55, pp. 1391-1393, 1989.
- [67] J. B. Cui, J. Ristein, M. Stammer, K. Janischowsky, G. Kleber, and L. Ley, "Hydrogen termination and electron emission from CVD diamond surfaces: a combined secondary electron emission, photoelectron emission microscopy, photoelectron yield, and field emission study," *Diamond and Related Materials*, vol. 9, pp. 1143-1147, 2000.
- [68] F. J. Himpsel, J. A. Knapp, J. A. VanVechten, and D. E. Eastman, "Quantum photoyield of diamond(111)—A stable negative-affinity emitter," *Physical Review B*, vol. 20, pp. 624-627, 1979.
- [69] J. van der Weide, Z. Zhang, P. K. Baumann, M. G. Wensell, J. Bernholc, and R. J. Nemanich, "Negative-electron-affinity effects on the diamond (100) surface," *Physical Review B*, vol. 50, p. 5803, 1994.

- [70] I. L. Krainsky, V. M. Asnin, G. T. Mearini, and J. A. Dayton, Jr., "Negative-electron-affinity effect on the surface of chemical-vapor-deposited diamond polycrystalline films," *Physical Review B*, vol. 53, pp. R7650-R7653, 1996.
- [71] D. Takeuchi, S. G. Ri, H. Kato, C. E. Nebel, and S. Yamasaki, "Negative electron affinity on hydrogen terminated diamond," *physica status solidi (a)*, vol. 202, pp. 2098-2103, 2005.
- [72] R. U. Martinelli and D. G. Fisher, "The application of semiconductors with negative electron affinity surfaces to electron emission devices," *Proceedings of the IEEE*, vol. 62, pp. 1339-1360, 1974.
- [73] F. Maier, J. Ristein, and L. Ley, "Electron affinity of plasma-hydrogenated and chemically oxidized diamond (100) surfaces," *Physical Review B*, vol. 64, p. 165411, 2001.
- [74] M. Suzuki, T. Ono, N. Sakuma, and T. Sakai, "Low-temperature thermionic emission from nitrogen-doped nanocrystalline diamond films on n-type Si grown by MPCVD," *Diamond and Related Materials*, vol. 18, pp. 1274-1277, 2009.
- [75] M. Kataoka, C. Zhu, F. A. M. Koeck, and R. J. Nemanich, "Thermionic electron emission from nitrogen-doped homoepitaxial diamond," *Diamond and Related Materials*, vol. 19, pp. 110-113, 2010.
- [76] W. F. Paxton, M. Howell, W. P. Kang, and J. L. Davidson, "Influence of hydrogen on the thermionic electron emission from nitrogen-incorporated polycrystalline diamond films," *Journal of Vacuum Science & Technology B: Microelectronics and Nanometer Structures*, vol. 30, p. 021202, 2012.
- [77] D. Menzel, "Desorption Phenomena," in *Interactions on Metal Surfaces*, R. Gomer, Ed., ed New York: Springer-Verlag, 1975, p. 310.
- [78] T. Nishimori, H. Sakamoto, Y. Takakuwa, and S. Kono, "Methane adsorption and hydrogen isothermal desorption kinetics on a C(001)-(1 x 1) surface," *Journal of Vacuum Science & Technology A: Vacuum, Surfaces, and Films*, vol. 13, pp. 2781-2786, 1995.
- [79] J. B. Cui, J. Ristein, and L. Ley, "Dehydrogenation and the surface phase transition on diamond (111): Kinetics and electronic structure," *Physical Review B*, vol. 59, pp. 5847-5856, 1999.
- [80] R. E. Thomas, R. A. Rudder, and R. J. Markunas, "Thermal desorption from hydrogenated and oxygenated diamond (100) surfaces," *Journal of Vacuum Science & Technology A: Vacuum, Surfaces, and Films*, vol. 10, pp. 2451-2457, 1992.
- [81] X. M. Zheng and P. V. Smith, "The topologies of the clean and hydrogen-terminated C(100) surfaces," *Surface Science*, vol. 256, pp. 1-8, 1991.
- [82] A. V. Hamza, G. D. Kubiak, and R. H. Stulen, "Hydrogen chemisorption and the structure of the diamond C(100)-(2 x 1) surface," *Surface Science*, vol. 237, pp. 35-52, 1990.

- [83] M. T. Schulberg and G. D. S. Kubiak, Richard H., "Temperature Programmed Desorption of Hydrogen and Deuterium from Cvd Diamond Samples," presented at the Novel Forms of Carbon, 1992.
- [84] M. McGonigal, M. L. Kempel, M. S. Hammond, and K. D. Jamison, "Isothermal hydrogen desorption from the diamond (100)2 x 1 surface," *Journal of Vacuum Science & Technology A: Vacuum, Surfaces, and Films*, vol. 14, pp. 2308-2314, 1996.
- [85] T. E. Derry, C. C. P. Madiba, and J. P. F. Sellschop, "Oxygen and hydrogen on the surface of diamond," *Nuclear Instruments and Methods in Physics Research*, vol. 218, pp. 559-562, 1983.
- [86] P. K. Baumann and R. J. Nemanich, "Surface cleaning, electronic states and electron affinity of diamond (100), (111) and (110) surfaces," *Surface Science*, vol. 409, pp. 320-335, 1998.
- [87] J. Davidson, W. Kang, K. Holmes, A. Wisitsora-At, P. Taylor, V. Pulugurta, R. Venkatasubramanian, and F. Wells, "CVD diamond for components and emitters," *Diamond and Related Materials*, vol. 10, pp. 1736-1742, 2001.
- [88] A. Vescan, I. Daumiller, P. Gluche, W. Ebert, and E. Kohn, "1000°C operation of diamond Schottky diode," in *Device Research Conference Digest, 1997. 5th*, 1997, pp. 40-41.
- [89] A. Vescan, I. Daumiller, P. Gluche, W. Ebert, and E. Kohn, "High temperature, high voltage operation of diamond Schottky diode," *Diamond and Related Materials*, vol. 7, pp. 581-584, 1998.
- [90] A. Aleksov, A. Denisenko, M. Kunze, A. Vescan, A. Bergmaier, G. Dollinger, W. Ebert, and E. Kohn, "Diamond diodes and transistors," *Semiconductor Science and Technology*, vol. 18, p. S59, 2003.
- [91] M. W. Geis, "Diamond transistor performance and fabrication," *Proceedings of the IEEE*, vol. 79, pp. 669-676, 1991.
- [92] J. Walko. (2009, Researchers tout diamond transistor breakthrough. *EE Times* [Online Article].
- [93] G. Fursey, "Advances in Applications," in *Field Emission in Vacuum Microelectronics*, I. Brodie and P. Shwoebel, Eds., ed: Kluwer Academic/Plenum Publishers, 2005, pp. 137-170.
- [94] T. Utsumi, "Historical Overview," in *Vacuum Microelectronics*, W. Zhu, Ed., ed New York: Jon Wiley & Sons, Inc, 2001, pp. 1-12.
- [95] K. Subramanian, W. P. Kang, J. L. Davidson, Y. M. Wong, and B. K. Choi, "Nanocrystalline diamond lateral field emission diode fabrication by dual micropatterning technique," *Diamond and Related Materials*, vol. 16, pp. 1408-1412, 2007.

- [96] K. Subramanian, W. P. Kang, J. L. Davidson, and M. Howell, "Nanodiamond lateral field emitter devices on thick insulator substrates for reliable high power applications," *Diamond and Related Materials*, vol. 17, pp. 786-789, 2008.
- [97] K. Subramanian, W. P. Kang, J. L. Davidson, B. K. Choi, and M. Howell, "Nanodiamond lateral comb array field emission diode for high current applications," *Diamond and Related Materials*, vol. 15, pp. 1994-1997, 2006.
- [98] W. P. Kang, J. L. Davidson, A. Wisitsora-At, Y. M. Wong, R. Takalkar, K. Holmes, and D. V. Kerns, "Diamond vacuum field emission devices," *Diamond and Related Materials*, vol. 13, pp. 1944-1948, Nov-Dec 2004.
- [99] K. Subramanian, W. P. Kang, J. L. Davidson, R. S. Takalkar, B. K. Choi, M. Howell, and D. V. Kerns, "Enhanced electron field emission from micropatterned pyramidal diamond tips incorporating CH<sub>4</sub>/H-2/N-2 plasma-deposited nanodiamond," *Diamond and Related Materials*, vol. 15, pp. 1126-1131, Apr-Aug 2006.
- [100] W. P. Kang, J. L. Davidson, M. A. George, I. Milosevljevic, J. Wittig, and D. V. Kerns, "Characterization of the Microstructure of Diamond Pyramidal Microtip Emitters," presented at the International Conference on the New Diamond Science and Technology, Tours, France, 1996.
- [101] W. P. Kang, J. L. Davidson, A. Wisitsora-at, Y. M. Wong, R. Takalkar, K. Subramanian, D. V. Kerns, and W. H. Hofmeister, "Diamond and carbon-derived vacuum micro- and nano-electronic devices," *Diamond and Related Materials*, vol. 14, pp. 685-691, 2005.
- [102] J. L. Davidson, W. P. Kang, K. Subramanian, and Y. M. Wong, "Vacuum Cold Cathode Emitter Electronic Devices Comprised of Diamond or other Carbons," in *University/Government/Industry Micro/Nano Symposium, 2008. UGIM 2008. 17th Biennial*, 2008, pp. 102-106.
- [103] B. K. Choi, W. P. Kang, I. L. Davis, J. L. Davidson, S. T. Hu, and R. W. Pitz, "Thermionic electron emission from chemical vapor deposition diamond by nanosecond laser heating," *Journal of Vacuum Science & Technology B: Microelectronics and Nanometer Structures*, vol. 27, pp. 557-561, 2009.
- [104] Y. M. Wong, W. P. Kang, J. L. Davidson, S. Raina, and J. H. Huang, "Carbon nanostructures as thermal field emitters for waste heat recovery," *Diamond and Related Materials*, vol. 18, pp. 563-566, 2009.
- [105] F. A. M. Koeck and R. J. Nemanich, "Low temperature onset for thermionic emitters based on nitrogen incorporated UNCD films," *Diamond and Related Materials*, vol. 18, pp. 232-234, 2009.
- [106] F. A. M. Koeck, R. J. Nemanich, Y. Balasubramaniam, K. Haenen, and J. Sharp, "Enhanced thermionic energy conversion and thermionic emission from doped diamond films through methane exposure," *Diamond and Related Materials*, vol. 20, pp. 1229-1233, 2011.

- [107] S. Dushman, "Electron Emission from Metals as a Function of Temperature," *Physical Review*, vol. 21, pp. 623-636, 1923.
- [108] O. W. Richardson, "The Positive Ionization from Hot Salts," *Physical Review (Series I)*, vol. 33, p. 450, 1911.
- [109] W. B. Nottingham, "Thermionic Emission," Massachusetts Institute of Technology, Cambridge, Technical Report 321, December 10 1956.
- [110] G. N. Fleming, "The evolution of Pauli's exclusion principle," *Studies in History and Philosophy of Science Part B: Studies in History and Philosophy of Modern Physics*, vol. 38, pp. 202-208, 2007.
- [111] N. S. Rasor, "Thermionic Energy Converter," in *Fundamentals Handbook of Electrical and Computer Engineering*. vol. II, S. S. L. Chang, Ed., ed New York: John Wiley & Sons, Inc., 1983, pp. 668-679.
- [112] G. Medicus and G. Wehner, "Noble Gas Hot Cathode Diodes with Negative Arc Drop," *Journal of Applied Physics*, vol. 22, p. 1389, 1951.
- [113] L. L. Marton, *Advances in Electronics and Electron Physics*: Academic Press, 1963.
- [114] N. S. Rasor, "Thermionic energy conversion plasmas," *Plasma Science, IEEE Transactions on*, vol. 19, pp. 1191-1208, 1991.
- [115] J. K. Shultis and R. E. Faw, "Thermionic Electrical Generators," in *Fundamentals of Nuclear Science and Engineering*, ed New York: Marcel Dekker, Inc., 2002.
- [116] G. M. Gryaznov, "30th anniversary of the startup of Topaz—The first thermionic nuclear reactor in the world," *Atomic Energy*, vol. 89, pp. 510-515, 2000/07/01 2000.
- [117] G. Gaertner and H. W. P. Koops, "Vacuum Electron Sources and their Materials and Technologies," in *Vacuum Electronics*, J. A. Eichmeier and M. K. Thumm, Eds., ed: Springer, 2008, pp. 429-481.
- [118] C. Ferris, J. Whitaker, and S. Epstein, "Electron Vacuum Devices," in *The Electronics Handbook, Second Edition*, ed: CRC Press, 2005, pp. 353-474.
- [119] R. O. Jenkins, "A review of thermionic cathodes," *Vacuum*, vol. 19, pp. 353-359, 1969.
- [120] E. L. Chaffeem, "Practical Sources of Emission and some General Physical Aspects of Vacuum Tubes," in *Theory of Thermionic Vacuum Tubes*, ed New York and London: McGraw-Hill, 1933, pp. 95-137.
- [121] A. Taran, D. Voronovich, S. Plankovskyy, V. Paderno, and V. Filipov, "Review of LaB6, Re-W Dispenser, and BaHfO3-W Cathode Development," *Electron Devices, IEEE Transactions on*, vol. 56, pp. 812-817, 2009.

- [122] C. Oshima, E. Bannai, T. Tanaka, and S. Kawai, "Thermionic work function of LaB<sub>6</sub> single crystals and their surfaces," *Journal of Applied Physics*, vol. 48, pp. 3925-3927, 1977.
- [123] V. C. Wilson, "Conversion of Heat to Electricity by Thermionic Emission," *Journal of Applied Physics*, vol. 30, pp. 475-481, 1959.
- [124] B. Fiegl, R. Kuhnert, M. Ben-Chorin, and F. Koch, "Evidence for grain boundary hopping transport in polycrystalline diamond films," *Applied Physics Letters*, vol. 65, pp. 371-373, 1994.
- [125] W. F. Paxton, "Characterization of the Thermal Electron Emission Properties of Boron-Doped Polycrystalline Films for Use in Energy Conversion," Master of Science, Electrical Engineering, Vanderbilt University, Nashville, 2011.
- [126] B. P. Allen and T. Evans, "Aggregation of Nitrogen in Diamond, Including Platelet Formation," *Proceedings of the Royal Society of London. Series A, Mathematical and Physical Sciences*, vol. 375, pp. 93-104, 1981.
- [127] A. T. Collins, "A spectroscopic survey of naturally-occurring vacancy-related colour centres in diamond," *Journal of Physics D: Applied Physics*, vol. 15, p. 1431, 1982.
- [128] K. S. Krishnan and S. C. Jain, "Thermionic Constants of Graphite," *Nature*, vol. 169, pp. 702-703, 1952.
- [129] V. S. Robinson, Y. Show, G. M. Swain, R. G. Reifenberger, and T. S. Fisher, "Thermionic emission from surface-terminated nanocrystalline diamond," *Diamond and Related Materials*, vol. 15, pp. 1601-1608, 2006.
- [130] N. S. Rasor, "Emission physics of the thermionic energy converter," *Proceedings of the IEEE*, vol. 51, pp. 733-747, 1963.
- [131] K. G. Hernqvist, "Analysis of the arc mode operation of the cesium vapor thermionic energy converter," *Proceedings of the IEEE*, vol. 51, pp. 748-754, 1963.
- [132] H. L. Witting and E. P. Gyftopoulos, "An Ionization Process in a Low-Energy Cesium Plasma," *Journal of Applied Physics*, vol. 36, pp. 1328-1337, 1965.
- [133] G. N. Hatsopoulos, "Transport effects in cesium thermionic converters," *Proceedings of the IEEE*, vol. 51, pp. 725-733, 1963.
- [134] I. Langmuir and K. H. Kingdon, "THERMIONIC EFFECTS CAUSED BY ALKALI VAPORS IN VACUUM TUBES," *Science*, vol. 57, pp. 58-60, January 12, 1923.
- [135] G. O. Fitzpatrick, E. J. Britt, and B. Moyzhes, "Updated perspective on the potential for thermionic conversion to meet 21st Century energy needs," in *Energy Conversion Engineering Conference, 1997. IECEC-97., Proceedings of the 32nd Intersociety, 1997*, pp. 1045-1051 vol.2.

- [136] G. R. Caskey Jr, M. R. Louthan Jr, and R. G. Derrick, "Hydrogen transport in molybdenum," *Journal of Nuclear Materials*, vol. 55, pp. 279-283, 1975.
- [137] Y. Sato, H. Fujita, T. Ando, T. Tanaka, and M. Kamo, "Local epitaxial growth of diamond on nickel from the vapour phase," in *Thin Film Diamond*, A. Lettington and J. W. Steeds, Eds., 1st ed London: Chapman & Hall, 1994, pp. 58-59.
- [138] M. Araki, "PID Control," in *Control Systems, Robotics, and Automation* vol. 2, H. Unbehauen, Ed., ed. Oxford, UK: Eolss Publishers, 2004.
- [139] R. Vanselow, "Compensation effects in thermionic electron emission," *Surface Science*, vol. 149, pp. 381-393, 1985.
- [140] M. Myojo, "Thermionic Emission Properties of Emissive Oxides," *Journal of Light & Visual Environment*, vol. 34, pp. 24-34, 2010.
- [141] S. Bhattacharyya, "Mechanism of high n -type conduction in nitrogen-doped nanocrystalline diamond," *Physical Review B*, vol. 70, p. 125412, 2004.
- [142] W. F. Paxton, T. Wade, M. Howell, N. Tolk, W. P. Kang, and J. L. Davidson, "Thermionic emission characterization of boron-doped microcrystalline diamond films at elevated temperatures," *physica status solidi (a)*, pp. n/a-n/a, 2012.
- [143] S. Albin and L. Watkins, "Current-voltage characteristics of thin film and bulk diamond treated in hydrogen plasma," *Electron Device Letters, IEEE*, vol. 11, pp. 159-161, 1990.
- [144] C.-L. Chen, C.-S. Chen, and J.-T. Lue, "Field emission characteristic studies of chemical vapor deposited diamond films," *Solid-State Electronics*, vol. 44, pp. 1733-1741, 2000.
- [145] Y. L. Yang, L. M. Struck, L. F. Sutcu, and M. P. D'Evelyn, "Chemistry of hydrogen on diamond (100)," *Thin Solid Films*, vol. 225, pp. 203-211, 1993.
- [146] D. D. Koleske, S. M. Gates, B. D. Thoms, J. N. Russell Jr, and J. E. Butler, "Isothermal desorption of hydrogen from polycrystalline diamond films," *Surface Science*, vol. 320, pp. L105-L111, 1994.
- [147] D. D. Koleske, S. M. Gates, B. D. Thoms, J. J. N. Russell, and J. E. Butler, "Hydrogen on polycrystalline diamond films: Studies of isothermal desorption and atomic deuterium abstraction," *The Journal of Chemical Physics*, vol. 102, pp. 992-1002, 1995.
- [148] J. B. Cui, J. Ristein, and L. Ley, "Electron Affinity of the Bare and Hydrogen Covered Single Crystal Diamond (111) Surface," *Physical Review Letters*, vol. 81, p. 429, 1998.
- [149] C. Bandis and B. B. Pate, "Electron Emission Due to Exciton Breakup from Negative Electron Affinity Diamond," *Physical Review Letters*, vol. 74, pp. 777-780, 1995.

- [150] R. J. Nemanich, P. K. Baumann, M. C. Benjamin, S. W. King, J. van der Weide, and R. F. Davis, "Negative electron affinity surfaces of aluminum nitride and diamond," *Diamond and Related Materials*, vol. 5, pp. 790-796, 1996.
- [151] B. B. Pate, "The diamond surface: atomic and electronic structure," *Surface Science*, vol. 165, pp. 83-142, 1986.
- [152] W. F. Paxton, A. Steigerwald, M. Howell, N. Tolk, W. P. Kang, and J. L. Davidson, "The effect of hydrogen desorption kinetics on thermionic emission from polycrystalline chemical vapor deposited diamond," *Applied Physics Letters*, vol. 101, p. 243509, 2012.
- [153] J. E. House, *Principles of Chemical Kinetics*, 2nd ed.: Elsevier, 2007.
- [154] E. V. Anslyn and D. A. Dougherty, *Modern Physical Organic Chemistry*: University Science Books, 2006.
- [155] J. H. Espenson, "Kinetic Isotope Effect," in *Chemical Kinetics and Reaction Mechanisms*, ed New York: McGraw-Hill Inc., 1995, pp. 214-220.
- [156] J. D. Garcia and J. E. Mace, "Energy Level and Line Tables for One-Electron Atomic Spectra," *J. Opt. Soc. Am.*, vol. 55, pp. 654-661, 1965.
- [157] M. Wolfsberg, W. A. Van Hook, P. Paneth, and L. P. N. Rebelo, *Isotope Effects in the Chemical, Geological, and Bio Sciences*. New York: Springer, 2010.
- [158] K. Bobrov, H. Shechter, M. Folman, and A. Hoffman, "Deuterium adsorption-desorption from diamond (100) single crystal surfaces studied by TPD," *Diamond and Related Materials*, vol. 7, pp. 170-176, 1998.
- [159] K. Bobrov, B. Fisgeer, H. Shechter, M. Folman, and A. Hoffman, "Thermal-programmed desorption (TPD) of deuterium from Di(111) surface: presence of two adsorption states," *Diamond and Related Materials*, vol. 6, pp. 736-742, 1997.
- [160] C. Su, K.-J. Song, Y. L. Wang, H.-L. Lu, T. J. Chuang, and J.-C. Lin, "Hydrogen chemisorption and thermal desorption on the diamond C(111) surface," *The Journal of Chemical Physics*, vol. 107, pp. 7543-7558, 1997.
- [161] A. Hoffman, K. Bobrov, B. Fisgeer, H. Shechter, and M. Folman, "Effects of deuterium adsorption-desorption on the state of diamond: surface degradation and stabilization of sp<sup>3</sup> bonded carbon," *Diamond and Related Materials*, vol. 5, pp. 977-983, 1996.
- [162] R. P. Bell, *The Tunnel Effect in Chemistry*. London: Chapman and Hall, 1980.
- [163] A. E. Shilov, "Catalytic reduction of molecular nitrogen in solutions," *Russian Chemical Bulletin*, vol. 52, pp. 2555-2562, 2003/12/01 2003.
- [164] G. C. Baldwin, "Nitrogen total cross section for electrons below 2.0 eV," *Physical Review A*, vol. 9, pp. 1225-1229, 1974.

- [165] T. Oster, A. Kühn, and E. Illenberger, "Gas phase negative ion chemistry," *International Journal of Mass Spectrometry and Ion Processes*, vol. 89, pp. 1-72, 1989.
- [166] M. Born, S. Ingemann, and N. M. M. Nibbering, "Formation and chemistry of radical anions in the gas phase," *Mass Spectrometry Reviews*, vol. 16, pp. 181-200, 1997.
- [167] R. Balog, "Low Energy Electrons as a Soft Tool for Surface Modification," Doctor of Philosophy, Department of Biology, Chemistry, and Pharmacy, University of Berlin, Berlin, 2004.
- [168] B. L. Moiseiwitsch, "Electron Affinities of Atoms and Molecules," in *Advances in Atomic and Molecular Physics*, vol. 1, D. R. Bates and I. Estermann, Eds., ed New York: Academic Press, 1965, pp. 61-83.
- [169] S. R. Hunter, J. G. Carter, and L. G. Christophorou, "Electron transport measurements in methane using an improved pulsed Townsend technique," *Journal of Applied Physics*, vol. 60, pp. 24-35, 1986.
- [170] N. B. Ram and E. Krishnakumar, "Dissociative electron attachment to methane probed using velocity slice imaging," *Chemical Physics Letters*, vol. 511, pp. 22-27, 2011.
- [171] G. Drabner, A. Poppe, and H. Budzikiewicz, "The composition of the CH<sub>4</sub> plasma," *International Journal of Mass Spectrometry and Ion Processes*, vol. 97, pp. 1-33, 1990.
- [172] S. Motlagh and J. H. Moore, "Cross sections for radicals from electron impact on methane and fluoroalkanes," *The Journal of Chemical Physics*, vol. 109, pp. 432-438, 1998.
- [173] T. E. Sharp and J. T. Dowell, "Isotope Effects in Dissociative Attachment of Electrons in Methane," *The Journal of Chemical Physics*, vol. 46, pp. 1530-1531, 1967.
- [174] J. Gross, "Chemical Ionization," in *Mass Spectrometry*, ed: Springer Berlin Heidelberg, 2011, pp. 331-354.
- [175] X. Gao, L. Liu, D. Qi, S. Chen, A. T. S. Wee, T. Ouyang, K. P. Loh, X. Yu, and H. O. Moser, "Water-Induced Negative Electron Affinity on Diamond (100)," *The Journal of Physical Chemistry C*, vol. 112, pp. 2487-2491, 2008/02/01 2008.
- [176] M. J. Rutter and J. Robertson, "Ab initio calculation of electron affinities of diamond surfaces," *Physical Review B*, vol. 57, pp. 9241-9245, 1998.
- [177] G. Piantanida, A. Breskin, R. Chechik, O. Katz, A. Laikhtman, A. Hoffman, and C. Coluzza, "Effect of moderate heating on the negative electron affinity and photoyield of air-exposed hydrogen-terminated chemical vapor deposited diamond," *Journal of Applied Physics*, vol. 89, pp. 8259-8264, 2001.
- [178] A. Laikhtman, A. Lafosse, Y. Le Coat, R. Azria, and A. Hoffman, "Interaction of water vapor with bare and hydrogenated diamond film surfaces," *Surface Science*, vol. 551, pp. 99-105, 2004.

- [179] B. F. Mantel, M. Stammer, J. Ristein, and L. Ley, "The correlation between surface conductivity and adsorbate coverage on diamond as studied by infrared spectroscopy," *Diamond and Related Materials*, vol. 10, pp. 429-433, 2001.
- [180] S. Skokov, B. Weiner, and M. Frenklach, "Theoretical study of oxygenated (100) diamond surfaces in the presence of hydrogen," *Physical Review B*, vol. 55, pp. 1895-1902, 1997.
- [181] L. M. Struck and M. P. D'Evelyn, "Interaction of hydrogen and water with diamond (100): Infrared spectroscopy," 1993, pp. 1992-1997.
- [182] A. Laikhtman and A. Hoffman, "Interaction of thermally activated and molecular oxygen with hydrogenated polycrystalline diamond surfaces studied by synchrotron radiation techniques," *Surface Science*, vol. 522, pp. L1-L8, 2003.
- [183] O. Heber, R. Golser, H. Gnaser, D. Berkovits, Y. Toker, M. Eritt, M. L. Rappaport, and D. Zajfman, "Lifetimes of the negative molecular hydrogen ions:  $H_2^-$ ,  $D_2^-$ , and  $HD^-$ ," *Physical Review A*, vol. 73, p. 060501, 2006.
- [184] B. M. Schwarzschild, "Negative ions of molecular hydrogen," *Physics Today*, vol. 64, p. 23, 2011.
- [185] H. Eyring, J. O. Hirschfelder, and H. S. Taylor, "The Theoretical Treatment of Chemical Reactions Produced by Ionization Processes Part I. The Ortho-Para Hydrogen Conversion by Alpha-Particles," *The Journal of Chemical Physics*, vol. 4, pp. 479-491, 1936.
- [186] I. Fischer-Hjalmars, "Theoretical Investigation of the Negative Hydrogen Molecule Ion," *The Journal of Chemical Physics*, vol. 30, p. 1099, 1959.
- [187] R. D. Harcourt, "A bound  $2 \Sigma_g^+$  ground state for  $H_2^-$  - ? A valence-bond study," *Journal of Physics B: Atomic and Molecular Physics*, vol. 20, p. L617, 1987.
- [188] A. Dalgarno and M. R. C. McDowell, "Charge Transfer and the Mobility of  $H^-$  Ions in Atomic Hydrogen," *Proceedings of the Physical Society. Section A*, vol. 69, p. 615, 1956.
- [189] B. Jordon-Thaden, H. Kreckel, R. Golser, D. Schwalm, M. H. Berg, H. Buhr, H. Gnaser, M. Grieser, O. Heber, M. Lange, O. Novotný, S. Novotny, H. B. Pedersen, A. Petrigiani, R. Repnow, H. Rubinstein, D. Shafir, A. Wolf, and D. Zajfman, "Structure and Stability of the Negative Hydrogen Molecular Ion," *Physical Review Letters*, vol. 107, p. 193003, 2011.
- [190] V. I. Khvostenko and V. M. Dukel'skii, "Formation of negative  $H^-$  ions in electron collisions with hydrogen molecules," *Zhurnal Eksperimental'noi i Teoreticheskoi Fiziki*, vol. 33, p. 5, 1957.
- [191] R. Golser, H. Gnaser, W. Kutschera, A. Priller, P. Steier, A. Wallner, M. Čížek, J. Horáček, and W. Domcke, "Experimental and Theoretical Evidence for Long-Lived Molecular Hydrogen Anions  $H_2^-$  and  $D_2^-$ ," *Physical Review Letters*, vol. 94, p. 223003, 2005.

- [192] A. A. Shiryaev, D. Grambole, A. Rivera, and F. Herrmann, "On the interaction of molecular hydrogen with diamonds: An experimental study using nuclear probes and thermal desorption," *Diamond and Related Materials*, vol. 16, pp. 1479-1485, 2007.
- [193] M. S. Melnik, "Diamond Surfaces: Interactions with Hydrogen and Halogens," Doctor of Philosophy PDF, Applied Physics, California Institute of Technology, Pasadena, CA, 1997.
- [194] J. E. Bartmess, "Gas phase ion energetics data," in *NIST Chemistry WebBook, NIST Standard Reference Database* vol. 29, P. J. Linstrom and W. G. Mallard, Eds., ed. Gaithersburg MD, 20899: National Institute of Standards and Technology, 2013.
- [195] M. Allan and T. Skalický, "Structures in elastic, vibrational, and dissociative electron attachment cross sections in N<sub>2</sub>O near threshold," *Journal of Physics B: Atomic, Molecular and Optical Physics*, vol. 36, p. 3397, 2003.
- [196] J. C. Rienstra-Kiracofe, G. S. Tschumper, H. F. Schaefer, S. Nandi, and G. B. Ellison, "Atomic and Molecular Electron Affinities: Photoelectron Experiments and Theoretical Computations," *Chemical Reviews*, vol. 102, pp. 231-282, 2002/01/01 2002.
- [197] D. Yu, A. Rauk, and D. A. Armstrong, "Electron affinities and thermodynamic properties of some triatomic species," *The Journal of Physical Chemistry*, vol. 96, pp. 6031-6038, 1992/07/01 1992.
- [198] S. J. Nalley, R. N. Compton, H. C. Schweinler, and V. E. Anderson, "Molecular electron affinities from collisional ionization of cesium. I. NO, NO<sub>2</sub>, and N<sub>2</sub>O," *The Journal of Chemical Physics*, vol. 59, pp. 4125-4139, 1973.
- [199] F. Brüning, S. Matejčík, E. Illenberger, Y. Chu, G. Senn, D. Muigg, G. Denifl, and T. D. Märk, "Effects of temperature on the dissociative electron attachment to N<sub>2</sub>O," *Chemical Physics Letters*, vol. 292, pp. 177-182, 1998.
- [200] M. Z. Hossain, T. Kubo, T. Aruga, N. Takagi, T. Tsuno, N. Fujimori, and M. Nishijima, "Surface Phonons, Electronic Structure and Chemical Reactivity of Diamond (100)(2 x 1) Surface," *Japanese Journal of Applied Physics*, vol. 38, p. 8, 1999.
- [201] S. C. Jain and K. S. Krishnan, "The Thermionic Constants of Metals and Semi-Conductors. I. Graphite," *Proceedings of the Royal Society of London. Series A. Mathematical and Physical Sciences*, vol. 213, pp. 143-157, June 24, 1952 1952.